

HIGH PRESSURE METROLOGY

---

Seminar  
organized by the "HIGH PRESSURE" Working Group  
of the COMITE CONSULTATIF POUR LA MASSE  
ET LES GRANDEURS APPARENTEES

Laboratoire national d'essais  
Paris, 24-25 May 1988

G.F. Molinar - Editor  
Istituto di Metrologia G. Colonnetti  
Torino (Italy)  
Chairman of the CCM-High Pressure Working Group



## F O R E W O R D

High pressure Technology and new applications demand increasingly of metrologists that the best instrumentation should ensure the highest measurement accuracy, in particular in fluid media to some gigapascal.

In this perspective, the seminar of the CCM "High Pressures" Working Group held at the Laboratoire National d'Essais in Paris in May 1988 was organised with the purpose of presenting an updated survey of the research work carried out by metrological national laboratories and by industrial concerns in the high-pressure sector. With this in view, the seminar was planned as a forum open to discussion, to bring into focus the main area in which high-pressure metrologists are especially asked - and expected - to make their contributions of study and research.

The seminar was organised in two sections. One was mainly devoted to the calculation and measurement of elastic distortions in piston-cylinders and to the new trends and developments in piston gauges for relative and absolute pressure measurement in liquids and gas. In the other section there were discussed pressure transducers, transfer standards available for use in comparisons, and dynamic pressure measurements.

There are also given the results of the latest international comparisons particularly in the range around 0.8 GPa; some possible new fixed points are also considered.

The seminar were attended by 27 persons and the 23 contributions presented are collected here.

All the contributions here presented were refereed by drs. Bean (NBS - USA), Molinar (IMGC - I) and Stuart (NPL - UK), and are published with the permission of the contributors and of their institutions.

The editor wishes to thank the Director and the personnel of the Laboratoire National d'Essais (Paris) for hosting the seminar, the Director of BIPM for publication of the present monograph, and all the colleagues that have participated in the interesting discussions during the seminar.

GF. Molinar



LIST OF CONTRIBUTORS - I

(in order of presentation during the seminar)

- **J. Jäger, G. Klingenberg, P. Hilsch**  
Physikalisch Technische Bundesanstalt (PTB)  
Bundesallee 100  
D-3300 Braunschweig (F.R.G.)
- **GF. Molinar, L. Bianchi, P.C. Cresto, R. Maghenzani**  
Istituto di Metrologia "G. Colonnetti" (IMGC)  
Strada delle Cacce, 73  
10135 Torino (Italy)
- **J.C. Legras**  
Laboratoire National d'Essais (LNE)  
1 rue Gaston Boissier  
F-75015 Paris (France)
- **D.B. Francis, K. Solis**  
Ruska Instrument Corporation (RUSKA)  
3601 Dunvale  
Houston - Texas 77063 (USA)
- **B.E. Welch, R.E. Edsinger, V.E. Bean, C.D. Ehrlich**  
**C.R. Tilford, R.W. Hyland**  
National Institute of Standards and Technology (NIST), formerly (NBS)  
Center for basic standards  
Gaithersburg, MD 20899 (USA)
- **P.R. Stuart**  
National Physical Laboratory (NPL)  
Queens Rd.  
Teddington  
Middlesex TW11OLW (UK)
- **P. Delajoud**  
Desgranges et Huot (D. & H.)  
10 rue Bernard at Mazoyer  
93300 Aubervilliers (F)
- **V.M. Borovkov, V.E. Tarassov, Yu.A. Atanov**  
VNIIFTRI  
High Pressure Meas. Div.  
141570 Mendeleyevo  
Moscow Region (USSR)
- **A. Ooiwa, S. Yamamoto**  
National Research Laboratory of Metrology (NRLM)  
1-4, 1-chome, Umezono, Sakura-Mura, Niihari-gun  
Ibaraki 305, (Japan)
- **Yaw-Poo Lin**  
Chung Shan Institute of Science and Technology  
Lung-ten, Taiwan

- **R. Wisniewski, R. Sendys, D. Wisniewski, A. J. Rostocki  
J. Rogowski**  
Institute of Physics  
Warsaw University of Technology  
00-662 Warszawa, ul, Koszykowa 75  
Warsaw (Poland)
- **H. Lippman, L. Sterner, H. Arendt**  
A S M W  
Furstenwalder Damm 388  
1162 Berlin (DDR)
- **B. Gyarmati, G. Sarkani**  
O M H  
P.O. Box 19  
1531 Budapest (Hungary)
- **N. Bignell**  
C S I R O  
Div. of Applied Physics  
Lindfield, NSW (Australia)
- **Sheng Yi-tang**  
National Institute of Metrology (NIM)  
Beijing (The people Rep. of China)

## C O N T E N T S

Foreword .....	III
List of contributors - I .....	V
Contents .....	VII
List of contributors - II .....	X

### **PART 1 "Piston gauge"**

#### Sub-section "Elastic distorsion in piston-cylinders"

Critical remarks concerning the derivation of the elastic distorsion coefficient from the normally used theory <b>G. Klingenberg</b> .....	1
Elastic distorsions in a piston-cylinder unit for pressure measurements in liquids to 100 MPa: preliminary results <b>GF. Molinar, P.C. Cresto, R. Maghenzani</b> .....	12
A capacitance method of measuring the radial displacement of the outer diameter of the cylinder of a piston gage <b>V.E. Bean, Yaw-Poo Lin</b> .....	22
Determination of pressure coefficient of effective area of simple 0.3 GPa deadweight manometer by means of finite element method of strain calculation <b>R. Wisniewski, R. Sendys, D. Wisniewski, A.J. Rostocki</b> ....	27
The influence of fluid viscosity on the distortion of piston-cylinder assemblies in pressure balances <b>P.R. Stuart</b> .....	31

#### Sub-section "New developments and trends concerning piston-gauges or similar systems"

Piston gage used as high accuracy standards in the range 0.01 - 1000 MPa <b>J.C. Legras</b> .....	41
Design considerations for a new high pressure (100 MPa) gas lubricated piston pressure gage <b>D.B. Francis, K. Solis</b> .....	53
Comparison measurements up to 8 kbar between a Budenberg and a Harwood high pressure balance using undiluted di-ethylhexyl-sebacate as pressure fluid <b>P. Hilsch, J. Jäger</b> .....	62

Development of a highly stable air piston pressure gage with non rotational piston-cylinder system  
A. Ooiwa ..... 67

Dead weight piston gauge of mixed operation principle  
R. Wisniewski, J. Rogowski, A.J. Rostocki ..... 73

Sub-section "Piston gauges for relative and absolute gas pressure measurements"

Observations of gas species and mode of operation effects on effective areas of gas-operated piston gages  
B.E. Welch, R.E. Edsinger, V.E. Bean, C.D. Ehrlich ..... 81

Primary barometers and the BIPM International Intercomparison in the pressure region 10 kPa to 110 kPa  
P.R. Stuart ..... 95

Non-geometric dependencies of gas-operated piston gage effective areas  
C.R. Tilford, R.W. Hyland, Sheng Yi-tang ..... 105

**PART 2 "Pressure transducers, transfer standards, dynamic pressure measurements, fixed points"**

Sub-section "Pressure transducers and transfer standards"

The pressure multiplier: a transfer standard in the range 100 to 1000 MPa  
P. Delajoud ..... 114

InSb as a pressure sensor  
V.E. Bean ..... 125

VNIIFTRI High-Pressure transfer standards  
Y.M. Borovkov, V.E. Tarassov, Yu. A. Atanov ..... 132

Use of strain gauge pressure transducers as transfer standards up to 1.0 GPa at the 0.1% uncertainty level  
J. Jäger ..... 141

Stability and metrological characteristics of manganin gauges up to approximately 1 GPa  
GF. Molinar, L. Bianchi ..... 147

Manganin resistance manometer: III. Pressure coefficient of resistance  
S. Yamamoto ..... 157

Sub-section "Dynamic pressure measurements, intercomparisons and fixed points"

Dynamic calibration of pressure transducer J.P. Damion .....	161
Some experimental results of calibration of dynamic pressure resistance sensors by use of triangular pulse generator A.J. Rostocki, R. Wisniewski .....	162
The 700 MPa intercomparisons of high pressure standards of the USSR, GDR and Hungary V.M. Borovkov, V.E. Tarassov, Yu. A. Atanov, H. Lippman, L. Sterner, H. Arendt, B. Gyarmati, G. Sarkani .....	168
Pressure fixed points based on the Carbon Dioxide Vapor pressure at 273.16 K and the H <sub>2</sub> O(I) - H <sub>2</sub> O(III) - H <sub>2</sub> O(L) triple point N. Bignell, V.E. Bean. ....	175



PART 1

PISTON GAUGE

Sub-section: elastic distortion in piston-cylinders



Critical remarks concerning the derivation of the elastic  
distortion coefficient from the normally used theory

G.Klingenberg

Abstract

The reader is reminded of Dadson's formula giving the relation between the elastic distortion coefficient of the pressure balance and the elastic distortion of the piston and the cylinder.

The radial and axial distortions of a piston and a cylinder are calculated from exact solutions of the elastic differential equations in the case of a pressure distribution  $p(z) = \alpha + \beta z + \gamma z^2$  in the clearance between the piston and cylinder. The jacket surface of the cylinder is assumed to be exposed to a constant pressure  $p_j$ . The end faces of the piston are subjected to the gauge pressure  $p_0$  and to the gravitational force exerted by the load that creates the pressure  $p_0$ . It is assumed that a pressure  $p_{ce}$  acts on the end faces of the cylinder.

The sensitivity of the calculated distortion coefficient to the choice of boundary conditions is demonstrated.

Calculation of the distortion coefficient normally assumes the pressure gradient in the clearance to be constant along the engagement length which yields a linearly varying clearance. The assumption is not strictly valid. It is avoided by applying the theory of flow in a converging channel to the pressure balance to calculate the upward force on the flanks of the piston due to fluid friction.

Critical remarks concerning the derivation of the elastic distortion coefficient from the normally used theory

G.Klingenberg

The distortion coefficient is an important parameter to characterize a pressure balance, particularly in the case of higher pressures. It can be determined directly from the experiment only in the case of jacket pressure systems. The calculation of the distortion coefficient is, therefore, of considerable importance.

The derivation of the formula normally used to calculate the distortion coefficient is given by Zhokhovskii / 1 / and Dadson et al. / 2 /. The three contributions balancing the total weight force on the piston are: 1. the pressure acting on the distorted piston bottom; 2. the pressure acting on the distorted piston jacket and 3. the frictional force of the fluid. In 3., an important assumption is used: The width of the gap between piston and cylinder is assumed to be constant. Therefore, the well-known solution of the Navier-Stokes equations can be used. This solution is then adopted to describe the flow in a locally variable gap. The result is the well-known formula for the distortion coefficient of a pressure balance:

$$\lambda = \frac{u_{rp}(r=r_i, x=0) + u_{rc}(r=r_i, x=0)}{r_i p_0} + \frac{1}{r_i p_0^2} \int_0^l p(x) \left( \frac{du_{rp}(r=r_i)}{dx} + \frac{du_{rc}(r=r_i)}{dx} \right) dx \quad (1)$$

where  $u_{rp}$ : radial piston distortion,  $u_{rc}$ : radial cylinder distortion,  $l$ : engagement length,  $x=0$ : bottom of the piston,  $x=l$ : top of the piston,  $r_i$ : radius of the piston  $\approx$  radius of the bore in the cylinder,  $p_0$ : pressure to be measured,  $p(x)$  pressure in the gap. The reason why the cylinder distortion appears in (1) is that in the solution of the Navier-Stokes equations  $h=h(x)$  was written for the clearance between piston and cylinder. To be exact, the Navier-Stokes equations cannot always be applied to pressure balances. These equations assume the fluid to be incompressible and of constant dynamic viscosity. In the case of higher pressures, this is not a good

assumption. If the distortions are proportional to the pressure along the engagement length

$$u_{rp}(r=r_i) = R + S p(x) \quad , \quad u_{rc}(r=r_i) = R_1 + S_1 p(x) \quad (2)$$

then, using (1), the result is

$$\lambda = \frac{1}{2} \frac{1}{r_i p_0} [u_{rp}(r=r_i, x=0) + u_{rp}(r=r_i, x=l) + u_{rc}(r=r_i, x=0) + u_{rc}(r=r_i, x=l)] \quad (3)$$

This result is not obvious. Quite different pressure distributions may give the same distortion coefficient. This is in contrast to the formula given by Welch and Bean / 3 /.

In the case of a linear pressure distribution the distortions vary linearly, too. This yields

$$\lambda = \frac{1}{r_i p_0} [u_{rp}(r=r_i, x=l/2) + u_{rc}(r=r_i, x=l/2)] \quad (4)$$

If the pressure in the clearance is given by  $p=p_0 z/l$ , then the distortion of a piston-cylinder assembly in the middle of the engagement length is the same as in the case of a system under the constant pressure  $p_0/2$ . For the derivation of the well-known equations it is therefore sufficient to start from a constant pressure in the gap, as has been done by Heydemann and Welch / 4 / in their review article. Since the results in the case of a constant and a linear pressure distribution are well known, it seems reasonable to add a quadratic contribution.

It is appropriate to note the differential equations for the elastic equilibrium in cylindrical coordinates, the Lamé equations. They are valid in the case of homogeneous, isotropic solids, i.e. the density and the elastic modulus must be constant. Piston and cylinder are assumed to be rotationally symmetrical.

$$\frac{\partial}{\partial r} \frac{1}{r} \left[ \frac{\partial(r u_r)}{\partial r} + r \frac{\partial u_z}{\partial z} \right] + \frac{1}{2} \frac{1-2\mu}{1-\mu} \frac{\partial}{\partial z} \left[ \frac{\partial u_r}{\partial z} - \frac{\partial u_z}{\partial r} \right] = 0, \quad (5)$$

$$\frac{\partial^2 u_\varphi}{\partial z^2} + \frac{\partial}{\partial r} \frac{1}{r} \frac{\partial(r u_\varphi)}{\partial r} = 0, \quad (6)$$

$$\frac{\partial}{\partial z} \left[ \frac{\partial(r u_r)}{\partial r} + r \frac{\partial u_z}{\partial z} \right] - \frac{1}{2} \frac{1-2\mu}{1-\mu} \frac{\partial}{\partial r} r \left[ \frac{\partial u_r}{\partial z} - \frac{\partial u_z}{\partial r} \right] = 0. \quad (7)$$

Equations (5), (7) are separated from (6) for  $u_\varphi$ , the component in the transverse direction. For the computation of the distortion coefficient,  $u_\varphi$  is not required and (6) need not be considered further.

The strain-stress relations in cylindrical coordinates are as follows:

$$\sigma_{rr} = \frac{E}{1+\mu} \frac{1-\mu}{1-2\mu} \frac{\partial u_r}{\partial r} + \frac{E}{1+\mu} \frac{\mu}{1-2\mu} \left[ \frac{u_r}{r} + \frac{\partial u_z}{\partial z} \right], \quad (8)$$

$$\sigma_{zz} = \frac{E}{1+\mu} \frac{1-\mu}{1-2\mu} \frac{\partial u_z}{\partial z} + \frac{E}{1+\mu} \frac{\mu}{1-2\mu} \left[ \frac{\partial u_r}{\partial r} + \frac{u_r}{r} \right], \quad (9)$$

$$\sigma_{rz} = \frac{E}{2(1+\mu)} \left[ \frac{\partial u_r}{\partial z} + \frac{\partial u_z}{\partial r} \right]. \quad (10)$$

Young's modulus is denoted by E, and Poisson's ratio by  $\mu$ . Since the stress acting on the surface is given as a boundary condition, these equations may be solved. If the unit vector normal to the surface is denoted by  $n$ , the stress tensor by  $\sigma$ , and the force acting from the outside on a surface element dF by PdF, then

$$\sigma n = P \quad (11)$$

must be valid. The pressures acting on the piston-cylinder assembly are shown in Fig.1.

In / 5 /, the boundary conditions were fulfilled for the diagonal components of the stress tensor:

$$\sigma_{rr}(r=r_1, z) = -\alpha - \beta z - \gamma z^2 \quad \text{for the piston and the cylinder,} \quad (12)$$

$$\sigma_{zz}(r, z=0) = \sigma_{zz}(r, z=l) = -p_0 \quad \text{for the piston,} \quad (13)$$

$$\sigma_{zz}(r, z=0) = \sigma_{zz}(r, z=l) = -p_{0c} \quad \text{for the cylinder.} \quad (14)$$

$\alpha, \beta, \gamma$  are constants. In the limit of the linear pressure distribution this yields the correct distortion  $u_r$ ; in addition - if

$$\alpha_1 = -(1+\mu_c) \frac{r_1^2 R^2}{R^2 - r_1^2} \frac{\beta}{E_c} \quad (15)$$

is chosen -  $\sigma_{rz}=0$  is the result. In the case of a pressure distribution with quadratic contribution, the  $\sigma_{rz}$  calculated from  $u_r, u_z$  using (10) yields a non-realistic distribution and its absolute value is indeed small compared with  $p_0$  but larger than a realistic value calculated from the fluid friction. As an example, a piston-cylinder system commercially available for the 500 MPa pressure range with  $r_1 = 0.79$  mm,  $R = 8.5$  mm,  $l = 26.5$  mm,  $\mu_p = 0.28$ ,  $\mu_c = 0.22$ ,  $E_p = 2.0 \cdot 10^5$  MPa,  $E_c = 6.3 \cdot 10^5$  MPa is considered. The subscript p denotes the piston, c the cylinder. In Fig.2  $\sigma_{rz}/p_0$  is shown as a function

of  $z/l$ . The attempt was therefore, made to find solutions of the differential equations (5), (7) for the boundary conditions (12),

$$\sigma_{rz} = 0 \quad \text{on all the piston and cylinder surfaces,} \quad (16)$$

$$2\bar{\pi} \int_0^{\bar{r}} r \sigma_{rz} dr = -\bar{\pi} \bar{r}^2 p_0 \quad \text{for the piston,} \quad (17)$$

$$2\bar{\pi} \int_{\bar{r}_i}^{\bar{R}} r \sigma_{rz} dr = -\bar{\pi} (\bar{R}^2 - \bar{r}_i^2) p_{ce} \quad \text{for the cylinder.} \quad (18)$$

The two final conditions are a generalization of an equation given by Chree / 6 /. He calculated the distortion of a solid cylinder for the condition  $\bar{\sigma}_{rz} = 0$  and a quadratic pressure distribution acting on the cylindrical surface. Indeed, his solution does not allow  $\bar{\sigma}_{zz} = 0$  on the end faces, but for the mean value he finds:

$$2\bar{\pi} \int_0^{\bar{r}} r \bar{\sigma}_{zz} dr = 0. \quad (19)$$

In the case of the piston, just as in an earlier paper / 5 /, a series in  $r$  and  $z$  up to the third order is used:

$$u_{rp} = a_1 r + a_2 rz + a_3 r^3 + a_4 rz^2, \quad (20)$$

$$u_{zp} = b_1 + b_2 z + b_3 r^2 + b_4 z^2 + b_5 r^2 z + b_6 z^3. \quad (21)$$

Some terms, for example those proportional to  $z$  and  $r^2 z$  do not appear in  $u_{rp}$ . The differential equations or the boundary conditions do not allow these terms. Terms proportional to  $1/r$  and  $\ln r$  should not be considered because they would lead to infinite distortions on the piston's axis. In the case of the cylinder, these terms must be taken into account:

$$u_{rc} = \frac{c_1}{r} + c_2 \frac{z}{r} + c_3 \frac{z^2}{r} + c_4 r \ln \frac{r}{\bar{r}_i} + c_5 r + c_6 rz + c_7 r^3 + c_8 rz^2, \quad (22)$$

$$u_{zc} = d_1 \ln \frac{r}{\bar{r}_i} + d_2 z \ln \frac{r}{\bar{r}_i} + d_3 z + d_4 r^2 + d_5 z^2 + d_6 r^2 z + d_7 z^3. \quad (23)$$

The same coefficients  $a_1, \dots, d_7$  differ from zero as in the case of the boundary conditions (12), ..., (14) / 5 /. They may depend on the geometrical quantities  $r_i, R, l$ ; the elastic constants  $\mu_p, \mu_c, E_p, E_c$ ; the pressures  $p_0, p_{ce}, p_j$  and the coefficients of the pressure distribution  $\alpha, \beta, \gamma$ . If the origin of the  $z$ -axis is fixed at the top on the axis of the piston,  $b_1 = 0$  results. The remaining coefficients  $a_1, \dots, d_7$  have been compiled in the appendix.

$\Delta \bar{\epsilon}_{zz}$  denotes the deviation of the stress  $\bar{\epsilon}_{zz}$  calculated from (9) using (20), (21) from  $-p_0$  (piston) or using (22), (23) from  $-p_{ce}$  (cylinder). In the case of the example mentioned above  $\Delta \bar{\epsilon}_{zz}/p_0$  yields substantially smaller absolute values than  $\bar{\epsilon}_{rz}/p_0$  (Fig.2) from the earlier paper / 5 /.  $\Delta \bar{\epsilon}_{zz}/p_0$  varies almost proportionally to  $r_i^2/l^2$ , and  $\bar{\epsilon}_{rz}/p_0$  proportionally to  $r_i/l$ . It must, therefore, be concluded that the boundary conditions (12), (16) ... (18) describe the elastic distortions more realistically than the conditions (12) ... (14). A theory allowing the calculation of values of  $\bar{\epsilon}_{rz}/p_0$  from the fluid friction acting on the cylindrical surface would possibly be better. From equations (1), (20) ... (23) for the distortion coefficient of a simple piston-cylinder assembly the well known formula is found:

$$\lambda = \frac{3\mu_p - 1}{2E_p} + \frac{1}{2E_c} \frac{1}{R^2 - r_i^2} [R^2(1 + \mu_c) + r_i^2(1 - \mu_c)] \quad (24)$$

This result shows the sensitivity of the solutions to a change of the boundary conditions. In the example mentioned above with the boundary conditions (12) ... (14) / 5 /, the distortion coefficient shows, mainly due to the piston distortion, a relative deviation of 36 % from the usual theory, while the deviation disappears if (12), (16) ... (18) are used.

As mentioned earlier, equation (1) starts from a solution of the Navier-Stokes equations in the case of a constant gap along the engagement length. The piston radius of pressure balances is much larger than this gap. For the calculation of the fluid friction using the usual approximations, it is therefore also possible to investigate the flow between two plane, parallel walls. Thus, the pressure drops linearly along the engagement length. The solutions of the Lamé equations for this simple pressure distribution yield a gap varying linearly with  $x$ . Therefore, the boundary condition of the Navier-Stokes equation is not exactly valid. To avoid this problem, the

theory of the flow in a converging channel / 7 / is applied. It is appropriate to note the differential equations for the steady flow between two plane walls meeting at an angle  $\Theta$ , expressed in cylindrical coordinates  $\zeta, \phi$

(Fig.4):

$$\nu \frac{\partial v}{\partial \zeta} = -\frac{1}{\rho} \frac{\partial p}{\partial \zeta} + \nu \left( \frac{\partial^2 v}{\partial \zeta^2} + \frac{1}{\zeta^2} \frac{\partial^2 v}{\partial \phi^2} + \frac{1}{\zeta} \frac{\partial v}{\partial \zeta} - \frac{v}{\zeta^2} \right), \quad (25)$$

$$-\frac{1}{\rho \zeta} \frac{\partial p}{\partial \phi} + \frac{2\nu}{\zeta^2} \frac{\partial v}{\partial \phi} = 0, \quad (26)$$

$$\frac{\partial(\zeta v)}{\partial \zeta} = 0. \quad (27)$$

$v$  is the component of the flow velocity in direction OA. The meaning of the coordinate  $\zeta$  can also be seen from Fig.4.  $\nu$  denotes the kinematic viscosity,  $\rho$  the density; both are supposed to be constant in this theory. From the equation of continuity it can be seen that

$$U = \frac{\zeta v}{6\nu} \quad (28)$$

is a function of  $\phi$  only. The important quantity for the calculation of the frictional force is (Fig.4):

$$\frac{dv}{d\tau} = -6\nu \frac{d[U(\phi)/\zeta]}{\zeta d\phi} = -\frac{6\nu}{\zeta^2} \frac{dU(\phi)}{d\phi} \quad (29)$$

In this case it is not necessary to use (1). Using (28) it is possible to separate the Navier-Stokes equations. This yields an equation for the pressure distribution

$$\frac{p}{\rho} = \frac{12\nu^2}{\zeta^2} \left( U - \frac{C_1}{2} \right) + \text{const.} \quad (30)$$

and an equation for the flow across the gap:

$$2\phi = \pm \int_{-u_0}^u \frac{dU}{\gamma(U+u_0)[-U^2-(1-U)U+q]} \quad (31)$$

$U$  does not depend on  $\zeta$  and  $C_1$  is a constant. Thus, it can be seen from (30) that the pressure distribution does not vary linearly with  $x$ . In the case of low pressures and correspondingly small distortions, however, it is possible to use the theory of the flow in a converging channel as an improved approximate description. The flow is symmetric to  $\phi=0$  (Fig.4).

This yields the two signs in (31). The boundary conditions are: 1. the fluid is at rest at the walls; 2. the mass of fluid passing in unit time through

any cross-section  $\zeta = \text{const.}$  is independent of  $\zeta$ , giving two equations for the determination of  $U_0, q$ :

$$\Theta = \int_{-u_0}^0 \frac{dU}{\sqrt{(U+U_0)[-U^2-(1-U_0)U+q]}} \quad (32)$$

$$\frac{\Theta}{6\eta} = \int_{-u_0}^0 \frac{U dU}{\sqrt{(U+U_0)[-U^2-(1-U_0)U+q]}} \quad (33)$$

$\eta$  is the dynamic viscosity,  $Re = |\Theta|/\eta$  the Reynolds number for this problem. The function  $f(U) = [-U^2-(1-U_0)U+q]^{-\frac{1}{2}}$  in the integrand of equations (31) ... (33) is expanded as a Taylor series in  $-U_0$ . In the lowest approximation for the

frictional force / 8 /

$$K_f = -2\bar{\tau} \tau_i \eta \int_{\phi=\frac{\pi}{2}}^{\phi} \left| \frac{dU}{d\tau} \right| dx = 12\bar{\tau} \tau_i \frac{\eta^2}{\Theta^2} Re \left( \frac{1}{\zeta_0} - \frac{1}{\zeta_0 + \ell} \right) \quad (34)$$

is found. The Reynolds number can be determined from the measurement of the fall rate / 8 /:

$$Re = \frac{r_0}{2\nu} v_{FR} \quad (35)$$

This is a possible approximation since the vertical piston movement is essentially slower than the flow velocity in the middle of the gap. However, the kinematic viscosity must be known with sufficient accuracy. As this often is not the case, the lowest order approximation of (31) is used:

$$U = -\frac{Re}{4\Theta} + \frac{Re}{\Theta^2} \phi^2 \quad (36)$$

Its arithmetic mean is used in (30) where according to / 7 /  $C_1$  is expressed by  $U_0$  and  $q$ . In the zero order approximation / 8 /

$$Re = \frac{1}{\zeta_0^{-2} - (\zeta_0 + \ell)^{-2}} \frac{\Theta^3 p_0}{6\eta^2 \nu^2} \quad (37)$$

is obtained. The contribution of the fluid friction to the distortion coefficient is given by / 8 /:

$$K_{fc} = \pi \tau_i p_0 \frac{h(x=\ell)h(x=0)}{h(x=\ell/2)} - \pi \tau_i p_0 h_0 \quad (38)$$

The meaning of the clearances  $h_0, h(x=1), \dots$  can be seen from Fig.4. The usual theory yields:

$$K_{fu} = \pi \tau_i p_0 h(x=\ell/2) - \pi \tau_i p_0 h_0 \quad (39)$$

and this gives  $K_{fc} \cong K_{fu}$ . The equality sign is valid only in the case of a constant clearance between piston and cylinder.

As an example, a simple piston-cylinder system made from tungsten carbide is considered with  $E_p = E_c = 6.3 \cdot 10^5$  MPa;  $\mu_p = \mu_c = 0.22$ ;  $r_i = 1.8$  mm;  $R = 13$  mm;  $l = 20$  mm. When (38) is used to calculate the distortion coefficient, a value,  $5.8 \cdot 10^{-7}$  MPa<sup>-1</sup> / 8 / is obtained, which is smaller by 20 % than that calculated from the usual theory.

### References

- / 1 / M.K.Zhokhovskii: Theory and Design of Instruments with Packing-free Pistons (in Russian) (Moscow, 1959)
- / 2 / R.S.Dadson, R.G.P.Greig, A.Horner: Metrologia 1 (1965), 55-68
- / 3 / B.E.Welch, V.E.Bean: Rev.Sci.Instrum. 55 (1984), 1901-1909
- / 4 / P.L.M.Heydemann, B.E.Welch: Experimental Thermodynamics. Volume II: Experimental Thermodynamics of Non-reacting Fluids, B. Le Neindre, B.Vodar (eds.) (Butterworths, London 1975), pp.147-202
- / 5 / G.Klingenberg: Metrologia 22 (1986) 259-263
- / 6 / C.Chree: Philos.Mag., Ser.6:2 (1901), 532-558
- / 7 / L.D.Landau, E.M.Lifshitz: Course of Theoretical Physics. Volume 6: Fluid Mechanics (Pergamon Press, Oxford, London, Edinburgh, New York, ..., 1959), pp.81-84
- / 8 / G.Klingenberg: Metrologia 24 (1987), 89-95

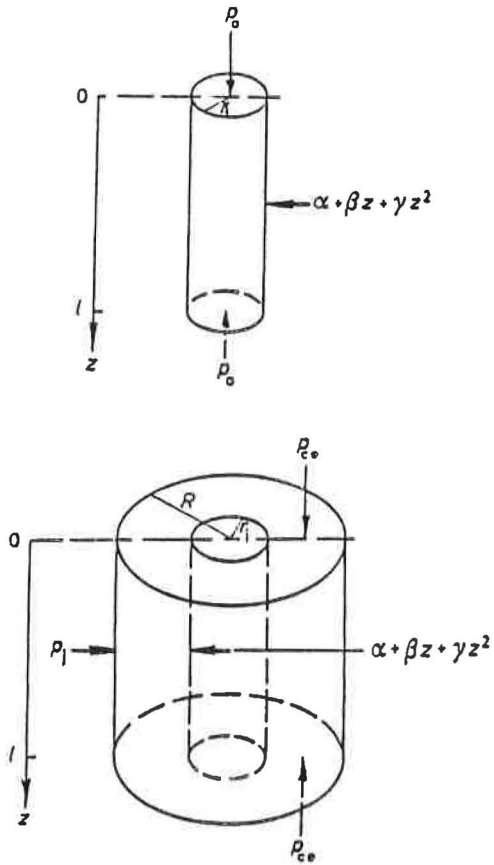


Fig.1 Pressures acting on the piston-cylinder assembly

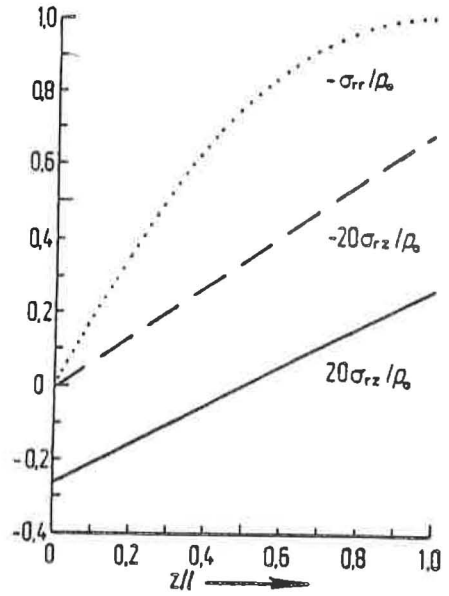


Fig.2 Calculated normalized shear stress  $\sigma_{rz}/\rho_0$  for the piston and the cylinder (---) to the relative pressure distribution  $-\sigma_{rr}/\rho_0$ , plotted against the normalized axial coordinate

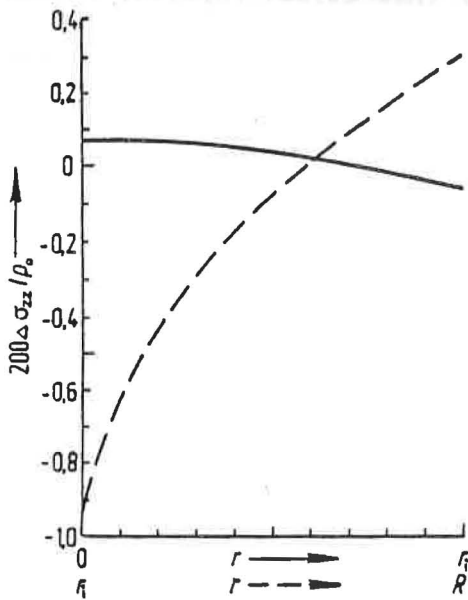


Fig.3 Relative deviations  $\Delta\sigma_{zz}/\rho_0$  for the piston and cylinder (---) subjected to the same pressure distribution as in Fig.2, plotted against the radial coordinate

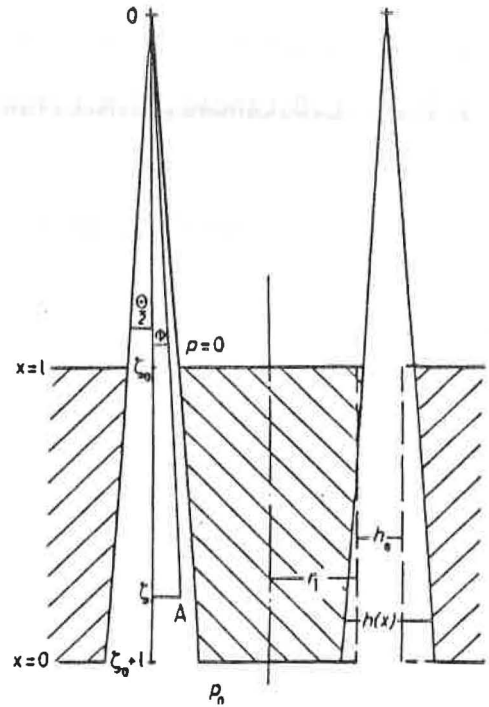


Fig.4 Diagrammatic sketch of a distorted piston-cylinder assembly (clearance shown greatly exaggerated). --- Undistorted boundaries of piston and cylinder

Appendix

$$a_1 = \frac{\mu_0}{E_p} p_0 - \frac{1-\mu_0}{E_p} \alpha + \frac{\mu_0}{4E_p} \gamma \tau_i^2, \quad (\text{A } 1)$$

$$a_2 = -\frac{1-\mu_0}{E_p} \beta, \quad (\text{A } 2)$$

$$a_3 = -\frac{\mu_0}{4E_p} \gamma, \quad (\text{A } 3)$$

$$a_4 = -\frac{1-\mu_0}{E_p} \gamma, \quad (\text{A } 4)$$

$$b_2 = -\frac{p_0}{E_p} + 2 \frac{\mu_0}{E_p} \alpha - \frac{1-\mu_0}{2E_p} \gamma \tau_i^2, \quad (\text{A } 5)$$

$$b_3 = \frac{1-\mu_0}{2E_p} \beta, \quad (\text{A } 6)$$

$$b_4 = \frac{\mu_0}{E_p} \beta, \quad (\text{A } 7)$$

$$b_5 = \frac{1-\mu_0}{E_p} \gamma, \quad (\text{A } 8)$$

$$b_6 = \frac{2\mu_0}{3E_p} \gamma. \quad (\text{A } 9)$$

$$c_1 = \frac{1+\mu_0}{E_c} \frac{R^2 \tau_i^2}{R^2 - \tau_i^2} (\alpha - p_j) + \frac{1+\mu_0}{1-\mu_0} \frac{\mu_0}{E_c} \frac{\tau_i^4 R^4}{(R^2 - \tau_i^2)^2} \gamma \ln \frac{R}{\tau_i} + \frac{1}{4} \frac{\mu_0}{E_c} \frac{\tau_i^4 R^2}{R^2 - \tau_i^2} \gamma, \quad (\text{A } 10)$$

$$c_2 = \frac{1+\mu_0}{E_c} \frac{R^2 \tau_i^2}{R^2 - \tau_i^2} \beta, \quad (\text{A } 11)$$

$$c_3 = \frac{1+\mu_0}{E_c} \frac{R^2 \tau_i^2}{R^2 - \tau_i^2} \gamma, \quad (\text{A } 12)$$

$$c_4 = \frac{\mu_0}{1-\mu_0} \frac{1+\mu_0}{E_c} \frac{R^2 \tau_i^2}{R^2 - \tau_i^2} \gamma, \quad (\text{A } 13)$$

$$c_5 = -\frac{1-\mu_0}{E_c} \left[ \frac{R^2}{R^2 - \tau_i^2} p_j - \frac{\tau_i^2}{R^2 - \tau_i^2} \alpha \right] + \frac{\mu_0}{E_c} p_{c0} - \frac{1+\mu_0}{1-\mu_0} \frac{\mu_0}{E_c} \frac{\tau_i^4 R^4}{(R^2 - \tau_i^2)^2} \gamma \ln \frac{R}{\tau_i} - \frac{\mu_0}{4E_c} \tau_i^2 \gamma \left[ 1 + \frac{2\tau_i^2}{R^2 - \tau_i^2} \right], \quad (\text{A } 14)$$

$$c_6 = \frac{1-\mu_0}{E_c} \frac{\tau_i^2}{R^2 - \tau_i^2} \beta, \quad (\text{A } 15)$$

$$c_7 = \frac{\mu_0}{4E_c} \frac{\tau_i^2}{R^2 - \tau_i^2} \gamma, \quad (\text{A } 16)$$

$$c_8 = \frac{1-\mu_0}{E_c} \frac{\tau_i^2}{R^2 - \tau_i^2} \gamma, \quad (\text{A } 17)$$

$$d_1 = -\frac{1+\mu_0}{E_c} \frac{R^2 \tau_i^2}{R^2 - \tau_i^2} \beta, \quad (\text{A } 18)$$

$$d_2 = -2 \frac{1+\mu_0}{E_c} \frac{R^2 \tau_i^2}{R^2 - \tau_i^2} \gamma, \quad (\text{A } 19)$$

$$d_3 = -\frac{p_0}{E_c} + 2 \frac{\mu_0}{E_c} \left[ \frac{R^2}{R^2 - \tau_i^2} p_j - \frac{\tau_i^2}{R^2 - \tau_i^2} \alpha \right] + 2 \frac{1+\mu_0}{E_c} \frac{R^4 \tau_i^2}{(R^2 - \tau_i^2)^2} \gamma \ln \frac{R}{\tau_i} - \frac{\tau_i^2}{R^2 - \tau_i^2} \frac{\gamma}{2E_c} \left[ (1+3\mu_0)R^2 - (1-\mu_0)\tau_i^2 \right], \quad (\text{A } 20)$$

$$d_4 = -\frac{1-\mu_0}{2E_c} \frac{\tau_i^2}{R^2 - \tau_i^2} \beta, \quad (\text{A } 21)$$

$$d_5 = -\frac{\mu_0}{E_c} \frac{\tau_i^2}{R^2 - \tau_i^2} \beta, \quad (\text{A } 22)$$

$$d_6 = -\frac{1-\mu_0}{E_c} \frac{\tau_i^2}{R^2 - \tau_i^2} \gamma, \quad (\text{A } 23)$$

$$d_7 = -\frac{2\mu_0}{3E_c} \frac{\tau_i^2}{R^2 - \tau_i^2} \gamma. \quad (\text{A } 24)$$

**ELASTIC DISTORTIONS IN A PISTON-CYLINDER UNIT  
FOR PRESSURE MEASUREMENTS IN LIQUIDS TO 100 MPa:  
PRELIMINARY RESULTS**

G.F. Molinar, P.C. Cresto, R. Maghenzani  
Istituto di Metrologia "G. Colonnetti"  
Strada delle Cacce 73, 10135 Torino, Italy

**ABSTRACT**

The primary standard for pressure measurements from atmospheric pressure to about 2 GPa is represented by a piston gauge. Recent results showed that the accuracy of systems of this type is limited mainly by insufficient knowledge of the elastic distortion in the piston-cylinder unit, even with pressure values only to 100 MPa.

Distortion phenomena are here studied by calculating the elastic distortion of a tungsten carbide piston-cylinder unit (0.2 cm<sup>2</sup> effective area) at a maximal pressure of 100 MPa. The elastic distortions are calculated as a function of the applied pressure by solving the differential equations of the deformation state, with the unknown functions expressed by Tschebyschef's polynomials and by adopting an iteration method to obtain solution convergence.

The pressure distribution in the clearance is calculated through an iteration method derived from appropriately modified Navier-Stokes equations, in which account is taken both of fluid viscosity and, iteratively, of the deformations of the piston-cylinder unit. The calculated displacements of the outer surface of the cylinder are compared with measurements made by means of strain gauges. The results of this comparison, which are in satisfactory agreement, are discussed.

**ELASTIC DISTORTIONS IN A PISTON-CYLINDER UNIT  
FOR PRESSURE MEASUREMENTS IN LIQUIDS TO 100 MPa:  
PRELIMINARY RESULTS**

G.F. Molinar, P.C. Cresto, R. Maghenzani  
Istituto di Metrologia "G. Colonnetti"  
Strada delle Cacce 73, 10135 Torino, Italy

**1. INTRODUCTION**

For the measurement of pressure in the range from atmospheric pressure to some gigapascals the primary standard is a piston gage in which pressure is obtained from the application of a known gravitational force in equilibrium with an upward force generated by pressure on a known area of a piston-cylinder unit.

Area determination involves:

- the determination of the effective area  $A_0$  at atmospheric pressure and at a specified reference temperature  $t_r$  (generally 20°C) by means of dimensional measurement or by comparison with other standards;
- the determination of the dependance of such effective area on the applied pressure, account being taken of the elastic distorsion of the piston and of the cylinder.

Both the above parameters being known, the effective area  $A_e$  at pressure  $P$  and at the working temperature  $t$  is:

$$A_e(P,t) = A_0(P_{atm},t_r) (1 + \lambda \cdot P) [1 + (\alpha_p + \alpha_c) (t - t_r)]$$

where  $\lambda$  is the coefficient of elastic distorsion of the piston-cylinder unit,  $\alpha_p$  and  $\alpha_c$  are the linear thermal expansion coefficients for the piston and the cylinder, respectively.

The results /1/ of a recent comparison between thirteen national metrological laboratories showed that the determining factor limiting the accuracy of piston gauges is an imperfect knowledge of the coefficient of elastic distortion in the piston-cylinder unit. In fact, for typical values of  $\lambda$  of

about  $1 \cdot 10^{-6}$  MPa $^{-1}$  for a piston gauges of 100 MPa capacity, the effect of a typical uncertainty  $\Delta\lambda = 0.3 \cdot 10^{-6}$  MPa $^{-1}$  on the uncertainty of full-scale pressure measurements is equal to 30 ppm, which is too high a value. Studies on this problem have been carried out mainly at NPL /2/ and, more recently, at NBS /3, 4, 5/ and PTB /6, 7/. At IMGCC a study on such elastic distortion was begun not long ago, with the purpose of establishing a calculation method that could satisfactorily be applied for the redetermination of the accuracy of any configuration of piston gauges. The elastic distortion in a piston-cylinder unit as a function of applied pressure is calculated by solving the differential equations representing the deformation state, with the unknown functions expressed by Tschebyschef's polynomials, and by adopting iterative methods in order to obtain solution convergence.

The pressure distribution in the clearance is calculated through an iteration method derived from appropriately modified Navier-Stokes equations, in which account is taken both of fluid viscosity and, iteratively, of the deformation of the piston-cylinder unit. The calculated displacements of the outer surface of the cylinder are compared with measurements made by means of strain gauges. The piston-cylinder unit used for this study (Fig. 1) is made of tungsten carbide and is characterized by:  $A_0$  nominal = 0.2 cm $^2$ ; piston diameter ( $z = 0$ ) = 5.0462 mm; internal cylinder diameter ( $z = 0$ ) = 5.0474 mm; external cylinder radius  $r_e = 15$  mm; engagement length of piston-cylinder unit  $l_0 = 51$  mm; piston fall rate = 0.0078 mm/min at 9.8 MPa; Young's modulus  $E = (6.47 \pm 0.065)10^5$  MPa; Poisson's ratio  $\nu = 0.2178 \pm 0.0007$ . The pressurizing fluid was Spinesso 10, for which the dynamic viscosity  $\eta_0$  and its variation with pressure, density  $\rho$  and its variation with pressure and temperature, and surface tension  $\gamma$  are known.

## 2. EXPERIMENTAL MEASUREMENTS

Strain  $\epsilon_\theta$  in the outer cylinder surface was measured as a function of applied pressure by means of a string of strain gauges bonded to the surface. The behaviour of  $\epsilon_\theta$  was then obtained as a function of the applied pressure and as a function of position in the engagement length of piston-cylinder unit.

In Fig. 1 the black rectangles indicate strain-gauge positions. In the portion of the maximal pressure,  $P_0$ , three strain gauges were bonded and in the engagement length  $l_0$  eight strain gauges were placed.

Strain was measured by means of a strain-gauge fast scanner-equipped system with  $\pm 0.05 \mu\epsilon$  resolution.

At least twenty measurements were carried out for each strain gauge at each pressure point, the standard deviations ranging between  $\pm 0.05 \mu\epsilon$  and  $\pm 0.5 \mu\epsilon$ ; that is well within 5% at each measurement point and at each pressure value.

The temperature was measured inside the cylinder within an uncertainty of  $\pm 0.05 \text{ }^\circ\text{C}$  and the relevant corrections to the strain-gauge signals were applied ( $0.29 \mu\epsilon/^\circ\text{C}$ , which is the apparent strain between  $20 \text{ }^\circ\text{C}$  and  $21 \text{ }^\circ\text{C}$  of the strain gauges used).

The uncertainty in the measured displacements  $U_r$  of the outer cylinder surface is  $\pm 6\%$  which was calculated as the linear sum of the contribution due to calibration of the instrumentation, measurement repeatability, and the effect of the uncertainty in the temperature measurements.

Fig. 2 illustrates the behaviour of displacement  $U_r = r \epsilon_\theta$  on the external cylinder surface as a function of the engagement length at pressures of 47.5 MPa and 97.5 MPa. Displacement magnitude and behaviour are similar to those reported by Bean /4/ for a 25 MPa capacity piston gauge, but no substantial discontinuity was observed in the data reported here.

The tungsten carbide used for the piston and cylinder was of class ISO-K20 (6% cobalt content). Young's modulus was measured with an uncertainty of  $\pm 1\%$  on a specimen of this material by means of Tuckermann optical strain gauges.

Poisson's ratio was measured with  $3 \cdot 10^{-3}$  uncertainty by means of strain gauges in a compression test to 100 kN.

The effective area of the piston-cylinder unit,  $A_0$  ( $P_{atm}$ ,  $20 \text{ }^\circ\text{C}$ ) was determined by comparison with an IMGC piston gauge to 10 MPa; a value equal to  $0.199997 \text{ cm}^2$  (uncertainty  $\pm 27 \text{ ppm}$ ) was obtained. The average clearance between the piston and the cylinder was determined from measurements of the fall rate of the piston. The piston gauge was compared with another 100 MPa piston gauge (IMGC-100) already employed in international comparisons /1/, to determine experimentally the value of  $\lambda$ .

The results of this comparison confirmed the value of  $A_0$  and allowed us to calculate  $\lambda_{exp} = 0.747 \cdot 10^{-6} \text{ MPa}^{-1}$ . The value of  $2\sigma/A_0$  of fitting  $A_e = f(P)$  based on the cross-floating results was equal to 6 ppm. The values of  $A_e$  are thus known with an uncertainty of  $\pm 66 \text{ ppm}$ , which depends largely on the inadequate accuracy of the old IMGC-100 piston gauge.

The roundness measurements made on the tungsten carbide piston and cylinder at

three different positions showed that the maximal roundness error can be stated to lie within  $\pm 0.06 \mu\text{m}$  for the cylinder and within  $\pm 0.08 \mu\text{m}$  for the piston.

### 3. THEORETICAL CALCULATIONS

The differential equations for a linear elastic solid of revolution in the cylindrical coordinates  $r$ ,  $\theta$ , and  $z$  (Fig. 1) are:

$$\left\{ \begin{array}{l} \frac{\delta\sigma_r}{\delta r} + \frac{\delta\tau_{rz}}{\delta z} + \frac{\sigma_r - \sigma_\theta}{r} = 0 \\ \frac{\delta\tau_{rz}}{\delta r} + \frac{\delta\sigma_z}{\delta z} + \frac{\tau_{rz}}{r} = 0 \\ (1 + \nu)(\sigma_r - \sigma_\theta) - r \frac{\delta\sigma_\theta}{\delta r} + \nu \cdot r \left( \frac{\delta\sigma_r}{\delta r} + \frac{\delta\sigma_z}{\delta r} \right) = 0 \\ \frac{\delta\sigma_z}{\delta r} - \nu \left( \frac{\delta\sigma_r}{\delta r} + \frac{\delta\sigma_\theta}{\delta r} \right) - 2(1+\nu) \frac{\delta\tau_{rz}}{\delta z} + r \frac{\delta^2\sigma_\theta}{\delta z^2} - \nu \cdot r \left( \frac{\delta^2\sigma_r}{\delta z^2} + \frac{\delta^2\sigma_z}{\delta z^2} \right) = 0 \end{array} \right. \quad (1)$$

The first two equations express the equilibrium of the stress state and the last two the compatibility of the strain state.

In these equations  $\nu$  denotes Poisson's ratio and components  $\sigma$  and  $\tau$  have their usual well-known meanings and refer to variables  $r$ ,  $\theta$ , and  $z$ . It must be remarked that Young's modulus,  $E$ , which will strongly affect the strain calculation, does not appear in these equations.

The equations are applicable both to the piston (by multiplying the first two equations by  $r$ , the singularity for  $r = 0$  is avoided) and to the cylinder. With the method adopted to solve the equation system (1), each of the four unknown functions ( $\sigma_r$ ,  $\sigma_\theta$ ,  $\sigma_z$ ,  $\tau_{rz}$ ) is expressed in a double series of Tschebyschef's orthogonal polynomials.

It is therefore necessary to obtain a linear transformation of variables, such that the integration domain lies between  $-1$  and  $+1$ .

One then puts:

$$\left\{ \begin{array}{l} u = K_1 \cdot r + K_2 \\ v = h_1 \cdot z + h_2 \end{array} \right. \quad \begin{array}{l} K_1 = \frac{2}{r_e - r_i} \\ h_1 = \frac{2}{l_0} \end{array} \quad \begin{array}{l} K_2 = -\frac{r_e + r_i}{r_e - r_i} \\ h_2 = -1 \end{array} \quad (2)$$

where  $l_0$  is the engagement length of the piston-cylinder unit in the working position,  $r_i$  and  $r_e$  are the internal and external cylinder radii, respectively (for the piston,  $r_i = 0$  and  $r_e$  is its radius).

By denoting by  $T_{i-1}$  the Tschebyschef's polynomial of order  $i-1$ , the four unknown functions can be expressed in the following form:

$$\left\{ \begin{array}{l} \sigma_r(u, v) = \sum_{i=1}^{MU} \sum_{j=1}^{MV} a_{ij} T_{i-1}(u) \cdot T_{j-1}(v) \\ \sigma_\theta(u, v) = \sum_{i=1}^{MU} \sum_{j=1}^{MV} b_{ij} T_{i-1}(u) \cdot T_{j-1}(v) \\ \sigma_z(u, v) = \sum_{i=1}^{MU} \sum_{j=1}^{MV} c_{ij} T_{i-1}(u) \cdot T_{j-1}(v) \\ \tau_{rz}(u, v) = \sum_{i=1}^{MU} \sum_{j=1}^{MV} d_{ij} T_{i-1}(u) \cdot T_{j-1}(v) \end{array} \right. \quad (3)$$

By substitution of eqs. (3) into eq. (1) which have been suitably modified according to eq. (2), a system is thus established of  $4 \cdot MU \cdot MV$  equations, which are algebraically linear and homogeneous with respect to unknowns  $a_{ij}$ ,  $b_{ij}$ ,  $c_{ij}$ , and  $d_{ij}$  ( $MU$  and  $MV$  being the maximal polynomial order with respect to  $u$  and  $v$ ). The following boundary conditions are associated with eqs. (3):

		<u>Piston</u>	<u>Cylinder</u>
$r = r_i$	$u = -1$	/	$\left\{ \begin{array}{l} \sigma_r = -p(z) \\ \tau_{rz} = 0 \end{array} \right.$
$r = r_e$	$u = +1$	$\left\{ \begin{array}{l} \sigma_r = -p(z) \\ \tau_{rz} = 0 \end{array} \right.$	$\left\{ \begin{array}{l} \sigma_r = 0 \\ \tau_{rz} = 0 \end{array} \right.$
$z = 0$	$v = -1$	$\left\{ \begin{array}{l} \sigma_z = -P_0 \\ \tau_{rz} = 0 \end{array} \right.$	$\left\{ \begin{array}{l} \sigma_z = 0 \\ \tau_{rz} = 0 \end{array} \right.$
$z = l_0$	$v = +1$		

From these conditions it is possible to obtain one, and only one, solution of the elasticity problem and to derive the  $a_{ij}$ ,  $b_{ij}$ ,  $c_{ij}$  and  $d_{ij}$  coefficients by which, through eqs. (3), the stress state for the piston and the cylinder can be known.

With  $\sigma_r$ ,  $\sigma_\theta$ ,  $\sigma_z$ , and  $\tau_{rz}$  being known, strains ( $\epsilon_r$ ,  $\epsilon_\theta$ ,  $\epsilon_z$ , and  $\gamma_{rz}$ ) and the main displacements ( $u_r = r\epsilon_\theta$ ) can be obtained. For the calculation of the pressure distribution inside the clearance, one has to start from the Navier-Stokes equation, account being taken of fluid compressibility and, iteratively, of variations of clearance  $h = f(z)$  caused by elastic distortions.

$$p(z) - p_1 = K \int_{z_1}^z \frac{\eta_0(p)}{\rho(p)} \cdot \frac{1}{h^3(z)} dz \quad K = \frac{dm}{dt} \cdot \frac{6}{\pi \cdot r} = \text{const.} \quad (4)$$

is then obtained.

In the specific case in question,  $P_1 = P_0$  which is the pressure at  $Z = Z_1$  and  $z_1$  denotes the beginning of piston engagement length.

Eq. (4) is an integral equation that can be solved by applying the Peano-Picard method of successive approximations. Let a linear pressure distribution be assumed for the first iteration, namely:

$$\left\{ \begin{array}{l} p(z) = p_1 + \frac{P_2 - P_1}{z_2 - z_1} (z - z_1) \\ K = \frac{P_2 - P_1}{\int_{z_1}^{z_2} \frac{\eta_0(p)}{\rho(p)} \cdot \frac{1}{h^3(z)} dz} \end{array} \right. \quad (5)$$

For all subsequent iterations, let us take the value of the function  $P(z)$  defined by eq. (4), using the preceding iteration obtained by the use of equation (5).

The iterative process is developed in a number of stages:

- a) the deformations and displacements of the piston and the cylinder are calculated on the assumption of a constant clearance and linearly-distributed pressure;
- b) the deformation and displacement data obtained at stage a) are entered in the program for the calculation of the pressure distribution; a new pressure distribution is then obtained;

c) the elastic deformations and displacements are re-calculated on the basis of the pressure distribution obtained at the preceding stage.

The process is continued in this way until solution convergence for both the deformation and the pressure distribution is obtained.

Fortran IV is used in all calculation program, which can be run on a computer of at least 4 Mbyte. The program for the deformation calculation may be very slow. It may take from some tens of minutes to several hours depending on the model of the piston-cylinder unit and, especially, on the density of the data defining the geometry of the unit from which calculation has been begun.

#### 4. PRELIMINARY RESULTS

Fig. 2 compares the experimentally obtained displacement values  $U_r = r \cdot \epsilon_\theta$  on the outer cylinder surface with those calculated according to the method described in the preceding section. The agreement between these values in the piston-cylinder engagement length is within  $\pm 6\%$ .

Fig. 3 illustrates the displacements of the piston surface and of the internal cylinder surface; Fig. 4 shows pressure distribution in the clearance. The illustrated data are those obtained by means of application of all the calculations and procedures indicated in section 3. With the data in Figs. 3 and 4 it is possible to calculate  $\lambda_{\text{theor}}$  of the investigated piston-cylinder unit by means of the well-known formula /2/:

$$\lambda_{\text{theor}} = \frac{1}{2h} \left[ \frac{U(o)+u(o)}{r \cdot P_o} + \frac{1}{r \cdot P_o^2} \int_0^{l_0} P(x) \left( \frac{dU}{dx} + \frac{du}{dx} \right) dx \right] \quad (6)$$

A value of  $\lambda_{\text{theor}}$  equal to  $0.741 \cdot 10^{-6} \text{ MPa}^{-1}$  is obtained.

#### 5. CONCLUSIONS

5.1 The above value of  $\lambda_{\text{theor}}$  agrees to within 0.8% with the value of  $\lambda_{\text{exp}}$  obtained from cross-floating (see section 2). This, as it is, cannot be considered a satisfactory result, since  $\lambda_{\text{exp}}$  is determined with a too large uncertainty.

5.2 The Navier-Stokes equation used has iteratively taken account of the distortions of the piston and the cylinder. This procedure reflects the

desire of considering the clearance modification in the piston-cylinder unit according to distortion variations and to change in pressure distribution.

- 5.3 The calculations demonstrate the necessity of taking due account of the geometry of the piston-cylinder unit, especially of profile and roundness.
- 5.4 The physical behaviour of distortion is highly dependent on piston-cylinder geometry. A variation of, for instance,  $\pm 0.1 \mu\text{m}$  (a value close to the accuracy of dimensional measurements) in input model data is sufficient to produce substantial differences in the determination of the deformation and the pressure distribution in the clearance.
- 5.5 It is difficult to estimate the accuracy with which  $\lambda$  can be calculated with the method adopted. Tests will be continued on other piston-cylinder units, also of different materials. It will then be possible to compare the ratio of the coefficients of the elastic deformation calculated by means of this method with the ratio that will be obtained experimentally from cross-floating of two piston gauges.
- 5.6 It is hoped that studies of piston-cylinder distortion may become a matter of cooperation with other metrological organisations so that the same effects may be evaluated with different methods and results may be compared.

#### REFERENCES

- /1/ J.C. Legras et al, Metrologia, 25, 21-28 (1988)
- /2/ R.S. Dadson et al, Metrologia, 1, 55-68 (1965)
- /3/ B.E. Welch, V.E. Bean, Rev. Sci. Instr. 55 (1984), 1901-1909
- /4/ V. Bean, Physica 139 & 140B, 739-742, (1986)
- /5/ R. Lazos-Martinez, V. Bean, Physica 139 & 140B (1986) 785-787
- /6/ G. Klingenberg, Metrologia, 22, 259-263 (1986)
- /7/ G. Klingenberg, Metrologia, 24, 89-95 (1987)

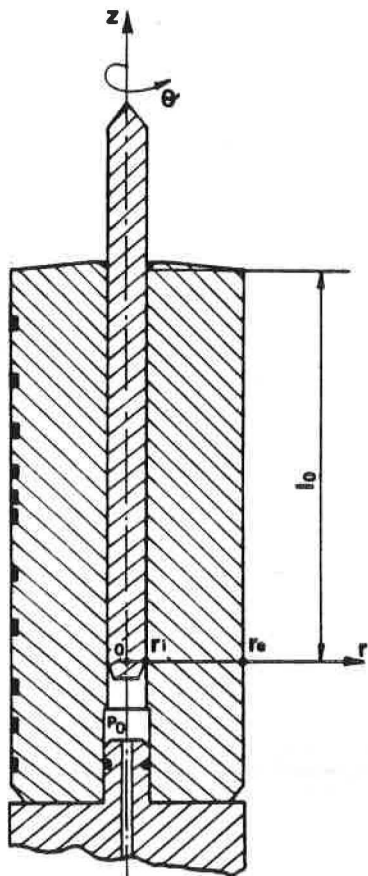


Fig. 1 100 MPa piston-cylinder unit. The black rectangle at the left indicate the locations of the strain gages.

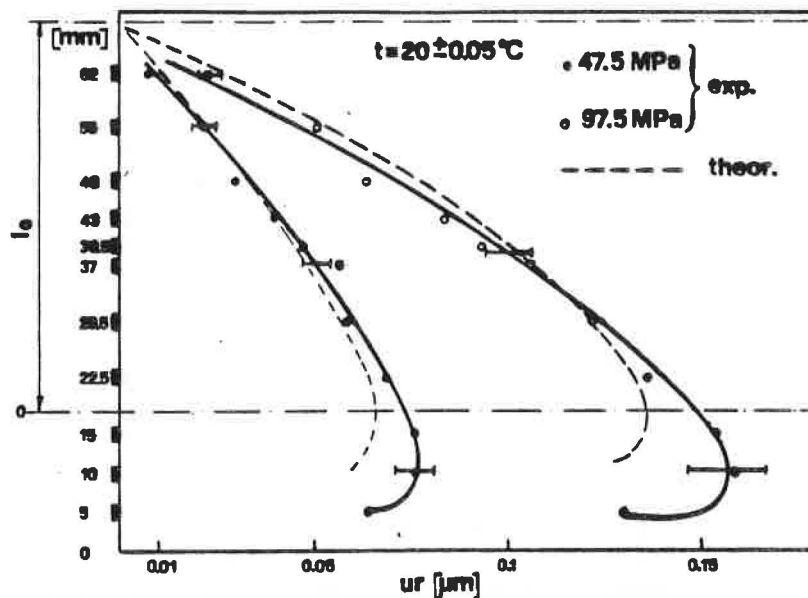


Fig. 2 Radial displacements on the outer cylinder surface in the coupling zone of the piston-cylinder unit at two pressure levels.

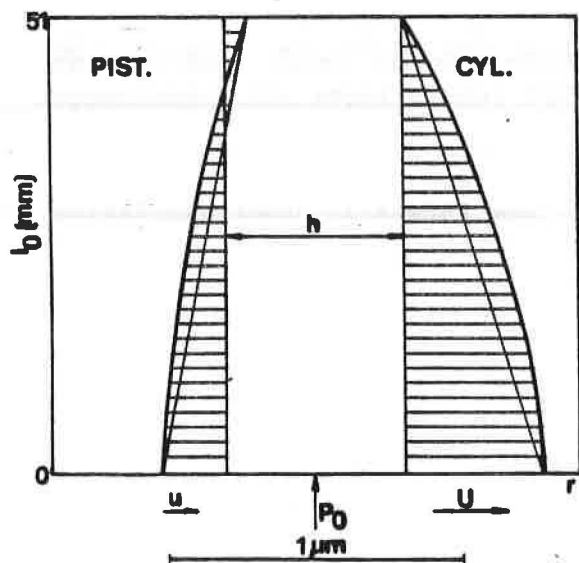


Fig. 3 Radial displacement in the piston and the cylinder at 97.5 MPa

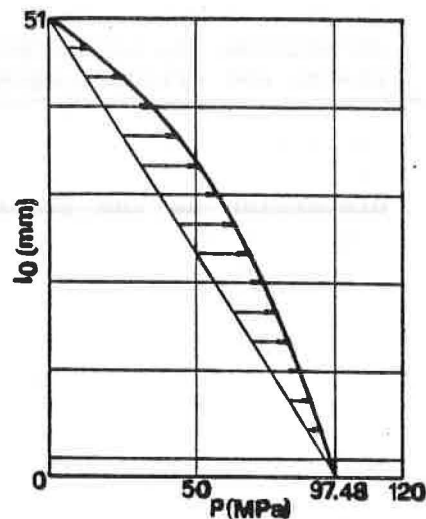


Fig. 4 Pressure distribution in the clearance with  $P_0 = 97.5$  MPa

A Capacitance Method of Measuring the Radial Displacement of  
the Outer Diameter of the Cylinder of a Piston Gage

Vern E. Bean  
National Institute of Standards and Technology  
Center for Basic Standards  
Gaithersburg, Maryland 20899

and

Yaw-Poo Lin  
Chung Shan Institute of Science and Technology  
Lung-tan, Taiwan

*Theoretical calculations of the distortion coefficients for piston gages require experimental verification in order to establish a basis for error analysis. We have developed a three-terminal capacitance method for measuring the radial displacement of the outer radius of the cylinder of a piston gage as a function of pressure to test such calculations. The measurements are repeatable at the nanometer level.*

The piston gage, also known as the pressure balance, dead weight tester, and piston manometer, is a fundamental pressure measurement instrument. The essential features of the device are a cylinder which is closed at the bottom with appropriate seals and plumbing connections to a pressure generating system and closed at the top with a close-fitting piston floating in the pressurizing fluid at the specified reference level. The piston is loaded with known weights and rotated to relieve friction and assure concentricity. The pressure is then determined as the ratio of the force to the effective area of the piston and cylinder assembly.

The leading cause of uncertainty in these pressure measurements is the lack of knowledge of how the effective area changes due to elastic distortion as the pressure increases. The generally used expression for calculating  $b$ , the distortion coefficient for the area, is based on elastic theory and is [1, 2]

$$b = \left[ \frac{\nu}{E} + \frac{P_a}{PE}(\nu-1) \right] + \left[ \frac{P_a}{P} \frac{(1+\nu)\omega^2 + (1-\nu)}{E(\omega^2-1)} \right]$$

where the first bracketed term is the contribution of the piston and the second is due to the cylinder,  $\nu$  is Poisson's ratio,  $E$  is Young's modulus,  $P_a$  is the pressure in the annular space between the piston and cylinder,  $P$  is the pressure under the piston, and  $\omega$  is the ratio of the cylinder's outer diameter to its inner diameter. This expression is for a right circular cylinder, free of end loading or external pressure, and a solid piston.

Two assumptions upon which Eq. 1 is based are:

- 1) The pressure is uniform over the entire length of the cylinder.

- 2) There are no shear stresses between planes through the cylinder normal to the cylindrical axis.

Both of these assumptions are invalid for a piston gage. Direct measurements of the pressure profile in the annular space between the piston and cylinder have shown that the pressure falls from essentially  $P$  to zero within a few millimeters [2]. Clearly, the relatively abrupt decrease in pressure will result in shear stresses of the sort assumed not to exist.

In an earlier paper [3], we reported our progress in developing a more rigorous method to calculate the elastic distortion in order to test the accuracy of Eq. 1 and to develop a basis for error analysis. The approach was to determine the radial displacement,  $u$ , for both the piston and cylinder separately from the expression [4]

$$u = - \frac{1}{2G} \frac{\partial^2 \Psi}{\partial r \partial z} \quad (2)$$

where  $G$  is the bulk modulus,  $r$  is the radial coordinate,  $z$  is the axial coordinate, and  $\Psi$  is the potential function which satisfies the biharmonic equation

$$\nabla^4 \Psi = 0 \quad (3)$$

and the appropriate boundary conditions, including the pressure profile in the annulus. The pressure profile for an oil-operated piston gage can be accurately calculated from dimensional measurements of the clearance between the piston and the cylinder as a function of piston working length [2].

In addition to providing the radial displacement of the cylinder bore and the piston, the approach also provides the radial displacement of the cylinder outer radius, which since it can be measured, affords an opportunity for experimental verification of the method.

Herein we report on the method we have developed to measure the changes in cylinder outer radius as a function of pressure.

The apparatus is shown in Fig. 1. The piston and cylinder are mounted between fixed steel surfaces such that the piston is held at its reference level as the cylinder is pressurized. The piston is not rotated. The change in cylinder outer radius upon pressurization is measured using a three-terminal capacitance technique. The sensor is mounted on a micrometer head (not shown in Fig. 1) so that the sensor can be located anywhere along the cylinder. Capacitance measurements are made by an automated bridge with the oscillator connected to the cylinder, the detector connected to the center electrode of the sensor, and the guard connected to ground.

The capacitance,  $C$ , of a concentric cylindrical capacitor is

$$C = \frac{2\pi \epsilon_0 Lk}{\ln(r_1/r_2)} = \frac{K}{\ln(r_1/r_2)} \quad (4)$$

where  $\epsilon_0$  is the permittivity of free space;  $L$  is the effective height of the center electrode, 0.3 mm;  $k$  is the dielectric constant of the air between the cylinder and the center electrode;  $r_1$  is the inner

radius of the center electrode; and  $r_2$  is the outer radius of the cylinder. All the terms in the numerator are constants whose product we set equal to  $K$ . Solving for  $r_2$ , we obtain

$$r_2 = r_1 e^{-K/C} \quad (5)$$

The radial displacement resulting from increasing the pressure from zero to  $P$  is

$$u = r_2(P) - r_2(0) = r_1 [e^{-K/C(P)} - e^{-K/C(0)}] \quad (6)$$

The measured value of  $u$  is an inherent average around the circumference of the cylinder and over a vertical distance of 0.3 mm.

The technique is to measure the capacitance at zero pressure, increase the pressure to the desired value and remeasure the capacitance, and then reduce the pressure to zero and again measure the capacitance. This cycle is done in a few seconds so that it is complete before the cylinder has time to respond to the heat generated by the compression of the pressurizing fluid, thus effectively separating elastic and thermal effects.

Radial displacement values derived from repeated measurements under the same conditions rarely differ by more than one percent. The clearance between the center electrode and the cylinder is on the order of 20  $\mu\text{m}$ , which is so small compared to the cylinder diameter that errors due to a lack of concentricity are negligible.

Radial displacement values obtained at 14, 17.5, 21, and 24.5 Ma are plotted in Fig. 2 relative to their location with respect to the piston and cylinder. They are spaced at 0.6 mm intervals. These measurements will be compared with the theory when the dimensional measurements needed to calculate the pressure profile are finished.

As it now stands, the net result of the measurements and the theoretical calculations will be an expression for the distortion coefficient as a function of cylinder length that will vary much like the data plotted in Fig. 2. What is needed is an experimentally justifiable method of selecting a constant value for the coefficient to be used in the calculation of the effective area. A method that seems to have been successful in one case is to examine the slope of the pressure profile curve for an abrupt change (if indeed, one exists), identify the location among the piston working length where it occurs, and calculate the distortion coefficient at that location [2]. This, or any other method, will (of course) require experimental verification.

One practical application of the data of Fig. 2 in their present form is that they can be used to set the upper limit of the distortion coefficient.

#### REFERENCES

1. P. L. M. Heydemann and B. E. Welch, Experimental Thermodynamics, Volume II: Experimental Thermodynamics of Non-reacting Fluids,

edited by B. Le Neindre and B. Vodar (Butterworths, London, 1975), pp. 147-202.

2. B. E. Welch and V. E. Bean, *Rev. Sci. Instrum.* 55, 1901 (1984).

3. R. J. Lazos-Martinez and V. E. Bean, *Pysica* 139, 785 (1986).

4. A. E. H. Love, *A Treatise on the Mathematical Theory of Elasticity*, 4th ed. (Dover, New York, 1944), pp. 274-276.

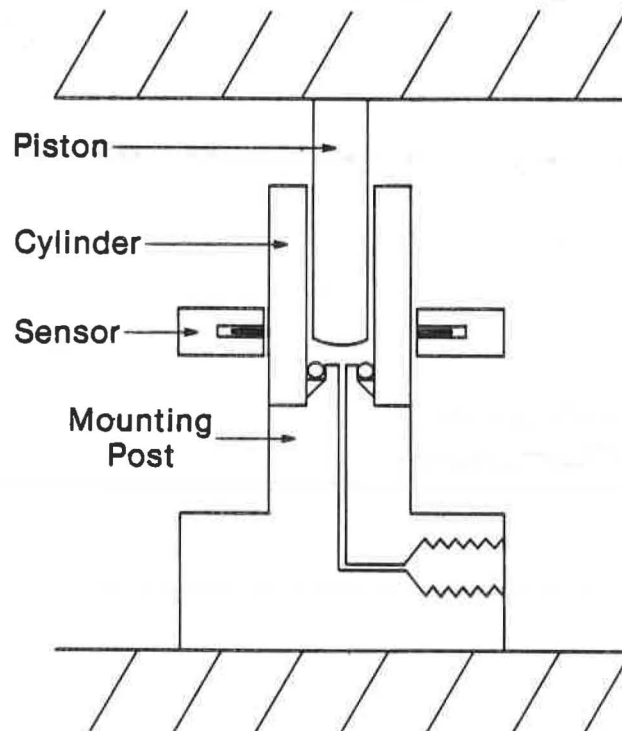


Figure 1. Piston and cylinder mounted between two fixed steel surfaces. The sensor is mounted on a micrometer head which is not shown.

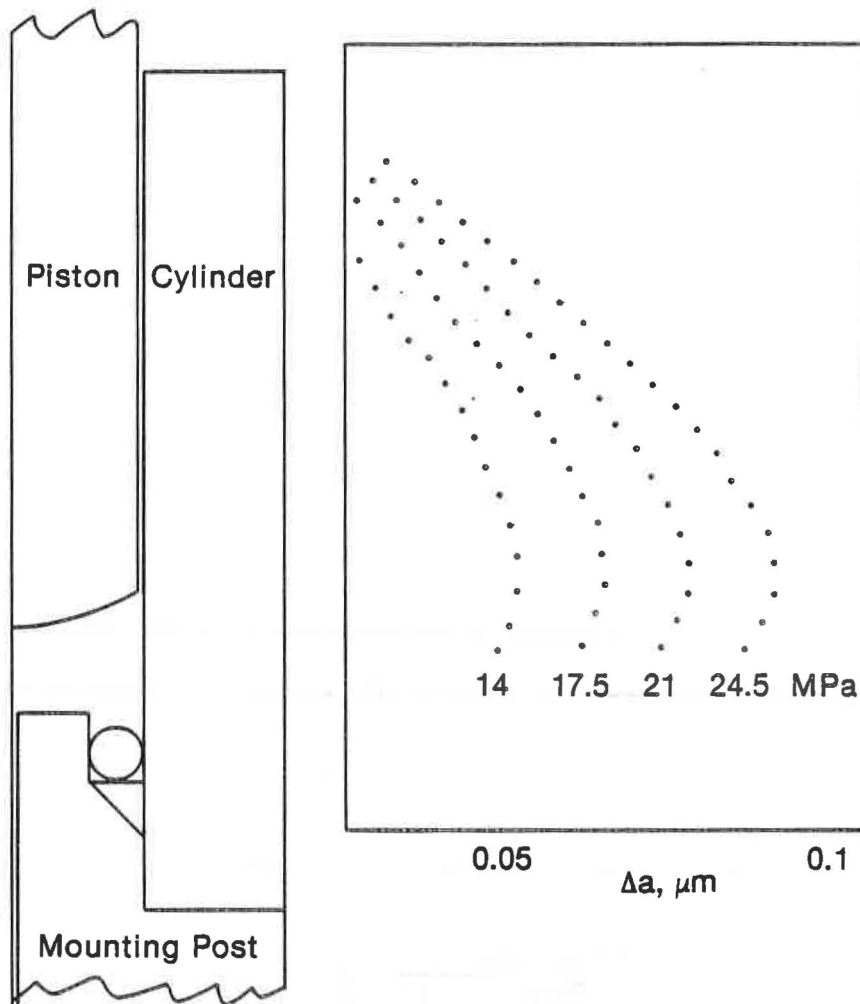


Figure 2. Radial displacement measurements of the cylinder outer radius relative to their location along the cylinder.

DETERMINATION OF THE PRESSURE COEFFICIENT OF THE EFFECTIVE AREA  
OF A SIMPLE 0.3 GPa DEADWEIGHT MANOMETER BY MEANS OF  
THE FINITE ELEMENT METHOD OF STRAIN CALCULATION

by

R.WISNIEWSKI, R.SENDYS, D.WISNIEWSKI and A.J.ROSTOCKI

Institute of Physics,  
Warsaw University of Technology  
00-662 Warszawa, ul.Koszykowa 75,  
WARSAW, POLAND

(Research sponsored by the Government Research Coordination  
Office under the Project CPBR-02.20 )

ABSTRACT

This paper is concerned with an attempt to increase the accuracy of a high pressure piston gauge with the guide piston . The aim of these efforts was to improve the metrological class of accuracy of an industrial model of pressure balance claimed by the maker to be 0.2%. It was assumed by the authors that the existance of "the guide piston" ,the low accuracy of the basic measurements of piston cylinder assembly parameters, and very approximate methods of calculation of effective area were the reasons for the low accuracy of that gauge. To eliminate the above sources of errors the authors have considered a model for the piston-cylinder assembly in which the changes of both piston and cylinder radii are calculated by the finite element method.

INTRODUCTION

Since 1972 the High Pressure Laboratory of the Institute of Physics has worked on the design and construction of pressure standards as well as on the improvment of standards currently manufactured in Poland. One of the prototypes manufactured in the specialised factory was the subject of several modifications done in our laboratory and also was used for testing various versions of piston cylinder assemblies designed by the authors. The initial class of accuracy was specified by the manufacturer as 0.2% . One of the reasons for the low accuracy was the method of calculation of the effective area based on Zhokhovski's model. The analysis done by the authors has shown that even with simple piston cylinder assemblies much better accuracy, up to 0.05% can be approached , although it requires the pressure dependence of effective area be calculated using more advanced models than the well known Zhokhowski model.

CALCULATIONS

The subject of the calculations, a simple piston gauge with a rotating loads and so-called guide piston has been shown in fig.1 . The schematic cross section of the piston cylinder assembly is shown in fig.2 . For the calculations the following notation has been used:  $p_0$  - pressure in the chamber,  $h_0$  -initial value of the clearence,  $h(z)$  - clearence at a distance  $z$  from the piston end ,  $U(z)$  - radial deformation of cylinder,  $u(z)$  - radial deformation of piston,  $\lambda$  - pressure coefficient of effective area ,  $\rho$  - current radius. The initial effective area

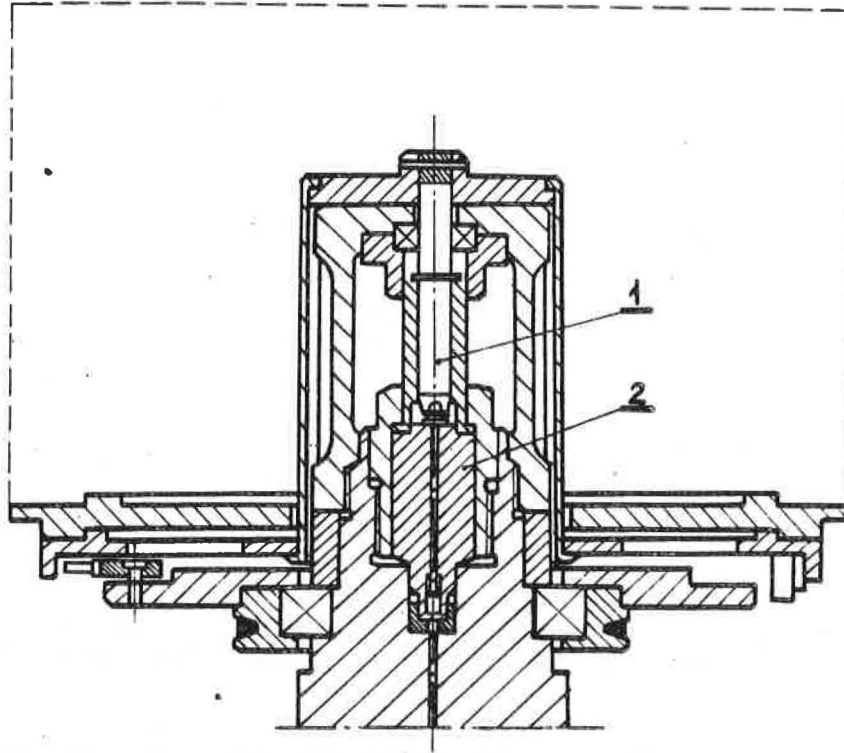


Fig.1. Diagram of deadweight piston gauge for pressures up to 300 MPa. 1 - "dead weight axis", 2 - p-c assembly.

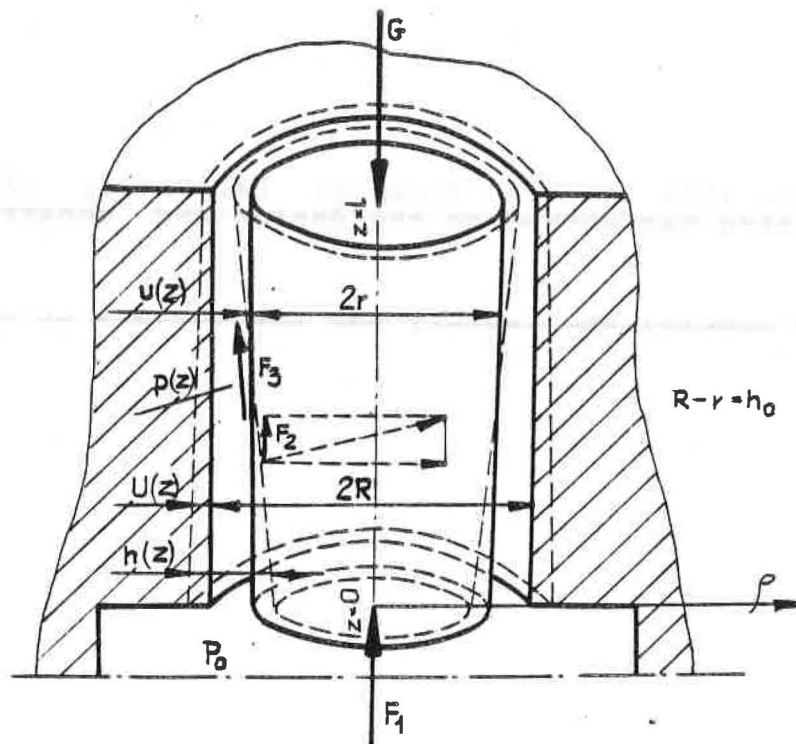


Fig.2. Diagram illustrating the piston-cylinder assembly of the pressure gauge.

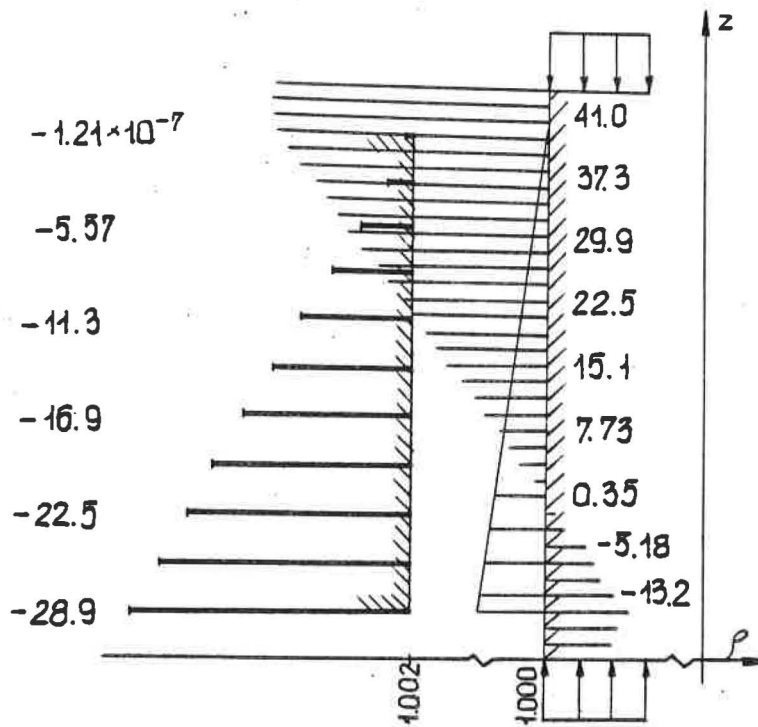


Fig.3. Radial increments of piston and cylinder assuming linear drop of pressure in the clearance.

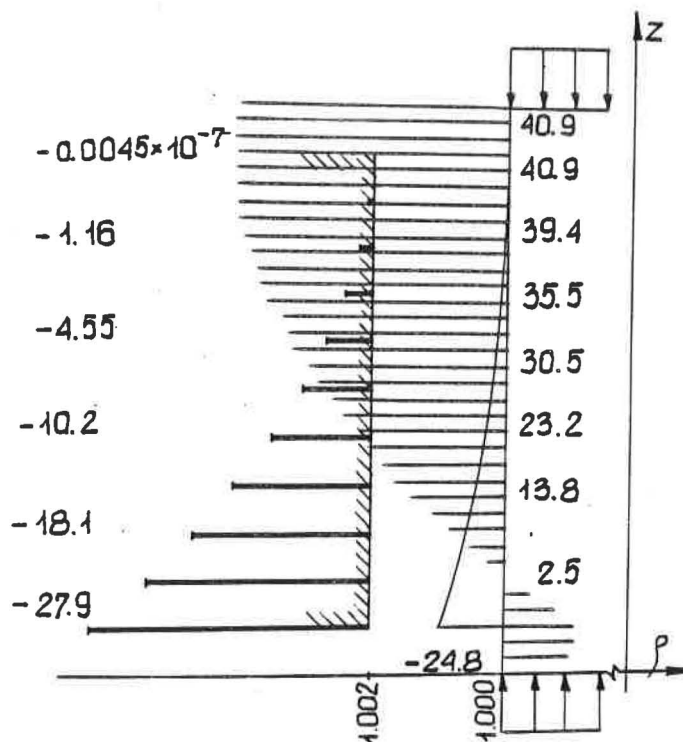


Fig.4. Radial increments of piston and cylinder assuming parabolic drop of pressure in the clearance.

was calculated from the formula:

$$A_{\text{oeff}} = \pi r^2 \left( 1 + \frac{h_0}{r_0} \right) \quad (1)$$

The dependence of effective area on pressure was numerically determined from the formula:

$$A_{\text{eff}}(p) = A_{\text{oeff}} \left[ 1 + \frac{U(a)+u(a)}{r} + \frac{1}{\pi P_0} \int_0^l P \left( \frac{dU}{dz} + \frac{du}{dz} \right) dz \right] \quad (2)$$

(notations as in fig.2).

The values of  $U(z)$  and  $u(z)$  were determined by the finite element method assuming both linear and parabolic decrease of pressure in the clearance. The results of calculations are shown graphically in figures 3 and 4.

Using the standard form for the expression for  $A$  as a function of pressure:

$$A_{\text{eff}}(p) = A_{\text{oeff}} ( 1 + \lambda P_0 ) \quad (3)$$

We calculated:

$$\lambda_{\text{lin}} = 2.5 \times 10^{-6} \text{ MPa}$$

$$\lambda_{\text{par}} = 2.8 \times 10^{-6} \text{ MPa}$$

In our calculation, we have assumed the following constant values: Young's Modulus =  $2.05 \times 10^5$  MPa, Poisson ratio  $\nu = 0.28$ , piston radius  $r_0 = 1.000$  mm, cylinder radius  $r = 1.002$  mm, cylinder outside radius  $R = 10$  mm, cylinder height  $l = 30$  mm. The values of the pressure coefficient of the effective area  $\lambda$  obtained by the authors are very close to the values presented in literature. For example R.S.Dadson [2] gives  $\lambda_{\text{teor}} = 2.95 \times 10^{-6}$  MPa,  $\lambda_{\text{exp}} = 3.00 \times 10^{-6}$  MPa for a very similar design of the piston-cylinder pressure gauge assembly.

#### CONCLUSIONS:

The obtained results it is:

- (1) calculation of the pressure coefficient with high reliability, and
  - (2) study of the influence of the dead weight axis upon the gauge error, which has been proved to be negligibly small in its unsystematic part and impossible to eliminate, allowed the increase of the pressure gauge accuracy to 0.05 %.
- It is worth noticing that the evaluated variation of  $U(z)$  and  $u(z)$  is similar to the assumed functions of  $p(z)$  in the gauge clearance. Thus it is possible to explain the good results of the calculations of deformation based on the "extremely untrue" assumptions that  $U \sim p$  and  $u \sim p$ , as presented for example by Zhokhovskii [1]. The result is also very close to the one obtained from the extremely simplified theory

#### REFERENCES

1. Zhokhovskii, M.K., Theory and computation of instruments with packless pistons, Standartgiz, Moscow, 1966
2. Dadson, R.S., The precise measurement of steady pressures, in High Pressure Measurement Techniques, ed. G.N.Peggs, Applied Science Publishers, London, 1983

THE INFLUENCE OF FLUID VISCOSITY ON THE DISTORTION OF  
PISTON-CYLINDER ASSEMBLIES IN PRESSURE BALANCES

P R STUART

National Physical Laboratory  
Teddington  
Middlesex TW11 OLW  
Great Britain

ABSTRACT

The paper commences with examples of how the viscosities of oils used in pressure balances increase with increasing applied pressure.

An iterative method is described for computing the pressure gradient in the oil along the gap between the piston and the cylinder in the absence of elastic distortion.

Examples show that for applied pressures below about 120 MPa the pressure gradient is essentially uniform and only slightly influenced by the choice of oil. For higher applied pressures the pressure gradient becomes very much more concentrated at the bottom, high pressure, end of the gap and will be much more dependent on the choice of oil.

It is concluded that a realistic calculation of the elastic distortion of pressure balance piston-cylinder assemblies at high applied pressures can be obtained only if the consequences of the dependence of viscosity on pressure are allowed for. An iterative approach with viscosity and elastic distortion calculations in alternation is proposed.

## 1 INTRODUCTION

Pressure balances, otherwise known as piston gauges or deadweight testers, are one of the most commonly used instruments for the accurate measurement of high pressures. The upward force due to pressure acting on the bottom of an accurately made piston in an accurately made cylinder is balanced by the gravitational force acting on the piston and on weights supported by it. In equilibrium, the relationship between the pressure  $P$  and the supported mass  $M$  is given by the equation:

$$P = \frac{M \cdot g}{A} \quad (1)$$

where  $g$  is the local acceleration due to gravity and  $A$  is the effective area of the piston-cylinder combination. In practice the effective area  $A$  generally increases as the applied pressure increases because the cylinder distorts more than the piston. The effective area  $A_p$  at an applied pressure  $P$  can usually be related to the effective area  $A_o$  at zero applied pressure by the linear equation:

$$A_p = A_o (1 + \lambda \cdot P) \quad (2)$$

where  $\lambda$  is known as the distortion coefficient or the pressure coefficient of area.  $\lambda$  is commonly calculated by stress analysis [1,2,3] or, less frequently, is determined by the "similarity method" [4,5].

In calculating the distortion by stress analysis several interdependent influences should be taken into account; the distortion depends not only on the shape and elastic properties of the piston and cylinder but also on the pressure distribution along the engagement length. The latter depends on the viscosity-pressure relationship of the working fluid and on the width of the annular gap which, in its turn, depends on the distortion.

Because of the complexity of the situation it is proposed that for pressures above about 100 MPa, where viscosity becomes very pressure dependent an iterative approach should be used, with calculations of pressure distribution and the resultant distortion being carried out in alternation until one arrives sufficiently close to a limiting value.

This paper concentrates on the steps involved in the calculation of the pressure distribution and assumes that the piston and cylinder are perfectly rigid and that the width of the annular gap is uniform along the whole engagement length. The equations for this special case are easily modified to take into account the subsequent steps in the procedure in which, because of elastic distortion, the gap is no longer uniform.

## 2 THE DEPENDENCE OF VISCOSITY ON PRESSURE

Since viscosity is very pressure dependent, the choice of an operating fluid for a pressure balance is a compromise between two conflicting requirements. The oil must be sufficiently viscous at low pressures for the leakage to be acceptably low to enable the pressure to be sustained but it must not become so viscous at the top of the pressure range that lubricating powers and balancing sensitivity are lost.

Measurements of viscosity at high pressures are usually made by determining the rate at which a close-fitting ball or slug falls through pressurised oil contained in a vertical tube [6-11]. The results obtained by different workers are not always in very good agreement, probably because viscosity is also very dependent on temperature and the experimental temperature conditions are not always strictly comparable. Nevertheless, the results all show the same general trend, which is illustrated in Figure 1.

Curve 1 is for a typical straight mineral oil of Viscosity Grade 15 (ISO 3448). Above about 150 MPa such oils tend to become waxy and can no longer be considered as fluids. Curve 2 is for di-2-ethyl hexyl sebacate, a synthetic ester of molecular weight 426 developed as a high temperature lubricant. Note that, although it remains fluid up to at least 800 MPa, its viscosity at this pressure is 1000 times greater than at 100 MPa.

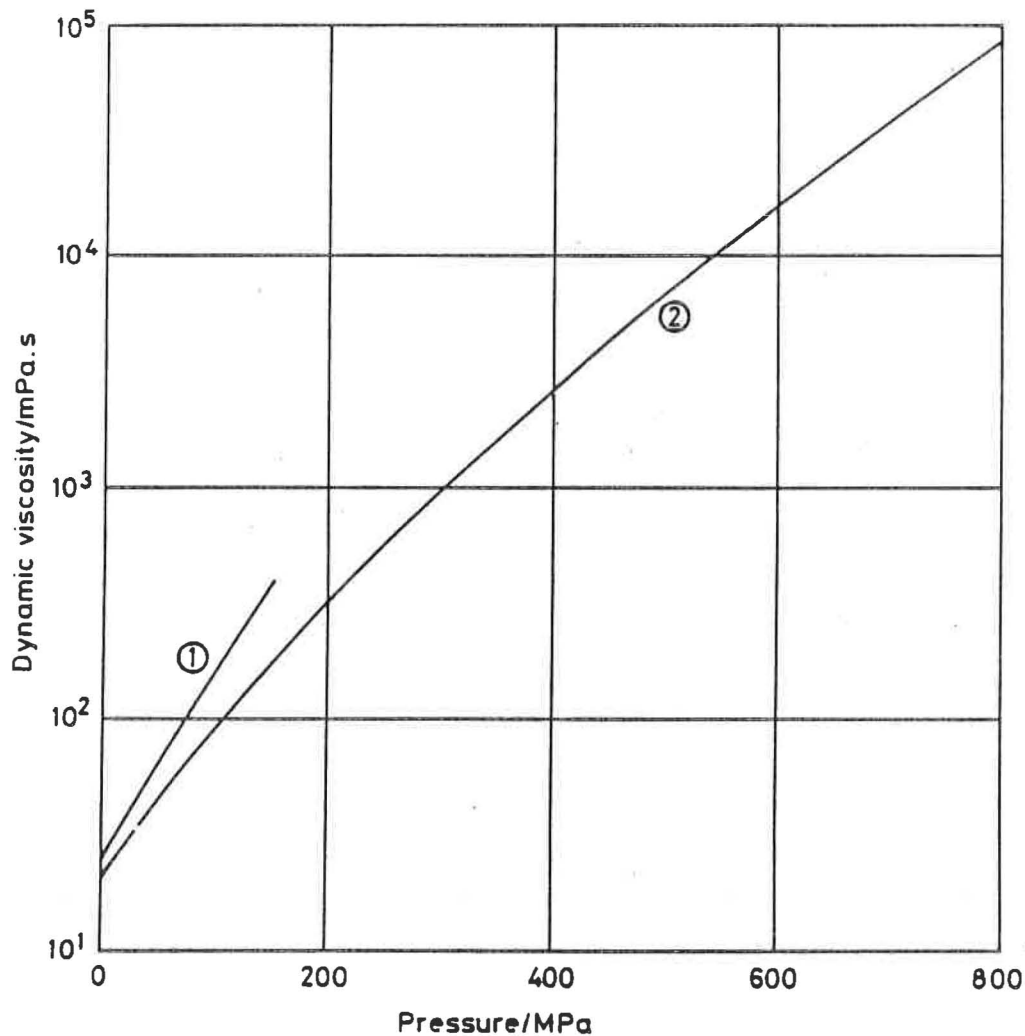


Figure 1 Calculated dependence of dynamic viscosity on pressure at 20 °C

Curve 1 Straight mineral oil:  $\eta_0 = 25.8 \text{ mPa.s}$ ,  $z = 0.67$

Curve 2 di-2-ethyl hexyl sebacate:  $\eta_0 = 21.1 \text{ mPa.s}$ ,  $z = 0.55$

The dependence of viscosity on pressure has been extensively discussed by Roelands [12], who found that the rapid increase in viscosity with increasing pressure can be represented reasonably well for most oils by the equation:

$$\log \eta + 1.200 = (\log \eta_0 + 1.200) \left(1 + \frac{P}{200}\right)^z \quad (3)$$

where:  $\eta$  is the coefficient of dynamic viscosity at pressure P  
 $\eta_0$  is the coefficient of dynamic viscosity at ambient pressure  
and  $z$  is a dimensionless quantity which is slightly temperature-dependent and differs from one oil to another.

In practice the viscosity of the fluid will be slightly modified due to the shear forces resulting from the rotation and fall of the piston and the upward flow of oil due to leakage. These are assumed to be relatively minor effects and are disregarded in the treatment that follows.

### 3 VISCOUS FLOW OF FLUID THROUGH AN ANNULAR GAP

Dadson [4] has shown that the rate of flow,  $F$ , of a fluid through the annular gap between a piston and cylinder may be expressed by the following relationship, which is readily derived from the basic equations for viscous flow:

$$F = \frac{P}{L} \cdot \frac{1}{\eta} \cdot \frac{Rt^3}{6} \quad (4)$$

where:  $P$  is the pressure difference between the ends of the gap  
 $L$  the length of the gap (the engagement length)  
 $\eta$  the coefficient of dynamic viscosity, assumed pressure independent  
 $R$  the mean of the radii of the piston and cylinder  
and  $t$  is the width of the gap between the piston and the cylinder.

Equation 4 may be re-written in the form

$$F = \frac{P}{L} \cdot \frac{1}{\eta} \cdot K \quad (5)$$

where  $K$  is constant for constant geometry.

If the engagement length is divided into a number of horizontal layers, equation 5 may be applied to each layer. Since  $F$  is constant along the whole length, the pressure developed across each layer will be proportional to the mean viscosity in that layer and the normalised pressure distribution along the whole engagement length will be independent of the actual magnitude of  $R$ ,  $t$  or  $L$ .

#### 4 ITERATIVE METHOD OF CALCULATING THE PRESSURE DISTRIBUTION

Figure 2 is a schematic representation of a piston-cylinder assembly.

To determine the pressure distribution along the engagement length by an iterative process, the parallel-sided annular gap is first divided into a number of layers,  $n$ , each of thickness  $dL$ . The number of layers will depend upon the accuracy required and upon the extent to which the viscosity varies with pressure. 100 layers are normally sufficient for an applied pressure of 100 MPa but at least 500 layers are necessary for an applied pressure of 800 MPa.

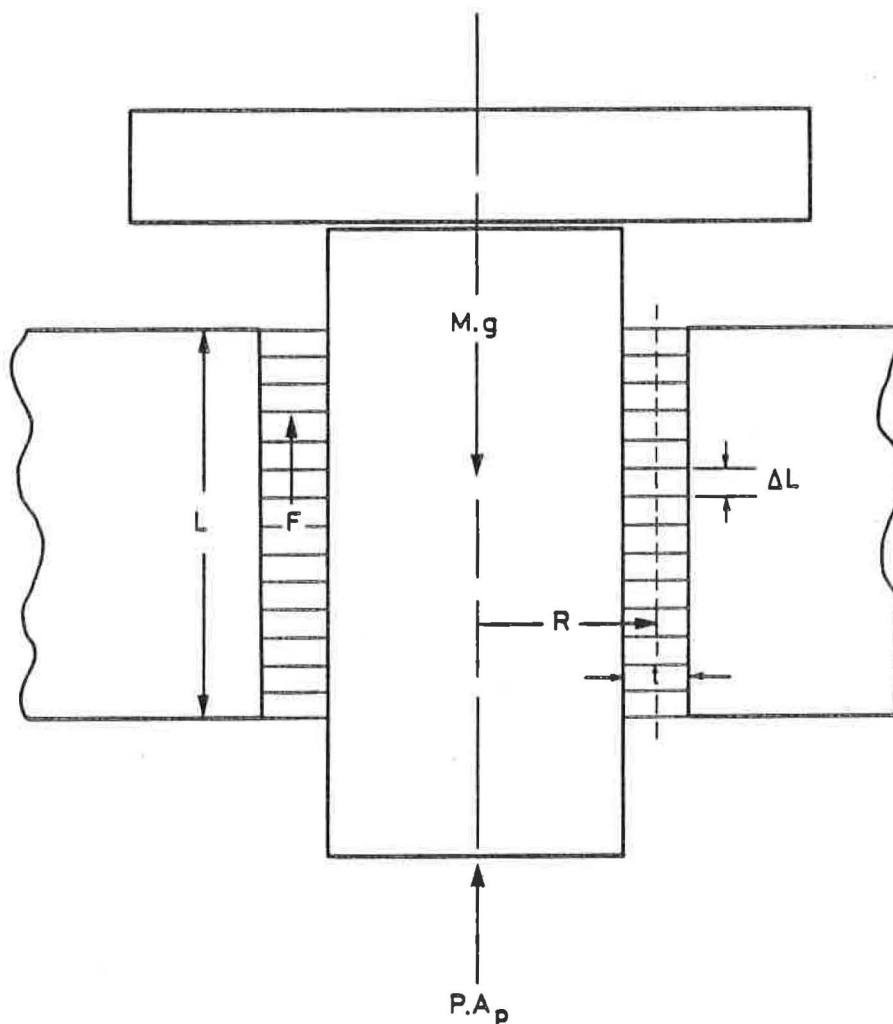


Figure 2 Schematic representation of piston-cylinder assembly, showing division of annular gap into layers for iterative calculation

The stages of the iterative processes are as follows:

1. Assuming a uniform pressure gradient along the whole engagement

length, calculate the pressure at the mid-plane of each layer.

2. Calculate the viscosity at the mid-plane of each layer, using the relationship given in Equation 3.
3. Calculate the pressure drop across each layer, in terms of  $F$ , using Equation 5.
4. Sum the pressure terms containing  $F$  for all the layers, equate to  $P$ , and hence determine  $F$ .
5. Substituting for  $F$ , determine the actual pressure drop across each layer.
6. From the cumulative totals of the pressure drops, determine the pressures at the centres of each layer.
7. Repeat stages 2 to 6 until the adjustments made become insignificant compared with the required accuracy. 100 iterations, which take only a few minutes on a microcomputer, should be quite sufficient for 100 layers but at least 1000 iterations are necessary for applied pressures of 800 MPa.

As in the case of the single layer considered in the previous section, the normalised pressure distribution is independent of the magnitude of  $R$ ,  $t$  or  $L$ , provided that  $t$  is constant along the whole engagement length.

## 5 RESULTS AND DISCUSSION

Figure 3 shows the pressure distribution along the engagement length calculated for 3 situations, all at 20 °C.

The following points should be noted:

- i) For 120 MPa applied pressure the pressure distributions are not far from linear.
- ii) For 120 MPa applied pressure there is only a slight difference between the pressure distributions in the mineral and synthetic

oils.

- iii) For 800 MPa applied pressure the pressure distribution is very far from linear. Over 90% of the pressure drop occurs in the bottom 10% of the engagement length. In the top 96% of the engagement length the pressure is actually less than is the case when the applied pressure is only 120 MPa.

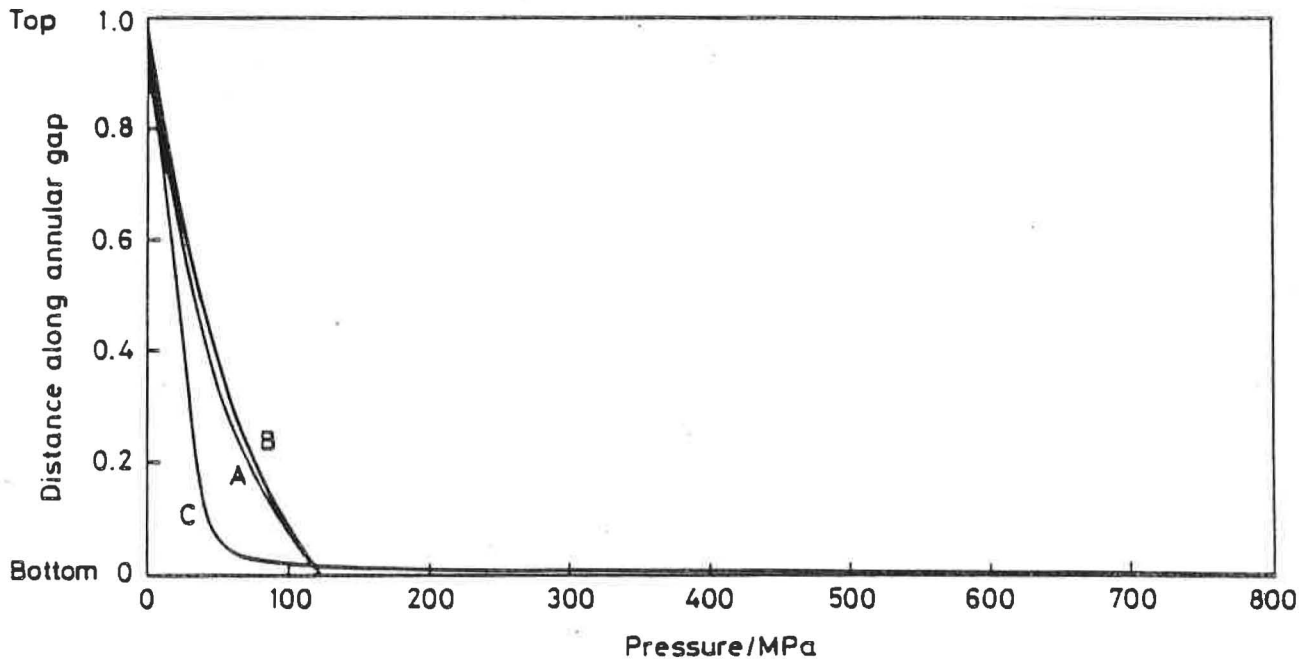


Figure 3 Variation of pressure along length of annular gap

Curve A A straight mineral oil of Viscosity Index 15 with an applied pressure of 120 MPa.  $\eta_0$  has been taken to be the measured value of 25.8 mPa.s and Z has been assumed to be 0.67.

Curve B di-2-ethyl hexyl sebacate with an applied pressure of 120 MPa.  $\eta_0$  has been taken to be measured value of 21.1 mPa.s and Z has been assumed to be 0.55

Curve C As in B above but with an applied pressure of 800 MPa.

## 6 CONCLUSIONS

The following conclusions may be drawn:

- a) The dependence of viscosity on pressure should not be overlooked when using stress analysis to calculate the dependence of effective area on pressure.
- b) Numerical analysis using finite elements is a suitable technique for calculating the consequences of the dependence of pressure on viscosity.
- c) Such analysis shows that for applied pressures below about 120 MPa the choice of oil is unlikely to have a great effect on the pressure distribution and therefore is unlikely to influence the distortion coefficient significantly.
- d) At pressures above about 120 MPa the pressure distribution along the annular gap is far from linear: the greatest pressure gradients are at the bottom end of the gap and the geometry of the cylinder in this region is therefore much more important than elsewhere in determining the distortion coefficient of the assembly as a whole.
- e) To allow for both elastic distortion and viscosity effects it will be necessary to use an iterative approach, performing both types of calculation in alternation.

## 7 REFERENCES

1. DADSON, R.S., LEWIS, Sylvia L. and PEGGS, G.N. The Pressure Balance. Theory and Practice. HMSO, London, 1982.
2. HEYDEMANN, P.L.M. and WELCH, B.E. Piston Gages. In: Experimental Thermodynamics Vol II. Eds: Le Neindre, B. and Vodar, B. Butterworths, London, 1975.
3. KLINGENBERG, G. Critical Remarks Concerning the Derivation of the Elastic Distortion Coefficient from Normally Used

Theory. See these proceedings.

4. DADSON, R.S., GREIG, R.G.P. and HORNER, Angela. Developments in the Accurate Measurement of High Pressures. *Metrologia* 1 55-68 (1965)
5. DADSON, R.S., LEWIS, Sylvia L. and PEGGS, G.N. *The Pressure Balance: Theory and Practice*. London, HMSO (1982)
6. BRADBURY, D., MARK, M. and KLEINSCHMIDT, R.V. Viscosity and Density of Lubricating Oils from 0 to 150,000 Psig and 32 to 425 F. *Trans. ASME* 73 667-676 (1951)
7. IRVING, J.B. and BARLOW, A.J. An Automatic High Pressure Viscometer. *J. Phys. E.* 4 232-236, 1971
8. ISDALE, J.D. and SPENCE, C.M. A Self-centering Falling Body Viscometer for High Pressures. UK National Engineering Laboratory Report No 592, 1975
9. SHARMA, J.K.N., JAIN, Kamlesh K., BEAN, V.E. and WELCH, B.E. Effects of Viscosity, Temperature and Rate of Rotation on Pressure Generated by a Controlled-clearance Piston Gauge. *Rev. Sci. Instrum.* 55 563-569 (1984)
10. BEAN, V.E., WOOD, Sarrill D. and LAZLOS, R.J. Pressure Dependence of Viscosity of Pressure Transmitting Fluids. *Mat. Res. Soc. Symp. Proc.* 22 Part III (High Pressure in Science and Technology) 289-293 (1984)
11. NISHIBATA, K. and IZUCHI, M. A Rolling Ball Viscometer for High Pressure Use. *Physica* 139 and 140B 903-906 (1986)
12. ROELANDS, C.J.A. Correlational Aspects of the Viscosity-Temperature-Pressure Relationship of Lubricating Oils. Doctorate Thesis, University of Delft, 1966.

PART 1

PISTON GAUGE

Sub-section: New developments and trends concerning piston-gauges  
or similar systems



**PISTON GAGES USED AS HIGH ACCURACY STANDARDS  
IN THE RANGE 0.01 - 1 000 MPa**

**J.C. LEGRAS - LABORATOIRE NATIONAL D'ESSAIS - PARIS -**

The pressure balances, the principle of which is an application of the definition of the unit of pressure, can be used as primary standard. To define the pressure from the fundamental units, it is necessary to determine the mass applied on the piston, the local gravity, and the effective area of the piston-cylinder unit.

L.N.E. and DESGRANGES et HUOT have worked since about 20 years to develop standards. These standards have been designed to optimize the accuracy of the effective area, that is to say its value at null pressure and the pressure distortion coefficient for the high pressure ranges.

The main methods used have been as follows :

- development of the machining of tungsten carbide to increase the quality of the geometry of the piston and the cylinder
- optimization of the measurement of the diameters of the piston-cylinder units
- use of the flow method on controlled-clearance type balances to measure the pressure distortion coefficient
- comparative methods to extrapolate the effective area to high pressure.

By this way, the typical accuracies have been estimated to be  $\pm 5$  ppm up to 1 MPa,  $\pm 7$  ppm at 10 MPa,  $\pm 18$  ppm at 200 MPa, and better than 100 ppm at 1 GPa (in development).

**PISTON GAGES USED AS HIGH ACCURACY STANDARDS  
IN THE RANGE 0.01 - 1 000 MPa**

**J.C. LEGRAS - LABORATOIRE NATIONAL D'ESSAIS - PARIS -**

Twenty years ago, the accuracy of the measurement of high pressures was about  $5 \cdot 10^{-4}$ . This was inadequate for industry, specially energy and military applications. The usual standard for the high pressures measurement is the pressure balance.

In such a standard, the pressure is applied on the lower surface of a piston which is vertically rotating in a cylinder. The pressure is equilibrated by the mass of weights subjected to the gravity and applied on the piston. The pressure is expressed as a function of the apparent mass  $m_a$  of the weights, the gravity  $g$  and the effective area  $A_e(p,t)$  of the piston-cylinder unit (that will be indicated below as "unit") :

$$p = m_a \times g / A_e(p,t) \quad (1)$$

To define a standard from this principle, it is necessary to measure the masses and the local gravity : an accuracy inside 1 ppm in this range is usual. It is more difficult to realize piston-cylinder units and to measure their effective area with an high level of accuracy. Since about 15 years, we have worked to increase the accuracy in the definition of the effective area of pressure balances.

So, the LNE has worked in close and fruitful collaboration with Desgranges et Huot to develop four levels of standards of simple piston type in the range 10 kPa to 1 GPa. All the works were supported by the BUREAU NATIONAL DE METROLOGIE (BNM).

The effective area of a pressure balance is expressed from the effective area  $A_0$  at null pressure and at a reference temperature (we use 20 °C) :

$$A_e = A_0 [1 + (\alpha_p + \alpha_c) (t - 20)] [1 + \lambda p] \quad (2)$$

where  $\alpha_p$  and  $\alpha_c$  are the linear thermal expansion coefficients of the materials of piston and cylinder ( $\alpha_p + \alpha_c$  is noted  $2\alpha$  when the material is the same for the two pieces)

$t$  is the temperature of the unit

$\lambda$  is the pressure distorsion coefficient of the unit.

It was demonstrated (in [1] for example) by the theory of the viscous flow that the effective radius  $R$  of the unit composed of a piston (radius  $R_0$ ) and a cylinder (internal radius  $R_1$ ) is :

$$R^2 = (R_1^2 - R_0^2) / 2 \ln (R_1 / R_0) \quad (3)$$

This formula is available for perfectly cylindrical pieces. By using  $R_1 = R_0 (1 + \epsilon)$  to define the radius of the cylinder, the effective area can be defined from the mean radius.

$$R = R_0 (1 + \epsilon/2) \quad (4)$$

It is easy to demonstrate that this relation is equivalent to the previous one. The error on the effective area due to this approximation is equal to  $(\pi \epsilon^2 / 12)$ .

So, it appeared that the conditions to realize a good reference of effective area were :

- to manufacture pieces of a very good shape (near perfect cylinder).
- to have a small clearance between the two pieces (measured by  $\epsilon$ ).
- to realize pieces as larger as possible to decrease the relative uncertainty of the measurement of the diameters (it will be seen that it is difficult to implement such measurements inside  $0.05 \mu\text{m}$ ).

In fact, pieces never are perfect. The measurement of the diameters of the pieces at different levels allows to determine the surface distortion ; then, the effective area  $A_0$  is calculated by integration of these distortions from well known equations [2,3].

To increase the range of the pressure balance by keeping low masses, it is necessary to decrease its effective area. Then the accuracy of the diameters measurements is decreasing. Comparative methods by crossfloating have been developed at LNE to measure an effective area from a reference unit.

This implies to have a sufficient common range of pressure where the sensitivity of the balances allows to determine the ratio of their effective areas with standard deviations inside 1 ppm. It is the reason why the ranges of our standards have been changed in time, by increasing the masses applied on the piston.

The effective area to determine is measured at the low part of its range ; it is calculated as a function of the pressure from the pressure measured by the reference balance by using the development of the expression (1). A numeric method or a differential method [4] are used to eliminate the zero effects in view to measure the effective area with the better accuracy.

For example, the following equation gives the effective area measured from two equilibria at the pressures  $P_1$  and  $(P_1 + P)$

$$A'_0 = A_0 \cdot \frac{\Delta m'}{\Delta m} \cdot \frac{1 + 2\alpha(t-20)}{1 + 2\alpha(t'-20)} \cdot \frac{1 + \lambda(\Delta p + 2p_1)}{1 + \lambda(\Delta p + 2p_1)} \quad (5)$$

where  $\Delta m$  and  $\Delta m'$  are the increments of masses ;  
the other notations have been defined in (2).

When the pressure increases, it is necessary to determine the pressure distortion coefficient for pressures up to 10 MPa,  $\lambda$  is calculated from the analysis of the strains applied to the material.

For higher pressures, the piston and the cylinder are bended. The notations are defined in Fig.1.

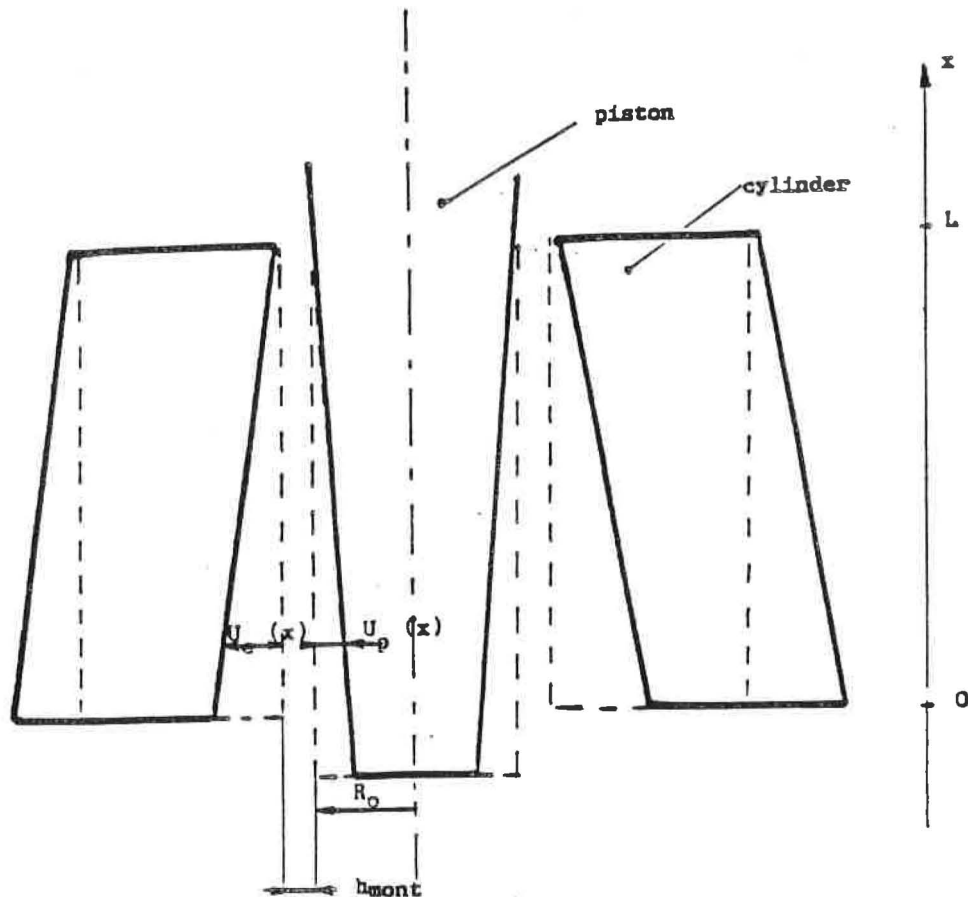


Fig. 1 - Distortions of a piston-cylinder unit -- Notations

The effective area is calculated from the analysis of all the forces applied to the piston [4].

$$A_p = \pi R_0^2 \left[ 1 + \frac{H_{mont}}{R_0} + \frac{U_p(o) + U_c(o)}{R_0} + \frac{1}{R_0 P} \int_0^P p(x) \left( \frac{dU_p}{dx} + \frac{dU_c}{dx} \right) dx \right] \quad (6)$$

By using the results of the materials resistance theory applied to a thick-wall cylinder the equation (5) becomes :

$$A_p = \pi R_0^2 \left[ 1 + \frac{P}{E} (3\mu - 1) + \frac{1}{R_0 P} \int_0^P H dp \right] \quad (7)$$

The radius  $R_0$  is determined at low pressure from an equation derived of (4)

$$A_0 = \pi R_0 (R_0 + H_{Mont}) \quad (8)$$

$A_0$  is measured at low pressure by comparison with a reference effective area from the equation (5).

The clearance at null pressure is measured by the flow method. The flow rate of the oil in the clearance is expressed from the viscosity of the oil, the gradient of pressure, and the clearance :

$$q(x) = -\pi R \frac{1}{\nu(x)} \frac{dp}{d(x)} \frac{H^3(x)}{6} \quad (9)$$

At low pressure where the clearance is considered as constant, it is easy to integrate this expression. The clearance is determined at a few low pressures by measurement of the flow rate and  $H_{Mont}$  is calculated by extrapolation to the null pressure.

The second term of the equation (7) is the distortion of the piston. It is due to the compression of the material due to the pressure. This term is calculated.

The third term is the mean clearance H between piston and cylinder. It is determined with a controlled clearance type balance : a jacket pressure is applied outside the cylinder and allows to change its distortions. The first method used at NBS [6] consists to extrapolate at null flow : the radius of the cylinder is then assumed to be the same that the radius of the piston. The method is difficult to use because at high jacket pressure it is opposite to a good operation of the unit by a concentration of the strains at the upper part of the cylinder.

At LNE, we use a method by variation of jacket pressure in the good operation zone of the unit : we combine the flow rate method with a comparative method to minimize the errors due to the theory.

The mean clearance is calculated from (9)

$$\bar{H} = - \left( \frac{6 R_0 D}{t} \right)^{1/3} \cdot \frac{1}{P} \cdot \int_0^P \left( \nu(x) \frac{d(x)}{dp} \right)^{1/3} dp \quad (10)$$

where D is the distance got down by the piston in the time t.

The standard is made up with two balances. The unit to study is compared with an other one for two jacket pressures. The variation of the effective area is measured by the variation of mass between the two equilibria :

$$A_1 - A_2 = mg / P \quad (11)$$

From (10) and (11) we easily calculate respectively the ratio and the difference of the mean clearances for the two jacket pressures, and then the clearance :

$$H_1 = \frac{mg}{P \pi R^2 [1 - t_1 / t_2]^{1/3} \times I_2 / I_1} \quad (12)$$

Where I is the integral of the equation (10).

So the determination of  $H_1$  is reduced to the calculation of the ratio of the integrals I for two jacket pressures : all the other terms are experimental.

To determine I, different hypothesis on the gradient of pressure were tested. The better way to reproduce the experimental data obtained by comparison when changing the jacket pressure is to use a parabolic form for the gradient of the pressure in the interspace between piston and cylinder. This result is in agreement with the experimental data obtained at NBS by measuring the pressure in the interspace of a special unit with pressure transducers [7].

Finally, the gradient of pressure, and the integral I are both determined by a numeric method. The whole method has been described in details in [5].

All the methods described in the first part of this paper allow to determine the effective area of a piston-cylinder unit with an associated uncertainty. To have an internal verification of these uncertainties, it was interesting to have several units. All the developed standards are equipped with sets of units (3 to 6) and two balances in view to compare the units of same technology and geometry two by two. The ratio of the effective areas at the pressure p is expressed as a function of the masses m and m' applied on each piston and the temperature t and t' of the units :

$$K = A/A' = [m' / m] \times [1 + 2 \alpha (t - t')] \quad (13)$$

The validity of the different equations taken into account has been tested by measuring this ratio with a high level of accuracy (the uncertainties on masses are the highest components because the standard deviations are typically 0.2 ppm).

With the equation (13) applied at high pressure, we can test the homogeneity of the pressure distortion coefficients

$$K_0 [1 + (\lambda - \lambda') P] = [m' / m] \times [1 + 2 \alpha (t - t')] \quad (14)$$

The calculation of the best least squares straight line gives the values of the ratio of the effective area at null pressure and the difference of the pressure distortion coefficients.

The last common parameter of all our standards is the tungsten carbide used as material of the pistons and the cylinders. It was chosen for different advantages :

- possibility to have a better machining than with the usual materials.
- high mechanical characteristics.
- low thermal expansion coefficient.

From these basis 4 levels of standards have been successively put in LNE. They will be described in order of increasing pressure, not in the chronological order.

### Standard 0.01 to 1 MPa

The first step of standards has been developed in view to define a reference of effective area. It is equipped with 3 units of 10 cm<sup>2</sup> effective area working in the gas pressure range 0.01 - 1 MPa.

Diametral measurements of the pistons and cylinders have been realized with an uncertainty of about 0.05 μm. We have used an interferometric method described in details in [3]. Ten measurements distributed on the whole working part of the pieces have allowed a first approach of the geometric shape. They have shown defects of circularity and straightness inside 0.1 to 0.2 μm.

The effective area has been calculated from (4) by integrating the distortions of the pieces :

$$A = \pi R_0 \left( R_0 + H_0 + \frac{1}{L} \int_0^L (U_p + U_c) dx \right) \quad (15)$$

where L is the length of the cylinder,

$U_p$  and  $U_c$  are the distortions of the piston and the cylinder.

For the integration, we have assumed that the gradient of pressure varies linearly in the interspace and we have made a few hypothesis on the evolution of the distortions. It was demonstrated that the application of the variation of the pressure gradient from the viscous flow laws implies deviations on the value of the effective area inside 1 ppm.

We have verified the homogeneity of the measurement of diameters by determination of the ratio of two effective areas from (5) where and have been eliminated in this range of pressure. The accordance between the absolute method and the comparative method is shown in table 1, from the determination of the ratio of the effective area of 2 units.

PISTONS	RATIO $K_1$ (dim. meas.)	RATIO $K_2$ (comp. meas.)	DEVIATION (ppm)
2/5	0.9999790	0.9999784	0.6
2/6	0.9999740	0.9999737	0.3
5/6	0.9999950	0.9999937	1.3

TABLE 1 : DETERMINATION OF THE EFFECTIVE AREA OF  
THE STANDARD 0.01 - 1 MPa

The standard was also compared with the mercury column of the INM in the range 0.01 to 0.09 MPa. The indications of the two standards of independent technologies are in a very good agreement inside 0.3 Pa. The results have been published in [8].

In the other hand, a direct comparison of diameters measurement with the dimensional metrology laboratory of ETCA (Etablissement Technique Central de l'Armement) through a transfer unit has been made in 1987. The agreement of the measurement is inside 0.07  $\mu\text{m}$  (the accuracy claimed by ETCA is  $\pm 0.16 \mu\text{m}$ ). During this comparison, we have also tested the stability of the unit (the same measurements have been made in 1985 and 1987 with different devices and operators). The measured deviation of the effective area (+ 0.7 ppm) was not significant. All the results will be published in the Journal of BNM [9].

From all these data, the uncertainty of the measurement of the effective area is estimated to be  $\pm 4$  ppm with a high level of confidence. We have now in development more precise methods of measurement of the roundness and the straightness of the pistons and the cylinders to evaluate their distortions.

#### Standard 0.2 to 10 MPa

The second step of standards is equipped with 1  $\text{cm}^2$  effective area. It is a twin oil operated system. An oil-gas interface is integrated into the balance. Until 1985, it was our reference of effective area, defined by measurement of the diameters of about 11 mm. All the comparisons realized before this date were referenced to this standard.

By comparison with the former standard, the relative accuracy of the determination of the effective area is estimated to be  $\pm (5 \cdot 10^{-6} + 1 \cdot 10^{-7} P)$  with P expressed in MPa.

The interface oil-gas is constituted with a needle placed in contact with oil. By using a cathetometer to adjust the point of the needle, the repeatability of the measurement is better than 0.5 Pa. The difference of height between the reference level and the level of the interface has been calculated by a numeric method. It has been found the same value for the 3 units tested inside 0.05 mm. So, the effective area has been measured between 0.4 and 1 MPa with an experimental standard deviation of about 0.2 ppm.

The pressure distortion coefficient has been calculated and the homogeneity between the units has been verified at high pressure from the equation (5). All the results are inside 1.5 ppm.

### Standard 6 - 200 MPa

This standard is constituted with 5 units of  $0.5 \text{ cm}^2$  effective area on which is applied a mass of 1 ton. It has been developed to determine experimentally the pressure distortion coefficient.

The effective area at null pressure of each unit has been measured by comparison with the 10 MPa standard, by an increasing mass method. The accuracy has been estimated to be  $\pm 7.5 \text{ ppm}$ .

Then the pressure distortion coefficient of each unit has been measured by the method of variation of jacket pressure presented in the first part of this paper. The experimental coefficients have been compared to the theoretical coefficients with or without the jacket pressure. The agreement of all the units with the theoretical coefficients is inside  $\pm 0,09 \text{ MPa}^{-1}$ .

Comparative measurements of the units two by two have shown an agreement at 200 MPa inside 5 ppm. Since two years, we have changed the working oil from UNIVIS J 13 to di-ethyl hexyl SEBACAT. No significant change has appeared in the measurement of the effective area. The uncertainty of the measured pressure due to the uncertainty of the pressure distortion coefficient was estimated to be  $\pm 0.05 \times 10^{-6} \text{ MPa}^{-1}$ .

### Standard 30 - 1 000 MPa

The last standard is constituted with the same balances and new piston-cylinder units of effective area  $0.1 \text{ cm}^2$ . They are of controlled clearance type with a sleeve in steel.

The effective area at null pressure and the pressure distortion coefficient have been measured between 30 and 200 MPa by comparison with the 200 MPa standard. The linearity deviations are inside 2 ppm.

The better sensitivity is obtained for a jacket pressure equal to the fifth of the measured pressure. Comparative measurements up to 800 MPa of units two by two have shown an agreement between the results at low pressure and the results at high pressure inside 20 ppm. The sensitivity and the linearity deviations have been found inside a few ppm.

The same method by variation of jacket pressure that for the 200 MPa standard will be applied to determine the pressure distortion coefficients. The results on  $\lambda$  measured up to 200 MPa are also in good agreement with the theoretical values. The accuracy, estimated from these first results, would must to be inside 80 ppm at 1 GPa.

Accuracy on pressure measurement

In conclusion, the presented standards form a performant reference in a large scale of pressure. The uncertainties, shown in a log-log scale in fig. 2, are the following :

0.01 to 1 MPa :  $\delta p/p = \pm (0.14 \text{ Pa} + 4.4 \times 10^{-6} \times P + 4 \times 10^{-13} \times P^2)$

0.2 to 10 MPa :  $\delta p/p = \pm (0.6 \text{ Pa} + 6 \times 10^{-6} \times P + 1 \times 10^{-13} \times P^2)$

6 to 200 MPa :  $\delta p/p = \pm (70 \text{ Pa} + 8 \times 10^{-6} \times P + 0.5 \times 10^{-13} \times P^2)$

30 to 1000 MPa :  $\delta p/p = 15 \text{ to } 80 \text{ ppm}$

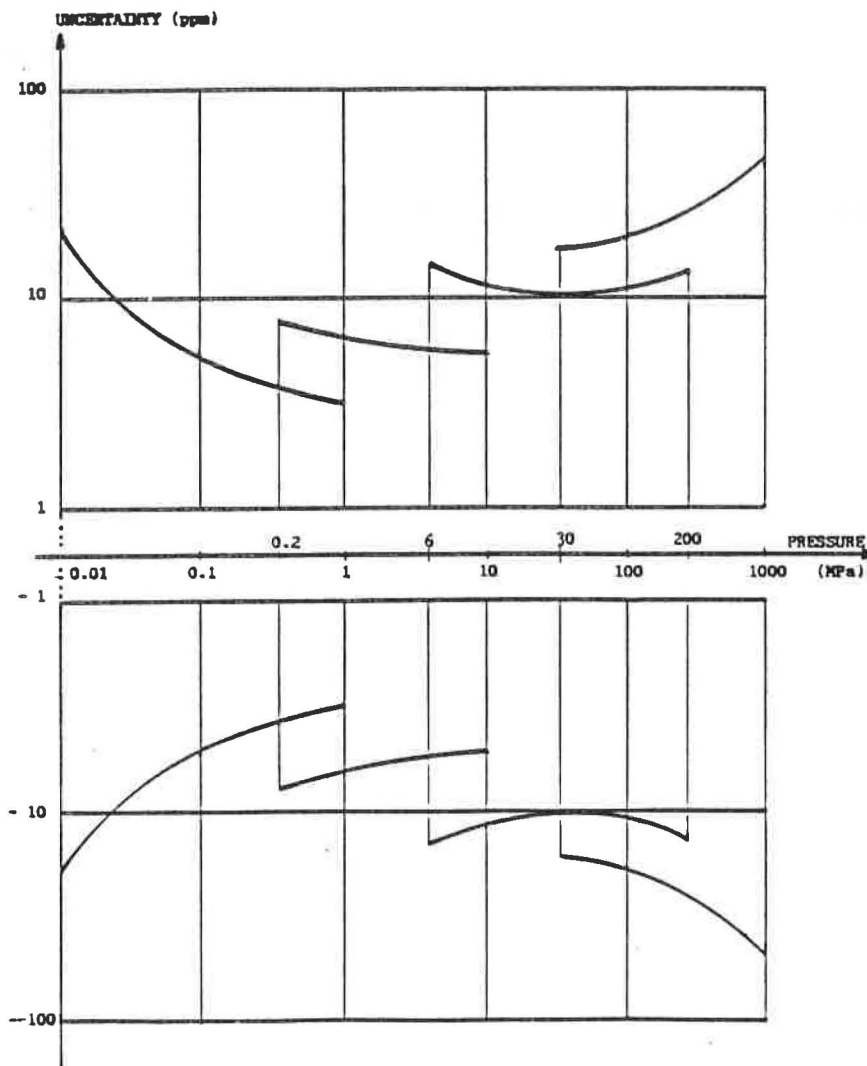


Fig. 2 - Uncertainties of the pressure measured by the standards of L.N.E.

## REFERENCES

- [1] R.S. : DADSON, S.L. LEWIS, G.N. PEGGS - The pressure balance. Monograph of NPL, 1982.
  
- [2] G.N. PEGGS - A method for computing the effective area of a pressure balance from diametral measurements. NPL report MOM 23, mars 1977.
  
- [3] J.C. LEGRAS, B. SCHATZ, P. DELAJOUD - La référence nationale de pression du BNM dans le domaine de 10 à 400 kPa. Bulletin d'Information du BNM n° 65, juillet 1986.
  
- [4] J.C. LEGRAS, P. DELAJOUD - Comparaison des étalons de pression du Gosstandard et du BNM - BI du BNM n° 28, 1977.
  
- [5] J.C. LEGRAS, A. HUOT, P. DELAJOUD - La référence nationale de pression du BNM dans le domaine de 5 à 200 MPa - BI du BNM n° 48, avril 1982.
  
- [6] P.L.M HEYDEMANN, B.E. WELCH - Experimental thermodynamics, volume II - Part 3 - Piston gages.
  
- [7] B.E. WELCH, V.E. BEAN - Pressure and temperature measurements in the annulus between the piston and cylinder of a simple dead-weight piston gage-contribution of the NBS.
  
- [8] P. RIETY, J.C. LEGRAS - Comparaison entre le manomètre à mercure de l'INM et la balance de pression de 400 kPa du LNE - BI du BNM n° 70, octobre 1987.
  
- [9] J.C. LEGRAS, B. SCHATZ - Mesure de la section effective d'un ensemble piston-cylindre de balance de référence de pression. To be published in BI du BNM.

## **DESIGN CONSIDERATIONS FOR A NEW HIGH PRESSURE (100 MPA) GAS LUBRICATED PISTON PRESSURE GAGE**

**DONALD B. FRANCIS, DIRECTOR OF QUALITY ASSURANCE  
KURT SOLIS, VICE PRESIDENT OF TECHNICAL SERVICES  
RUSKA INSTRUMENT CORPORATION**

In a market-driven, profit-oriented economy, individuals and firms determine what will be produced and how. The laws of supply and demand serve to distribute profits and point out what goods and services should be produced. Since resources are limited, the production of one set of goods and services will be at the expense of another resulting in compromises often referred to as "opportunity costs". This then sets the stage for the design process. When an instrument is designed that meets the requirements of the market, a profit may be realized through supplying the "goods", or instruments. To assure the best profit we must consider the opportunity costs. This is done through a "Design Goal" or specification. What is the demand of the market? -- Will our design meet the demands?

Review of the improvements in sensors and instruments for pressure measurement and the need for better accuracy has increased the need for better calibration standards. The need for a high pressure, accurate, and clean gas calibration standard is apparent. The benefits of such a piston gage are clear. The calibration of pneumatic gages would be easier, faster, and less expensive and at the same time more accurate.

One could say, in round figures that the measurements normally achievable with a top-quality deadweight tester carry an uncertainty in pressure of about +/-100 ppm or 0.01%. A large percentage of that error is due to the systematic uncertainty from the national standards laboratories. Each calibration further down in the hierarchy increases the cumulative uncertainty. The market is not satisfied and is demanding better calibration standards.

## **BASIC SPECIFICATIONS - "DESIGN GOAL"**

**PRESSURE RANGE** - A market survey indicates most pneumatic calibration work is at pressures under 10,000 psi (67 MPa), with minimal requirements up to 100 MPa (15,000 psi). Calibration equipment now on the market using oil-to-gas technology has a range to 100 MPa.

**GOAL** - The instrument must work to 10,000 psi and every effort should be made for a pressure range of 15,000 psi (100 MPa).

**PRESSURE MEDIUM** - All who have worked with a very small hole (leak) in a pneumatic pressure vessel can begin to understand the importance of the fit of the piston in the cylinder using gas as the lubrication and pressure medium. As the pressure increases we want to keep the sink rate small but not at the expense of sensitivity. However, all who have cleaned liquid and hydrocarbon contamination from sensors and instruments will strongly demand the use of oil-free technology.

**GOAL** - nothing in the design will introduce contaminants into the test instrumentation.

**ACCURACY** - It is well known by practicing metrologists and certainly the scientific community that the objective and realistic knowledge of accuracy of a measurement (with a high degree of confidence) is not easily achieved. It requires knowledge of the value of mass and the area as the foundation. This information cannot be used without good instruments, and control over the procedures and environment where the measurement is performed.

A triangle of responsibilities (Figure 1) exists and when combined will account for the total accuracy or error budget of the measurement process.

- The respective national standards facility is the foundation of the process, that is, it is responsible for providing and disseminating the best possible national primary standards for mass and effective area.
- The instrument manufacturer is responsible for the quality of the instrument itself. Here we can incorporate the effects of the instruments precision, stability, resolution and so forth, as reflected in performance qualities such as drift, and the residual uncertainties in the instrument.
- Finally, the user's environment and procedures are responsible for the remaining error-budget. Part is derived from uncertainties in the values used for local gravity, air density, and fluid density in the corrections normally made.

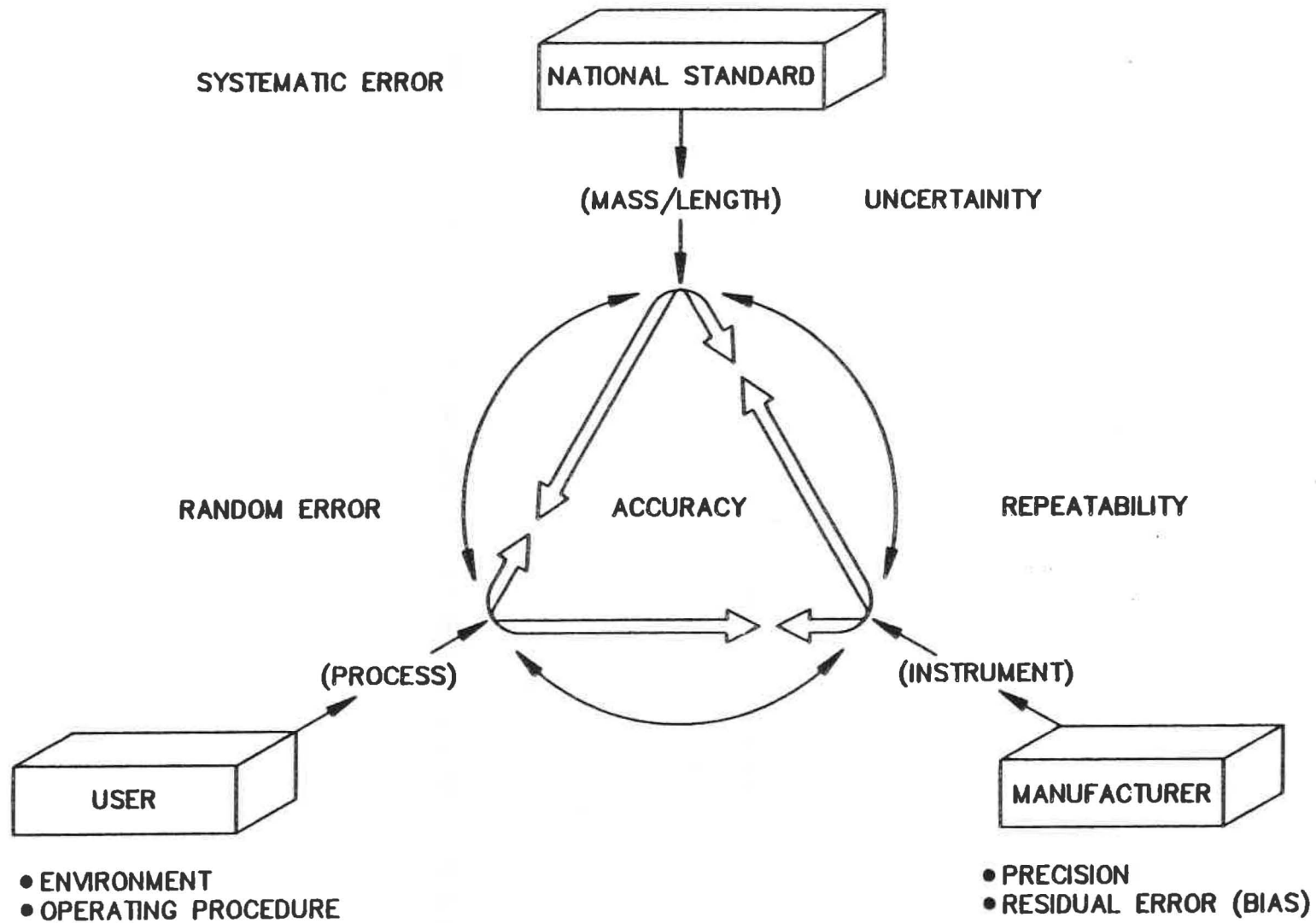


FIGURE 1

**RESIDUAL ERRORS** - Each of the disturbances of the process creates a certain amount of inaccuracy in a pressure measurement. That inaccuracy is described in terms of uncertainty. The amount of the disturbance we know (quantity and polarity) is a correction. The part we are not certain about is the uncertainty. For example the thermal expansion coefficient of the piston gage material might be  $4.55E-06$  per  $^{\circ}C$  with an uncertainty of  $\pm 10\%$  the  $4.55E-06$  is the correction and  $4.55E-7$  the uncertainty. The basic problem of temperature gradients will give us residual errors in the value of the temperature of the piston material. These residual errors and uncertainties are components of the total accuracy.

**GOAL** - Identify and include an estimated uncertainty for each residual error in the error budget.

**MEASUREMENT OF THE PERFORMANCE** - The performance of a piston pressure gage can be measured by the freedom of the piston within the cylinder. If the piston is free it may fall too fast, however, one that will not fall is not free enough and will not show the sensitivity required. At best, one has a trade-off. In establishing the specifications for a new instrument values must be set for the fall rate and the sensitivity threshold. Even though the instrument may respond to a small change in pressure will it repeat this value time and time again or what specification can we set for repeatability?

Furthermore, what can be reproduced over a long period of time?

**GOAL** - We can set the goal for sensitivity at 1 ppm, repeatability at 3 ppm and with drift included we can set reproducibility at 6 ppm per year. The maximum sink rate can be set at 4mm/minute (0.15 in/min.)

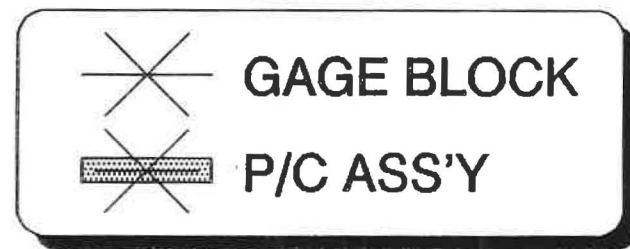
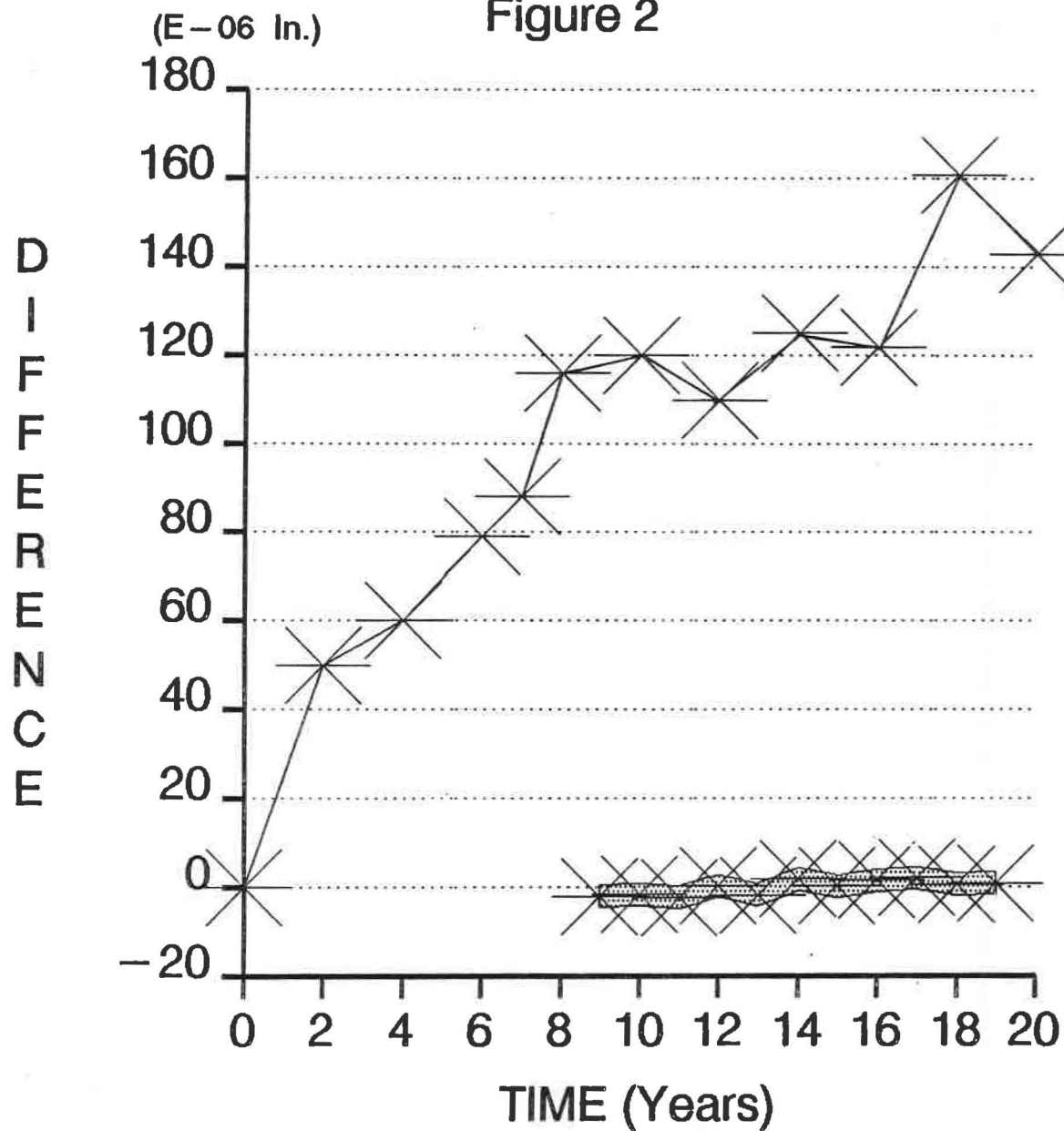
## CONSIDERATIONS TO MEET THE GOALS

**MATERIAL FOR THE PISTON/CYLINDER** - An optimum material must be chosen to minimize the residual errors in expansion of the piston and cylinder due to temperature, to have the required elastic constants and to maintain long-term stability.

**STABILITY** - Very accurate gages or tools must be ground and lapped to size and must then hold this size indefinitely. Pistons and cylinders are not the only metrological tools that fit this requirement. Others are plug or ring gages and gage blocks. As ordinarily hardened, a tool made from tool steel may change size or shape by a few microns over a period of years. This comes about through a natural "aging" process. To show an illustration of this change we have been comparing the size of a one inch (25.4 mm) gage block to a standard gage block for the past twenty (20) years (Figure 2). This block has changed size by approximately 5 microns in this time. Armed with this information we set procedures in place where many years of aging can be crowded into a few hours when manufacturing pistons. On the other hand, if we can use a material not requiring this aging, stabilizing will not be a large constraint on our design.

# STABILITY

Figure 2



**MOUNTING OF THE PISTON/CYLINDER ASSEMBLY** - Careful considerations must be given to the methods used to contain the P/C Assembly within the superstructure of the instrument base and the connection means to the mass.

**ATTITUDE STABILITY** - Centerline and alignment surfaces must be controlled to ensure with minimal uncertainty contribution that the axis of the piston/cylinder is aligned with the direction of gravity. This mechanical relationship must be repeatable with removal/insertion of the P/C Assembly and must be mechanically translated to some external, user-accessible, surface.

**DISTORTION IN MOUNTING THE P/C ASSEMBLY** - The P/C in Figure 3, which is a re-entrant type, has a pressure seal on the bore of the housing and outside of the cylinder. With this design high torque is not required of the nut to seal pressure. However, in search of a leak one might torque down all fasteners. This action will end-load the cylinder and deform it. In this case the deformation can change not only the area at the low pressure but also the re-entrant effect. To caress the cylinder is not enough - it must be held stable. The attitude of the assembly as a function of pressure/load must be stable. Figure 4 conceptually demonstrates the improved design. The pressure seal has been relocated to the lower surface of the cylinder (face-seal). This minimizes vertical external forces onto the cylinder by the retaining nut. Radial forces are also eliminated. The re-entrants property is optimized by the "thin-wall" extension.

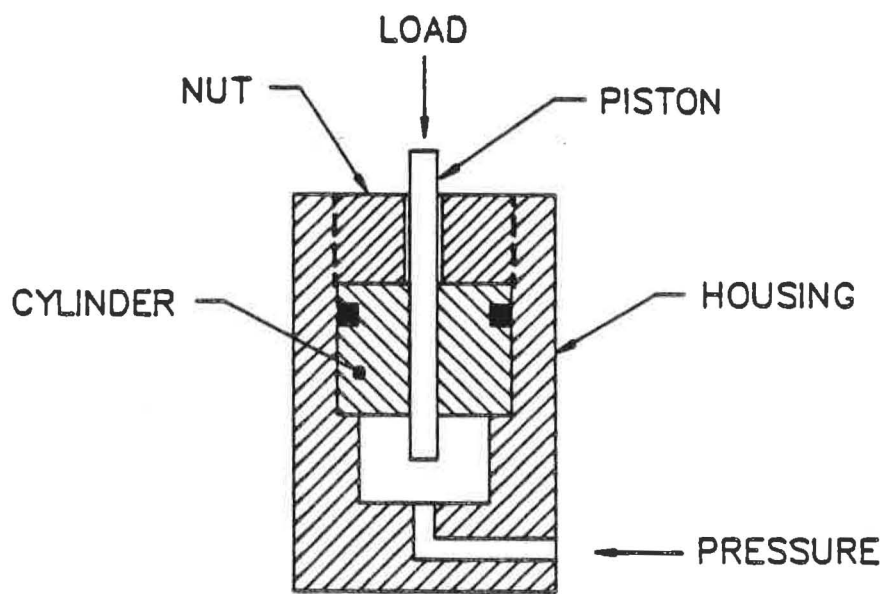


FIGURE 3

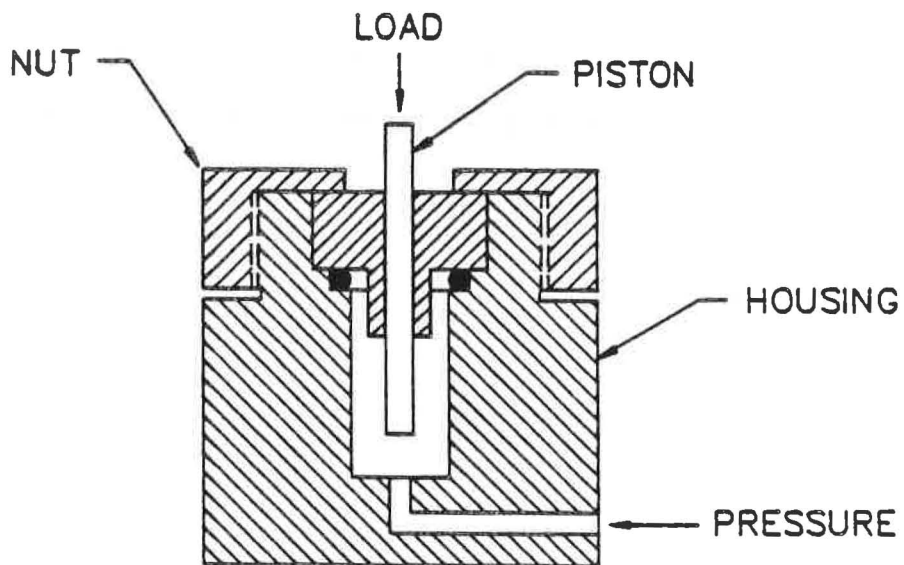


FIGURE 4

**FORCE TRANSLATION TO PISTON** - The point at which the mass mechanically contacts the piston must be configured such that the force is translated totally through the vertical axis of the piston. Additionally, sufficient contact area is required to ensure the rotation of the mass is translated to the piston.

## **THE MASS SET**

**STABILITY OF MASS** - Trouble is sometimes experienced from forces caused by magnetization of the components of the Piston Gage. To reduce trouble of this type, it is preferred to construct the components from nonmagnetic material, check for magnetization of the components, and monitor the environment. To insure long term stability of the mass, sharp edges and other features such as movable parts, cracks or crevasses should not be designed into the mass. The knowledge of a mass is of greater importance than how precisely it is adjusted to a given value. Given this, the necessity of calibration seals on the adjusting cavity and monitoring of loose adjustment material need not be tolerated. Each mass can therefore be constructed of one homogeneous material.

Comparison measurements up to 8 kbar between a Budenberg and a Harwood high pressure balance using undiluted di-ethylhexyl-sebacate as pressure fluid

P.Hilsch, J.Jäger

### Abstract

Because of the nonlinear correlation observed at constant fall rate between the jacket pressure  $p_j$  and the measured pressure  $p$ , the equation  $A_e = A_0 (1 + \lambda p - dp_j)$  is used to characterize a controlled-clearance high-pressure balance. From pressure comparison experiments with a standard pressure balance the coefficients  $\lambda$  and  $d$  were found to be independent of  $p$  and  $p_j$ , as had been expected. Whereas  $d$  agrees with the value calculated from the well-known theory,  $\lambda$  deviates considerably from its theoretical value.

Comparison measurements up to 8 kbar between a Budenberg and a Harwood high pressure balance using undiluted di-ethylhexyl-sebacate as pressure fluid

P.Hilsch, J.Jäger

The effective area  $A_e$  of a controlled-clearance piston-cylinder (p-c) system at its reference temperature can be described by eq.(1):

$$A_e = A_0 (1 + \lambda p - d p_j) \quad (1)$$

$A_0$  is the effective area at zero pressure and  $\lambda$  and  $d$  describe the dependence of the effective area on the measured pressure  $p$  and on the "jacket" pressure  $p_j$  applied to the external surface of the cylinder in order to control the clearance between piston and cylinder.

Instead of eq.1 a well-known alternative expression is normally used:

$$A_e = \pi r_p^2 [1 + b p + d(p_{j0} - p_j)] \quad (2)$$

Eq.(2) is based on the cross-section  $\pi r_p^2$  of the piston as obtained from geometrical measurements, on the piston and cylinder deformation coefficients  $b$  and  $d$  and on the "zero-clearance" jacket pressure  $p_{j0}$ , which can be obtained from fall rate measurements by extrapolation of the results.

Eq.(1) and eq.(2) can be equivalent only if a linear dependence exists between  $p_{j0}$  and  $p$ , which is the case for pressure transmitting media of comparatively low viscosity at high pressures / 1 /. In this case, small clearances between piston and cylinder are, however, required to ensure acceptable fall rates for practical pressure measurements. These small clearances involve the risk of deterioration of the p-c system. Experience has shown that at least on some commercially available systems traces of friction and wear are observed, which are unacceptable in view of possible shifts of the effective area with time.

Such effects can be avoided if more viscous fluids are used, such as undiluted di-ethylhexyl-sebacate. Then, however, the increase of  $p_j$  with  $p$  observed at constant fall rate is much smaller at higher measured pressures than at lower pressures / 1 /, so that eq.(2) cannot be used to find  $A_e$ .

Despite a nonlinear dependence of  $p_{j0}$  on  $p$ , the effective area of a controlled-clearance p-c system should still show a linear dependence on both the measured pressure and the jacket pressure, so that it should be possible to calibrate the system on the basis of eq.(1). In the pressure range between 0.3 and 0.8 GPa we have checked this by performing pressure comparison measurements between two high-pressure balances (Budenberg, model 284, and Harwood), one equipped with a simple p-c system ( $p_j = 0$ ) and one with a controlled-clearance system for the 1.5 GPa range of measurement. From these measurements the parameters  $d$ ,  $\lambda$  and  $A_0$  of eq.(1) were determined for the Harwood p-c system. The Budenberg pressure balance was used as the standard characterized by the expression  $A_e' = A_0' (1 + \lambda'p)$  with  $A_0'$  and  $\lambda'$  as obtained from pressure measurements with standard instruments for lower pressures. The standard was known to measure the melting pressure of mercury at 0 °C in agreement with the internationally accepted value to within  $\pm 0.2$  MPa.

The value of  $d$  was found from measurements of the change of the load on the controlled-clearance gauge with  $p_j$ , when the equilibrium condition between both balances was being maintained at constant  $p$ . Using the experimental value of  $d$ ,  $\lambda$  and  $A_0$  were determined from pressure comparison measurements performed at various values of  $p$  and  $p_j$ .

From the results of our measurements as presented in fig.1 and fig.2 we find  $\lambda_{\text{exp}} = 3.8 \text{ TPa}^{-1}$  and  $d_{\text{exp}} = 9.58 \text{ TPa}^{-1}$ , both independent of  $p$  and  $p_j$

as had been expected. Applying the well known formulae for  $\lambda$  and  $d / 2$  / we obtain  $\lambda_{\text{calc}} = 2.79 \text{ TPa}^{-1}$  and  $d_{\text{calc}} = 9.584 \text{ TPa}^{-1}$ . Whereas  $d_{\text{exp}}$  and  $d_{\text{calc}}$  are in perfect agreement in this case, there is a striking disagreement between  $\lambda_{\text{exp}}$  and  $\lambda_{\text{calc}}$ . The relative standard deviation of the data obtained for  $A_0$  when using  $\lambda_{\text{exp}}$  and  $d_{\text{exp}}$  was  $3 \cdot 10^{-5}$ . This value characterizes the experimental uncertainty of the pressure comparison measurements.

In conclusion it may be said that the effective area of the investigated controlled-clearance p-c system exhibits the expected linear pressure dependence, independent of the non-linear correlation between  $p_j$  and  $p$  for constant fall rate. The deformation coefficient  $\lambda$  reflects, however, individual properties of this system and is difficult to predict theoretically with reasonable accuracy.

Results similar to those described in this note have been obtained earlier using a Harwood p-c system designed for the 1.0 GPa range / 3 /.

### References

- / 1 / J.K.N.Sharma, K.K.Jain, V.E.Bean, B.E.Welch and R.L.Lazos:  
Rev.Sci.Instrum. 55 (1984), 563-569
- / 2 / P.L.M.Heydemann and B.E.Welch: Experimental Thermodynamics,  
Vol.II; Ed.: B. LeNeindre and B.Vodar; Butterworths, London (1975),  
p. 152-155
- / 3 / A.K.Bandyopadhyay, P.Hilsch and J.Jäger: PTB-Mitteilungen 97 (1987),  
264-269

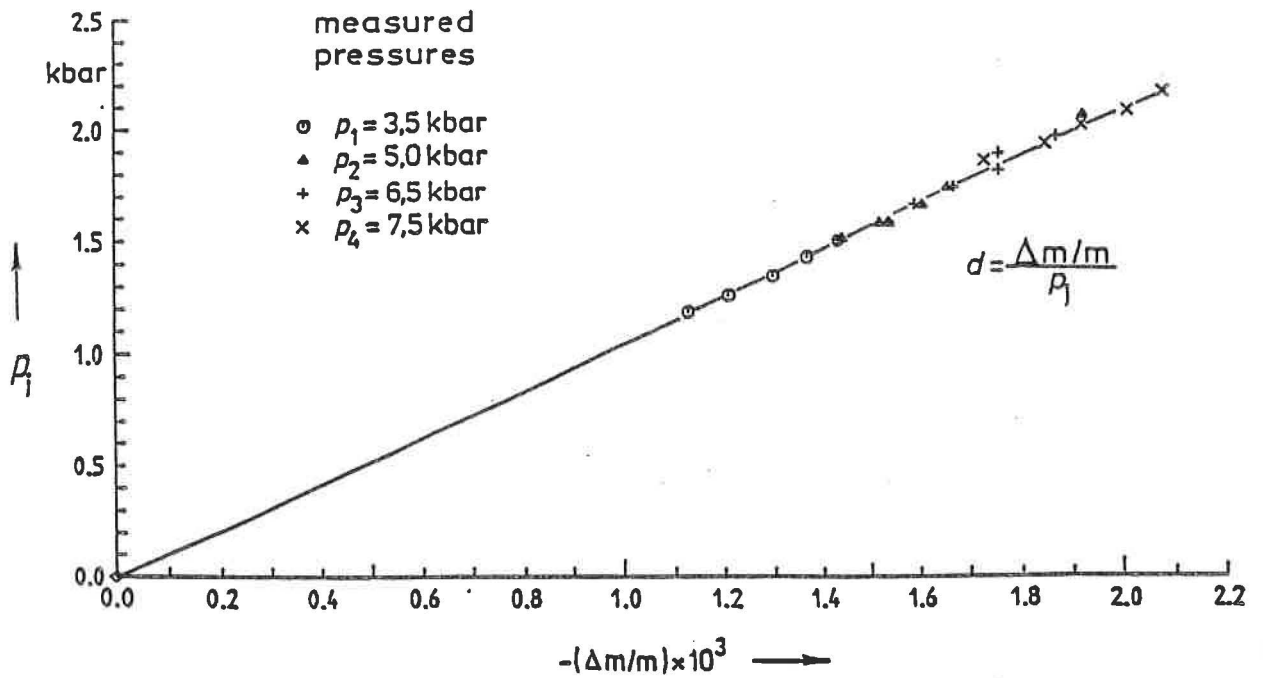


Fig.1 Change  $\Delta m$  of load  $m$  required to compensate for changes in jacket pressure  $p_j$  at constant measured pressure  $p$ .

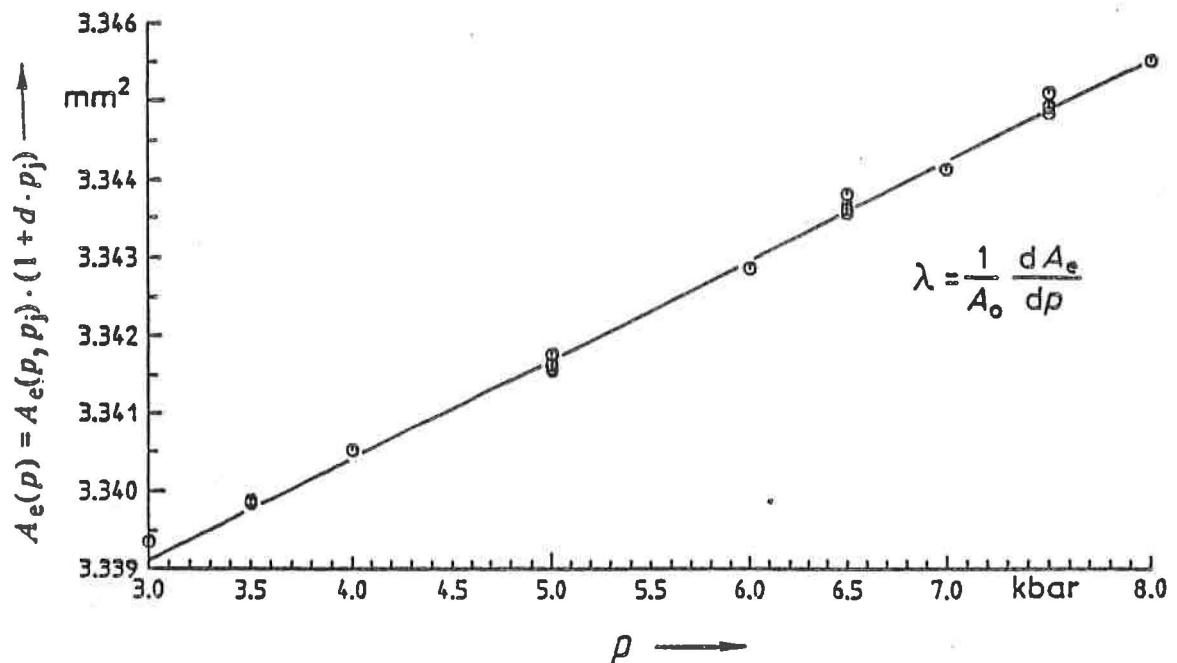


Fig.2 Change of effective area  $A_e$  with measured pressure  $p$  at zero jacket pressure  $p_j$  (data calculated from measurements performed at various jacket pressures).

DEVELOPMENT OF A HIGHLY STABLE AIR PISTON PRESSURE GAGE  
WITH NON-ROTATIONAL PISTON-CYLINDER SYSTEM

A.Oiwa  
National Research Laboratory of Metrology,  
A.I.S.T., M.I.T.I.,  
JAPAN

ABSTRACT

A newly developed pressure gage has such a high stability that the fluctuation level of a generated pressure is measured less than 0.1 Pa or 1 ppm. This high stability is obtained by applying the non-rotational system, because the pressure fluctuation level of the usual piston gage, which is more than 10 ppm, mainly results from the rotation, being employed to lubricate the piston cylinder assembly. The non-rotational system consists of two specially designed mechanisms. One is the shape of the clearance between piston and cylinder. The other is suspending method for weights. Detailed discussion covers the numerical simulation of the flow in the clearance between the piston and cylinder, the evaluation method of the performance, the balancing mechanism of weights, and the monitoring technique of piston's inclination.

KEY WORDS

Pressure measurement; pressure standard; air piston gage; piston cylinder assembly; pressure balance; stabilized piston.

INTRODUCTION

The air piston gage consists of a piston cylinder assembly and weights those are applied on the piston. Because of their high accuracy, piston gages are used as the pressure standards over wide pressure ranges. During the operation, the piston and cylinder must be rotated relatively in order not to contact each other. The rotation makes viscous flow in the clearance between piston and cylinder. This flow lubricates them, and generates the centralizing force acting on the piston's surface (Dadson, Lewis, and Peggs, 1982).

There are some problems in the rotation method.

- a) The rotation is generated by the force from outside which brings noises to the measured pressure.
- b) When the rotational velocity is high, the piston and weights are affected and pushed by stirred fluids around them (Prowse, and Hatt, 1976).
- c) As increasing the weights, the inclination force acting on the piston also increases, and piston becomes unstable.
- d) The rotation generates heat by friction in the clearance, and causes the temperature rises which change the effective area of the piston-cylinder assembly (Welch, and Bean, 1984).

The non-rotational piston cylinder system has been developed to remove or reduce these problems, and to make piston gages more accurate and simple.

## PRINCIPLES

**Stabilizing Mechanism** The main principle of the non-rotational piston cylinder system is a slightly tapered clearance between piston and cylinder, shown illustratively in Fig.1. The wider and narrower ends of this tapered clearance must be opened to the higher and lower pressure sides respectively. In this system we can observe the stabilizing effect.

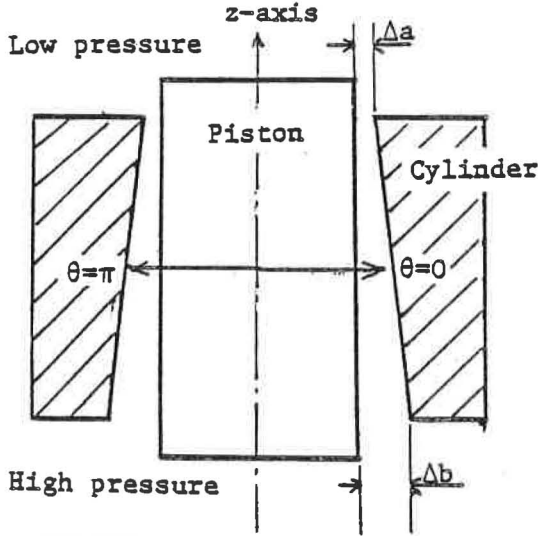


Fig.1 The schematic shape of non-rotational piston-cylinder assembly. the gap of clearance and the tapering rate are exaggerated.

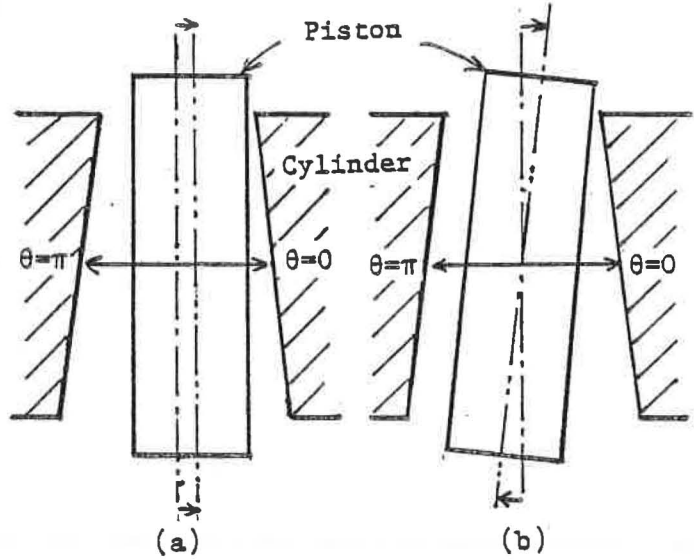


Fig.2 Displacement forms of the piston in the cylinder. (a) Lateral displacement (Eccentricity), (b) Tilting displacement (Inclination)

The stabilizing mechanism is described as follows. The clearance of the piston and cylinder is filled with a pressure medium fluid and the fluid flows through the clearance according to the pressure fall. The flow rate and the pressure distribution in the clearance depend upon the size and shape of the clearance and the pressure drop between top and bottom of the piston. The piston is assumed to be exactly cylindrical and the clearance can be neglected compared with the radius. I adopt the co-ordinate system indicated in Fig.1 and denote by  $p(z, \theta)$  the pressure distribution function in the clearance. For convenience in calculation the zero of  $z$  is taken to be midway of the fitting part of the piston. The circumferential force by pressure  $f_p(z)$  acting on the piston's surface at a level  $z$  is integrated as Eq. (1). Then the lateral force  $F_p$  and the tilting moment  $M_p$  are acquired by integrating  $f_p$  on  $z$ , as defined by Eq. (2).

$$f_p(z) = \oint_{\theta} p(z, \theta) \frac{\mathbf{n}}{|\mathbf{n}|} d\theta \quad (1)$$

where  $\mathbf{n}$  is a surface vector of the piston, the direction of which is at right angle to the surface.

$$F_p = \int_{-l/2}^{l/2} f_p(z) dz, \quad M_p = \int_{-l/2}^{l/2} f_p(z) z dz \quad (2)$$

When the piston is positioned concentrically at the center of the cylinder as shown in Fig.1, the clearance is thought to be cylindrical annular channel. Therefore the flow direction has only the axial component and the pressure distribution function is varied only with  $z$  ( $p(z, \theta) = p(z)$ ).

$$f_p(z) = p(z) \oint_{\theta} \frac{\mathbf{n}}{|\mathbf{n}|} d\theta = 0 \quad \text{then} \quad F_p = M_p = 0 \quad (3)$$

Accordingly the integrated circumferential force  $f_p$  at any  $z$  becomes null as indicated in Eq.(3). The lateral force and tilting moment are also zero. When the piston is eccentrically positioned or inclined in the cylinder, The shape of clearance is varied at any level and the pressure distribution has also some asymmetric value. For simplicity, the piston's departures from the ideal condition are classified into two forms, illustrated in Fig.2, one is a lateral displacement of piston while the axes of the piston and cylinder are parallel (Fig.2(a)), and the other is a tilting displacement of the piston around it's center (Fig.2(b)). For the lateral displacement, the profile of clearance on the approaching side ( $\theta=0$ ) is choked at the top part, and therefore, the pressure distribution on this side has an elevated value comparing with that in the ideal condition. On the contrary, the clearance profile on the opposite side ( $\theta=\pi$ ) is spread, and the pressure distribution has a reduced value comparing with the ideal one. Therefore the circumferential force  $f_p(z)$  has a value pushing the piston back to the central position, and is, so to speak, a centralizing force for the piston. This force is thought to have the stabilizing effect for the lateral displacement of the piston. For the tilting displacement, the mechanism is similar to that for the lateral displacement. On the upper part of the piston ( $z>0$ ), the circumferential force  $f_p(z)$  has a centralizing effect, but on the lower part ( $z<0$ ), it has a centrifugal effect. Supposing that the centralizing effect is greater than the centrifugal one, it could be concluded that the tilting moment of the pressure works as the stabilizing force.

Numerical Simulation for Flow in Clearance As it is difficult to solve analytically the Navier-Stokes equation in the asymmetric annular tapering channel, a numerical simulation with computer was adopted to get the pressure distribution in the clearance for various displacement of the piston. The flow equation is solved numerically in the condition as follows.

- a) No-slip condition; the velocities of fluid are same as those of solid body at the contacting places.
- b) Incompressibility; For easiness of comparing the results, the fluid was supposed to be incompressible. As the equation is linear for pressure, the profiles of flow and pressure distribution are similar for any pressure drop.
- c) Constant viscosity:

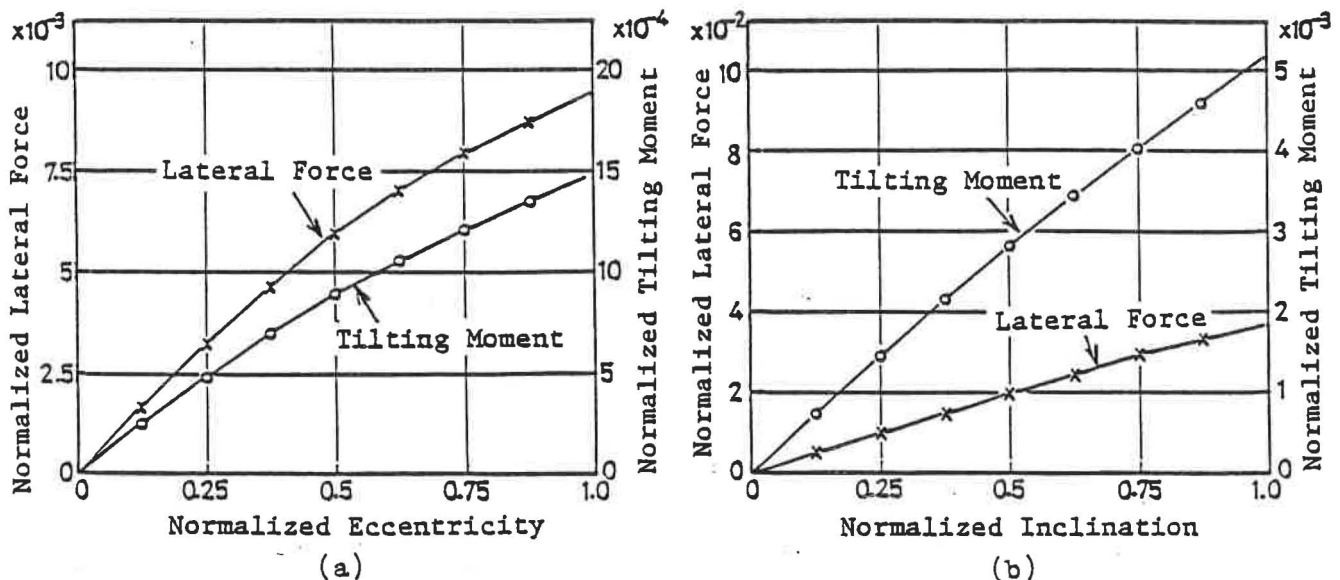


Fig.3 Lateral force  $\bar{F}_p$  and tilting moment  $\bar{M}_p$ , under the fixed tapering ratio  $\Delta b/\Delta a = 2$ , (a) as the functions of eccentricity, and (b) as the functions of inclination.

Results are obtained for normalized lateral forces  $\tilde{F}_p$  and tilting moments  $\tilde{M}_p$ , the normalizing treatments of which are defined in eq.(4).

$$\tilde{F}_p = \frac{F_p}{2\pi r \cdot l \cdot \Delta p}, \quad \tilde{M}_p = \frac{M_p}{2\pi r \cdot l^2 \cdot \Delta p} \quad (4)$$

In the process, piston's displacements are also normalized by the maximum displacement  $\Delta a$ . Results are graphed in Fig.3 and Fig.4. Rateral forces  $\tilde{F}_p$  and tilting moments  $\tilde{M}_p$  are calculated for various eccentricity in Fig. 3(a) and for various inclination in Fig. 3(b). We find that the forces are increasing proportionally to the displacement. In Fig.4, the tilting moment and the lateral forces are obtained and plotted for various tapering ratio  $\Delta b/\Delta a$ . The lateral force by eccentricity and the tilting moment by inclination are playing as stabilizing forces, which have maximum values in the range where the tapering ratio is from 5 to 7. And the tilting moment by eccentricity and the lateral force by inclination don't have stabilizing effect and are, so to speak, parasitic forces, which are varied exponentially with the tapering ratio.

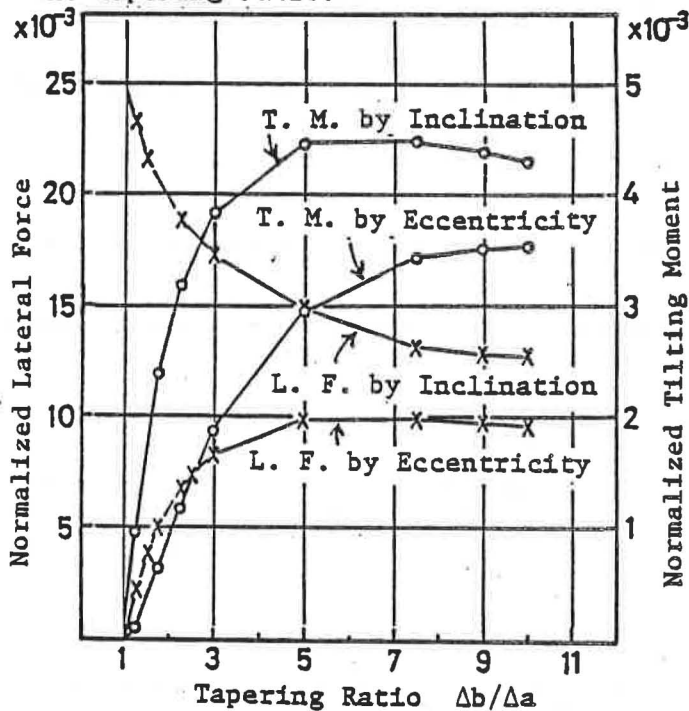


Fig.4 Lateral force  $\tilde{F}_p$  and tilting moment  $\tilde{M}_p$  for various tapering ratio  $\Delta b/\Delta a$  under the fixed displacements, n. eccentricity is 0.5 and n. inclination is 0.5.

#### APPARATUS

The picture and the specifications of the developed apparatus is shown in Fig.5 and Table 1. The piston-cylinder assembly is set inside of the hat and the cylinder is put on the stand.

Piston and Cylinder Assembly The piston and cylinder were made of 440C stainless steel, and after finishing, they were carefully demagnetized. The shape and dimensions of the piston and cylinder were measured by means of comparative method with gage blocks. The profiles of piston-cylinder are shown in Fig.6. The average gaps of the top and bottom of the clearance are  $1.2 \mu\text{m}$  and  $3.4 \mu\text{m}$  respectively.

Table 1 Specifications of the developed non-rotational air piston gage

Medium	gas	Effective area	6 cm <sup>2</sup>
Pressure range	$0.5 \sim 4 \times 10^5$ Pa	Accuracy	9 ppm

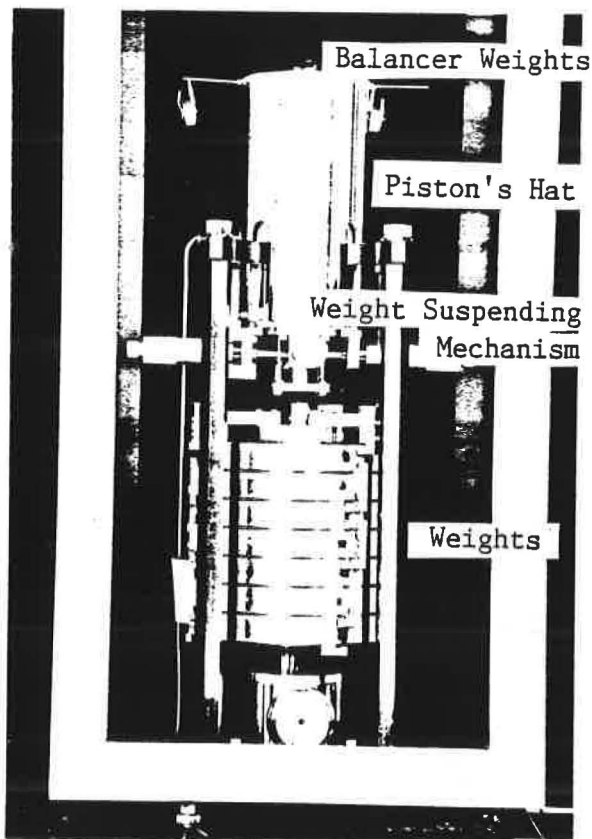


Fig.5 Picture of the developed non-rotational piston gage.

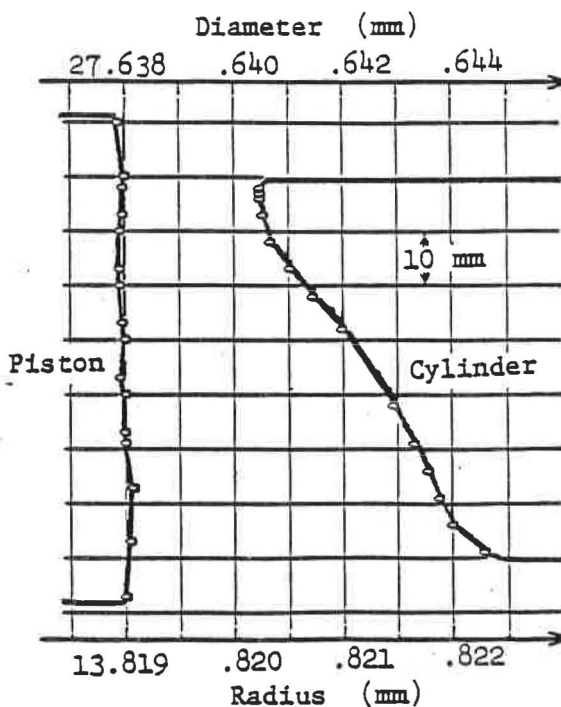


Fig.6 Profiles of the piston and cylinder.

Weight Suspension Mechanism The weights suspension mechanism plays another important role for the non-rotational stabilizing system as well as the tapering clearance of the piston-cylinder assembly. The fluctuation force acting on the piston is mainly caused by an unbalance of weights. In order to eliminate this fluctuation force below the maximum level of the stabilizing force, the weights must be suspended under the piston exactly on the extended line of the piston's axis. The micro adjusting mechanism for suspending the weights is set at the bottom of the piston's hat, which enables us to adjust the suspending point of weights. The residual unbalance may be adjusted by suitable positioning of the small weights on the rods which are stuck on the top edge of the piston's hat. By this suspension mechanism, after the adjustment has done, the alignment is stable and does not easily get out of order even when the weights are changed. It should be noted that this suspending mechanism could be adopted owing just to the non-rotational relation between the piston and cylinder.

Monitoring Technique The piston's inclination can be monitored by using an auto-collimator watching the top surfaces of the piston and cylinder which were polished to work as reflecting mirrors. The piston's inclination angle can be measured against the reference level, the free surface of silicone oil, with the accuracy of about  $4.8 \times 10^{-6}$  rad. By this monitoring technique, the floating condition can be easily watched.

#### EXPERIMENTAL RESULTS

The piston keeps floating in the cylinder while the inclination angle of the piston against the cylinder's axis is smaller than  $1.4 \times 10^{-5}$  rad. The maximum inclination angle is about  $3.2 \times 10^{-5}$  rad which is almost equal to the tapering

angle of the cylinder  $2.4 \times 10^{-5}$  rad. The actual tilting moment can be measured from the relation between the inclination angle and the adjusting state of the small balancer weights. The tilting moment is proportional to the inclination angle  $\alpha$  and the pressure difference  $\Delta p$ , and is represented as  $M_p = 1.7 \times 10^{-3} \cdot \Delta p \cdot \alpha$ . When the pressure difference is  $10^5$  Pa (1 atm.) and the inclination angle is  $5 \times 10^{-6}$  rad, the tilting moment becomes  $8.3 \times 10^{-3}$  Nm, which can be easily controlled by adjusting the small balancer weights.

Sensitivity and Stability The sensitivity of the gage is estimated by small masses added to the weights. The pressure change is monitored by the pressure transducer using a quartz oscillator as a sensing element, the resolution of which is about 0.4 Pa (3 $\mu$ mHg). The stability of the non-rotational pressure gage has been also monitored by the transducer, but the pressure fluctuation level is less than the resolution and cannot be detected. therefore, we can say just that the stability of this gage is less than 1 ppm. The total accuracy of the developed non-rotational air piston gage is estimated as shown in Table 2. The main error is that of effective area which is derived from the uncertainty in measuring the dimensions of the piston-cylinder assembly.

Table 2 Estimation of the accuracy of the developed gage

Factor	Estimating accuracy ( $\pm$ )
Mass of weights	0.3 ppm
Gravity	0.3 ppm
Correction of buoyancy	< 0.4 ppm
Effective area	8.0 ppm
Total accuracy	< 9.0 ppm

### CONCLUSIONS

The non-rotational piston pressure gage has some advantages over the usual piston gage with rotation. These advantages are summarized as follows.

- a) There is no necessity of forcing the piston or cylinder to rotate, the generated pressure is highly stable, better than 1 ppm, for rather long period of time.
- b) The non-rotational state can reduce the errors due to rotation, such as temperature rises and convections.
- c) As the structural relation between the piston and cylinder is simple with non-rotational system, the suspending mechanism can be designed easily to have a high stability.
- d) It is easy to analyze theoretically the flow in the clearance so as to estimate accurately the effective area of the piston-cylinder assembly.
- e) The non-rotational stabilizing mechanism is available for also higher pressure ranges because the stabilizing forces increase proportionally to the increase of the measured pressure difference.

### REFERENCES

- Dadson, R. S., S. L. Lewis, and G. N. Peggs. (1982). The Pressure Balance. HMSO, London. pp34-45.
- Prowse, D. B., and D. J. Hatt. (1976). The effect of rotation on gas operated free-piston pressure gauge, J. Phys. (E), 10, 450-451.
- Welch, B. E., and Vern E. Bean. (1984). Pressure and temperature measurements in the annulus between the piston and cylinder of a simple dead-weight piston gauge, Rev. Sci. Instrum., 55(12), 1901-1909.
- A. Ooiwa, Non-rotational type dead weight pressure gauge, NRLM news, vol.30, no.12.
- A. Ooiwa: Proc. of the International Symposium on Fluid Control and Measurement (FLUCOME Tokyo '85), pp959-964.

# DEAD WEIGHT PISTON GAUGE OF MIXED OPERATION PRINCIPLE

by

R. WISNIEWSKI, J. ROGOWSKI and A.J. ROSTOCKI

Institute of Physics,  
Warsaw University of Technology  
00-662 Warszawa, ul.Koszykowa 75,  
WARSAW, POLAND

(Research sponsored by the Government Research Coordination  
Office under the Project CPBR-02.20 )

## ABSTRACT

This paper presents the design of the mixed operation principle piston-cylinder assembly for a dead-weight manometer for pressures up to 1GPa, built in The Institute of Physics of Warsaw University of Technology. Both the theory and the method of calculation of effective area and the problem of its optimization have been presented. To confirm the principle of action and theoretical calculations of deformations, an examination of large scale models built of different materials for the piston and cylinder have been done. Pressure characteristics of the new piston-cylinder assembly have been determined partially by comparison with a simple piston-cylinder pressure standard within the range of pressures up to 0.3GPa. The pressure dependence of the effective area of the piston gauge of mixed operation principle has been found to be approximately parabolical. The accuracy for the prototype assembly has been estimated to be 0.1% or better. The experience gained from the above experiments has been used to design a new model of dead-weight manometer for pressure range 1-1.2 GPa .

## INTRODUCTION

In 1980 one of the authors of this paper published two papers [1],[2] introducing a mixed principle piston gauge for pressures up to 1 GPa . The term "mixed operating principle" has been used to emphasize the fact that the device combines the idea of the reentrant cylinder in its lower part with the properties of simple piston-cylinder assembly in the upper part . The schematic diagram of such a piston-cylinder assembly is shown in fig.1 . The variations of the effective area for both parts are of opposite sign thus compensating each other (see fig.2).A more developed theory of calculation of the effective area for this type of pressure gauge has been presented in paper [3].A similar manometer up to 160MPa, which was partially a simple system and partially a controlled clearance was described by Eremev [6], but no information regarding the pressure changes of effective area was given there.

The aim of this paper is to present the further development in the theory of effective area calculation of this type of manometer and also to present experimental data leading to the construction of new models of dead-weight piston gauges for pressures up to 1.2 GPa.

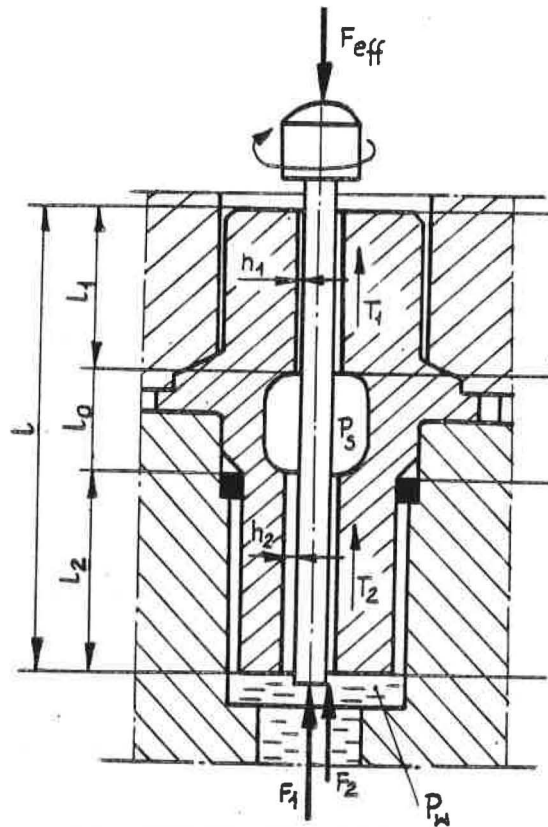


Fig.1. Schematic cross section of mixed operation principle piston cylinder system; at left side situation for low pressure ( $p_w \rightarrow 0$ ), at right side for high pressure.

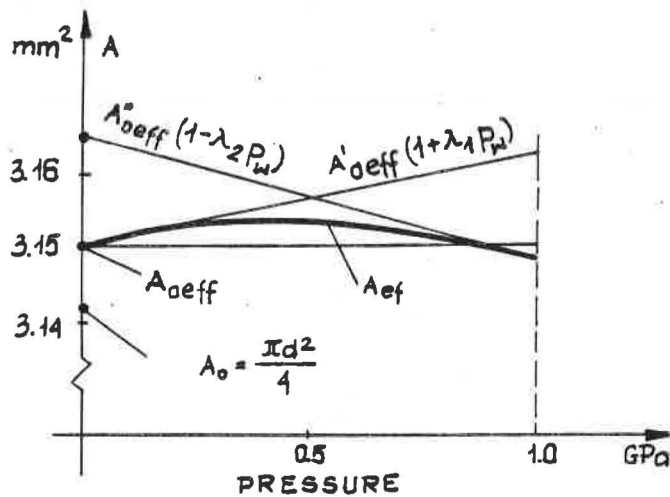


Fig.2. Pressure dependence of  $A_{eff}(p)$  with asymptotic lines  $A'_{oeff}(p)$  for simple system and  $A''_{oeff}(p)$  for reentrant system.

## THEORETICAL CALCULATIONS OF EFFECTIVE AREA

To define the effective area of the mixed operation principle dead-weight manometer, the force acting on the piston must be taken into consideration at the equilibrium condition, that is when the piston rate of fall is constant. Assuming that local deformations of piston and cylinder are determined only by the local pressure we have:

$$F_1 + F_2 = \pi b^2 p_w \left[ 1 - \frac{p_w}{E_1} (1 - \mu_1) \right] \quad (1)$$

and

$$T_1 + T_2 = \pi b^2 \left\{ p_s \left[ \frac{h_1}{b} + \left( \frac{k}{2} - k_1 \right) \frac{1}{b} \right] + (p_w - p_s) \left[ \frac{h_2}{b} + \frac{k_5}{2b} (p_w + p_s) - \frac{k_6}{b} \right] \right\} \quad (2)$$

where:  $F_1$  - is a force acting on a face of the piston  
 $F_2$  - is a force acting on a flank of the piston  
 $T_1$  and  $T_2$  viscous friction forces corresponding to the simple piston and reentrant cylinder regions respectively.  
 $p_s$  is the pressure in the intermediate, nonactive space.

In the last equation it was assumed that:

$$h_1(p) = h_1 + k p - k_1 p_w \quad \text{and} \quad h_2(p) = h_2 k_2 + k_5 p - k_6 p \quad (3)$$

where:  $k_1, k, \dots, k$  are coefficients of deformation of the piston and of cylinder [7].

All those forces balance the applied force  $F_{\text{eff}}$  acting on the rotating piston and we have:

$$A_{\text{eff}} = \pi b^2 \left\{ 1 - \alpha \frac{p_w}{p_s} + \frac{p_s}{p_w} (\tilde{h}_1 + \beta p_s) + \left( 1 - \frac{p_s}{p_w} \right) \left[ h_2 + \gamma (p_s + p_w) - \delta p_w \right] \right\} \quad (4)$$

where:  $\alpha = \frac{1-3\mu_1}{E_1}$ ,  $\beta = \frac{0.5k - k_1}{b}$ ,  $\gamma = \frac{k_5}{2b}$ ,  $\delta = \frac{k_6}{b}$ ,  $\tilde{h}_1 = \frac{h_1}{b}$ ,  $\tilde{h}_2 = \frac{h_2}{b}$

The pressure  $p_s$  is a function of nominal pressure  $p_w$ . Assuming that the pressure dependence of viscosity has a form:

$\eta = \eta_0 \exp(cp)$ , where  $\eta_0$  is a viscosity at  $p \rightarrow 0$  and  $c$  is a const. for the continuous flow rate we have:

$$Q \int_{l+l_0}^l dl = - \frac{\pi b}{6\eta_0} \int_{p_s}^0 \frac{(h_1 + k p - k_1 p_w)^3}{\exp(cp)} dp \quad (5)$$

$$Q \int_0^{l_2} dl = - \frac{\pi b}{6\eta_0} \int_{p_w}^{p_s} \frac{(h_2 + k_5 p - k_6 p_w)^3}{\exp(cp)} dp \quad (6)$$

where  $Q$  is a volumetric flow rate. From those equations one can obtain the dependence  $p_s(p_w)$ .

The results obtained by Eq. 5 and 6 are shown as the lower curves in figures 3 and 4. Having  $p_s(p_w)$  it is easy to obtain a pressure dependence of  $A_{\text{eff}}$  which is shown by the upper curves in fig. 3 and 4. The results shown in fig. 3 and 4 have been obtained for the nominal piston diameter  $d=2\text{mm}$  for a steel cylinder - steel piston as well as steel cylinder - tungsten carbide piston.

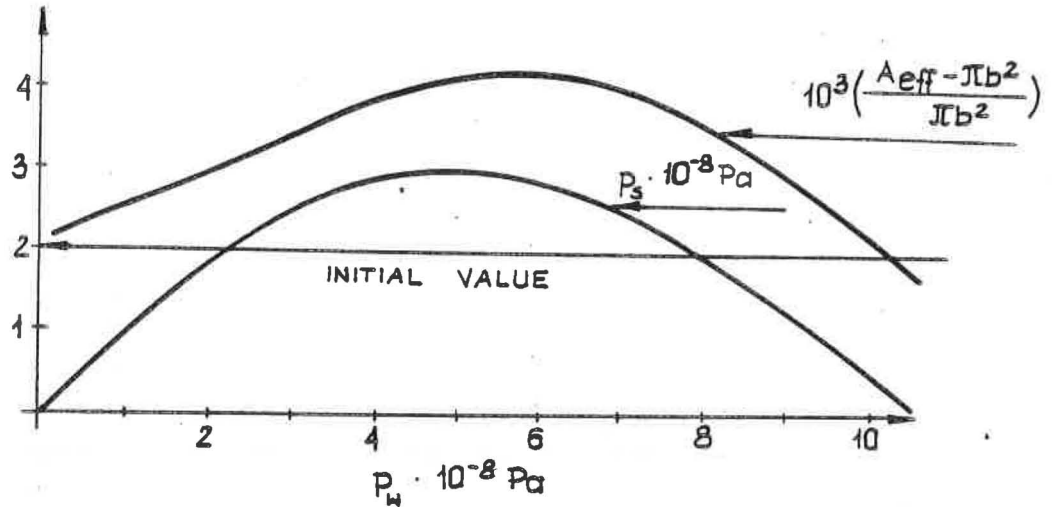


Fig.3. Dependence of effective area and intermediate pressure  $p_s$  on generated pressure  $p_w$  for LH15 steel piston with 45HMNFA steel cylinder.

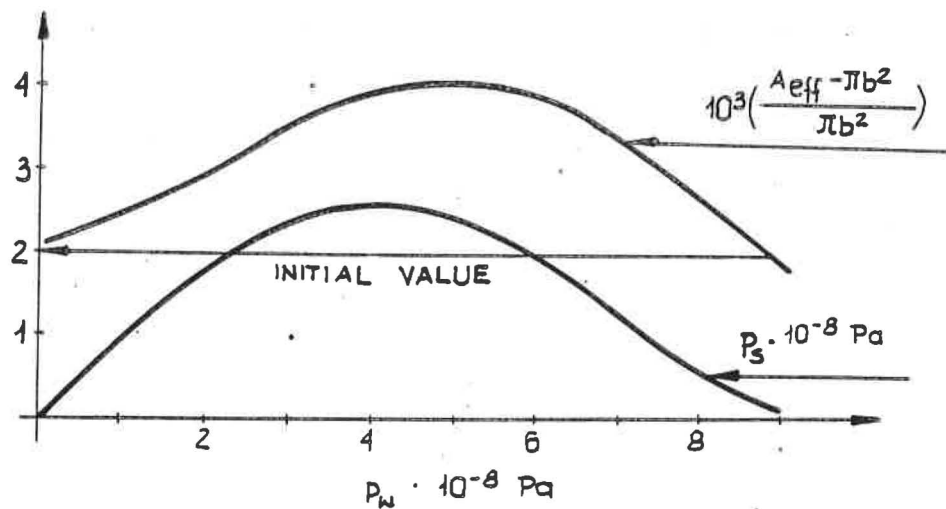


Fig.4. Dependence of effective area and intermediate pressure  $p_s$  on generated pressure  $p_w$  for Carbolloy 907 piston with 45HMNFA steel cylinder.

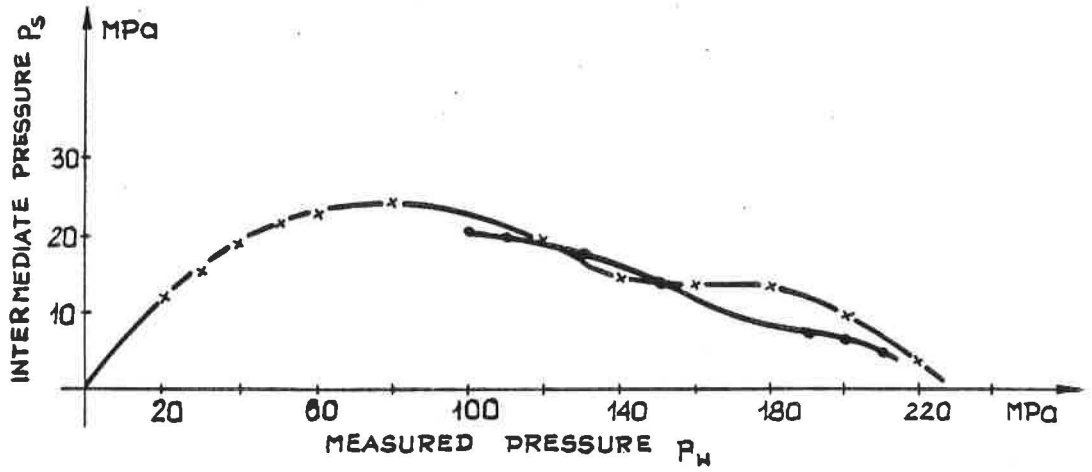


Fig.5. Intermediate pressure  $p_s$  as a function of pressure in the chamber  $p_w$  obtained on large scale model of piston cylinder assembly.

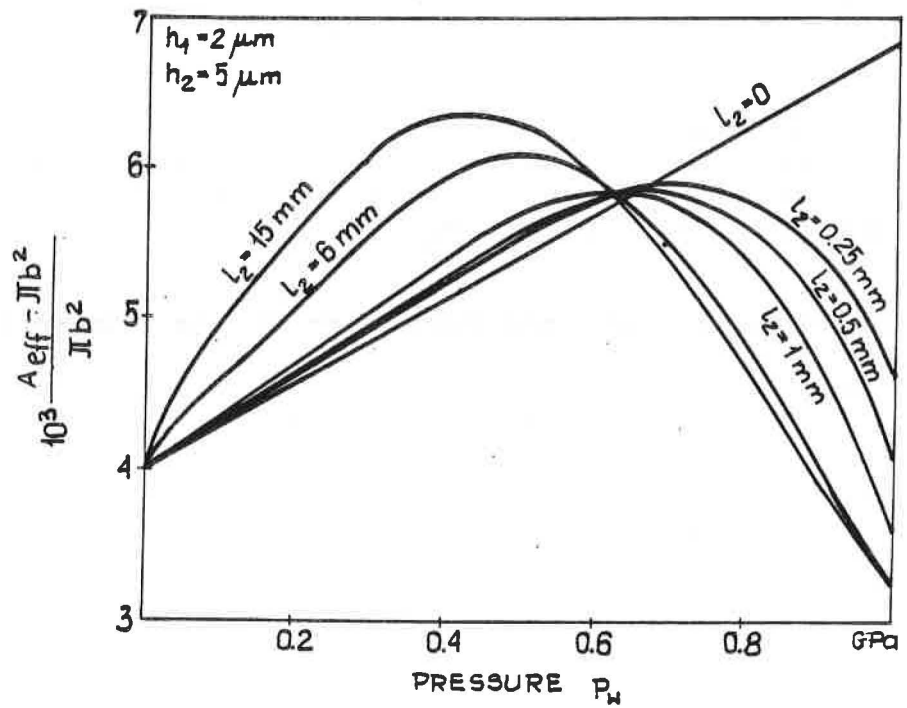


Fig.6. Pressure dependence of effective area for simple and mixed operation assemblies for various magnitude of clearance length  $l_2$ .

## EXPERIMENTAL

The results of theoretical considerations of the relation  $p_s(p)$  were confirmed in experiments where a 10 mm diameter steel piston was operated in a brass cylinder. The relation  $p_s(p)$  is shown in fig.5 and it confirms the concept of operation of the pressure standard of this type. Paper [5] contains discussion of the results of the optimization of the smallest possible change of the effective area in the pressure standard under conditions:

$$\langle A_{eff}(p) - A_{oeff} \rangle \rightarrow \min \quad \text{or} \quad \left| A_{eff}^{max} - A_{oeff} \right| \rightarrow \min \quad (7)$$

The results are shown in fig.6. It is very surprising that the optimal situation is when  $l_2 = 1\text{mm} - 6\text{mm}$ . All calculations were performed under the assumption of proportional changes of piston diameter and cylinder internal diameter as a function of effective pressure in the clearance. On the basis of those experiments the authors have built a piston gauge for pressures up to 1 GPa by installing a mixed principle assembly into the one of their earlier gauges. The cross section of this manometer is shown in fig.7. The piston gauge shown in that figure has the nominal piston area  $A_0 = \pi b^2 \text{ mm}^2$ , a rotating load and the primary clearances are  $h_1 = 3\mu\text{m}$  and  $h_2 = 10\mu\text{m}$ .

Due to the high mass of standard dead weights, the auxiliary piston of known characteristics has been applied.

The pressure fluid was Castor oil + 20% of methyl alcohol.

The maximum pressure was  $p_{max} = 1.02\text{GPa}$ , working pressure 0.99GPa and the nominal pressure increment was 0.03GPa.

The effective area was primarily determined by comparing it with a simple piston standard of  $p_{max} = 0.06\text{GPa}$ .

The lower part of characteristic was compared with the characteristics of a simple pressure standard of  $p_{max} = 0.3\text{GPa}$ .

The obtained results prove that the effective area changes parabolically with pressure.

The middle and the upper parts of characteristic were determined by means of calculations, taking under consideration the phase transition  $Hg_{L \rightarrow S}$  and the fact that at the pressure of seizing the piston in the lower cylinder, the situation is corresponding to the one in the manometer with adjustable clearance.

It was possible then to calculate with high accuracy the value of effective area at the seizing pressure, which was 1.05GPa.

## CONCLUSIONS

In the recent years it was decided to build a new pressure gauge for pressures up to 1 GPa basing on the experience gained from the use of the existing one. The following suggestions have been considered as a starting point for the design of the new gauge :

1. The system of loading will be similar to the one applied in the Harwood dead weight testers with standard loads hanging on a non rotating ram.
2. The effective area will be determined using the finite element method .

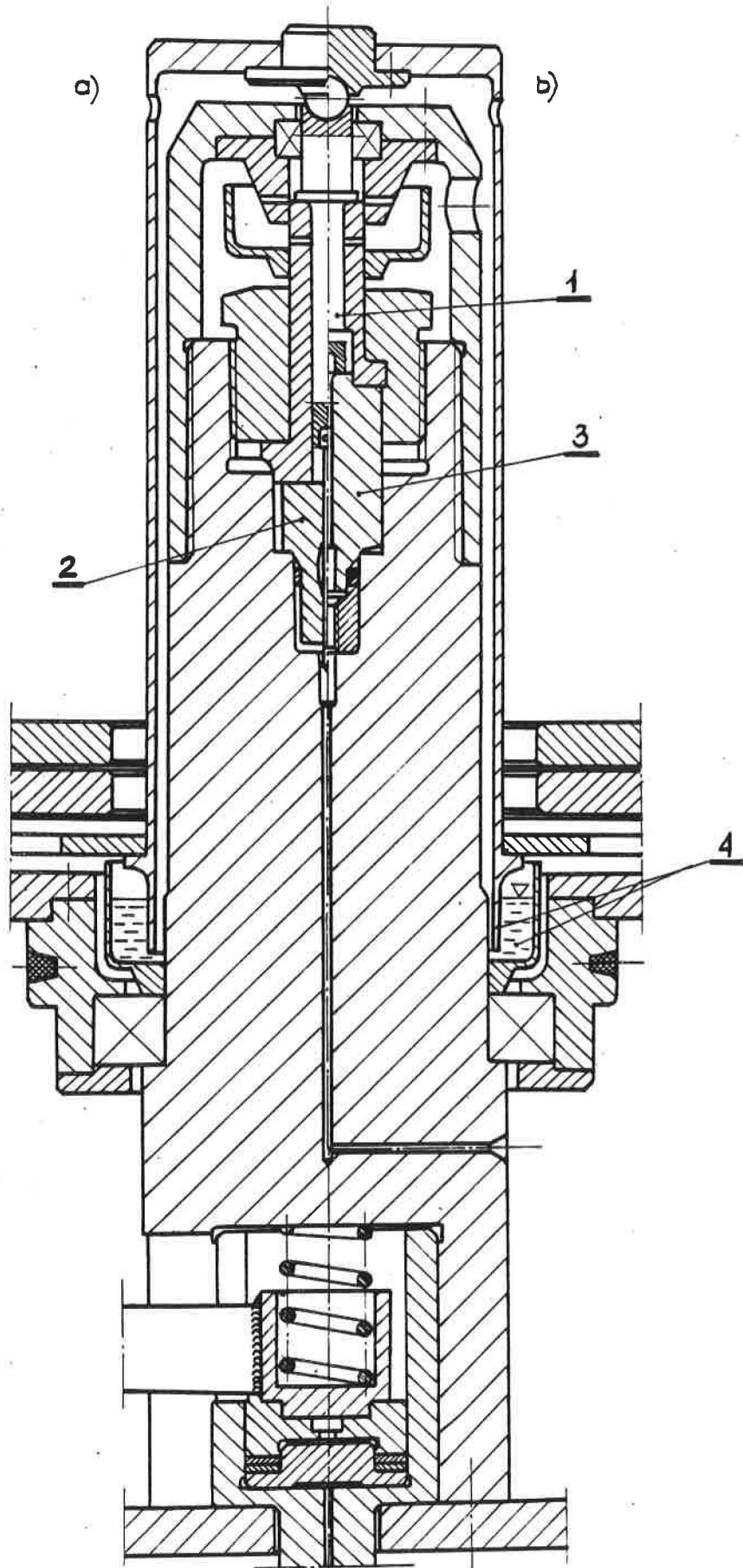


Fig.7. Cross section of the main part of manometer: a) simple version, b) new version. 1-dead-weight axis, 2-mixed operation p-c assembly, 3-simple p-c assembly, 4-angular motion hydraulic stabilizer.

#### REFERENCES

1. Wisniewski R, Rev.Sci.Instum. v53(6),920-922,(1982)
2. Wisniewski R, Polish Patent No P 194 635
3. Wisniewski R, Urbanski M, Golkowska A, High Temp.High Press. v.14,311-314,(1982)
4. Wisniewski R, Urbanski M, Mat. conf."Metrologia 86"
5. Urbanski M, Wisniewski R, Siemko A , High Pressure Techniques Conference.,Libice,Czechoslovakia,1983
6. Erenev A E, Meas. Tech. USSR (7) 18-20 (1971)
7. Zhozhovski m K, Theory and computation of instruments with packless pistons, Standartgiz,Moscow, 1966

PART 1

PISTON GAUGE

Sub-section: Piston gauges for relative and absolute gas pressure measurements



Observations of Gas Species and Mode of Operation Effects  
on Effective Areas of Gas-Operated Piston Gages

B. E. Welch, R. E. Edsinger, V. E. Bean and C. D. Ehrlich

National Institute of Standards and Technology  
Center for Basic Standards  
Gaithersburg, Maryland 20899

ABSTRACT

*The effective areas of four gas-operated piston gages have been determined by the pressure calibration technique with a state-of-the-art manometer using both helium and nitrogen in the absolute mode. For all four gages, the effective areas with nitrogen are greater than the effective areas using helium. The differences range from 4 to 28 parts-per-million.*

*Pairs of these gages have been cross-floated in both the gage and the absolute modes with helium, neon, nitrogen, argon, carbon dioxide, and krypton. For a given gas, the effective area in the absolute mode is greater than that for the gage mode. The magnitude of the difference is dependent upon the species of gas.*

Introduction

The piston gage (pressure balance, piston manometer, dead-weight tester) is widely accepted as the instrument of choice for precise pressure measurement over a wide range of pressures [1-4]. The essential features include a vertical hollow cylinder fitted with a matching piston and closed at the bottom with appropriate plumbing to admit the pressurizing fluid. The piston is loaded with known weights, floated at the reference level by applying pressure to its bottom end, and rotated to relieve friction. The pressure is calculated as the ratio of the force due to the weights and the effective area of the piston and cylinder. This calculated result is the difference in pressure applied to each end of the piston. If the top of the piston is exposed to the ambient atmosphere pressure, the piston gage is being used in the gage mode. The piston gage is operated in the absolute mode when the top of the piston is in a vacuum.

In recent studies at NIST designed to explore the limits of precision and accuracy of gas-operated piston gages, the effective areas of four piston gages have been determined in the absolute mode with both helium and nitrogen through calibration with a state-of-the-art mercury manometer. The technique is to apply a pressure which is accurately measured by the manometer to an operating piston gage with an accurately known load on the piston and then calculate the effective area of the piston gage. Also pairs of these piston gages have been cross-floated in both the absolute and gage modes with helium, neon, nitrogen, argon, carbon dioxide, and krypton. The results indicate that the effective area of a gas-operated piston gage is a function of both the gas and the mode of operation.

## Apparatus

The manometer used in these measurements was developed at NIST for the purposes of gas thermometry. It has a pressure range of 10 kPa to 130 kPa and an uncertainty of 2 parts-per-million (ppm) at the 99 percent confidence level. It was designed to be operated only in the absolute mode [5].

The four piston gages are of two types. Two have pistons and cylinders made of tungsten carbide and are commercial units, identical in make and model. They are designated as PG28 and PG29. The other two were custom made by a tool-and-die maker rather than a piston gage manufacturer. In this case the pistons and cylinders are made of tool steel. They are designated as PG30 and PG31. These two types of gages differ in area, annular space between the piston and cylinder, and surface finish of both piston and cylinder.

The commercial units were modified in two ways. The mechanisms for both the top and bottom stops were replaced with parts made of Kel-F. We thought it prudent to remove any part located above the piston that had any possibility of being difficult to clean and thus becoming a source of dirt. Also the rotative mechanism was changed such that the piston, weight stack, and cylinder could be rotated all together by means of a drive motor until the desired angular speed was reached, then the piston was floated and the cylinder was stopped allowing the piston and weight stack to coast while the pressure measurements were made. All four gages were operated in this same manner. The coasting time is an excellent indication of the cleanliness and quality of the gage [6]. All four of the gages would coast for more than 1.5 hours after an initial angular frequency of 60 revolutions per minute.

The bottom stops in all four gages were made of plastic and were coated with a conductive layer of aluminum and grounded to the cylinder to prevent the accumulation of electrostatic charges on the plastic parts as the rotating weight hangers rub against the stops. Without the conductive coatings, it is possible to accumulate sufficient electrostatic charges to generate forces on the piston corresponding to change in pressure of several ppm at atmospheric pressure [6].

All four pistons and cylinders were examined for residual magnetic fields with a Hall probe and were demagnetized as necessary [6].

The temperatures of the piston gages were measured using an array of ten thermistors attached to the stationary part of the cylinder mounting of each piston gage and calibrated in situ.

Fig. 1 is a schematic diagram of the experimental arrangement for determining the effective areas of the piston gages from pressure measurements with the manometer. Item A is a calibrated differential pressure transducer having a full range of 130 Pa and a sensitivity of  $7 \times 10^{-2}$  Pa. It was calibrated by using two piston gages, one supplying pressure to each pressure port of the transducer. The use of the transducer provides two advantages: it allows both the piston gage and the manometer to work against a limited-volume pressure system which mitigates departures from equilibrium and thus the apparatus is much easier to operate. The transducer was also used to measure small differential pressures between the manometer and the piston gage which makes the establishment of a perfect equilibrium

unnecessary. The zero was checked before each measurement by applying the identical pressure to both sides of the transducer via the bypass valve. Typically, the differential pressure for a given measurement was a fraction of a pascal. Both of these advantages provide a great saving of time and labor.

Item B of Fig. 1 is another calibrated differential pressure transducer of the same make, model, range, and sensitivity as item A and was used to measure the pressure in the bell jar surrounding the weights when operating the gage in the absolute mode. The reference side of transducer B is continuously evacuated by an ion pump.

These same two pressure transducers were used for the same purposes when cross-floating two gages in the absolute mode as shown in Fig. 2.

### Results

Each of the four piston gages was repeatedly calibrated with the manometer using helium at 27, 61, and 95 kPa and nitrogen at 27 and 95 kPa all in the absolute mode. The effective area of the piston gage was calculated using the expression

$$A = \frac{Mg}{(P - P_b - \rho gh + \epsilon) [1 + (\alpha_p + \alpha_c)(T - T_R)]} \quad (1)$$

where

- M is the total mass supported by the pressure including the weights and piston
- g is the local acceleration due to gravity
- P is the pressure at the lower mercury surface of the manometer
- $P_b$  is the pressure in the bell-jar surrounding the weights
- $\rho$  is the density of the gas
- h is the height of the reference level of the piston gage above the level of the lower mercury surface of the manometer
- $\epsilon$  is the differential pressure measured by transducer A
- $\alpha_p$  and  $\alpha_c$  are the linear thermal expansion coefficients for the piston and cylinder, respectively
- T is the temperature of the operating piston gage
- $T_R$  is the reference temperature defined to be 23 °C.

Figs. 3-6 are histograms wherein the number of measurements is plotted as a function of the deviation from the mean area, expressed in ppm, for PG28 and PG29 for both helium and nitrogen. Figs. 3 and 5 contain the helium data for PG28 and PG29 respectively at all three pressures; Figs. 4 and 6 contain the nitrogen data for each gage at both pressures. Note that the pressure at which each measurement was made is indicated. The repeatability of the data is excellent. The standard deviation of the worst case is 1.1 ppm. The effective areas for PG28 and PG29 are plotted as a function of pressure in Figs. 7 and 8. For both gages and for both gases, within the sensitivity of the measurements, the areas are independent of pressure over the range of the calibration. And for both gages the effective area with nitrogen is nominally 4 ppm greater than the area when using helium.

Figs. 9-12 are the histograms of the deviation from the mean area for PG30 and PG31. Figs. 9 and 11 show the helium data and Fig. 10 and 12

show the nitrogen data. It is not meaningful to attempt to combine the data for all three pressures for a given gas as was done in Figs. 3-6 since the effective areas of PG30 and 31 are definitely dependent upon the pressure as is shown in Figs. 13 and 14. Again, as is the case for PG28 and 29, the effective areas when using nitrogen is greater than when using helium, but in this case, the difference ranges from 20 to 28 ppm for PG30 and 19 to 25 ppm for PG31 over the pressure range of the measurements.

In the cross-float measurements, PG28 was compared with PG30 and PG31 in both the gage and absolute modes with helium, neon, nitrogen, argon, carbon dioxide, and krypton, all at a pressure of 100 kPa. In addition, helium, nitrogen, and carbon dioxide were used with cross-floats between PG28 and PG30 at 79 kPa and 127 kPa. The effective areas of PG30 and 31 were calculated using the expression

$$A_T = \frac{M_T g}{\frac{M_R g + P_{bR} - P_{bT} + \epsilon}{A_R}} \quad (2)$$

where

- $A_T$  is the effective area of the piston gage under test, either PG30 or PG31
- $M_T$  is the total mass supported by the pressure on the test gage
- $g$  is the local acceleration due to gravity
- $M_R$  is the total mass supported by the pressure on the reference gage, PG28
- $A_R$  is the effective area of the reference gage and is assumed to be invariant
- $P_{bR}$  is the bell jar pressure of the reference gage
- $P_{bT}$  is the bell jar pressure of the test gage
- $\epsilon$  is the differential pressure as measured by transducer A between the two piston gages.

The relative changes in these effective areas at three different pressures are listed in Table 1. In the first column, the gage-mode effective areas are compared with the gage-mode helium effective areas for each pressure which demonstrates that in the gage mode, the effective area is gas dependent. In the second column, the absolute mode effective areas are compared with the absolute mode helium effective areas for each pressure which demonstrates that in the absolute mode, the effective area is also gas dependent but to a greater degree. In the third column, the absolute mode effective area is compared with the gage mode effective area for each gas. The absolute mode effective area is generally greater than the gage mode effective area by an amount that varies with the gas used. The data for PG30 shows all of these effects to be a function of pressure.

The rates at which the floating piston of the operating piston gage sinks into the cylinder (fall rate) are also listed in Table 1 for each gage, gas, and pressure.

### Discussion

We have expressed our results as the relative changes of effective areas. These observed changes are apparently due to the change in the

gas flow conditions in the annulus as a function of gas and mode-of-operation.

The description of gas flow can be divided into three regions; the division being specified by three ranges of values of a dimensionless parameter known as the Knudsen number. The Knudsen number is defined as the ratio of the mean free path of a gas molecule,  $\lambda$ , to a characteristic dimension of the channel through which the gas is flowing [7]. For a piston gage, the characteristic dimension is  $r_2 - r_1$  where  $r_2$  is the cylinder bore radius and  $r_1$  is the piston radius. Practical assignments of limits to the Knudsen numbers and the flow conditions which pertain to them are:

$$\begin{aligned} \lambda/(r_2 - r_1) < 0.01, & \text{ the flow is viscous} \\ \lambda/(r_2 - r_1) > 1.00, & \text{ the flow is molecular} \\ 0.01 < \lambda/(r_2 - r_1) < 1.00, & \text{ the flow is in the transition range} \\ & \text{ between viscous and molecular flow.} \end{aligned}$$

Table 2 lists the mean free paths for the six gases and Table 3 lists the approximate value for the Knudsen numbers appropriate for the present experimental conditions. For the absolute mode measurements, the pressure at the top of the piston and for some unknown extent down into the annulus is on the order of 1 Pa and the flow condition is molecular while the pressure under the piston and for some unknown extent up the annulus is on the order of 27 to 127 kPa and the flow is in the transition range. For the gage-mode measurements, the pressure at the top of the piston is on the order of 100 kPa while the pressure under the piston ranges from 127 to 227 kPa. The flow is in the transition range all along the piston's working length for the gage-mode measurements.

There are no general derivations of flow equations in the transition range based on first principles. There are, however, methods of extending equations based on viscous flow into the transition region by adding terms which are proportional to the mean free path [9-11]. There is a problem with this approach. Since the mean free path is inversely proportional to the pressure, we must know the details of the pressure gradient in the annulus and have some method of selecting the appropriate mean free path for the calculations. The equations currently found in the literature for calculating the pressure in the annulus as a function of piston working length are based on viscous flow theory [12,13] and have not been demonstrated to be appropriate for the transition region. The next logical step to fully understand these results is to develop a proven method to determine the pressure profile in the annulus.

The fall rate data in Table 1 are curious in that the gage mode fall rates are greater than those for the absolute mode with the exception of the He data at all pressures and Ne data for PG31 at 100 MPa.

Based on flow measurements for several gases in the transition region by Porodnov, Suetin, Borisov, and Akinshin [14] and, Maegley and Berman [15], we would expect the fall rates for a given gage to be nearly equal for all six gases in the pressure range where the mean free path is less than about  $2 \times 10^{-6}$  m (about 4 kPa and above). As the pressure decreases and the mean free path increases, we would expect the fall rates to become increasingly dependent upon the species of gas. Ref. 15 shows a plot representing flow measurements in an annulus wherein

the ordinate is proportional to flow and the abscissa proportional to the reciprocal of the mean free path. There is a very pronounced minimum in the curve in the region of  $\lambda = 2 \times 10^{-6}$  m known as the Knudsen minimum. Whether or not the fall rates for the gage mode would be expected to be greater than those for the absolute mode would depend upon the effective mean free paths pertaining to those measurements in relation to the Knudsen minimum.

### Conclusion

Our measurements have shown that the effective area of a gas-operated piston gage is a function of the gas used and depends upon whether the gage is used in the absolute or gage modes. Progress toward a theoretical understanding of these effects would be greatly aided by a knowledge of the pressure in the annulus space as a function of the piston's working length.

### REFERENCES

1. M. K. Zhokhovskiy, Teoriya i Raschet Priborov s Neuplotnennym Porshnem, (Moscow, 1959). English translation, Theory and Design of Instruments with Packing-free Pistons, JPRS 27,722, (Clearinghouse for Federal Scientific and Technical Information, Superintendent of Documents, U.S. Government Printing Office, Washington D. C.).
2. P.L.M. Heydemann and B.E. Welch, Experimental Thermodynamics, Volume II: Experimental Thermodynamics of Non-reacting Fluids, Edited by B. Le Neindre and B. Vodar. [Butterworths, London, 1975) pp 147-202.
3. S. Lewis and G.N. Peggs, The Pressure Balance: A Practical Guide to its Use (National Physical Laboratory, Teddington, England, 1979).
4. R. S. Dadson, S. L. Lewis, and G. N. Peggs, The Pressure Balance, Theory and Practice, (Her Majesty's Stationery Office, London, 1982).
5. L. A. Guildner, H. F. Stimson, R. E. Edsinger, and R. L. Anderson, Metrologia, 6, 1 (1970).
6. B. E. Welch, L. A. Guildner, and V. E. Bean, Advances in Test Measurement, 22, 303 (1985).
7. S. Dushman and J. M. Lafferty, Scientific Foundations of Vacuum Technique, (John Wiley and Sons, New York, 1962) p 80-81.
8. J. O. Hirschfelder, E. F. Curtis, and R. B. Bird, Molecular Theory of Gases and Liquids, (John Wiley and Sons, New York, 1964), p 10 and p 528.
9. S. Dushman and J. M. Lafferty, op. cir. pp 35-36, pp. 104-111.

10. S. L. Thompson and W. R. Owens, *Vacuum* 25, 151 (1975).
11. E. H. Kennard, *Kinetic Theory of Gases*, (McGraw-Hill, New York, 1938) pp 292-300.
12. A. H. Bass, *J. Phys. E. Sci. Instrum.* 11, 682 (1978).
13. R. S. Dadson et al., op. cit. p. 32.
14. B. T. Porodnov, P. E. Suetin, S. F. Borisa, and V. D. Akinshin, *J. Fluid Mech.*, 64, 417 (1974).
15. W. J. Maegley and A.S. Berman, *The Physics of Fluids*, 15, 780 (1972).

Table 1. Fall rate data for PG28, PG30, and PG31, and relative change of areas resulting from cross-floats between PG28 and PG30 and between PG28 and PG31. The effective areas are denoted as follows: A(g), gage mode; A(g,He), gage mode using helium; A(a), absolute mode; A(a, He), absolute mode with helium.

Gage	P kPa	Gas	Relative change in area, ppm			fall rates mm/min	
			$\frac{A(g)-A(g,He)}{A(g,He)}$	$\frac{A(a)-A(a,He)}{A(a,He)}$	$\frac{A(a)-A(g)}{A(g)}$	gage	absolute
PG30	79	He	0	0	-.4	1.39	1.71
		N <sub>2</sub>	3.7	20.1	16.0	1.31	.99
		CO <sub>2</sub>	6.2	29.6	23.0	1.38	1.18
PG30	100	He	0	0	2.7	1.55	1.75
		Ne	2.3	4.7	5.1	.95	.92
		N <sub>2</sub>	4.9	21.4	19.2	1.41	1.14
		A	5.0	20.1	18.6	1.13	.88
		CO <sub>2</sub>	5.0	30.1	28.6	1.54	1.44
		Kr	7.4	27.8	23.1	1.05	.86
PG30	127	He	0	0	2.8	1.84	1.96
		N <sub>2</sub>	3.3	22.9	22.3	1.58	1.42
		CO <sub>2</sub>	4.5	32.4	30.6	1.89	1.73
PG31	100	He	0	0	2.8	2.21	2.52
		Ne	2.0	6.5	7.4	1.37	1.59
		N <sub>2</sub>	3.7	23.4	22.6	2.11	1.92
		A	3.2	21.8	21.5	1.56	1.49
		CO <sub>2</sub>	4.6	32.8	31.1	2.34	1.92
		Kr	4.4	27.6	26.1	1.34	1.18
PG28		He				.77	.88
		Ne				.49	.41
		N <sub>2</sub>				.73	.45
		A				.51	.37
		CO <sub>2</sub>				.65	.43
		Kr				.47	.29

Table 2. Mean free path,  $\lambda$ , [8] at 1 Pa

Gas	$\lambda, 10^{-4} \text{ m}$
He	141.8
Ne	120.9
N <sub>2</sub>	69.4
A	80.5
CO <sub>2</sub>	58.9
Kr	72.2

Table 3. Approximate Knudsen numbers for six gases at 3 pressure with the assumed clearance between piston and cylinder equal to  $2 \times 10^{-6}$  meters

P, Pa	He	N <sub>e</sub>	N <sub>2</sub>	A	CO <sub>2</sub>	Kr	flow condition
1	7000	6000	3000	4000	3000	4000	molecular
$1 \times 10^5$	.07	.06	.03	.04	.03	.04	transition
$2 \times 10^5$	.04	.03	.02	.02	.02	.02	transition

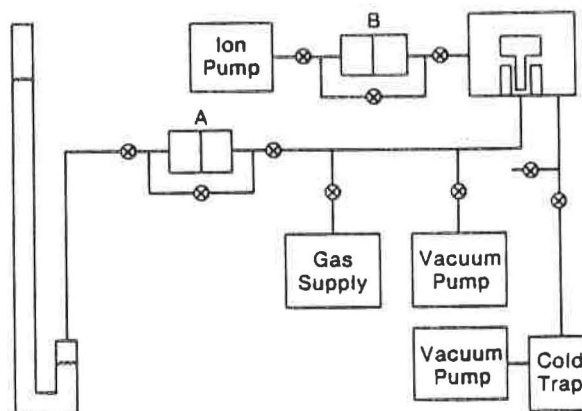


Fig. 1. Schematic diagram of the pressure system connecting the manometer to the piston gage. Items A and B are calibrated differential pressure transducers. Valves are shown as circled X's.

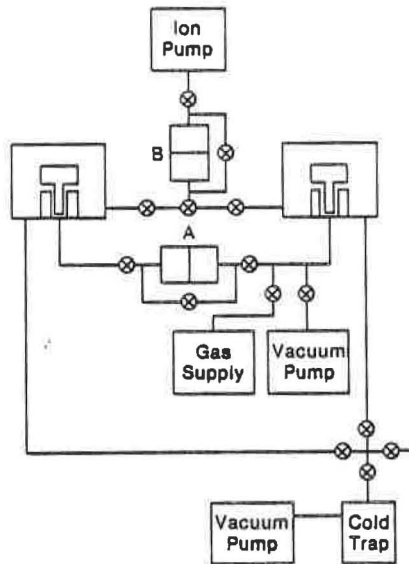


Fig. 2. Schematic diagram of the pressure system used to cross-float two piston gages. Items A and B are calibrated differential pressure transducers. Valves are shown as circled X's.

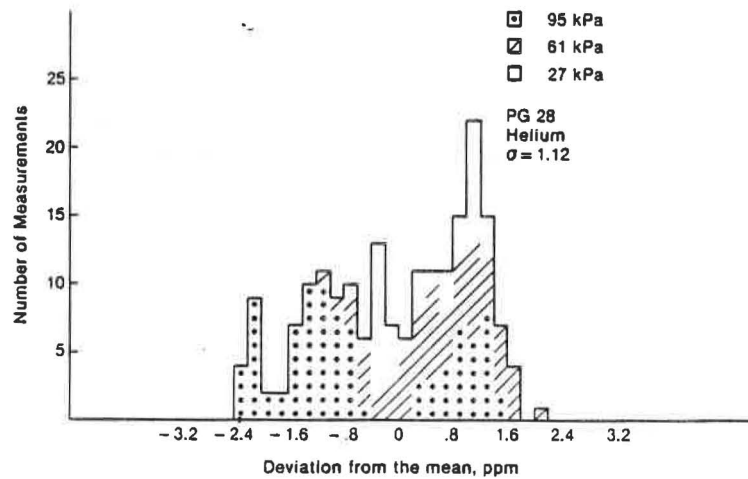


Fig. 3. Histogram showing the deviation from the mean of measured areas for PG 28 with helium at 27, 61, and 95 kPa.

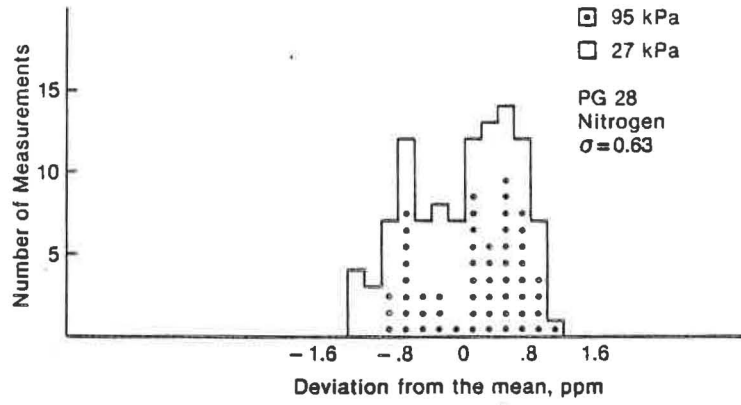


Fig. 4. Histogram showing the deviation from the mean of measured areas for PG 28 with nitrogen at 27 and 95 kPa.

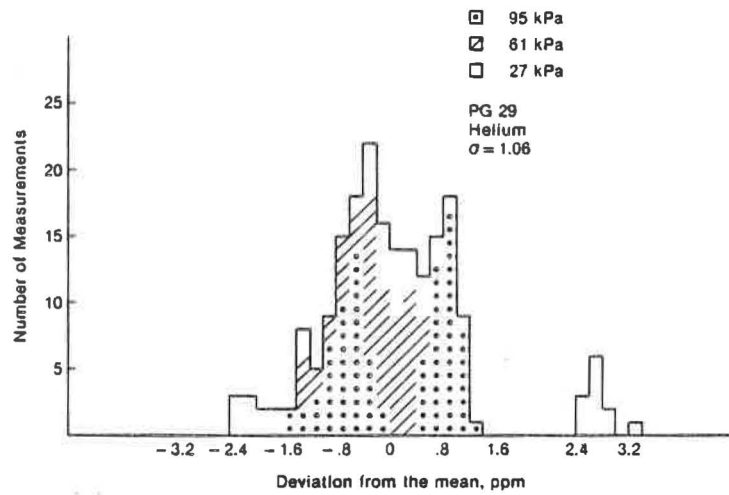


Fig. 5. Histogram showing the deviation from the mean of measured areas for PG 29 with helium at 27, 61, and 95 kPa.

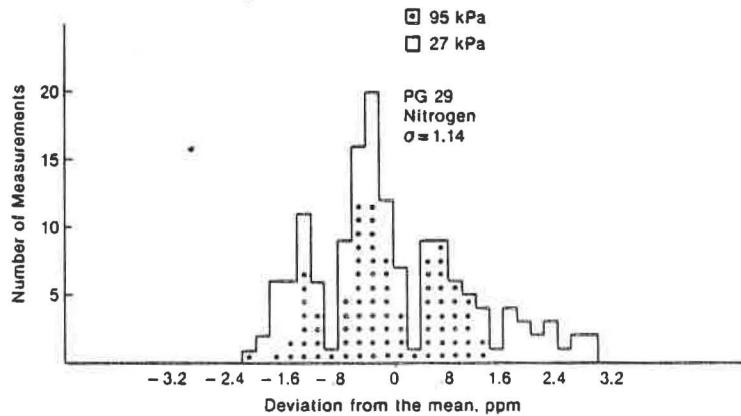


Fig. 6. Histogram showing the deviation from the mean of measured areas for PG 29 with nitrogen at 27 and 95 kPa.

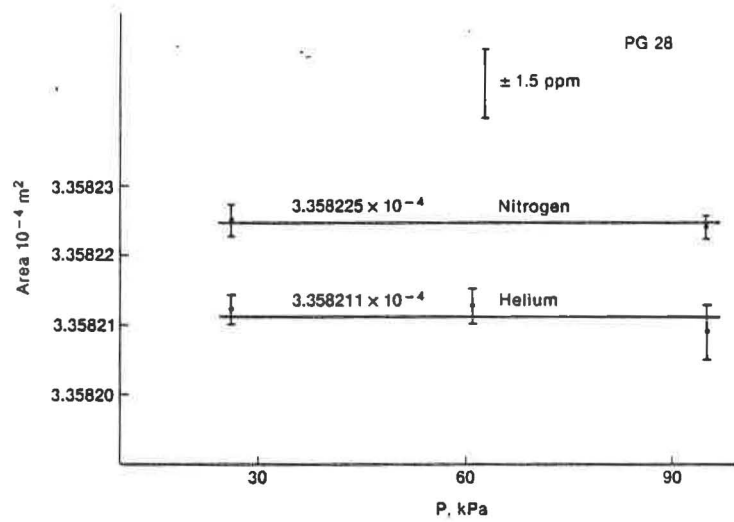


Fig. 7. Areas plotted as a function of pressure for PG 28 with helium and nitrogen.

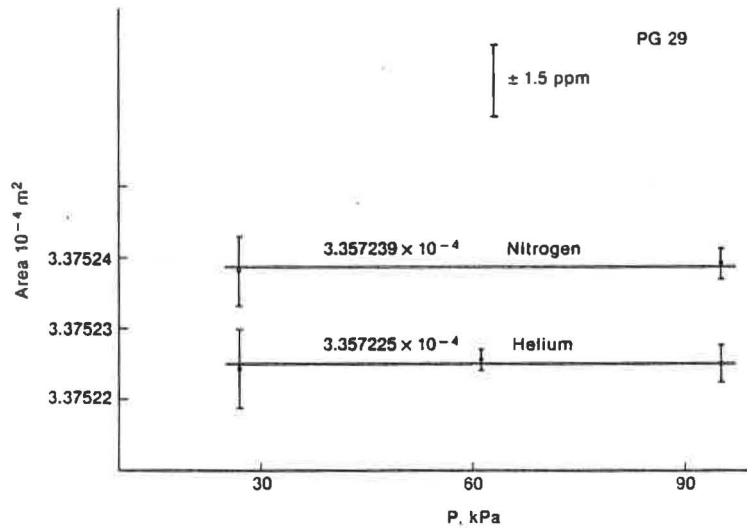


Fig. 8. Areas plotted as a function of pressure for PG 29 with helium and nitrogen.

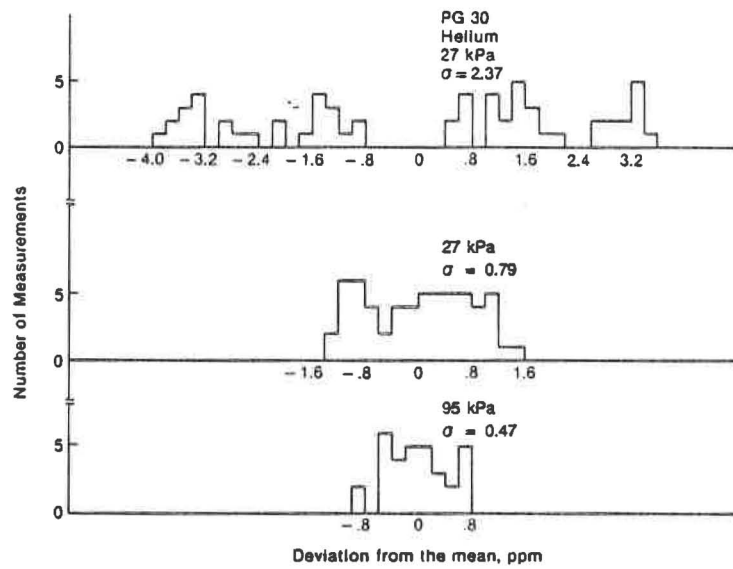


Fig. 9. Histograms showing the deviation from the mean of measured areas for PG 30 with helium at 27, 61, and 95 KPa.

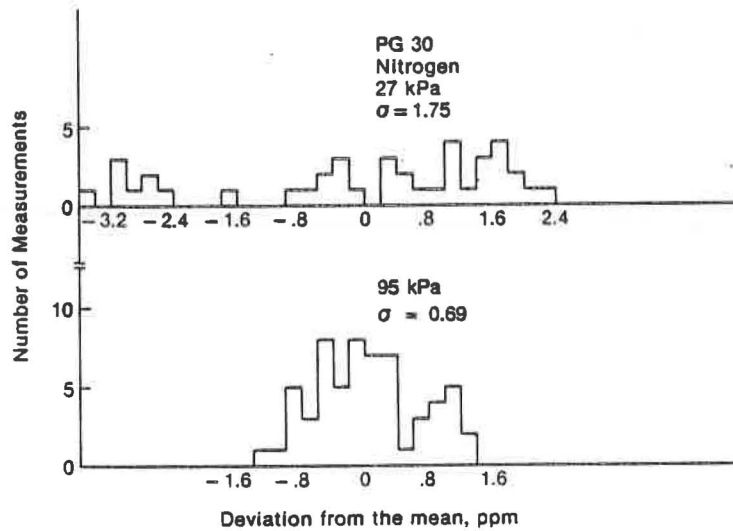


Fig. 10. Histograms showing the deviation from the mean of measured areas for PG 30 with nitrogen at 27 and 95 kPa.

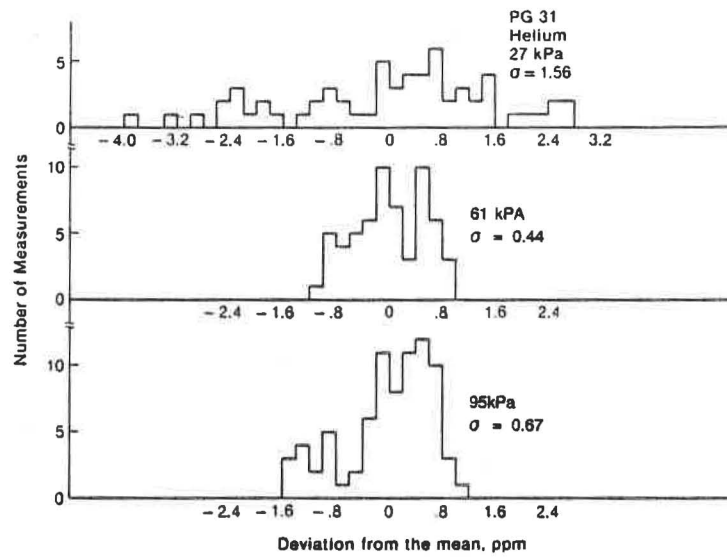


Fig. 11. Histogram showing the deviation from the mean of measured areas for PG 31 with helium at 27, 61, and 95 kPa.

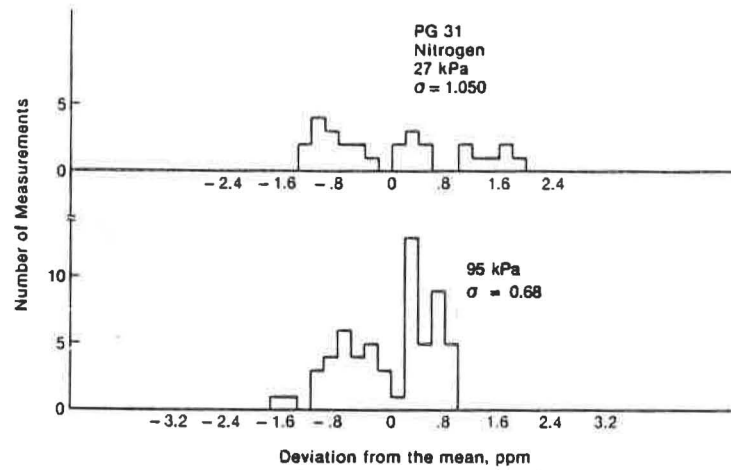


Fig. 12. Histogram showing the deviation from the mean of measured areas for PG 31 with nitrogen at 27 and 95 kPa.

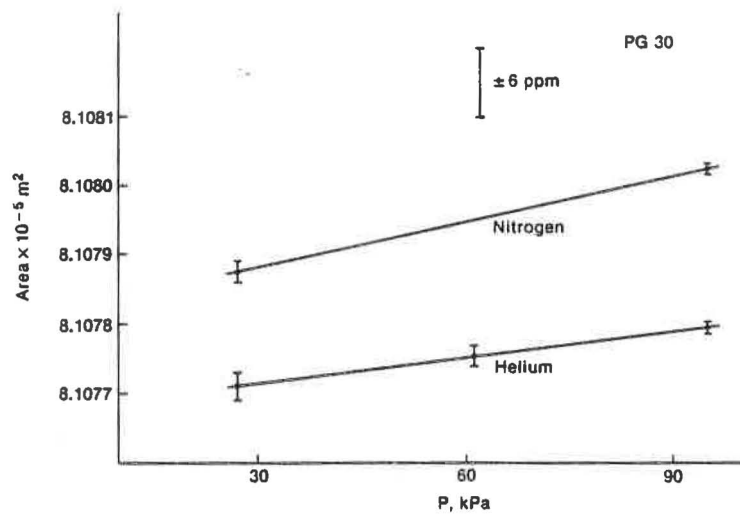


Fig. 13. Areas plotted as a function of pressure for PG 30 with helium and nitrogen.

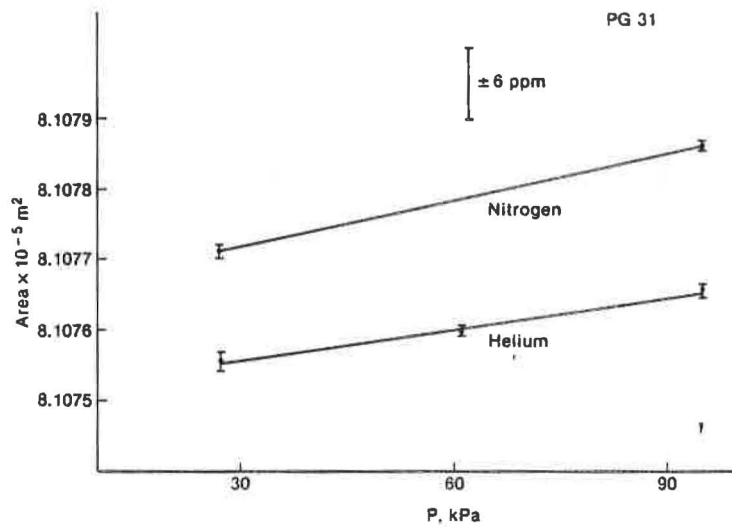


Fig. 14. Areas plotted as a function of pressure for PG 31 with helium and nitrogen.

PRIMARY BAROMETERS AND THE BIPM INTERNATIONAL INTERCOMPARISON IN THE PRESSURE REGION 10 kPa TO 110 kPa.

P.R.STUART.

National Physical Laboratory, Teddington, Middlesex, TW11 OLW, U.K.

ABSTRACT

An international intercomparison in the pressure range 10 to 110 kPa has been organised by the Medium Pressure Working Group of the Consultative Committee for Mass of the International Bureau of Weights and Measures.

The paper begins with a review of the mercury primary barometers used by some of the participants. The main differences of design involve:

- i) the method adopted for the measurement of the mean heights of the mercury surfaces; this should minimize of the effects of external vibrations
- ii) the minimization of tilting when mercury is transferred from one column to another when the applied pressure is changed
- iii) methods of stabilizing and measuring the mean temperature of the mercury.

This review is followed by a description of the transfer standard used in the intercomparison - a specially constructed gas-operated pressure balance. The results obtained from the first 5 participants indicate that systematic differences exist between them which are higher than expected from the claimed uncertainties.

## 1. Introduction

The BIPM Medium Pressure Working Group has the responsibility for arranging international collaborative projects with the aim of improving pressure measurement standards in the pressure range 1 kPa to 1 MPa. The first activity of the Group has been to arrange an international intercomparison in the range 10 kPa to 110 kPa. The pilot laboratory is the NPL (UK).

Before describing the methods used in the intercomparison and the results obtained so far, it will be useful to review some of the primary standards being intercompared, taking as examples those of the 8 laboratories which are represented on the Working Group. In all these laboratories the primary standards are mercury U-tube barometers, although in some countries pressure balances, otherwise known as piston gauges or deadweight testers, are also used or are being seriously considered [1,2].

## 2. Primary Barometers

All designers of primary barometers have certain problems in common. These include:

- i) the measurement of the difference between the mean heights of the mercury surfaces, which will inevitably be shimmering due to externally generated vibrations
- ii) minimising the tendency of the mercury columns to tilt as a result of possible movement of the centre of mass when mercury is transferred from one column to another
- iii) the stabilisation and measurement of the mean temperature of the mercury, which has a very significant influence on its density.

At most long-established national standards laboratories the value of  $g$ , the acceleration due to gravity, is known to better than 1 ppm, so this factor adds a relatively minor contribution to the total uncertainty and is therefore not a major problem.

The NPL Long Range Primary Barometer is shown schematically in figure 1. Floats in the two limbs of the U-tube have internal diameters of 45 mm, so the mercury surfaces are essentially flat near the axes and form

mirrors in two interferometers which share a single helium-neon laser light source. Changing the applied pressure over the full range gives a fringe count of approximately 2.5 million. The floats carry convex lenses which focus the light beams on to the mercury surfaces, thereby ensuring that, even if there are slight surface ripples due to vibrations, the reflected beams are returned to the beam-splitter rather than being deflected out of the vertical [3]. The resulting reduced sensitivity to vibrations has the advantage that it has been possible to mount the manometer on a rigid base which does not tilt significantly when mercury is transferred from one column to another. The mercury in the manometer is part of a batch the density of which was measured by Cook [4,5]. By using 2 platinum resistance thermometers and a 3-stage temperature control system, the mercury temperature may be estimated to within  $\pm 5\text{mK}$ , enabling the temperature contribution to the uncertainty of density to be no more than  $\pm 1$  ppm.

The primary barometer of the BIPM [6], the second laboratory to participate in the intercomparison, is shown schematically in figure 2. It is mounted on anti-vibration springs and to avoid tilting when mercury is transferred as the applied pressure is changed, one column is placed at the centre, surrounded by 3 interconnected, equilaterally spaced, columns. Vibration isolation is good enough for the mercury surfaces to be used as simple mirrors in a white-light interferometer which also incorporates corner cubes mounted on a carriage which is moved horizontally by the observer to compensate for the change in optical path length due to the movement of the mercury. The movement of the carriage is measured against an Invar scale.

The third participant in the intercomparison was INM, France. Their barometer [7] is shown schematically in figure 3. Two reservoirs, one fixed and one moveable, are connected by a flexible tube. The moveable reservoir may be traversed vertically, by means of a lead-screw, until pre-determined capacitances are obtained between the mercury surfaces and capacitor electrodes within the reservoirs. The moveable reservoir has a corner-cube fixed to it, so that its position may be measured interferometrically. The 4th participant, CSMU in Czechoslovakia, has concentric columns and also uses the capacitance technique with a laser interferometer above the moveable axial reservoir [8].

The 5th participant, NML in Australia, uses an optical reflection system

with retro-reflectors similar in many ways to those used at NPL [9]. However, unlike NPL, the 2 mercury surfaces are part of the same interferometer rather than parts of 2 separate interferometers.

The 6th participant, NBS in the USA, has used 2 completely different standards, an ultrasonic manometer and a piston gauge (pressure balance), the calibration of which is traceable to the primary barometer developed by Guildner et al [10]. In the latter, the positions of the mercury surfaces are determined by the capacitance method and calibration is achieved by supporting the moveable reservoir on gauge blocks. The columns are in the configuration of a "W", so that the centre of mass does not change when the applied pressure is changed (figure 4).

The other NBS standard is an ultrasonic manometer [11], also in the form of a "W". The difference in heights between the mercury surfaces is calculated from the difference in transit times of ultrasonic pulses which are generated by piezoelectric transducers at the bases of the columns and reflected back by the surfaces.

The next laboratory to participate will be NRLM, Japan, where the movement of the mercury surfaces in the primary barometer is measured by means of a white-light interferometer as at BIPM [12]. The movement of the carriage is measured with a HeNe laser interferometer. After NRLM will be the primary barometer at IMGC, Italy, which is based on a commercial version of the primary barometer at BIPM.

The estimated total uncertainties of all the barometers described above lie within the range  $0.1 \pm (4 \times 10^{-6} \times p)$  Pa to  $0.7 \pm (8 \times 10^{-6} \times p)$  Pa, ie between about 5 and 15 ppm at 100 kPa.

### 3. The Transfer Standard

Primary barometers may have total measurement uncertainties of as little as  $0.1 \pm (4 \times 10^{-6} \times p)$  Pa, and a transfer standard therefore needs to have a repeatability significantly better than this if it is to be suitable for an intercomparison. A gas-operated pressure balance is capable of meeting this specification, provided that it incorporates a specially selected piston-cylinder assembly mounted on a base of special design. No commercially available device is entirely suitable,

particularly in respect of the speed of evacuation of the bell jar, the measurement of the residual vacuum obtained therein and the measurement of the temperature of the piston-cylinder assembly. To meet the requirements of the intercomparison a special pressure balance base was constructed by the NML in Australia (figure 5). It incorporates a mechanism for changing the ring masses within each of 2 interleaved sequences of 5 combinations without breaking the vacuum, thereby reducing the time between observations and hence reducing random errors. The piston-cylinder assembly is a selected commercial unit loaned by NBS. The anodised surface of the aluminium mass-carrier had to be machined off and replaced by a plated coating in order to reduce mass variations due to the sorption and desorption of water vapour. The thermal-conductivity vacuum gauge, the thermistor thermometer and a volume displacer for adjusting the pressure were provided by NPL.

The reproducibility of the transfer standard was assessed at NPL using the Long-Range Primary Barometer. The mean of the standard deviations of the pressures generated for the 10 ring-mass combinations was only 0.08 Pa. Following calibration at BIPM and INM the transfer standard was returned to NPL, where the effective cross-sectional area of the piston-cylinder assembly was redetermined. It was found to be within 0.6 ppm of the initial value, indicating an impressive degree of stability.

#### 4. Procedure for the Intercomparison

A "petal" form of intercomparison has been adopted; the first loop involved 2 laboratories and there are 5 in the second loop. So far, all the participants have carried out measurements in the absolute mode; measurements in the gauge mode are optional. Participants are required to measure the pressures generated by the transfer standard with the various ring-mass combinations for 2 increasing and 2 decreasing pressure sequences for both clockwise and counterclockwise rotations. Next, the participant calculates the pressures that would have been obtained at 20 °C and standard gravity. Finally, the pilot laboratory calculates the effective area of the piston-cylinder assembly at each nominal pressure, using the values it has previously obtained for the masses of the floating elements. Each time a new set of results is received by the pilot laboratory it is stored on a computer, following which an analysis can be promptly produced and sent to all the previous

participants.

## 5. Results of the Intercomparison

The results obtained in the intercomparison prior to March 1988 are shown in figure 6. No scale markings are given on the ordinate axis because the intercomparison is "blind", i.e participants are not permitted to see any results until after they have completed their own observations.

If a participant's values of effective area fall on a horizontal line but are significantly above or below the mean values then a pressure-proportional systematic error is indicated. If the results fall on a curve which deviates increasingly from the horizontal as lower pressures are approached then a zero-error is indicated. Deviations of both types can of course occur simultaneously.

The results show convincingly that systematic differences of both kinds have occurred, and the intercomparison is therefore fully justified. Another beneficial consequence of the intercomparison is that it has prompted many laboratories to overhaul and improve their instruments prior to participating.

## 6. References

1. RIETY, P and LEGRAS, J.C. Bull. BNM 70, 3-7 (1987)
2. RIETY, P. Bull. BNM 70, 8-16 (1987)
3. BENNETT, S.J., CLAPHAM, P.B., DABORN, J.E. and SIMPSON, D.I. J.Phys.E. 8, 5 (1975)
4. COOK, A.H. and STONE, N.W.B. Phil. Trans. Roy. Soc., Series A, 250, 279-323 (1957)
5. COOK, A.H. Phil. Trans. Roy. Soc., Series A, 254, 125-154 (1961)
6. BONHOURE, J. and TERRIEN, J. Metrologia 4, 59-68 (1968)
7. RIETY, P. and LECOLLINET, P. Bull. BNM 28, 13-21 (1977)
8. SKROVANEK, T., LANEK, D. and KEPRT, A. Ceskoslovenska standardizace c 11, 442-448 (1978)
9. HARRISON, E.R., HATT, D.J., PROWSE, D.B. and WILBUR-HAM, J. Metrologia 12, 115-122 (1976)
10. GUILDNER, L.A., STIMSON, H.F., EDSINGER, R.E. and ANDERSON, R.L.

Metrologia 6, 1-18 (1970)

11. HEYDEMANN, P.L.M., TILFORD, C.R. and HYLAND, R.W.

J. Vac. Sci. Technol. 14, 597 (1977)

12. KANEDA, R., SUDO, S. and NISHIBATA, K. Bull. NRLM 9, 24-36 (1964)

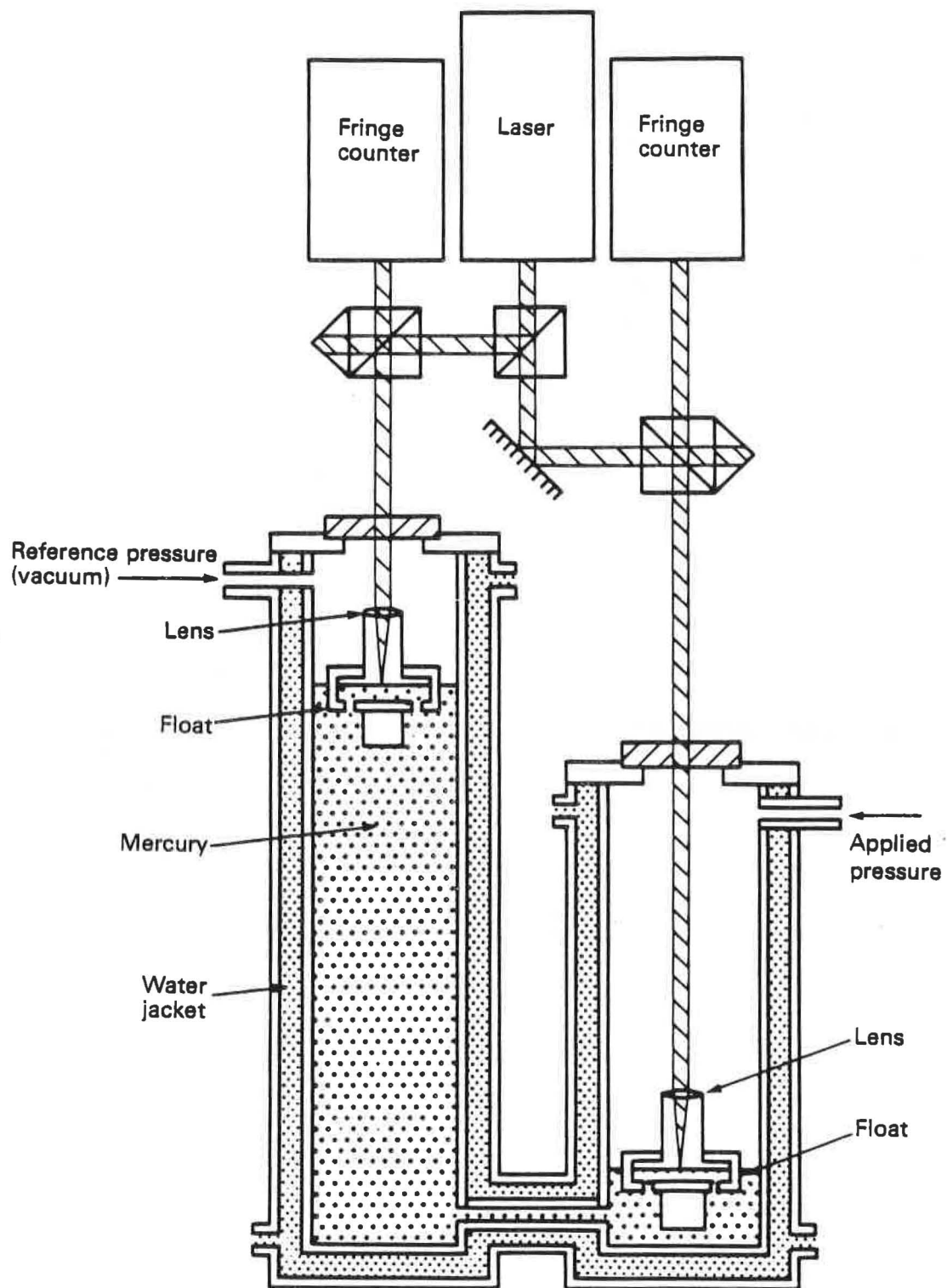


Fig.1 The NPL Long-Range Primary Barometer

Fig.2 Principle of the BIPM primary barometer

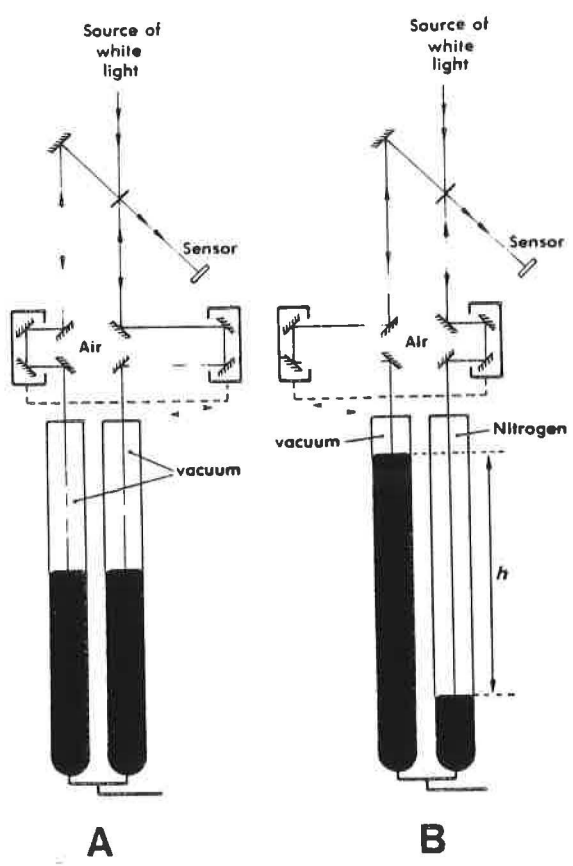


Fig.3 Schematic diagram of the INM primary barometer

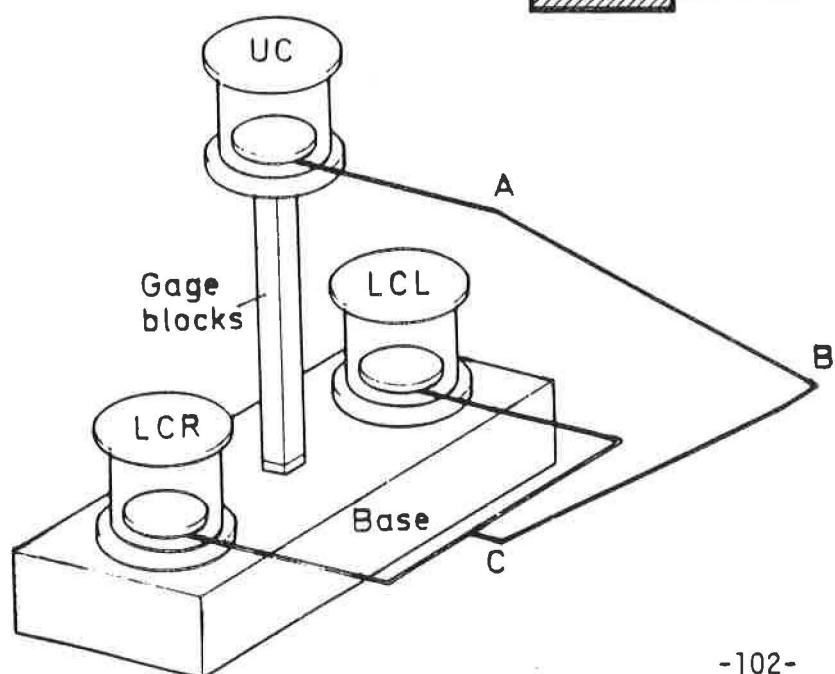
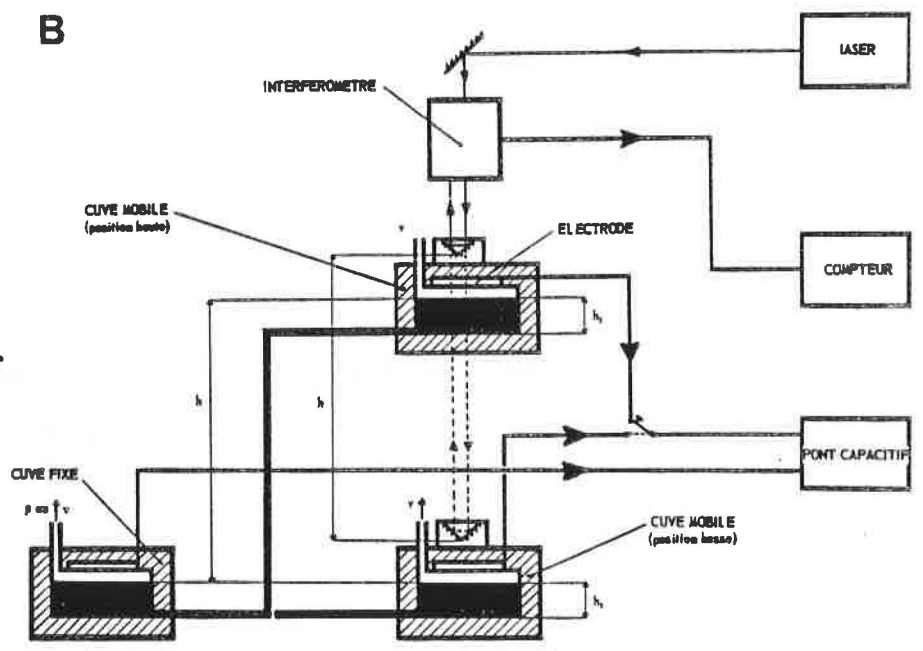


Fig.4 The configuration of the NBS primary barometers

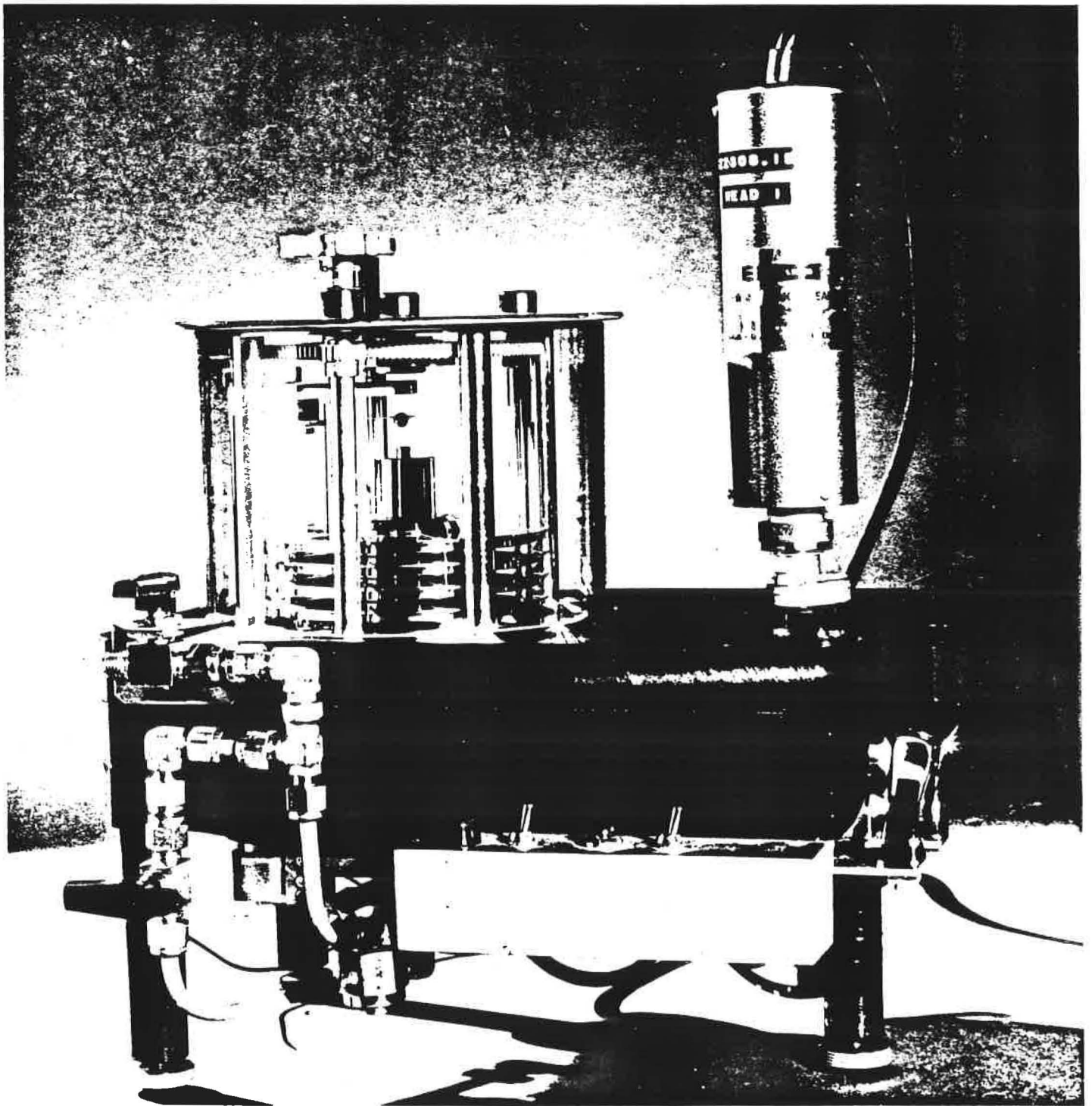


Fig. 5 The transfer standard

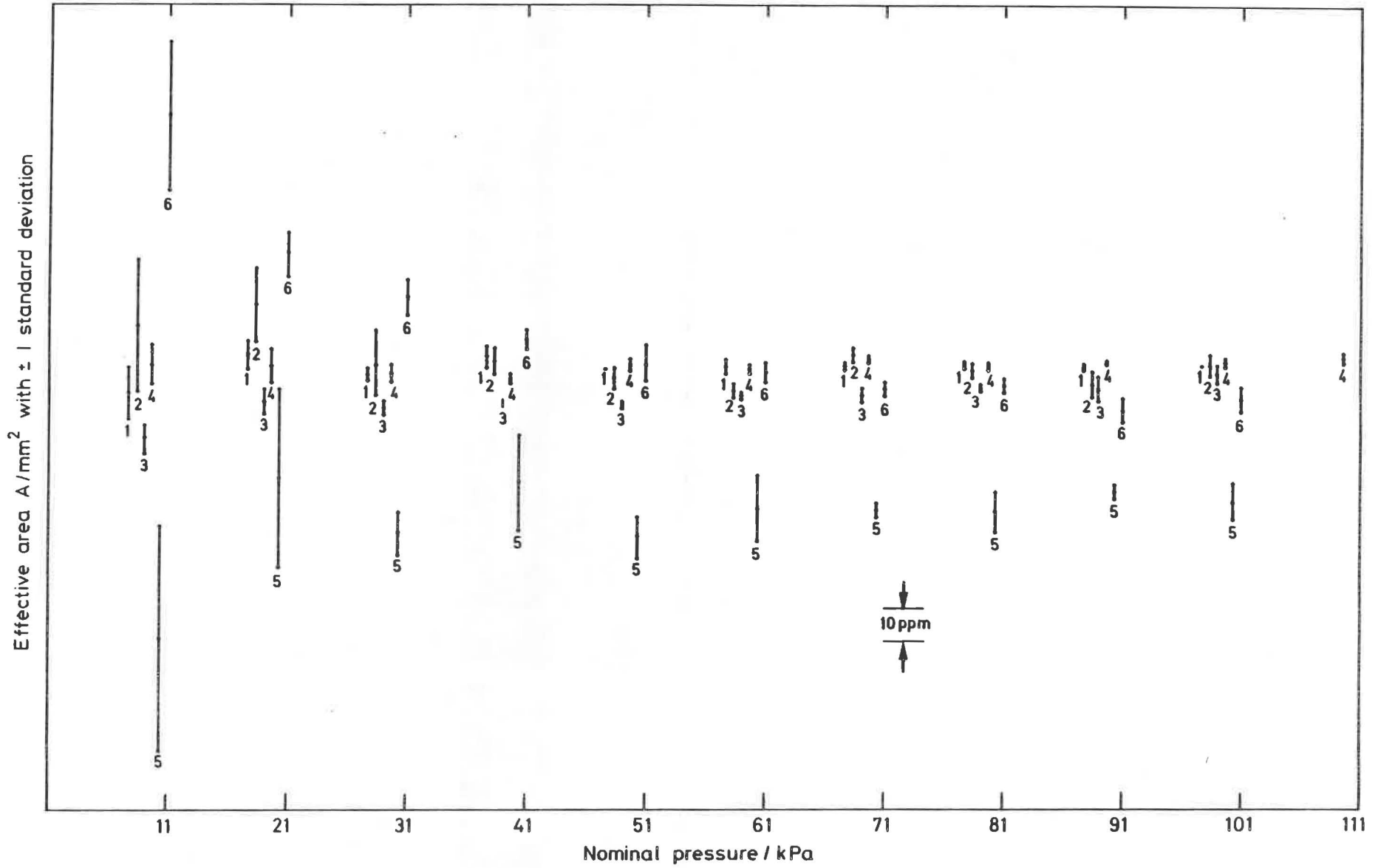


Fig.6 Relative values of the effective cross-sectional area of the piston-cylinder assembly of the transfer standard calculated from the results of the 1st six calibrations (two at the pilot laboratory).

# Non-Geometric Dependencies of Gas-Operated Piston Gage Effective Areas

C.R. Tilford and R.W. Hyland  
National Bureau of Standards  
Gaithersburg, MD 20899

and Sheng Yi-tang\*  
National Institute of Metrology  
Beijing, China

## ABSTRACT

Using a mercury manometer, we have determined the effective areas of different gas-operated piston gages as a function of pressure, mode of operation (absolute or differential), and gas species. We have observed changes in the effective area of individual gages that vary from zero to 25 ppm as these parameters are changed. Over the 5-160 kPa range of these experiments, changes in the geometry of the pistons and cylinders cannot explain these effects. These results demonstrate the need for a more refined theory of the interaction of the pressure fluid and the piston/cylinder. Until that is available effective areas of primary standard piston gages calculated on the basis of geometric factors alone can have significant uncertainties.

## INTRODUCTION

Piston gages, also known as pressure balances or deadweight testers, are widely used as pressure standards for both gas and liquid media over a wide range of pressures. In the case of gas-operated gages they are used in both the absolute mode ("zero" reference pressure), and differential or gage modes, the latter being a special case of differential operation in which the reference pressure is atmospheric. In all cases the common operating assumption is that the pressure generated by the gage when it is properly balanced or "floating" is

$$P = F_g / A_{eff} \quad (1)$$

where  $F_g$  is the gravitational force exerted on the piston and attached weights, corrected for gas buoyancy effects, and  $A_{eff}$  is the effective area. The effective area is generally assumed to be an invariant property of the gage, determined by the geometry of the piston and cylinder combination. The effective area can be determined by calibrating the piston gage against another pressure standard, or, in the case of a primary standard piston

\*NBS Guest Researcher

latter case the calculation generally follows the derivation of Meyers and Jessup (Ref. 1), in which it is assumed that the viscous drag of the pressure fluid flowing through the annulus between the piston and cylinder acts equally on the piston and cylinder, so that the effective area is very nearly the average of the mean cross sectional areas of the piston and cylinder. Attempts have been made to refine this model with a more detailed analysis of the molecular interactions between the pressure fluid and the piston (Refs. 2-4). However, it is still generally the case that the interaction of the gas and the piston are assumed to be independent of the gas species and the pressure, and the uncertainty of the calculated effective area is believed to be determined solely by the uncertainty of the dimensional measurements and the deviations of the piston and cylinder from perfect cylindrical shapes.

Over the past five years we have measured effective areas for a number of gas-operated piston gages between 5 and 160 kPa, using a mercury Ultrasonic Interferometer Manometer (UIM, Refs. 5-8) as a reference standard, and we find that in many cases the effective area of a particular gage depends on the pressure, gas, and/or mode of operation. The changes in area for some gages have been as large as 25 parts per million (ppm). For other gages we cannot detect area changes to within the 2-4 ppm random errors that are typical of these measurements. We present here results for several of the gages that have been measured in the absolute (reference pressure of 0.2 to 0.5 Pa) and differential (reference pressure of 93 kPa) modes with nitrogen, helium, and argon.

## RESULTS

Since the pistons and cylinders are not perfect geometric shapes the effective area of most gages varies as a function of the height of the piston relative to the cylinder (engagement length). In order to establish an optimum operating height for the piston, one of the first steps in characterizing a gage is to determine the absolute mode effective area as a function of the piston height. Figure 1 illustrates the change of effective area as a function of height for a gage with a tungsten carbide cylinder, a hollow steel piston, and a nominal piston diameter of 2 cm. This gage is identified within NBS as PG36. Negative piston heights indicate that the bottom of the piston protrudes below the bottom of the cylinder, for heights

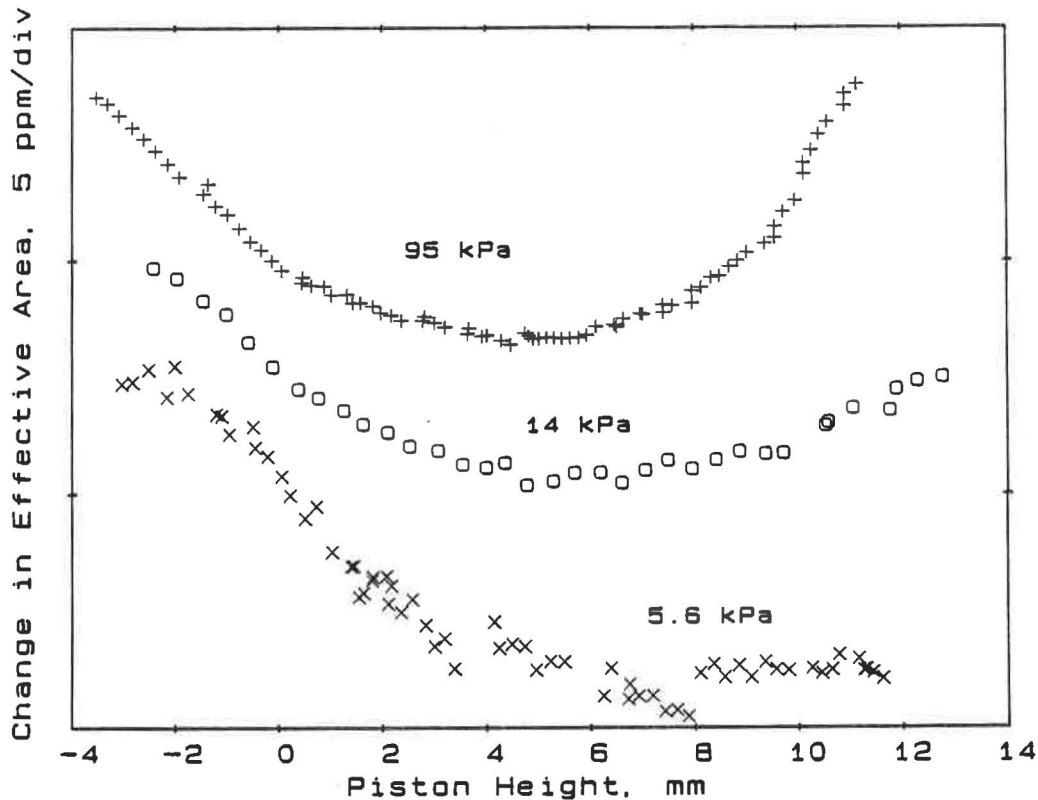


Figure 1: Changes in the absolute mode nitrogen effective area, as a function of piston height (distance between the bottom of the piston and the bottom of the cylinder), for one gage at three different pressures.

above 10 mm the top of the piston protrudes above the top of the cylinder (the cylinder is 55 mm long, the piston is 45 mm long). The 95 kPa data are quite characteristic of data obtained at higher absolute pressures for this gage, and on the basis of this data the reference piston height was defined to be 5 mm and the average of data obtained between 3 and 7 mm was used to determine an effective area. In general, the height dependence would be ascribed to height-dependent imperfections in the piston and cylinder geometries. However, at low absolute pressures the piston height dependence changes character as illustrated by the 5.6 and 14 kPa data. These changes cannot be due to changes in piston or cylinder geometry and must be due to changes in the interaction between the gas and the piston. Similar changes with pressure in the dependence of area on piston height have been observed for some, but not all other gages.

For the sake of clarity the individual data sets in Fig. 1 were plotted in the reverse order of their actual relative positions. As defined by the average of the data between 3 and 7 mm, the smallest effective area was found at high pressures, the effective area at 14 kPa is about 5 ppm larger

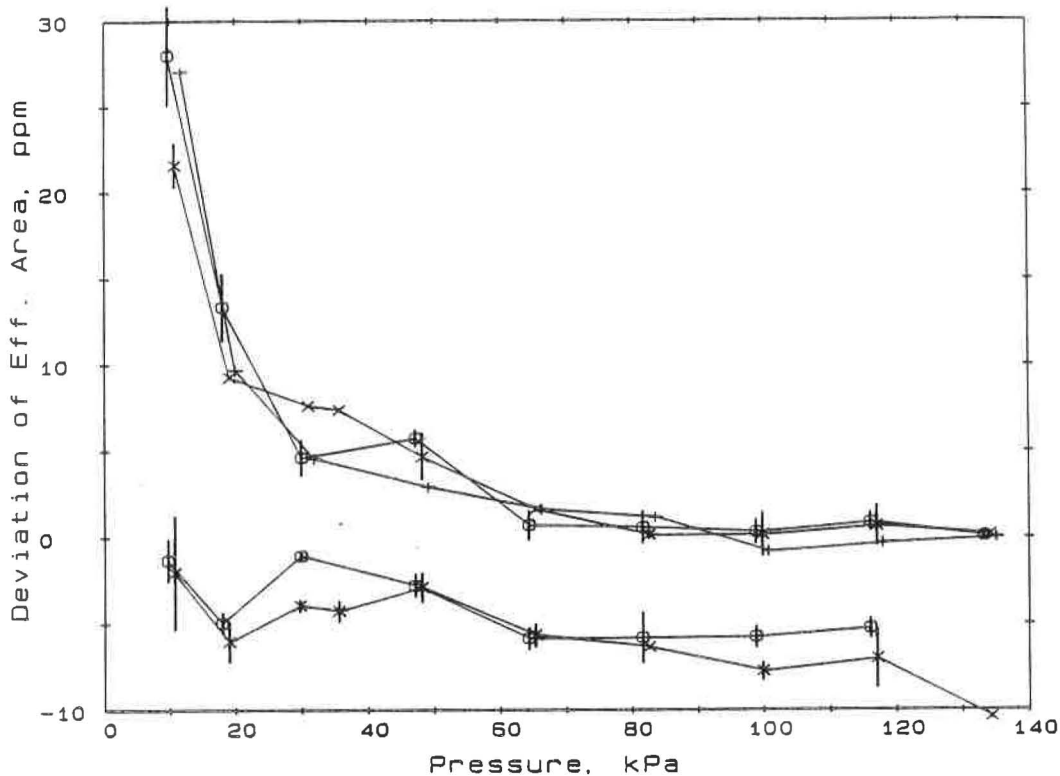


Figure 2: Changes in the effective area for one gage as a function of pressure, gas (x- nitrogen, o-helium, +-argon), and mode of operation. The bottom data sets for nitrogen and helium were obtained in the differential mode, reference pressure of 93 kPa, and the top sets for all three gases were in the absolute mode. Where multiple determinations were made at a pressure, plus and minus one standard deviation of the mean is indicated by the error bars, single determinations have no error bars. Data for different gases at the same pressure have been displaced slightly in pressure for clarity.

than the higher pressure area, and the 5.6 kPa area is about 25 ppm larger. Such changes in effective area at low absolute pressures have been observed for several gages, one example of which is illustrated in Fig. 2. In this case the gage is of the same type as that in Fig. 1 except that both the piston and cylinder are of tungsten carbide. This gage is identified within NBS as PG28. Fall rates for this gage were between 1/2 and 3/4 mm/min. A significant increase in the absolute mode effective area of this gage below 40 kPa is evident. Above 40 kPa the data are affected by a systematic nonlinearity of a few ppm known to exist in the UIM. The apparent changes in the absolute mode effective area above 40 kPa could thus be due to the manometer. Similarly, this same UIM nonlinearity and the larger random errors found for differential mode piston gage operation, particularly at

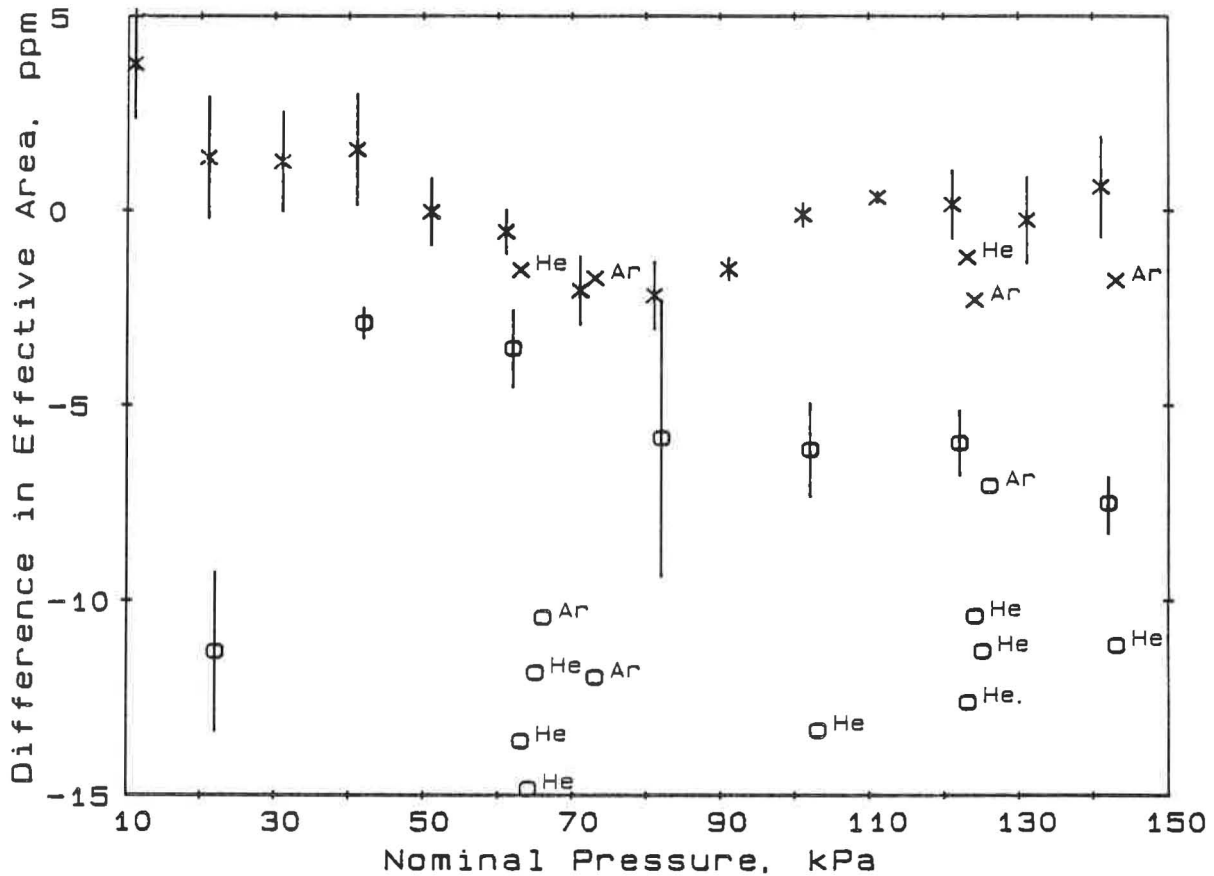


Figure 3: Changes in effective area in the absolute, "x", and differential, "o", modes. Nitrogen data are average values and are plotted with error bars indicating plus and minus one standard deviation of the mean. Helium and argon data are single determinations and are labelled with gas species.

low pressures, could account for the apparent changes in the differential mode areas. In other words, these data are consistent with the differential mode area being independent of pressure, and the absolute mode area independent of pressure above 40 kPa, but there is clearly a significant increase in the absolute mode effective area below 40 kPa.

To within the precision of these data, the effective area appears to be the same for the different gases in a given mode. However, the differential mode area is systematically 6 ppm less than the absolute mode effective area at higher pressures.

The data in Fig. 3 are for a second type of gage which has a nominal piston diameter of 1 cm and is fabricated from 440C, a hardenable stainless steel. Fall rates for this particular gage were on the order of 1 mm/min. In this

case a large amount of data were obtained for nitrogen, and only a few determinations made with helium and argon. Allowing for the previously mentioned nonlinearities of the UIM above 40 kPa, and the increased random errors at the lowest pressures, the data are consistent with there being no significant change in the absolute mode nitrogen effective area of this gage with pressure, and surely no changes of the magnitude observed for the two gages previously discussed. Nor, to within the precision of the data, does there appear to be a significant difference in the absolute mode effective areas for nitrogen, helium, and argon. The differential mode nitrogen areas are definitely less, on the order of 3-7 ppm less, than the absolute mode areas, although it is not clear how much credence should be given to the 21 kPa differential mode point since the operation of the gage under these conditions is less than optimal. The absolute-to-differential differences are greater for argon and helium, on the order of 5-8 ppm for argon, and 10-13 ppm for helium.

It should be noted that we have determined effective areas for five other gages of this same type (Ref. 8), although the amount and quality of data are generally smaller and poorer than for the gage just discussed. For two of those gages there is a significant increase in the absolute mode area at low pressures, on the order of 15 ppm, for one there is no change, and we do not have low pressure data for the other two. For the two gages that show a change at low pressures, the absolute mode effective areas are the same for helium and nitrogen to within 2-4 ppm. Differential mode areas differed from absolute mode areas by less than 6 ppm, if at all.

Figure 4 illustrates data obtained for a gage of the same design as that used to obtain the data in Fig. 3, but constructed of tool steel. This gage is identified within NBS as PG31. These data are few in number, but are in qualitative agreement with independent absolute mode data obtained by Welch (Ref. 11) on this same gage, and illustrate different types and larger changes in effective area than observed for other gages. The differences indicated between the differential mode nitrogen, differential mode helium, and absolute mode helium areas are comparable to or smaller than the errors of this experiment. However, the large differences between these values and the absolute mode nitrogen area are larger than the gas or mode dependent differences that we have observed for any other gage. In addition, the dependence of the area on pressure occurs in a pressure range where we have not observed such effects for other gages, and is much larger than can be explained by nonlinearities in the manometer or mechanical distortion.

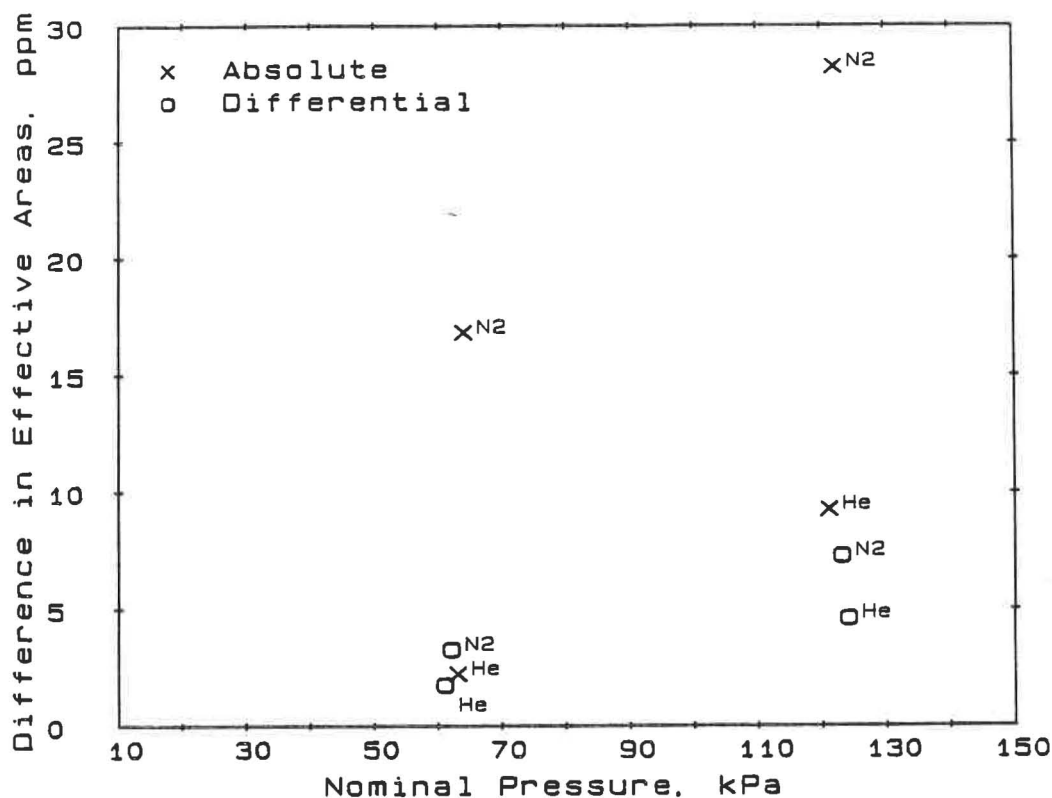


Figure 4: Effective areas for helium and nitrogen in the absolute and differential modes.

#### DISCUSSION

Since these results contradict several common assumptions about piston gage behavior we have examined possible systematic sources of error with great care. Particular attention has been paid to the mass and density of the weights, hydrostatic head corrections, pressure gradients between the piston gage and the manometer, reduction of magnetic and electrostatic forces, temperatures of the piston gage and the manometer, and correction for aerodynamic forces on the weights in the differential mode (Refs. 8-10). We believe that errors due to these effects do not exceed 1 ppm, except for the aerodynamic forces, which may cause residual errors of a few ppm for some of the gages that will not operate at low piston rotation rates. The three-sigma systematic uncertainty of the UIM is estimated to be 15 ppm, including the systematic nonlinearity previously discussed, and systematic differences between the results in the absolute or differential modes should not exceed 1 ppm. Operation of the UIM is independent of the pressurizing gas. The lack of a systematic pattern in the results for different gages confirms that there are no major systematic errors, e.g., if mass errors are responsible for the change in absolute mode effective area at low pressures seen in Fig. 2, the differential mode data should be similarly affected.

Random errors varied with the gage, ambient conditions, pressure, and mode of operation. Data obtained over a period of weeks with a "good" gage in the absolute mode typically had standard deviations of 1-2 ppm, but differential mode operation was always more difficult, with generally increased standard deviations, and errors increased at the lowest pressures for all gages. The increased errors are obvious in the standard deviations plotted in Figs. 2 and 3.

Taking possible errors into account, we believe that the data show significant changes in the effective area for some gages as a function of: pressure at low absolute pressures, mode of operation, and gas species. The magnitude of these changes varies from gage to gage, and in some cases no significant change could be detected. At this time no consistent pattern is evident for the behavior with different gases; the data of Fig. 3 show the area to depend on the gas in the differential mode, but not in the absolute mode, the data of Fig. 4 show a gas dependence in the absolute mode, but not in the differential mode, and the data of Fig. 2 do not indicate a gas dependence in either mode.

The observed changes in area cannot be due to changes in the piston or cylinder geometry, and must be due to changes in the interaction between the pressurizing gas and the piston. For the gages we have studied the contribution of the annular space to the effective area is on the order of 100 to 400 ppm, so relatively small changes in gas dynamics or tangential momentum accommodation coefficients could cause the observed 5 to 25 ppm changes. Presumably the magnitude of possible area changes will decrease as the piston diameter is increased and/or the annular gap width is decreased.

It is clear that if piston gages are to be used as ppm transfer standards these effects must be better understood, and that the accuracy of primary standard piston gages will be limited until the theory of force or momentum transfer between the gas and the piston can be better developed and experimentally verified.

#### ACKNOWLEDGMENTS

These experiments owe a great deal to the expert technical assistance of Fred Long and Donald Martin. We are indebted to Richard Davis, Jerry Keller, and Bernie Welch for numerous mass and density determinations.

## REFERENCES

1. Meyers, C.H., and Jessup, R.S., J. Res. Nat. Bur. Stand. 6, 1061 (1931).
2. Dadson, R.S., and Greig, R.G.P, "The air operated pressure balance as a standard for sub-atmospheric pressures", Proceedings of the Conference on Fundamental Problems of Low Pressure Measurements, National Physical Laboratory, Teddington U.K., Sept., 1964, Institute of Physics, London, 1964.
3. Sutton, C.M., "The air-operated pressure balance as a primary pressure standard", Report 562 of the Physics and Engineering Laboratory, Lower Hutt, N.Z., Jan., 1977
4. Dadson, R.S., Lewis, S.L., and Peggs, G.N., The Pressure Balance, Theory and Practice, Her Majesty's Stationery Office, London, 1982
5. Heydemann, P.L.M., Tilford, C.R., and Hyland, R.W., J. Vac. Sci. Technol. 14, 597 (1977).
6. Tilford, C.R., Metrologia 24, 121 (1987).
7. Tilford, Charles R., "New developments in barometric range pressure standards", pgs. 35-1 to 35-15 of the proceedings of the 1988 Symposium of the National Conference of Standards Laboratories, Washington, D.C., August, 1988.
8. Tilford, C.R. and Hyland, R.W., "The NBS ultrasonic interferometer manometer and studies of gas-operated piston gages", to be published in the proceedings of the 11th World Congress of the International Measurement Confederation (IMEKO), Houston, TX, October, 1988.
9. Prowse, D.B., and Hatt, D.J., J. Phys. E 10, 450-451 (1977).
10. Sutton, C.M., J. Phys. E 12, 466-468 (1979).
11. Publication of these results is in preparation.



P A R T 2

PRESSURE TRANSDUCERS, TRANSFER  
STANDARDS, DYNAMIC PRESSURE  
MEASUREMENTS, FIXED POINTS

Sub-section: Pressure transducers and transfer standards



## THE PRESSURE MULTIPLIER

### A TRANSFER STANDARD IN THE RANGE 100 TO 1000 MPA

P. DELAJOURD - DESGRANGES ET HUOT  
AUBERVILLIERS - FRANCE

#### ABSTRACT

Many pressure calibration laboratories need to maintain capability in a range from less than 1 kPa to 1000 MPa. Various manufacturers have adapted basic piston gauge technology to cover segments of this wide range with separate and distinct instruments. Modern high quality piston gauges are extremely reliable and easy to use in a broad mid-range from roughly 0.1 MPa to as high as 500 MPa. At the extremes outside of this range however, their application from both a practical and metrological viewpoint, is much more difficult. A concept applied successfully in other fields of metrology, multiplying and dividing values supplied by one reliable mid-range standard rather than using several independent standards, presents a useful alternative for covering very wide pressure ranges.

This presentation examines the use of a multiplier to cover the upper extremes of the pressure range.



## INTRODUCTION

Pressure is defined as a force per unit of area as expressed by :

$$P = \frac{F}{A}$$

Where     P = pressure (Pa)  
           F = force (N)  
           A = area (m<sup>2</sup>)

Pressure then, is derived from the fundamental units of mass, length and time. Primary standards are needed to define pressure directly from the fundamental units.

Two different types of primary standards are commonly used. The first, the manometer, uses a column of liquid of known density, usually mercury. Given the difficulties encountered as the column increases in height, the practical application of manometers is limited to a maximum of about 350 kPa. The second, called the piston gauge, deadweight gauge or deadweight tester, uses a piston rotating in a cylinder to define an area. Masses subjected to gravity are loaded onto the piston to define a force.

The accurate definition of pressure with a piston gauge depends upon the accurate definition of the piston-cylinder's effective area and the force applied to it. Given that the force can be defined with accuracy of better than 10 ppm with relatively little difficulty, the most important limitations to accuracy come in defining the effective area of the piston-cylinder at 0 pressure and the change of effective area with pressure.

Over the years, a great deal of effort has gone into trying to improve the definition of piston-cylinder effective areas. Tungsten carbide piston-cylinders with excellent geometry and operating characteristics have been produced. The effective area of these piston-cylinders has been measured directly by dimensional measurement and calculated from comparisons with manometers. The change in effective area with pressure has been predicted using knowledge of material properties and solid mechanics and studied experimentally by various methods.

The work has yielded some impressive results, particularly over the mid-range where, using current technology, traditional piston gauges offer their best performance. Today, in various national laboratories around the world, estimated uncertainties on piston-cylinder effective area on the order of 20 ppm at up to 5 MPa and 50 ppm at up to 100 MPa have been achieved. As pressures go higher and lower, special difficulties in using piston gauges are encountered and uncertainties increase.

The objectives of most calibration laboratories do not include fundamental research into primary standards and therefore the validity of their internal standards as a research tool is not a major concern. Rather, they require standards that combine the accuracy needed to calibrate the instruments for which they are responsible with sufficient reliability and ease of use to ensure that the operators will consistently achieve the desired results in an acceptable amount of time. At the extremes of the range, traditional piston gauges tend to be difficult to use and maintain. In addition, covering a very wide range using several independent standards with different designs and operating principles increases maintenance costs and the laboratory space required to house them.

An alternative to procuring and maintaining multiple, expensive and complex independent standards is presented by the use of devices that conveniently multiply and divide pressures supplied by a reliable and easy to use mid-range standard.

## THE PRINCIPLES OF RATIO-METRIC DIVICES FOR PRESSURE

Why multiply and divide ?

Finding ways to exactly multiply and/or divide values supplied by one central standard is attractive for several reasons other than those just mentioned :

- 1 - In most metrological fields, measuring the ratio of two values exactly is more easily accomplished than measuring a single value in the absolute sense.
- 2 - Covering a wide range using a mid-range standard and exact multiplying and dividing devices increases the likelihood that measurements will be homogeneous over the entire range.
- 3 - When an adimensional, ratio-metric device is used to multiply or divide a value, the only added uncertainty is the uncertainty on the ratio. The systematic uncertainty is not repeated in the ratio-metric device. The metrological characteristics of a divider or multiplier are independent from the fundamental units that define pressure and are limited only by our ability to determine a ratio, not our ability to measure an effective area in the absolute sense.

Using piston-cylinders

The use of combinations of piston-cylinders working together is an obvious choice for the basic design of ratio-metric devices for pressure. The excellent operating characteristics and stability over time of high quality tungsten carbide piston-cylinders are well documented.

The limitations in absolute accuracy in the field of pressure today do not come from limitations in the performance of piston-cylinders ; they come from our inability to measure effective area in the absolute sense. It follows that the value of the ratio of effective area of two piston-cylinders should be able to be measured much more accurately than the absolute value of the effective area of either one.

That this is the case is in fact recognized and exploited on a daily basis in the application of the crossfloat method of measuring piston-cylinder effective area. The crossfloat method can be described as the experimental determination of the ratio of effective area of two piston-cylinders. It is thanks to the intrinsic performance characteristics of piston-cylinders and the perfection of crossfloat techniques that reference values for effective area and pressure are transferred so efficiently through the measurement system. At the highest levels, the estimated three sigma uncertainty associated with the transfer of effective area from one high quality piston gauge to another is generally less than 5 ppm even though the systematic uncertainty on the gauge that is used as a reference may be five to ten times that. In other words, our ability to determine a ratio of effective areas is far greater than and is basically independent from our ability to measure one effective area in the absolute sense.

The importance of the quality and relative ease with which ratios can be measured cannot be overemphasized. It is of central importance to the characterization and exploitation of high accuracy dividers and multipliers.

## MULTIPLIER TECHNOLOGY

### Background

The first steps toward the practical application of the multipiston multiplier approach at DH occurred in the 1970's. A gauge manufacturer required a high accuracy 1000 MPa standard that would be more compact, easier to operate and less expensive than the traditional controlled clearance gauges that were usually used to cover the range. Studies showed that this could be accomplished by using the ratio of two piston-cylinders to multiply the pressure supplied by a 100 MPa piston gauge by 10.

The first multiplier to operate consistently with acceptable performance up to 1000 MPa was produced in 1976. Since then, 25 multipliers have been manufactured. Most of them work in intensive applications calibrating transducers used in ballistics measurements and have given complete satisfaction. A multiplier has been included in the Desgranges and Huot calibration chain since 1979 and the multipliers produced have been compared to it.

### The 10:1 Multiplier

Figure 1 gives the schematic of a 10:1 multiplier for pressure up to 1000 MPa.

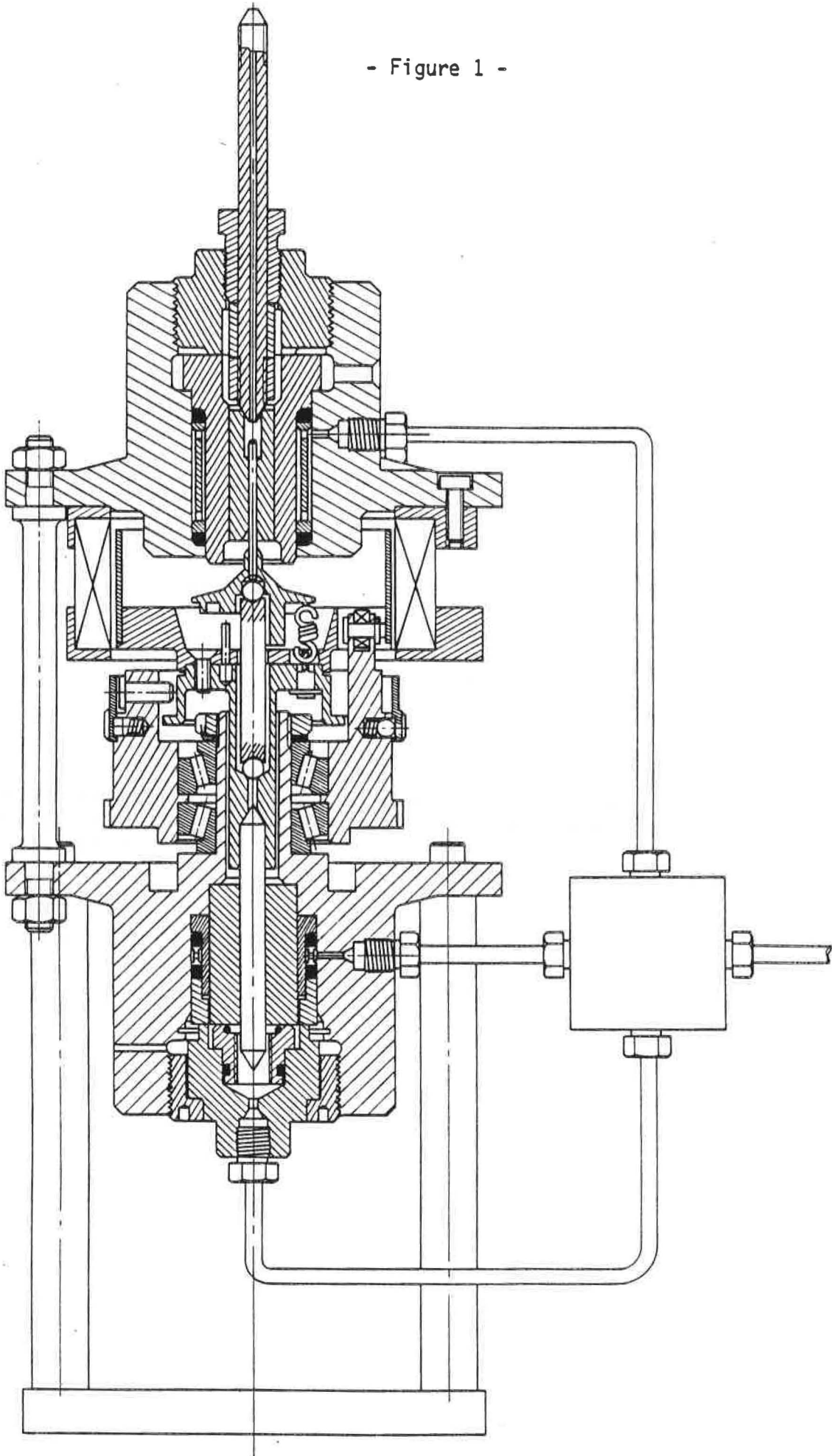
Both piston-cylinders are made out of tungsten carbide. The lower piston has a nominal diameter of 8 mm and radial clearance of about 0.5 micrometer. The upper piston has a nominal diameter of 2.5 mm and radial clearance of about 0.2 micrometer.

The multiplier operates in the range of 10 MPa to 1000 MPa. Generally, the piston gauge chosen to supply the low pressure side uses a 3.5 mm piston-cylinder and a 100 kg mass set to supply 1 MPa to 100 MPa.

Both piston-cylinders are mounted so that a pressure may be applied along the length of the cylinder. In operation, the pressure coming from the standard whose pressure is being multiplied will be used as a jacket pressure and applied to the outside of the multiplier cylinders. This means that the high pressure cylinder will receive a jacket pressure equal to 10 % of the pressure it is measuring and the relative values of the jacket pressures and measured pressures will be constant.

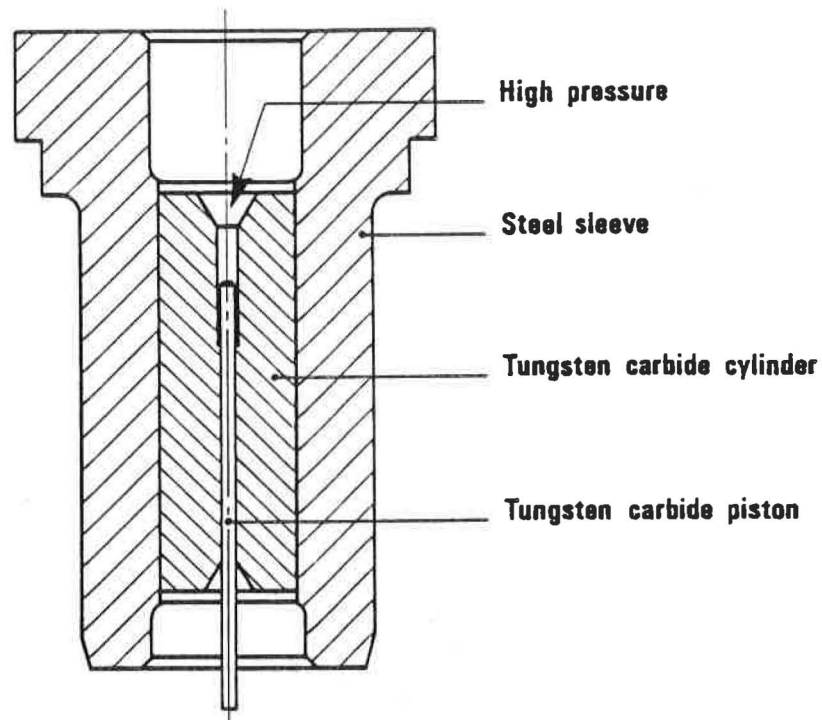
The multiplier's mobile assembly has a total stroke of 10 mm. How quickly the multiplier goes through that stroke depends upon the leak of oil through the space between the high pressure piston and cylinder. At 1000 MPa, the multiplier goes through its entire stroke in about 30 minutes. However, the piston gauge that is driving the multiplier must, by the downward movement of its piston, compensate for the leak of the high pressure piston, the leak and displacement of the low pressure piston and its own leak. At maximum pressure, the low pressure piston gauge goes through its 10 mm stroke in about 5 minutes. Since the piston gauge must compensate for the movement of the multiplier's lower piston and the lower piston displaces a volume ten times greater than the upper piston, any change in the leak rate of the upper piston changes the piston gauges drop rate radically.

- Figure 1 -



For this reason, the design of the high pressure piston-cylinder was studied very carefully.

Figure 2 - Design of the high pressure piston-cylinder



Due to its high Young's modulus that limits deformation, tungsten carbide is an excellent material from which to make piston-cylinder assemblies. However, though tungsten carbide has good compressive strength, the same is not true for tensile strength and a tungsten carbide cylinder can be expected to rupture at an internal pressure of around 700 MPa. In order to benefit from tungsten carbide's low deformation, we put a tungsten carbide cylinder into a steel sleeve which offers the advantages of high tensile strength and excellent fatigue resistance.

- Figure 3 -

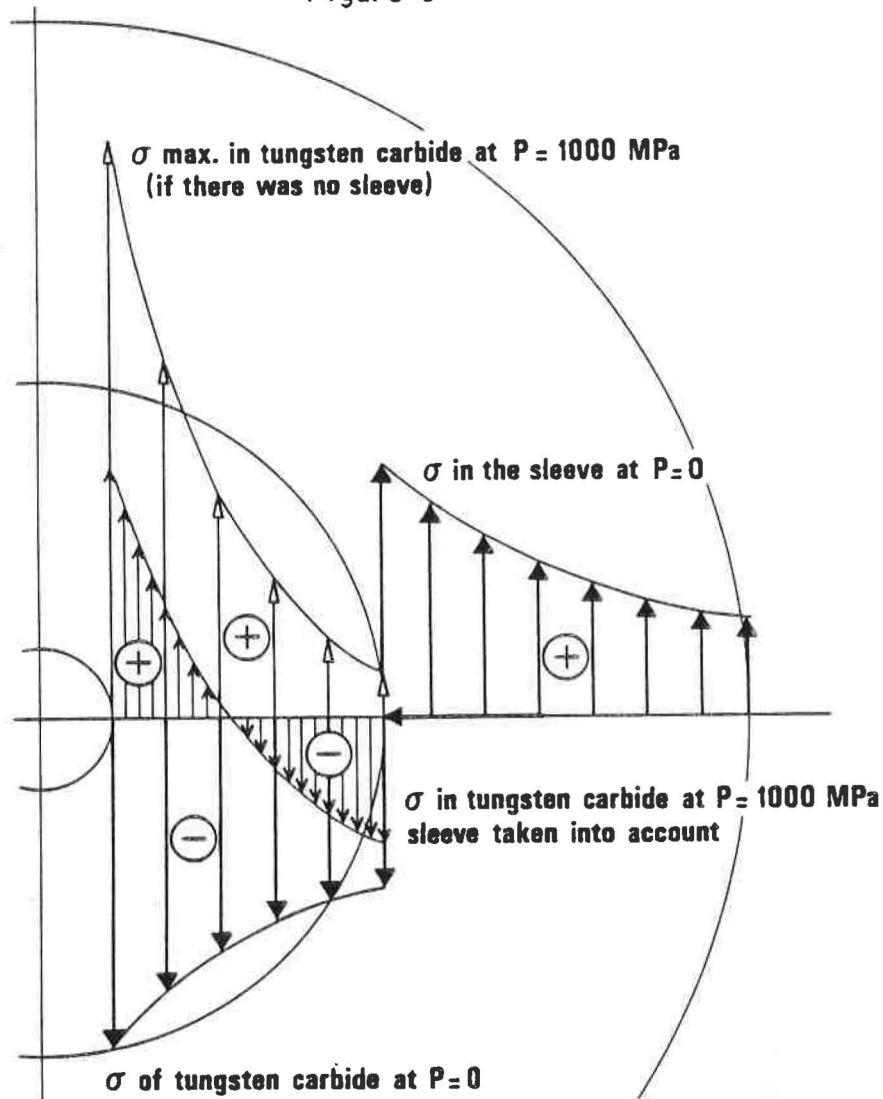


Figure 3 shows that the sleeving technique results in a negative tensile force for the tungsten carbide when the internal pressure is zero, which reduces the maximum stress in the carbide when the high pressure reaches its maximum value of 1000 MPa by redistributing the stress around a new null stress point.

Under these conditions, the low value of the jacket pressure applied to the sleeve (10 % of the measured pressure) limits the deformation of the high pressure cylinder such that the annular flow rate is ideal for the multiplier's operation. The manufacturing of the high pressure cylinder is a difficult process but produces a piston-cylinder assembly that performs extremely well at pressures up to 1000 MPa. For both parts of the cylinder, this design assures maximum stress levels that are well below the elastic limits of the materials while using low jacket pressures. This keeps the piston-cylinder deformation in the linear portion of the stress-strain curve over the range of pressure applied which allows the change in effective area with pressure to be predicted reliably.

## METROLOGICAL CHARACTERISTICS

To be used in practical applications, the intrinsic performance of the multiplier and the multiplying ratio and its change with pressure must be determined.

Intercomparing two multiplier/piston gauge combinations by direct crossfloat is useful in evaluating the multiplier's intrinsic characteristics. The crossfloat is set up by connecting the high pressure sides of the two multipliers together and using two separate piston gauges to supply the low sides.

A mobility check of all six pistons in the crossfloat is performed at maximum pressure by determining the mass change necessary on either of the piston gauge to break an equilibrium. With a 100 kg load on both piston gauges, once an equilibrium has been set, a mass of less than 1 g (10 ppm) placed on either gauge will break the equilibrium. This is equivalent to 1 kPa on the low pressure end and 10 kPa on the high pressure end of the multiplier.

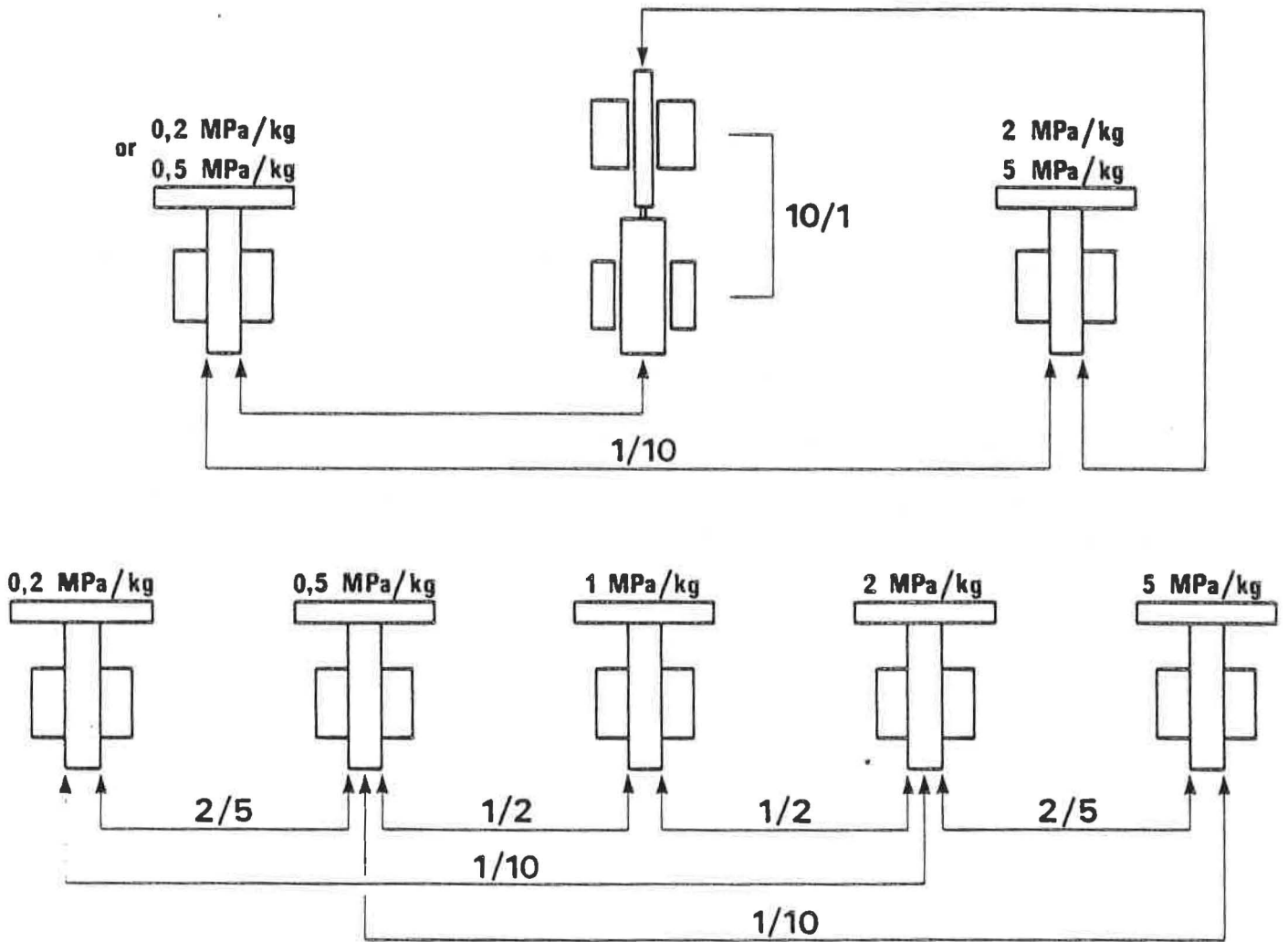
Although it is easier to determine the ratio of effective areas of two piston-cylinders than to determine the absolute value of one, optimal characterization of high performance multipliers requires some special techniques and equipment. In particular, piston gauges whose effective area ratios are known and can easily be verified over a wide range of pressure and over time are needed.

We have always felt that it is important that the ranging structure of the piston gauges used as internal standards be designed to meet these requirements. Reasons for this include a desire to be able to verify the homogeneity of internal measurements from the lowest to the highest pressures and dedication to the principle that maintaining a group of interrelated standards is preferable to relying on a single master standard.

To facilitate the establishment of a calibration chain the nominal effective areas of standard DH piston-cylinder sizes are in 1-2-5 progressions. Our internal standards consist of chains of these piston-cylinders. The links of the chain are closed by crossfloats and the chain is complete when each level has been crossfloatated with the level immediately above and below it. Between most levels the ratio of piston-cylinder effective areas can be determined to better than 5 ppm. The effective area ratio of piston-cylinders from non-contiguous levels can then be known with great accuracy by simple calculation. The uncertainty on all effective area ratios is completely independent from the absolute uncertainty on individual piston-cylinder effective areas.

The calibration chain allows the transfer of effective area values upwards and downwards from low pressures to high pressures and vice versa with minimum accuracy degradation. It also provides an excellent tool for the calibration of multipliers. Figure 4 illustrates how the calibration chain can be used to calibrate a 10:1 multiplier. The ratios of the effective areas of the 0.2 to 0.5, 0.5 to 1, 1 to 2 and 2 to 5 MPa/kg piston-cylinders are determined by crossfloat. From these experimentally determined ratios the ratio of the 0.2 with 2 MPa/kg and 0.5 with 5 MPa/kg effective areas, which would be very difficult to determine by direct crossfloat because of the large ratio, can easily be calculated. The ratio of the multiplier can then be determined by crossfloating the 0.2 and 2 MPa/kg piston-cylinders through the multiplier. The result is an experimentally determined ratio for the multiplier between 2 and 200 MPa whose uncertainty is completely independent from the relatively large uncertainties on the absolute values of individual effective areas. The 0.5 and 5 Mpa/kg piston-cylinders can also be used for the operation.

- Figure 4 -



The measured ratio of a multiplier is determined using the calibration chain as explained above. First the multiplier is crossfloated between a 0.2 MPa/kg and a 2 MPa/kg piston-cylinder and ratios at 50, 100 and 200 MPa are determined. Then the multiplier is crossfloated between a 0.5 MPa/kg and a 5 MPa/kg piston-cylinder and ratios at 250 and 500 MPa are determined. From the five ratios obtained the multiplying ratio and the evolution of that ratio with pressure can be calculated. The result shows a change in multiplying ratio with pressure that is linear from 50 MPa to 500 MPa.

If  $K_m(0)$  is the ratio of the multiplier at null pressure, the value of the multiplier ratio at a high pressure, HP, is written :

$$K_m(HP) = K_m(0) [1 + P(HP)]$$

The value of  $P(HP)$  is on the order of  $-0.4 \times 10^{-6} \text{ MPa}^{-1}$ , which leads to a reduction of the ratio of  $4.10^{-4}$  at 1000 MPa.

The effective area of a piston-cylinder changes when its temperature is changed due to the thermal expansivity of the material of which it is made. However, in a multiplier it is not the absolute change in one effective area that we are concerned with but the change in the ratio of two effective areas. All multiplier pistons are made of the same material, tungsten carbide, which means that all the piston-cylinders have the same thermal expansivity coefficient. Therefore, a temperature change might not alter the multiplier ratio. In fact, the high pressure cylinder is inside a steel sleeve whose thermal expansion coefficient is greater than that of tungsten carbide. A temperature change therefore leads to a variation in the stress applied by the sleeve to the high pressure cylinder due to the difference in thermal expansivity between the two materials.

The change in stress causes a change in effective area of the high pressure piston-cylinder which leads to a change in the multiplier ratio. The effect is quite small, about  $4 \times 10^{-6}/^{\circ}\text{C}$ , with increases temperature causing a decrease in the ratio.

The means of verifying the multiplying ratio have improved significantly over the past ten years with improvements in the piston gauges used, improvements in the calibration chain and extension of the range of the calibration chain. For this reason, in the data obtained in redetermining multiplying ratios over the years, it is difficult to completely isolate changes in the means used to make the measurements from actual changes in the multiplying ratio. It is possible to say, however that the change in multiplying ratio of our calibration chain multiplier since 1981, when our calibration chain structure was finalized, is on the order of 20 ppm.

At this time the calibration chain uses traditional piston gauges up to 500 MPa and a multiplier up to 1000 MPa. Therefore, for the moment, we cannot experimentally measure a multiplier's multiplying ratio above 500 MPa using internal standards.

Though we cannot experimentally determine the ratio of a multiplier above 500 MPa, we can study the behavior of multipliers by comparing them directly between 500 and 1000 MPa as described above. About 25 multipliers have been produced and the comparisons show that different multipliers behave in the same way above 500 MPa. In other words, the relationship between two multipliers at 1000 MPa can be predicted reliably using ratios and deformation coefficients that were determined experimentally between 100 and 500 MPa.

Given that the change in a multiplier's ratio is linear with pressure from 100 to 500 MPa, that the behavior of various multipliers is consistent above and below 500 MPa and taking into consideration the information that is available on the mechanical characteristics of the tungsten carbide from which the piston-cylinders are made, we apply the deformation coefficient that was experimentally determined for the ratio from 100 to 500 MPa to calculate the multiplying ratio between 500 and 1000 MPa. We then assume that the deformation coefficient could in fact change by as much as 20 %. Summing the uncertainty due to a possible change in deformation coefficient of 20 % with the uncertainty on the experimentally determined ratio at 200 MPa and 500 MPa leads to a total uncertainty on the multiplying ratio of : about 30 ppm at 200 MPa, about 70 ppm at 500 MPa, about 110 ppm at 1000 MPa.

### CONCLUSIONS

Multiplying devices offer a convenient and accurate way to extend the range of a reliable and easy to use mid-range standard. The combination of 1 to 100 MPa piston gauge with a multiplier covers the range from 1 to 1000 MPa in one system without piston changes. The complete system uses 100 kg of mass and has a footprint of about 1 m<sup>2</sup>. It can be fit onto one work bench into which the necessary pressure generation and control hardware is integrated.

The availability of versatile, easily implemented and relatively low cost automated piston gauges in the mid range area increases the advantage to be gained from extending the range rather than adding separate standards.

In addition, thanks to its compact size, the multiplier combines the reliability and transportability needed for use as a high pressure transfer standard.

The results obtained with pressure dividers and multipliers to date encourage us continue to develop new ways to exploit the technique.

## InSb As a Pressure Sensor

Vern E. Bean

National Institute of Standards and Technology  
Gaithersburg, Maryland 20899

*The resistivity of InSb increases exponentially with pressure. We have made a pressure transducer based on InSb that has nearly 70 times the sensitivity at 645 MPa of a manganin pressure transducer. The transducer has adequate sensitivity and short term stability to be used to measure the change of pressure generated by a controlled-clearance piston gage resulting from a change of jacket pressure from which the cylinder distortion coefficient can be determined. The long term performance data necessary to evaluate the suitability of the transducer as a transfer standard for laboratory intercomparison is not yet available.*

There is a need for a stable and sensitive pressure transducer capable of operating in the 700 MPa pressure range for use as a transfer standard for pressure measurement intercomparisons among laboratories and for experimentally determining the cylinder deformation coefficients for controlled-clearance primary standard piston gages [1]. Transducers based on the electrical resistance of a length of manganin wire are used for intercomparisons [2,3], but they lack the necessary resolution (on the order of 10 parts per million, ppm) needed to characterize a controlled-clearance piston gage. Konczykowski and co-workers [4] as well as Kraak and co-workers [5] have suggested that a transducer based on the electrical resistance of a narrow-band-gap semiconductor such as InSb will have far greater sensitivity than manganin, because semiconductor resistivity is an exponential function of pressure resulting in increased sensitivity as the pressure increases.

At NIST we have recently begun using an InSb transducer in the controlled-clearance piston gage characterization process with very satisfactory results. We do not yet have enough long-term data to evaluate the usefulness of this transducer as a transfer standard.

The essential feature of the transducer is a single crystal of undoped n-type InSb, 0.5 mm x 0.5 mm x 25 mm, with pairs of 0.1 mm diameter wires soldered to each end with indium so we can use the four lead resistance measurement technique. The crystal is mounted in a plastic holder so as to be free of strains. The holder fits into a commercially available pressure vessel intended for a manganin transducer. The pressure vessel is in a controlled temperature bath. The resistance measurements were obtained using either an automated resistance bridge or a general purpose digital multimeter.

We desire a transducer with a large pressure coefficient and a minimal temperature coefficient.

The resistance,  $R$ , of a semiconductor can be expressed as [6]

$$R = A \exp E_g / (2kT) \quad (1)$$

where A is a constant,  $E_g$  is the energy gap between the valence and the conduction bands, T is the absolute temperature and k is the Boltzman constant. Then

$$\ln R = \ln A + E_g/(2kT) \quad (2)$$

The measured resistances of the InSb sample described above over the temperature range of 263 to 313 K at atmospheric pressure are plotted semi-logarithmically in Fig. 1 as a function of  $1/T$ . The linearity of the data indicates that  $E_g$  is essentially independent of temperature over this temperature range.

The temperature coefficient of resistance is obtained by taking the partial derivative of Eq. 1 with respect to T and can be expressed as

$$\frac{1}{R} \frac{\partial R}{\partial T} = \frac{1}{2kT} \frac{\partial E_g}{\partial T} - \frac{E_g}{2kT^2} \quad (3)$$

Since  $E_g$  is essentially independent of T,

$$\frac{\partial E_g}{\partial T} \approx 0$$

and the temperature coefficient becomes

$$\frac{1}{R} \frac{\partial R}{\partial T} = - \frac{E_g}{2kT^2} \quad (4)$$

Thus the temperature coefficient can be minimized by using a semiconductor with the lowest value of  $E_g$ ; from this stand point, InSb is an excellent choice [7,8]. The temperature coefficient is also reduced by operating at elevated temperature.

From Eq. 2, the slope of the line in Fig. 1 is  $E_g/2k$  from which the value of  $E_g$ , 0.261 electron volts (ev) is obtained. This value compares well with the value of 0.236 ev given in Ref. 8 but less favorably with the value of 0.18 found in Ref. 7. Using our measured value of  $E_g$ , the temperature coefficient at 273.16 K is  $-0.0203 \text{ K}^{-1}$ . An uncertainty of 1 mK in the measurement of temperature corresponds to an uncertainty of 6 kPa in pressure.

The transducer has been repeatedly calibrated at pressures up to 645 MPa with a primary standard piston gage. During all of the calibration cycles the transducer remained in a temperature bath controlled to  $273.160 \pm 0.015 \text{ K}$ . The transducer temperature was monitored with a calibrated platinum resistance thermometer mounted on the pressure vessel containing the InSb. All of the resistance data were referenced to 273.160 K. The measured resistances as a function of pressure with the transducer at 273.16 K are plotted semi-logarithmically in Fig. 2.

A convenient way to write the calibration equation for this transducer is

$$P = B \ln \frac{R(P)}{R(0)} \quad (5)$$

$$0 = \frac{\Delta P}{P} + \frac{(\alpha_p + \alpha_c)\Delta T}{1 + (\alpha_p + \alpha_c)(T - T_r)} - \frac{d \Delta P_j}{1 + d(P_z - P_j)} \quad (7)$$

Since  $1 \gg (\alpha_p + \alpha_c)(T - T_r)$  and  $1 \gg d(P_z - P_j)$ , we can write

$$0 = \frac{\Delta P}{P} + (\alpha_p + \alpha_c)\Delta T - d\Delta P_j \quad (8)$$

Solving for d,

$$d = \frac{1}{\Delta P_j} \left[ -\frac{\Delta P}{P} + (\alpha_p + \alpha_c)\Delta T \right] \quad (9)$$

Based on our experience, the second term of Eq. 9 is negligible compared to the first, so

$$d = \frac{1}{\Delta P_j} \frac{\Delta P}{P} \quad (10)$$

We can measure  $\Delta P$  using the InSb transducer with the following scheme:

1. Operate the piston gage at some value of  $P_j$  and note the transducer reading  $R_1$
2. Increase  $P_j$  by  $\Delta P_j$  and note the transducer reading  $R_2$
3. Add a trim weight,  $\Delta W$  such that the resulting pressure change is approximately equal to that due to the increase in  $P_j$ . The transducer reading,  $R_3$ , will thus be approximately equal to  $2R_2 - R_1$ . This serves to calibrate the transducer under the conditions of use.

Then, with sufficient accuracy,

$$\Delta P = \frac{R_2 - R_1}{R_3 - R_2} \frac{\Delta W}{A_o} \quad (11)$$

#### REFERENCES

1. P.L.M. Heydemann and B.E. Welch, Part 3, Piston Gages, in Experimental Thermodynamics of Non-reacting Fluids, edited by B. LeNeindre and B. Vodar (Butterworths, London, 1975) pp 147-202.
2. S.E. Babb, Jr., The Measurement of Hydrostatic Pressure, in Mechanical Behavior of Materials Under Pressure, edited by H. Ll. D. Pugh, (Elsevier, London, 1970) pp 119-152.
3. G. F. Molinar and L. Bianchi, Metrological Characterization of Manganin Gages Calibrated Against the Mercury Melting Line, in High Pressure Science and Technology, Part III, edited by G. Homan, R. K. MacCrone, and E. Whalley, (North-Holland, New York, 1984) pp 285-288.
4. M. Konczykowski, M. Baj, E. Szafarkiewicz, L. Konczwicz and S. Porowski, Narrow Gap Semiconductors as Low Temperature Pressure

where B is the calibration coefficient, and R(P) and R(O) are the resistances measured at high pressure and at atmospheric pressure, respectively. The values of B for five calibration cycles are listed in Table I. These values were determined by fitting Eq. 5 to the calibration data separately for increasing pressure and decreasing pressure for each cycle. The short term repeatability of the transducer is indicated by the second and fourth columns of Table I where values of  $(B/B_0) - 1$  are listed for increasing and decreasing pressure respectively. For purposes of these comparisons, the value of  $B_0$  is arbitrarily defined as that resulting from the first calibration cycle with increasing pressure only. That the values on the fourth column are larger than the values on the second column is indicative of hysteresis. Longer-term data is needed to judge the suitability of the InSb transducer for use as a transfer standard.

The great advantage of the InSb transducer is its very high sensitivity. Fig. 3 is a plot of the sensitivity, defined as the ratio of the change of resistance to the change of pressure, plotted as a function of pressure. The sensitivity ranges from 0.0215 ohms/MPa at atmospheric pressure to 0.1703 ohms/MPa at 645 MPa. By the way of contrast, the sensitivity of a manganin transducer is on the order of 0.0020 ohms/MPa and is, in the first approximation, independent of pressure [2]. Thus, at atmospheric pressure, the InSb transducer is about 9 times more sensitive than the manganin transducer. At 645 kPa, the InSb sensitivity is nearly 70 times that of manganin.

The properties required of a transducer, in order to measure the cylinder distortion coefficient of a controlled-clearance piston gage, are sensitivity and short term stability, say on the order of 30 minutes. The InSb transducer is satisfactory on both counts. The method to measure the distortion coefficient is as follows:

The total downward force, W, on the piston of a controlled-clearance piston gage is [1]

$$W = PA_0 [1 + (\alpha_p + \alpha_c)(T - T_r)] (1 + bP_n) [1 + d(P_z - P_j)] \quad (6)$$

where

- P is the measured pressure
- $A_0$  is the area of the piston at temperature  $T_r$ ,
- $\alpha_p$  and  $\alpha_c$  are the linear thermal expansion coefficients for the piston and the cylinder respectively,
- T is the temperature of the operating piston gage when the measurements were made
- b is the distortion coefficient for the piston
- $P_n$  is the nominal pressure
- d is the cylinder distortion coefficient
- $P_z$  is the pressure on the outside of the cylinder resulting in zero clearance between the piston and the cylinder
- $P_j$  is the pressure on the outside of the cylinder (jacket pressure) during gage operation.

While W is held constant, we change  $P_j$  and measure the corresponding change in P. During the time required to make these measurements, T could also change so the variables are P,  $P_j$ , and T. Since d has already been employed as a symbol in Eq. 6, let us use  $\Delta$  to denote differentials. The normalized total differential of Eq. 6 is

- Gages, in High Pressure and Low Temperature Physics, edited by C. W. Chu and J. A. Wooam, (Plenum Press, New York 1979), pp 523-528.
5. W. Kraak, U. Schaller, and R. Herrmann, Phys. Stat. Sol., (a) 85, K183, 1984.
  6. C. Kittel, Introduction to Solid State Physics, (John Wiley and Sons, New York, 1956) p 348.
  7. C. Kittel, op.cit., p 351.
  8. H.P.R. Frederikse, Properties of Semiconductors, in American Institute of Physics Handbook, Third Edition, coordinating editor D. E. Gray, (McGraw Hill, New York, 1972) pp 9-56 to 9-72.

Table I.

Values of the calibration coefficient, B, obtained by fitting Eq. 5 to calibration data separately for increasing pressure and decreasing pressure for five calibration cycles and comparison of each of these values with  $B_0$ , arbitrarily defined as that resulting from the first calibration cycle with increasing pressure. That the values of  $B/B_0 - 1$  for decreasing pressure tend to be larger than for increasing pressure is indicative of hysteresis.

Increasing Pressure			Decreasing Pressure	
	B, MPa	$\frac{B}{B_0} - 1$ , ppm	B, MPa	$\frac{B}{B_0} - 1$ , ppm
( $B_0$ )	307.4340	0	307.5151	264
	307.4462	40	307.4563	73
	307.4684	112	307.4933	193
	307.4087	-82	307.4794	148
	307.4636	97	307.4607	87

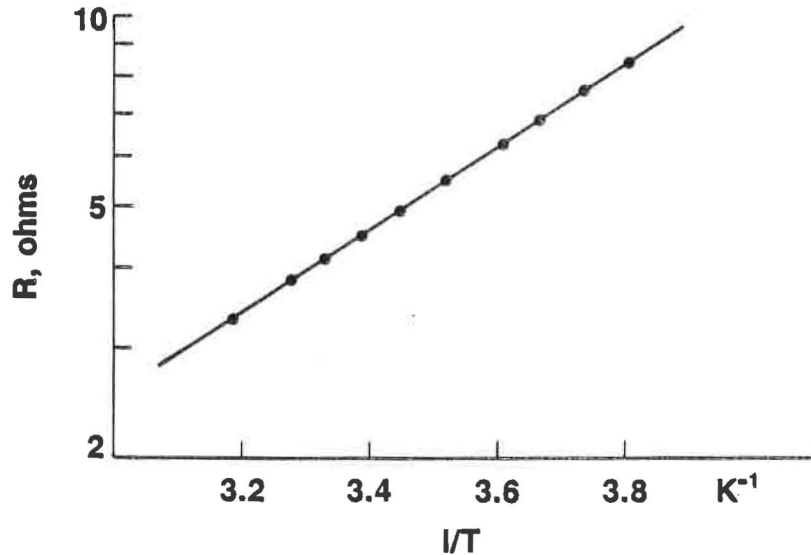


Fig. 1. Resistance plotted semi-logarithmically as a function of  $1/T$ .

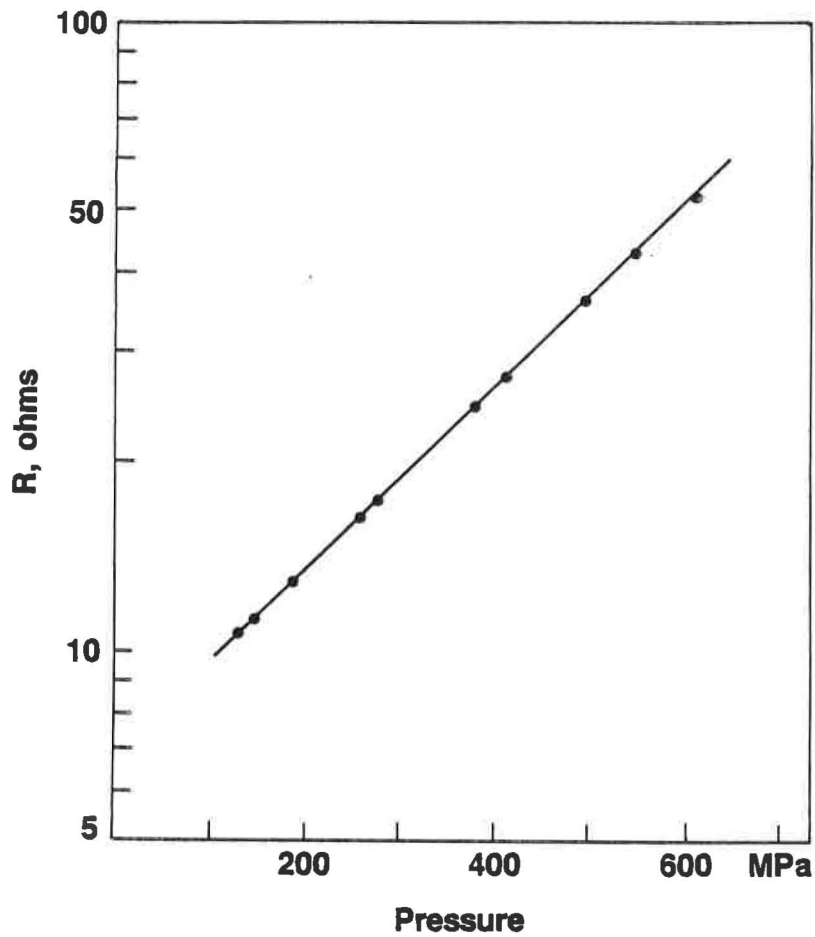


Fig. 2. Resistance plotted semi-logarithmically as a function of pressure.

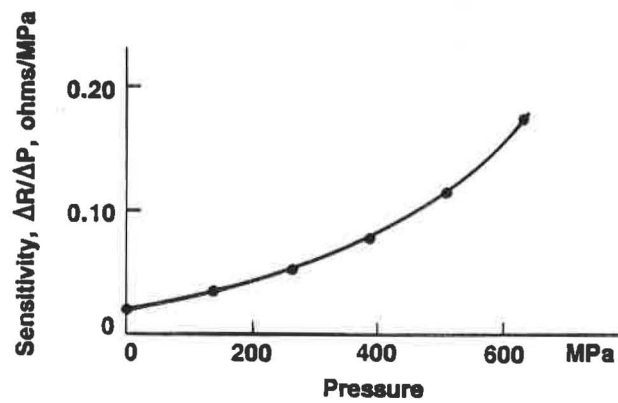


Fig. 3. Sensitivity, defined in the ratio of the change of resistance to the change of pressure, plotted as a function of pressure.

## VNIIFTRI High-Pressure Transfer Standards

Borovkov V.M., Tarassov V.E., Atanov Yu.A.

Two types of portable high-pressure standards have been developed and certified at VNIIFTRI up to 1.2 GPa: a hydraulic pressure multiplier and manganin gauge.

We have built two versions of a multiplier, the MULTIBAR and MULTIBAR-C. Each of them incorporates two unpacked piston-cylinder assemblies and a drive unit. The steel pistons are coated with chromium to increase wear resistance. The low-pressure piston is 50 mm in diameter (35 mm in the MULTIBAR-C). There is a choice of high-pressure piston-cylinder units with diameters from 16 to 2.7 mm allowing the upper limit of measured pressures to vary from 60 to 1200 MPa. The special lever system prevents any stray radial force being transmitted to the rotating pistons. The pistons are kept in a direct contact and aligned by means of conical surface. In the MULTIBAR a sleeve provides alignment of the high-pressure cylinder and simultaneously serves as a low-pressure cylinder. In the MULTIBAR-C the low-pressure cylinder is designed as a separate detachable component. After assembly, the gap between the high-pressure cylinder and the sleeve is taken up by the chuck clamp on the outside surface of the sleeve in the MULTIBAR and by three-contact-point cramp in the MULTIBAR-C. Another characteristic feature of the MULTIBAR-C is a worm reducer built in the drive unit. All interchangeable piston-cylinder units used to reproduce pressures over 100 MPa have partially re-entrant cylinders providing counter-pressure on a lower half of the cylinders. This design feature together with the special profile of the cylinder bore ensures low variation

of multiplication factor with pressure ( $\approx 0.02\%$  at 1.2 GPa) and satisfactory piston fall rates. The maximum fall rates are observed at pressures equal to about 20 or 30% of the maximum pressure of the range chosen.

The multiplier can be equipped with a separating polyethylene membrane permitting different pressure fluids to be used in piston gauges being compared.

The large diameter of low-pressure piston makes it possible to obtain high multiplication factors even for thick high-pressure pistons. Thus we can reproduce the pressures about 1000 MPa using a 10 MPa piston gauge available at any pressure measuring laboratory. When necessary, the multiplier can be easily incorporated into an automatic calibration complex.

On the other hand, the large diameter of low-pressure piston allows its accurate independent certification by direct linear dimensions measurements. With diameter measurement error of  $0.1\ \mu\text{m}$ , one can easily certify the effective area with uncertainty of 5 ppm, since the absolute error of clearance measurements can be reduced to few hundredths of a micrometer. Now the effective areas of distortion-free (zero-pressure) piston-cylinder units employing smaller piston diameters can be easily determined by direct cross-float comparison with the low-pressure piston-cylinder assembly certified earlier.

The pressure dependence of multiplication factor is found from comparison with the National High-Pressure Standard. Also determined are piston fall rates, resolution and uncertainties. We have built a special high-pressure plant to perform such comparisons. It comprises two separate pressure-generating units, two manganin cells used as a differential manometer, and high-pressure valve. The actual comparison of pressures reproduced by

piston gauges takes place when the valve is closed. In this case the gauges operate independently and keep their specific piston fall rates. After the comparison the valve is opened to check the stability of manganin gauges.

The total uncertainty of the multiplier is composed of the following contributions:

- (i) the error due to mechanical rotation drive;
- (ii) short-term instability;
- (iii) the drift of pressure due to inhomogeneous heating of piston-cylinder assembly during continuous operation;
- (iv) the slow drift of pressure due to wear of piston-cylinder assemblies.

The drive error is caused by friction in guide bearings and by stray forces arising from possible defects in bearing races and a guide fork, as well as diverse departures from vertical axis symmetry. This error may have both stationary and oscillating components which can be detected by means of a manganin gauge. The stationary component is obviously equal to the apparent pressure change observed on doubling the rotation velocity since this error is proportional to the rate of rotation. We managed to reduce the oscillating component to about 3 ppm and stationary one to 5 ppm over the whole operation range.

The random error of the multiplier is close to its sensitivity threshold and equals 10 ppm at low pressures and 3 to 5 ppm at maximum pressures of the range.

Since the drift due to temperature rise has a practically constant rate of 3 to 5 ppm per hour, the appropriate correction can be easily found for any moment during the total operation interval of 5 hours.

The drift caused by wear is determined from the results of

service tests after 100 hour operation. The maximum pressure variations amounting to  $40 \div 80$  ppm are observed for the thinnest high-pressure piston. As a rule, such wear resistance is sufficient to carry out an intercomparison. To cope with emergency, a back-up piston-cylinder unit covering the highest pressure range can be supplemented. Generally, the initial dimensions of the deteriorated pistons are easily restored by chrome-plating.

The 70/30 mixture of glycerol and ethylene glycol is usually used as a pressure transmitting liquid that stays Newtonian even above 1.6 GPa. Unfortunately, it has high electric conductivity and may induce electrochemical corrosion of hydraulic system components. If necessary, the MULTIBAR and MULTIBAR-C can operate with other pressure liquids. In this case, however, the pressure dependence of multiplication factor changes, so that during intercomparison it is advisable to operate the multiplier with the abovementioned mixture. If the piston gauge compared operates with different fluid, a separating polyethylene membrane is applied. The measurements show that there is no perceptible pressure difference across that membrane.

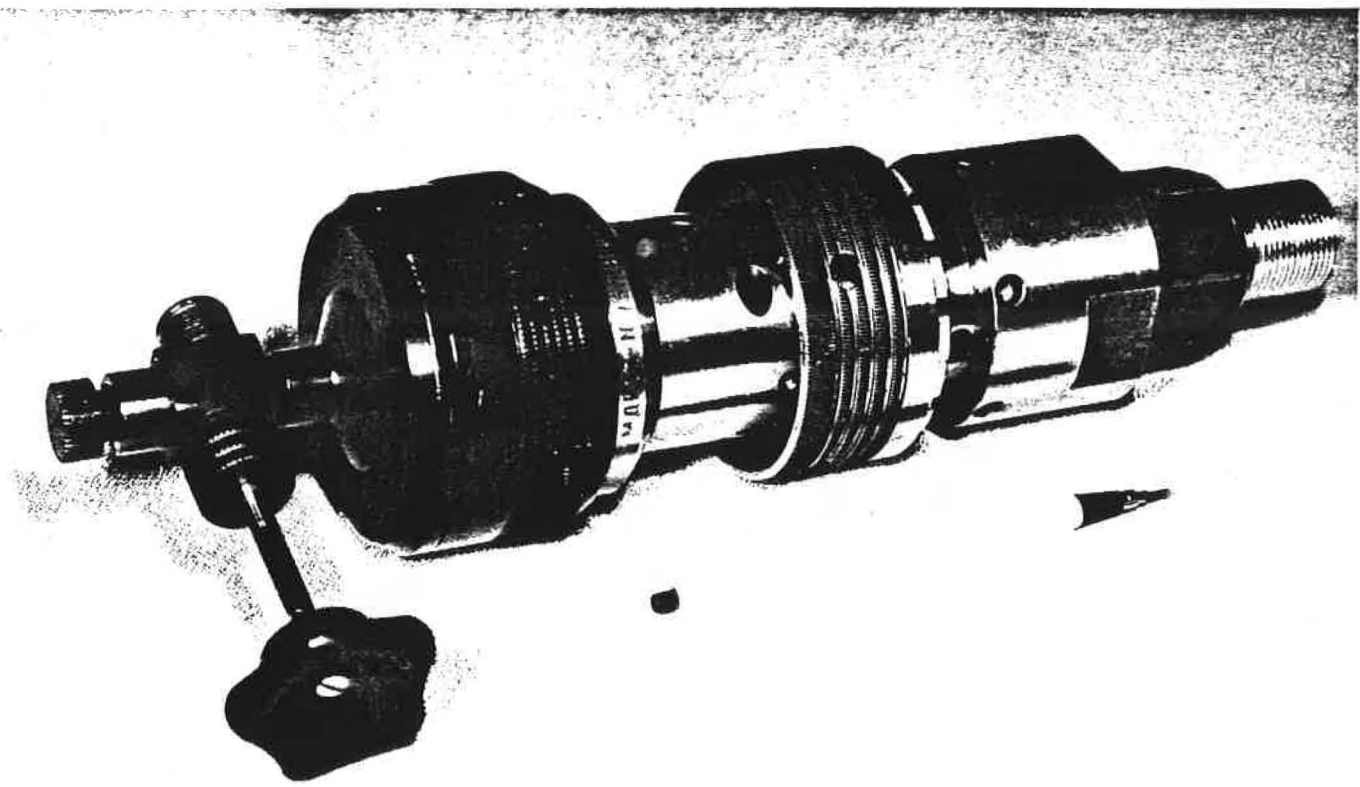
The low-pressure piston-cylinder assembly operates with transformer oil or the like, whose viscosity is about 20 mPa·s.

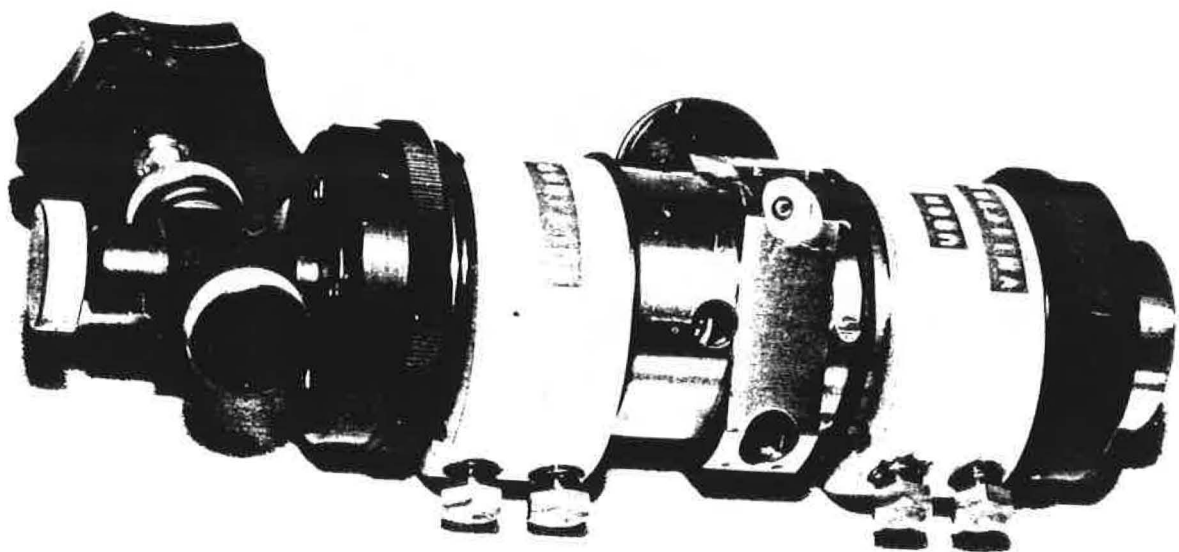
At present our multipliers are supplied with five high-pressure piston-cylinder units with piston diameters 2.7, 3.5, 7, 11, and 16 mm. The corresponding maximum pressures reproduced are 1200, 600, 300, 100, and 60 MPa. Since the low-pressure piston-cylinder unit is easily detached and can be used separately as a dead-weight piston gauge, the multipliers can be used for high precision comparison of pressure standards all over the range from 25 kPa to 1.2 GPa. On the basis of such a multiplier

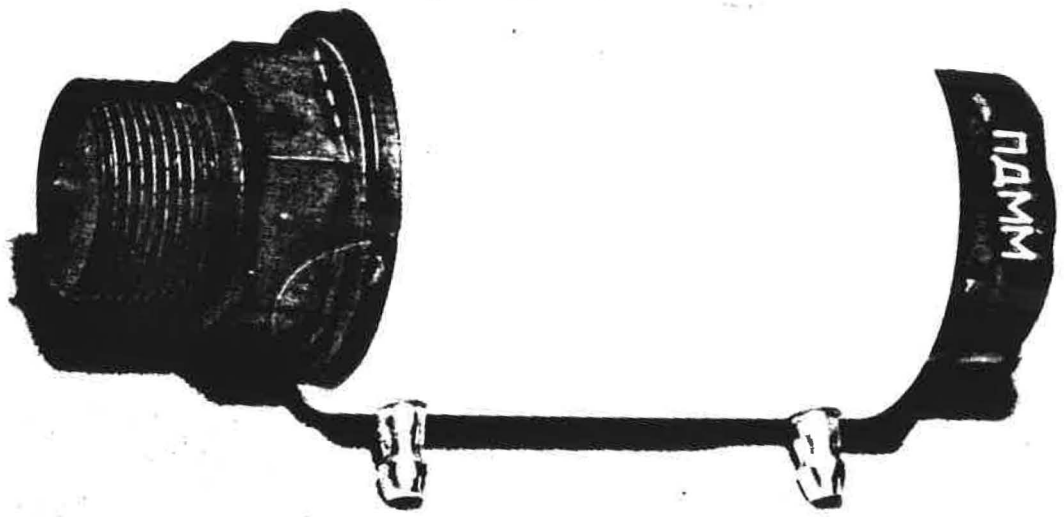
it is possible to develop a series of multirange self-calibrating standards, reference instruments and automatic calibration systems.

The standard manganin cell has a sensing element manufactured from seasoned manganin wire in the shape of a double helix. After proper heat treatment the element is placed in a pressure vessel equipped with thermostat jacket. The cell is calibrated against standard piston gauge to find the interpolation equation  $p = A \cdot (\Delta R/R_0) + B \cdot (\Delta R/R_0)^2$  relating pressure  $p$  with fractional change of electrical resistance of the gauge  $\Delta R/R_0 \equiv (R-R_0)/R_0$ .  $A$  and  $B$  are empirical constants calculated by regression analysis. The standard deviation of the gauge readings is 80 kPa. The drift did not exceed 120 kPa during the intercomparison interval. The total mass of the cell equals 2.4 kg. It can be used with any pressure transmitting liquid owing to special flexible sleeve fixed around the wire coil.

The transfer standards are transported in a vibration-proof metal case. The mass of MULTIBAR with a single high-pressure piston-cylinder unit is equal to 8 kg. The MULTIBAR-C weighs only 3.8 kg. Using these instruments, VNIIFTRI performs routine calibrations of high-pressure piston gauges at the local laboratories. Domestic calibrations of a piston gauge are carried out by a single person in one or two days. The international comparisons in GDR and Hungary were performed by two persons and took three weeks each including technical preparations, checking of hydraulic systems, maintenance repair, comparison data processing and preparation of the final document.









Use of strain gauge pressure transducers as transfer standards  
up to 1.0 GPa at the 0.1 % uncertainty level

J.Jäger

Abstract

Some calibration results are reported for a 1.4 GPa strain gauge transducer. It is concluded that under specified conditions this transducer can be used up to 1.0 GPa as a transfer standard at the 0.1 % uncertainty level, when only the data obtained from measurements in the direction of increasing pressure are evaluated.

Use of strain gauge pressure transducers as transfer standards  
up to 1.0 GPa at the 0.1 % uncertainty level

J.Jäger

Recently the possibility of interlaboratory high-pressure comparison measurements has been discussed in some detail. When national standards institutes perform such measurements they are able to use sophisticated techniques in order to minimize the uncertainty of the comparison. There are however industrial laboratories linked to national calibration services which, like the national standards institutes use piston-cylinder devices to measure fluid pressures up to 1.0 GPa. In view of the increasing international acceptance of calibration certificates issued by these laboratories, economic methods are required to carry out pressure audits in cooperation with the responsible national standard laboratory. Electrical instruments are generally preferred. Strain gauge transducers have the benefit of simplicity and tolerance of unwanted sudden pressure changes. It remains to be shown that the necessary precision and long-term stability can be achieved.

Recently calibration results obtained at the NPL (New Delhi) and the IMGC (Turin) in the 0.5 GPa range have been published / 1 /. In this note we will present measurements performed in the 1.0 GPa range with a strain gauge transducer designed for the 1.4 GPa range, the construction of which has been described by Birks and Gall / 2 /. This transducer, labelled T31, was first calibrated at the PTB in 1975. From measurement cycles up to 0.75, 1.10 and 1.38 GPa, the results of which are given elsewhere (/ 3 /, fig.5), a characteristic

$$V_1(p_e) = 0.11771 \frac{\text{mV}}{\text{V kbar}} p_e + 0.302 \cdot 10^{-3} \frac{\text{mV}}{\text{V kbar}^2} p_e^2 + 5.3 \cdot 10^{-6} \frac{\text{mV}}{\text{V kbar}^3} p_e^3$$

was derived which is valid for measurements at  $t = 20 \text{ }^\circ\text{C}$  in the direction of increasing pressures. Since high-pressure strain gauge transducers show considerable hysteresis effects / 3 /, it is advantageous with respect to the reproducibility of the calibration data to use this characteristic in metrological applications. Identical well-defined schedules must be observed for each calibration cycle and "overshooting" must be avoided when the measured pressures are adjusted.

In Nov.1987 the transducer was recalibrated. As during the measurements in 1975, it was exposed to a room temperature close to  $20 \text{ }^\circ\text{C}$ . A characteristic

$$V_2(p_e) = 0.117550 \frac{\text{mV}}{\text{V kbar}} p_e + 0.3787 \cdot 10^{-3} \frac{\text{mV}}{\text{V kbar}^2} p_e^2$$

was derived from ten measurement cycles up to 0.8 GPa (5 cycles) and up to 1.0 GPa (5 cycles). The standard deviation of the calibration data from this characteristic was  $0.22 \cdot 10^{-3} \text{ mV/V}$  corresponding to 1.9 bar. The relative difference  $2^{-1}\delta_r = [V_2(p_e) - V_1(p_e)]/V(p_e)$  in dependence on pressure is given below:

$p_e$ in kbar	1	2	3	4	5	6	7	8	9	10
$10^3 \cdot 2^{-1}\delta_r$	-0.75	-0.23	0.19	0.52	0.77	0.92	0.98	0.95	0.84	0.64

This result is in good agreement with earlier recalibrations, so that the long-term stability of the transducer may be regarded as satisfactory. However, the temperature coefficient of the zero reading was found to be rather large. A careful temperature stabilization of the transducer should therefore result in a much smaller standard deviation of the data. The thermostat used during a recalibration of the transducer in March 1988 after it had been used for comparison measurements within the German Calibration Service (DKD) is shown in fig.1. Five calibration cycles were performed up to 0.8 GPa.

The new characteristic

$$V_3(p_e) = 0.117669 \frac{\text{mV}}{\text{V kbar}} p_e + 0.3643 \cdot 10^{-3} \frac{\text{mV}}{\text{V kbar}^2} p_e^2$$

was obtained with a standard deviation  $s = 0.55 \cdot 10^{-4} \frac{\text{mV}}{\text{V}}$  corresponding to

0.47 bar. This value is comparable with the performance of the manganin transducers used at the PTB / 4 /. The relative differences

${}^{3-2}\delta_r = [V_3(p_e) - V_2(p_e)]/V(p_e)$  and  ${}^{3-1}\delta_r = [V_3(p_e) - V_1(p_e)]/V(p_e)$  are given below:

$p_e$ in bar	1	2	3	4	5	6	7	8
$10^3 \cdot {}^{3-2}\delta_r$	0.88	0.76	0.63	0.51	0.39	0.27	0.15	0.03
$10^3 \cdot {}^{3-1}\delta_r$	0.13	0.52	0.82	1.03	1.16	1.19	1.13	0.98

It is obvious from  ${}^{3-2}\delta_r$  that the difference between both characteristics expressed in % of reading is well below 0.1 % in the upper half of the measurement range. Since this is a realistic example of the use of the transducer in comparison measurements with a DKD laboratory, it may be concluded that the uncertainty of high-pressure comparison experiments in this pressure range using strain gauge transducers can be 0.1 % of reading and can be as low as 0.03 % at 0.8 GPa (see tab.1). The transducers used in such experiments should be operated well below their nominal full scale pressure and should be well autofrettaged at pressures above this value. The comparatively low sensitivity of such transducers can be compensated by digital measuring units such as the Hottinger DK 38, which permits a transducer signal of 2 mV/V to be resolved into 200 000 digital steps. The temperature of the transducer should be kept constant within  $\pm 0.1$  K.

Table 1. Reproducibility of measurements with a strain gauge transducer  
at  $p_e = 0.8$  GPa

$p_e$ [MPa]	READING $\left[\frac{mV}{V}\right]$	DATE	MEAN VAL. $(1 \pm \text{MAX.REL.DEV.})$	REL.DEV. OF MEAN
801.09	0.96609	15.3.1988		
	0.96609	17.3.		
	0.96608	18.3.	$0.96604 (1 \pm 1.5 \cdot 10^{-4})^*$	
	0.96590	23.3.		
	0.96606	25.3.		
				$2.1 \cdot 10^{-4}$
801.09	0.96616	26.11.1987		
	0.96576	7.12.		
	0.96560	8.12	$0.96584 (1 \pm 3.3 \cdot 10^{-4})^+$	
	0.96596	11.12.		
	0.96574	14.12.		

\* transducer thermostatted at  $20 \text{ }^\circ\text{C} \pm 0.05 \text{ K}$

+ transducer not thermostatted. Air conditioned room temp.:  $20 \text{ }^\circ\text{C}$

All readings taken from complete calibration cycles measured in the direction of increasing pressures.

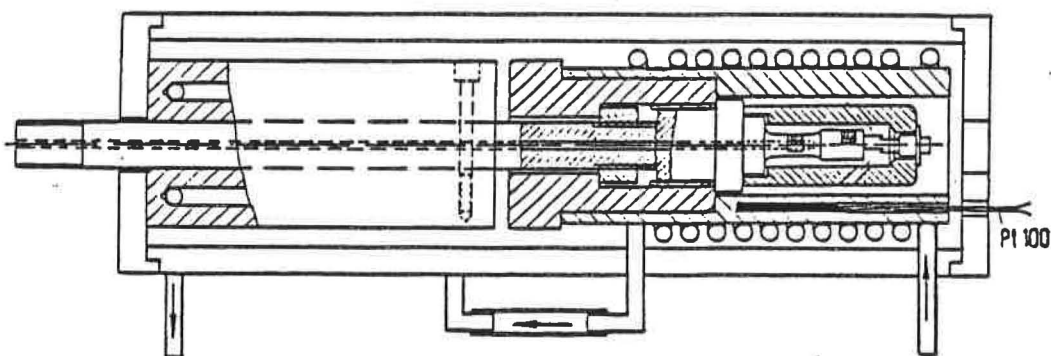


Fig.1

Strain gauge transducer mounted in a thermostat

## References

- / 1 / J.K.N.Sharma, K.K.Jain and G.F.Molinar: Sensors and Actuators, 11 (1987), 275-282
- / 2 / A.W.Birks and C.A.Gall: Strain, April 1973, 1-7
- / 3 / J.Jäger and W.Wanninger: Feinwerktechnik & Messtechnik 84 (1976), 387-391
- / 4 / J.Gieleßen: Z.Instr. 72 (1964), 182-186

STABILITY AND METROLOGICAL CHARACTERISTICS  
OF MANGANIN GAUGES UP TO APPROXIMATELY 1 GPa

G.F. Molinar and L. Bianchi  
Istituto di Metrologia "G.Colonnetti" - IMGC  
Strada delle Cacce 73 - 10135 TORINO, Italy

**ABSTRACT**

Progress on the study of manganin gauge pressure transducers is dealt with. Special attention is given to the stability with time of the electric resistance at atmospheric pressure of two manganin gauges, which were checked over a period of four years, and to the differences in calibration resulting from the use of different fluids and to those due to time. Conclusions are drawn and suggestions are given, especially on the basis of the experience of the last two years, for a possible use of such transducers as pressure transfer standards. Such experience showed that the satisfactory stability and the metrological characteristics of these transducers, particularly small changes of calibration in time, make them suitable for this use if the required uncertainty is less than  $5 \cdot 10^{-4}$  up to 1 GPa, and if they are used only up to 800 MPa when the pressurizing fluid is diethyl-hexyl sebacate (DHSeb).

**STABILITY AND METROLOGICAL CHARACTERISTICS  
OF MANGANIN GAUGES UP TO APPROXIMATELY 1 GPa**

G.F. Molinar and L. Bianchi  
Istituto di Metrologia "G.Colonnetti" - IMGC  
Strada delle Cacce 73 - 10135 TORINO, Italy

**1 INTRODUCTION**

The study of the metrological characteristics of manganin transducers began in 1981. The two transducers specifically tested, denoted as IN-1 and IN-2, and already described elsewhere /1/ from a constructional point of view, had been studied in past years working in a liquid medium, especially in connection with:

- their characterization, by comparison with pressure balances and by the aid of the mercury melting curve /1/;
- their characterization and stability in time when working over a wide temperature range from -20 °C to +80 °C /2/;
- their use to 500 MPa in comparisons between the national metrological laboratories of Italy and India /3/.

The present paper summarizes briefly the results achieved with the two manganin cells investigated and their stability in time. The behaviour in time of the electric resistance,  $R_0$ , of the transducers at atmospheric pressure and at a temperature of approximately 30.7 °C is analyzed. The results of calibrations made over a 1-year period and in longer time intervals and with the use of different fluids are compared and discussed, in particular those obtained during one year with the use of the same fluid (diethyl-hexyl sebacate, DHSeb). On the basis of the experience gained, suggestions are also advanced concerning the transportation of such transducers and operational procedures, which will make them suitable as transfer standards in international comparisons

over the 200 to 800 MPa range.

The measurement accuracy of these transducers, in a period of at least one year, is well within  $\pm 5 \cdot 10^{-4}$  provided that pre-established precautions are always taken.

## 2 APPARATUS USED IN CELL TESTING

The tests were carried out with manganin cells IN-1 and IN-2 immersed in a thermal active-control bath of silicone oil, in which the temperature can be maintained at the pre-established value of 30.7 °C, with  $\pm 0.02$  °C long-term (about 1 year) stability. A stability within a few thousandths of Celsius degree can be maintained over the shorter periods (days) required for a complete transducer calibration.

A controlled-clearance piston gauge of 1.2 GPa capacity and  $\pm 200$  ppm accuracy was used for the calibration of the manganin gauges. The temperature of the transducer body was measured by means of a shielded platinum resistance thermometer with an uncertainty not exceeding  $\pm 0.02$  °C. It was thus possible to detect the heat of compression so that through temperature measurement it was possible to estimate the time needed for pressure to stabilize after a pressure change.

The resistance of the manganin transducers was measured with an automatic a.c. double Kelvin bridge with a resolution of  $1 \times 10^{-7}$ . Account being taken of all systematic (including the accuracy of a standard resistor of  $\pm 1$  ppm) and random contributions, the accuracy of the electrical resistance value amounted to  $\pm 0.2$  milliohm (i.e.,  $\pm 2$  ppm).

Up to 1985 all the calibrations were performed with a mixture of gasoline and UNIVIS P38 mineral oil (10:1 in volume) as the pressurizing fluid, which can be used up to 1.2 GPa. However, since it was feared that possible effects of friction might cause instability of the cylinder

diameter of the piston gauge, in 1986 the UNIVIS mixture was replaced by pure DHSeb (Reolube DOS), which is still used.

This fluid proved to be a good choice from the point of view of the sensitivity of the manganin gauges and of the piston gauge up to 800 MPa. At higher pressures it starts to solidify. In the beginning of this process, the piston gauge becomes insensitive to small mass adjustments and the pressure transducer shows sizable instability of the electrical resistance of the manganin coil.

### 3 RESULTS

#### 3.1 Behaviour of $R_0$ in time at $P_{atm}$

Fig.1 illustrates the behaviour of  $R_0$  over a period of one year (February 1987 -February 1988) for the IN-2 manganin transducer maintained at a temperature of  $30.7 \pm 0.02$  °C and always used with the DHSeb pressurizing fluid. The behaviour in time of  $R_0$  of the IN-1 manganin transducer was nearly the same.

The value of  $R_0$ , for both manganin transducers, appears stable to within  $\pm 13$  ppm over one year, which is a

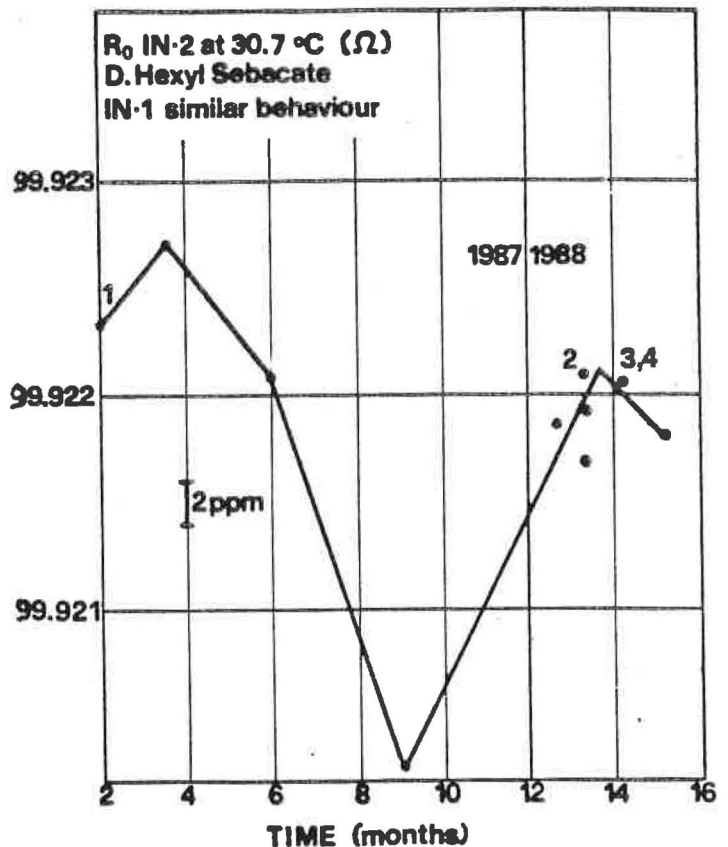


Fig.1 ·  $R_0$  at atm P for manganin gage IN-2 in 1 year.

satisfactory result. In the same period the average temperature remained constant at  $30.7 \pm 0.02$  °C; however, with temperature fluctuations due to the fluid compressibility taken into account, the uncertainty band is equal to  $\pm 0.06$  °C. In any case, even when considering this uncertainty band, the variations in  $R_o$  observed over one year are not significant.

Much larger variations were observed in  $R_o$  over a five-year period including an irregular increment reaching about  $1 \cdot 10^{-3}$ . The  $R_o$  shifts were much more substantial when the mixture of mineral oil and gasoline was used rather than DHSeb. It must be pointed out also that some measurement cycles carried out at temperatures between -20 and +80 °C in 1985 and some changes made in the electrical connections of the transducers at the end of 1986 were also responsible for the high increase in  $R_o$ .

Given this large variation in  $R_o$ , amounting to about 300 ppm, a comparison was made of the calibration cycles carried out with different fluids before and after this increase (see next section). Since the differences between the calibration factors when using gasoline-mineral oil were slightly higher than those using DHSeb (Fig. 2) it was considered necessary to adopt a procedure including an accurate determination of the value of  $R_o$  before and after each calibration cycle and the use of the same type of fluid. With DHSeb the  $R_o$  values were more stable than with other fluids over the period of one year. During a complete calibration cycle  $R_o$  is stable to within a few ppm which is about the same change observed during a week at atmospheric pressure.

3.2 Comparison of calibration cycles carried out with different fluids

Fig. 2 gives the calibration factor  $K = \delta/P = f(P)$ ,  $\delta = R/R_0 - 1$ , where  $R_0$  and  $R$  denote transducer resistance (specifically, of transducer IN-2), at atmospheric pressure and at pressure  $P$ , respectively.

When comparing cycle 11 (Sept. 1986), carried out with the mineral-oil and gasoline mixture, with cycles 1, 3, and 4 (Feb. 1988) made with the DHSeb fluid, a substantial difference of  $1.8 \cdot 10^{-3}$  at 186 MPa is noticeable in the calibration factor. For this difference there is no clear explanation.

There was a decrease of  $2.3 \cdot 10^{-4}$  in  $R_0$  between

the two calibration cycles of Sept. 86 and Febr. 88 which is by no means to be neglected, and neither is the fact that with a pressure balance and with the use of DHSeb much more regular and repeatable pressure equilibrium can be obtained. However, change in  $R_0$  account only partially for the high systematic deviation observed.

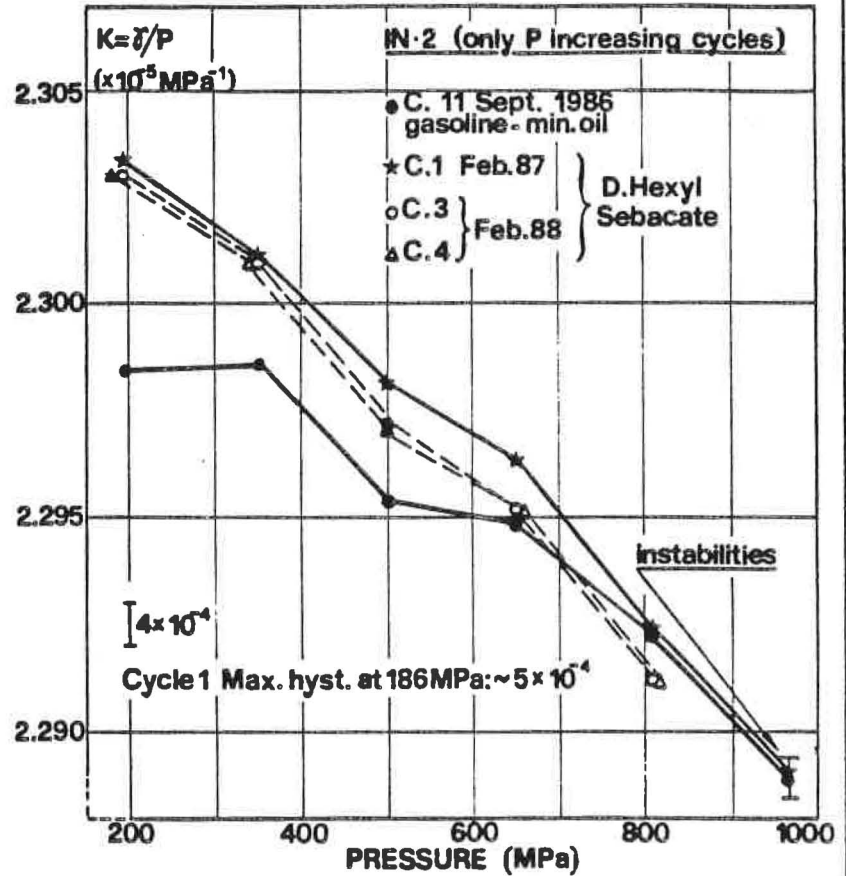


Fig. 2.  $K = \delta/P = f(P)$  in different calibration cycles over 18 months for IN-2 manganin gage using different fluids.

### 3.3 Comparison of calibration cycles carried out in a 1-year period with the same fluid

Fig. 2 shows also the results of calibration cycles 1 (Febr. 87), 3 and 4 (Febr. 88) using IN-2. Similar results were obtained with IN-1. In these cycles the value of  $R_0$  (see section 3.1) was satisfactorily stable as well as the temperature.

The transducer was not moved physically and the resistance measuring system was calibrated before and after the measurements by means of a standard resistance; the accuracy in the  $R_0$  and  $R$  values was confirmed to be  $\pm 2$  ppm. The same calibration procedure was always applied which consisted of three preloading cycles to  $P_{max}$  (about 800 MPa) and before passing from one pressure equilibrium point to the next, 10 minutes were allowed to elapse to wait for temperature stability. The pressure transmitting fluid was never removed from the manganin coils.

The cycles carried out allow the following conclusions:

- Repeatability of the calibration factor of both cells during one year's time and between 150 and 800 MPa always remained within  $\pm 4 \cdot 10^{-4}$ ; between 300 and 800 MPa repeatability was typically within  $\pm 2 \cdot 10^{-4}$ .
- With the DHSeb fluid the hysteresis of the tested transducers was definitely smaller than that observed using mineral oil and gasoline. At lower pressures (approx. 100 to 200 MPa) hysteresis may be of the order of a few parts in  $10^4$ , though it can be reduced by following a specific calibration procedure that defines the time intervals for pressure increase and for pauses at the established pressure points.
- When using the DHSeb fluid, it is better not to exceed 800 MPa. Attempts were made (Fig. 2) to realize a calibration point at 960 MPa, but very poor repeatability was obtained, because at this level the pressure

balance showed sensitivity loss and the indications of the manganin cells were made deceitful by the imperfect hydrostatic conditions of the fluid.

Fig. 3 shows the difference in the in calibrations of manganin cells IN-2 and IN-1 done in Febr. 87 and Febr. 88.

The standard deviations of the second order equations used are, typically, 0.1 MPa. No substantial differences were observed in linearity. The pressure differences of the calibrations remained within  $\pm 3 \cdot 10^{-4}$  during a period of one year. The IN-1 manganin cell proved to be better than IN-2 in reproducibility; which was estimated to be  $\pm 0.5 \cdot 10^{-4}$ , during the year.

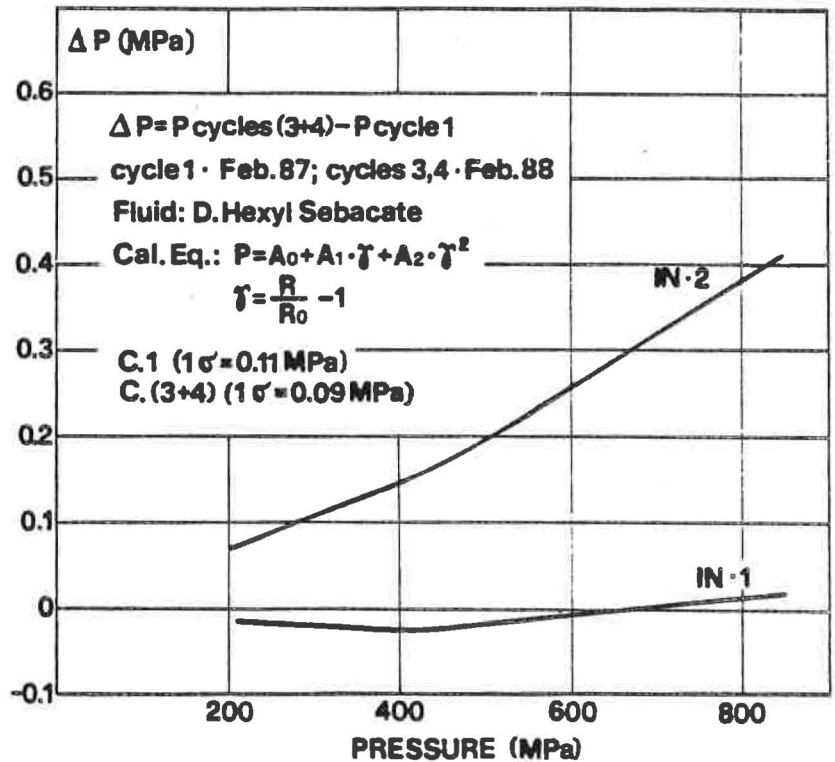


Fig.3. Pressure difference between two calibrations of manganin gages IN-1 and IN-2 in 1 year. Manganin gages maintained at  $30.75 \pm 0.05$  °C over a one year period.

#### 4 CONCLUSIONS AND RECOMMENDATIONS

The results obtained in the tests carried out during a period of one year using the DHSeb fluid confirm that the manganin cells tested can be used as transfer standards in international comparisons if the required uncertainty is not better than  $\pm 5 \cdot 10^{-4}$ . Short-term reproducibility can be better than

$2 \cdot 10^{-4}$ ; hysteresis, which may be high at pressures around 100 MPa, can be reduced by means of a careful calibration procedure. The above results were obtained, as a rule, when the electric resistance of the manganin cells at atmospheric pressure was highly stable. Even when it drifted by a value as high as 1 or  $2 \cdot 10^{-4}$ , similar results can be expected provided the calibration procedure includes the acquisition of several values of  $R_0$  in a calibration cycle. The main precautions to be taken to achieve the results indicated are summarized as follows:

- During tests, the manganin cells have to be always maintained at the temperature at which  $R_0$  is maximum; with the present manganin cells this temperature value is 30.7 °C.
- It is sufficient to maintain the temperature of the manganin cells constant to within  $\pm 0.05$  °C, which is easily obtained with an active-control bath.
- It is necessary to verify that no big  $R_0$  drift occurs in a calibration cycle.
- The manganin cells must be transported very carefully, to avoid mechanical shocks; it is also advisable to seal the cells so as to maintain the fluid in contact with the coils.
- It is recommended to use always the same pressurizing fluid. The DHSeb fluid has proved to be very satisfactory, especially as regards  $R_0$  stability.
- It is advisable not to alter the electric circuitry and cabling of the manganin cells, so that d.c. or a.c. resistance measurements may always be carried out in the same configuration. In any case, it is good practice to indicate whether  $R_0$  and  $R$  measurements are made in d.c. or a.c.

At IMGC the two manganin cells tested are at the disposal of those who

might wish to compare their calibration systems up to 800 MPa with an estimated uncertainty of  $\pm 5 \cdot 10^{-4}$ . Research work is still in progress for complete automation of signal recording for these manganin cells. The system is basically similar to others /4/, but applies a measuring system that should not resort to precision multimeters and employs, instead, devices for a/d conversion, in view of a direct use with personal computers /5/.

#### REFERENCES

- /1/ MOLINAR G.F. and BIANCHI L. Metrological characterization of manganin gages calibrated against the mercury melting line. Proc. IX AIRAPT Confer., Albany (USA) 1983. Nat. Res. Soc. Symp. Proc. vol. 22, 1984. Elsevier Publishing Co. USA.
- /2/ MOLINAR G.F., BIANCHI L., CERUTTI G. Pressure metrology up to 1.2 GPa with manganin gauges. Physica 139 and 140 B (1986) 743-745, Amsterdam, North Holland.
- /3/ MOLINAR G.F., BIANCHI L., SHARMA J.K.N., JAIN K.K. Intercomparison of pressure standards up to 500 MPa by means of pressure transducers. High Temperatures - High Pressures, 18, (1986), 241-247.
- /4/ NORELDIN O. and SCAIFE W.G. Automatic measurement of high pressures. J. Phys. E: Sci. Instrum. 20 (1987), 1212-1214.
- /5/ FASCIANI P. Studio e realizzazione di un sistema automatico per le misure di alte pressioni mediante sensori resistivi. Politecnico di Torino, Tesi di laurea, Dicembre 1987.

Manganin resistance manometer :  
III. Pressure coefficient of resistance

Shojiro Yamamoto  
National Research Laboratory of Metrology  
1-1, Umezono, Tukuba, Ibaraki 305, JAPAN

ABSTRACT

The pressure coefficients of manganin resistance have been investigated with Isabellenhutte and Driver Harris wires in a pressure range up to 1 GPa for ten years.

It may be expected that the pressure coefficients are constant within  $\pm 1$  % of the average values among the wires of the same manufacture, and  $\pm 0.2$  % among a spool of wire, and quite reproducible for a long period.

German wire has the largest pressure coefficient expressed by the following quadratic equation;

$$R_p = R_0 ( 1 + 2.51 \times 10^{-5} * P - 1.8 \times 10^{-10} * P^2 ) \quad [ P \text{ in MPa } ] .$$

1. Introduction

Since the manganin alloy was found to be a suitable material for pressure sensors in a high pressure range by Lisell in 1903, even nowadays it is still the best one. With recent progress in electronics, the resistance measurement has become so easy and precise just by using digital multimeters instead of conventional Mueller or Caray Foster bridges that the resistance manometer seems more convenient and useful to use as pressure transducers over a wider pressure range. In fact, Noreldin and Scaife(1987) use it connecting to a computer-controlled data gathering system to reduce measured resistances to the pressure scales automatically.

However, many researchers have reported the troubles with manganin gauges due to the drifts of the initial resistance and consequently the variations of the pressure coefficient. Recently, Klingenberg(1981), Molinar et al(1986) and Noreldin et al(1987) have described that their manganin gauges showed more or less increases in the initial resistance.

In the previous papers(1972), the construction and seasoning of the manganin gauges were studied with Japanese and Driver Harris wires. It was found that the pressure coefficients of resistance varied nearly proportionally with the manganese content in manganin alloy, and were almost constant among the wires of the same manufacture.

After the publications, a so-called German wire was available which was well known such a good wire as Bridgman had pointed out. On the other hand, some knowledge about the temperature and pressure coefficients for German wire have been published in literatures. Thus experiments were continued particularly with an intention to establish the metrological characteristics as resistance manometers of German wire as accurately as possible so that everyone may use the manganin gauge made from German wire without individual calibration for most purposes, just like platinum resistance thermometers in temperature measurements. This paper describes the results, referring to the literature values.

2. Experiments

The sample wires used were of B&S 38 (0.1mm dia), double silk covered, made in Isabellenhutte(German) and Driver Harris Co.(USA). The Driver Harris wire was that drawn in 1975, and 56  $\mu\Omega/\text{m}$  in resistivity, while the German wire was not known of the details but very old. The German wire featured somewhat brighter in appearance of metal and stiffer in feeling as compared with the Driver Harris'.

Three coils were wound from both the wires, respectively, into the shape of self-supported elliptic according to the previous experience. The overall size is about 5 mm in width and 25 mm in length.

The annealing was carried out for 15 hours at 140°C in argon gas. The resistances decreased during the annealing by approximately 2 % for the German wire, while 0.5 % for Driver Harris wire as reported in the previous paper.

The coils were carefully soft-soldered to the leads of insulated plugs, there being two types. One was of a small cone resined with Araldite and a piece of thin paper as insulator. The other was of sheathed wire. Both had only one leadwire insulated from the plug body. Outside the manganin cell, shield cable of 4 wires was used.

The resistances during calibrations were measured usually with digital multimeters ( HP 3456 ) of a resolution of 0.1 mΩ, connected to a computer, and have been followed for ten years with occasional calibrations and practical use in a pressure range up to 1 GPa at room temperature. The calibrations were done against a dead-weight piston manometer at pressures of 0.2, 0.4, 0.6, 0.8, and 1.0 GPa. The pressure transmitting liquid used was a mixture of UNIVIS P12 and white gasoline of 50 to 50 % by volume.

The other experimental details were already described elsewhere.

### 3. Results and Discussion

The resistances of all the coils were sufficiently stable to measure down to the resolution of the instruments. However, most of them showed gradual increases of the resistance with time. The rate depended on the gauge, but some amounted to as much as 50 mΩ per year. In the worst case, it reached the break of the circuit in the plug which was of the cone type. While the initial resistances of the two gauges have not changed at all for ten years, for which the sheathed wire plugs were used. It may be thought, therefore, that the cause of the resistance increase should be located to the change in the lead resistance of the plug and/or soldering.

The data of the calibration, i.e., the resistances as a function of pressure were fitted to the quadratic equation by the least squares method,

$$R_p = R_0 ( 1 + A P + B P^2 )$$

where  $R_p$  is the resistance [ $\Omega$ ] under pressure  $P$  [MPa],  $R_0$  the resistance at atmospheric pressure, and  $A$  and  $B$  are coefficients. The average values of the coefficients of the linear and quadratic terms are shown in Table 1. The standard deviations of the residuals from the regression equations were about 0.2 mΩ corresponding to about 0.1 MPa.

Table 1. Pressure coefficients of manganin resistances, determined at present study

Manufacture	$A \times 10^{-5} (\text{MPa})^{-1}$	$B \times 10^{-10} (\text{MPa})^{-2}$
German wire	2.510	-1.8
Driver Harris wire	2.395	-2.0

It is interesting to compare this result for the German wire with all the information available in the literatures, which being shown in Table 2. In spite of absolutely independent and wide spread in time experiments, it may be said that the pressure coefficients are in good agreement though those in early stage like Bridgman(1912) and Michels(1934) were considerably lower. The five researchers' values are within  $\pm 1\%$  of the average. This fact suggests that German wire is so well quality controlled that one may assume the pressure coefficient to be nearly constant.

It was realized that the dispersions of our pressure coefficients were

Table 2. Pressure coefficients of manganin gauges made from German wires, reported in the literatures

Researcher	A $\times 10^{-5}$ (MPa) $^{-1}$	B $\times 10^{-10}$ (MPa) $^{-2}$	Pressure(GPa)
Bridgman (1912)	2.34-2.37		1.3
Michels (1934)	2.346	-2.5	0.4
Lippmann (1970)	2.54-2.575	-3.2- -1.5	
Morris (1975)	2.52	-2.05	
Klingenberg(1981)	2.5	-2	0.81
Sundqvist (1987)	2.48		
Yamamoto (1988)	2.510	-1.8	1.0

partly due to the variations (not corrected) of the working conditions of the primary gauge but partly due to the contribution of the lead resistance. If the initial resistance of a manganin gauge include  $0.1\Omega$  of lead resistance, then the apparent pressure coefficient is smaller by 0.1 % than the true one. Our manganin gauges were not measured perfectly by 4-wire method, but had about  $0.1\Omega$  of the lead resistance at the insulated plugs of the sheathed wire type, while about  $0.05\Omega$  of the cone type plug. Furthermore, the lead resistances tend to vary temporarily and permanently under pressure. Also it should be noted that the insulate resistance between the lead and plug body does affect the reproducibility of the initial resistance. That was as high as  $1\text{ G}\Omega$  for the sheathed wire plug but about 10 to 100  $\text{M}\Omega$  for the cone plug. It appeared that Morris used 4 wires insulated plugs and his pressure coefficient was a little higher.

#### 4. Conclusions

With an intention to establish the resistance-pressure relation of manganin, some gauges made from German and Driver Harris wires have been investigated for ten years in a pressure range up to 1 GPa.

Followings were found;

- (1) the initial resistances were completely constant and stable for a long period unless the lead resistance changed.
- (2) the pressure coefficient may be expected to be fully reproducible within  $\pm 1\%$  of the average among the wires of the same manufacturer and  $\pm 0.2\%$  among wires of the same spool.
- (3) the resistance-pressure relation of German manganin wire can be expressed in terms of a quadratic equation with the linear coefficient  $2.51 \times 10^{-5}$  (MPa) $^{-1}$  and the quadratic  $-1.8 \times 10^{-10}$  (MPa) $^{-2}$ .

A recommendation is made that all high pressure experimenters should use, if possible, the same wire from a definite source, then one may measure pressure accurately better than  $\pm 0.2\%$  without individual calibration, and even perform an international comparison of his high pressure scale without transferring the actual gauge.

#### References

- Noreldin O and Scaife W G 1987 Automatic measurement of high pressures J.Phys.E: Sci.Instrum. 20 1212-4  
 Klingenberg G 1981 Untersuchung der Langzeitstabilitat einiger Manganinmanometer PTB-Mitteilungen 91 1/81 33-5  
 Molinar G F, Bianchi L and Cerutti 1986 Pressure metrology up to 1.2 GPa with Manganin gauges

Physica 139/140B 743-5  
Yamamoto S 1972 Manganin resistance manometer:I. Construction  
Bull.of NRLM(Japan) 24 23-31  
Yamamoto S 1972 Manganin resistance manometer:II. Seasoning  
Bull.of NRLM(Japan) 25 1-6  
Bridgman P W 1912 Measurement of hydrostatic pressures up to 20000 kg/cm<sup>2</sup>  
Proc.Amer.Acad. 47 321-43  
Michels A and Lenssen M 1934 An electric manometer for pressures up to 3000  
Atmospheres  
J.Sci.Instrum. 11 345-7  
Morris E C 1975 High-pressure measurement with manganin gauges  
J.Instrum. and Control(Australia) 32 77-80  
Sundqvist B 1987 Low T hydrostatic limits of n-pentane/iso-pentane mixture  
measured by a self-supporting Manganin pressure gauge  
J.Phys.E: Sci.Instrum. 20 984-6

P A R T    2

PRESSURE TRANSDUCERS, TRANSFER  
STANDARDS, DYNAMIC PRESSURE  
MEASUREMENTS, FIXED POINTS

Sub-section: Dynamic pressure measurements, intercomparisons and  
fixed points



## Dynamic calibration of pressure transducer

J.P. Damion

Ecole Nationale Supérieure d'Arts et Métiers  
Laboratoire de Métrologie Dynamique  
151 boulevard de l'hôpital 75013 PARIS

After a brief review of the different methods permitting the determination of the transfer function of a transducer this paper presents the means of dynamic calibration of pressure transducers in a gaseous condition working in the laboratory of dynamic metrology at the Ecole Nationale Supérieure d'Arts et Métiers of Paris and Moes, especially the shock tubes and the fast opening devices

### shock tubes

TO 10	static pressure(0-10 bar) step pressure (0.2-5 bar)
TO 100	static pressure(0-100 bar) step pressure (5-60 bar)
TOR	static pressure(0-4 bar) step pressure (0.2-3 bar)

### Fast opening devices

DOR 10	static pressure(0-10 bar) step pressure (0-10 bar)
DOR 100	static pressure(0-100 bar) step pressure (0-100 bar)

The functioning of the aperiodic pressure generators is described and the limit of use of amplitude and frequency are given.

Papers by J.P.Damion dealing with the same subject presented at the seminar:

- J.P. Damion, Moyens d'étalonnage dynamique des capteurs de pression  
Bulletin BNM, Oct. 1977, 30, 7-22
- J.P. Damion, Méthodes et moyens d'étalonnage dynamique des capteurs de pression en transitoire, Bulletin BNM, July 1981, 45, 15-17
- J.P. Damion, Intercomparaison des tubes à choc ETCA-ENSAM et CERT-ENSAM, Bulletin BNM, July 1982, 49, 15-26

SOME EXPERIMENTAL RESULTS OF CALIBRATION  
OF DYNAMIC PRESSURE RESISTANCE SENSORS  
BY USE OF TRIANGULAR PULSE GENERATOR

by

A.J. ROSTOCKI and R. WISNIEWSKI  
Institute of Physics,  
Warsaw University of Technology  
00-662 Warszawa, ul. Koszykowa 75,  
WARSAW, POLAND

ABSTRACT

The paper presents some results of the measurement of dynamic pressure characteristics of resistive transducers made of materials commonly used for static measurement such as manganin, zeranin, Au-Cr alloy, tellurium etc. The measurements have been made using the generator of triangular pressure pulses up to 500 MPa. The principle of operation of such system as well as the method of calculation of pressure rise in the chamber has been presented. An independent measurement of stress rise in various parts of the chamber has proved that the model used for pressure calculation has been developed correctly. The measurement of characteristics of manganin and Au-Cr alloy have shown good performance and usefulness for the measurement of quick variable pressures.

INTRODUCTION

The measurement of pressure which vary with time is of great importance in many fields of industry and research. The knowledge of dynamic characteristics of pressure transducers is very essential and therefore many efforts have been made to develop methods of dynamic pressure generation in fully controlled manner. In number of papers the experimental devices designed especially for generating of transient pressure have been described [1], [2]. Such devices usually used to investigate "response" of transducers have been developed on the basis of quick operating valves. A new method of quick generation of triangle pressure pulse has been presented in [3], [4] and [5]. The present work presents a modified version of such generator and some results of calibration of electroresistive transducers.

THE PRINCIPLE OF OPERATION OF TRIANGULAR PRESSURE  
GENERATOR

The cross section of triangle pressure generator has been shown in fig.1. The device consist of double piston cylinder systems, one inside the other with the cylinder of interior system acting simultaneously as a piston of the exterior one.

The piston (3) of the interior system being of small diameter if compared to that of high pressure chamber provides the compression of the liquid medium. It is stiffly fixed to the exterior cylinder (4) so that the motion of both parts is the same. The define angular velocity of the whole system as well as the fine fitting of cooperating parts provides the tightness

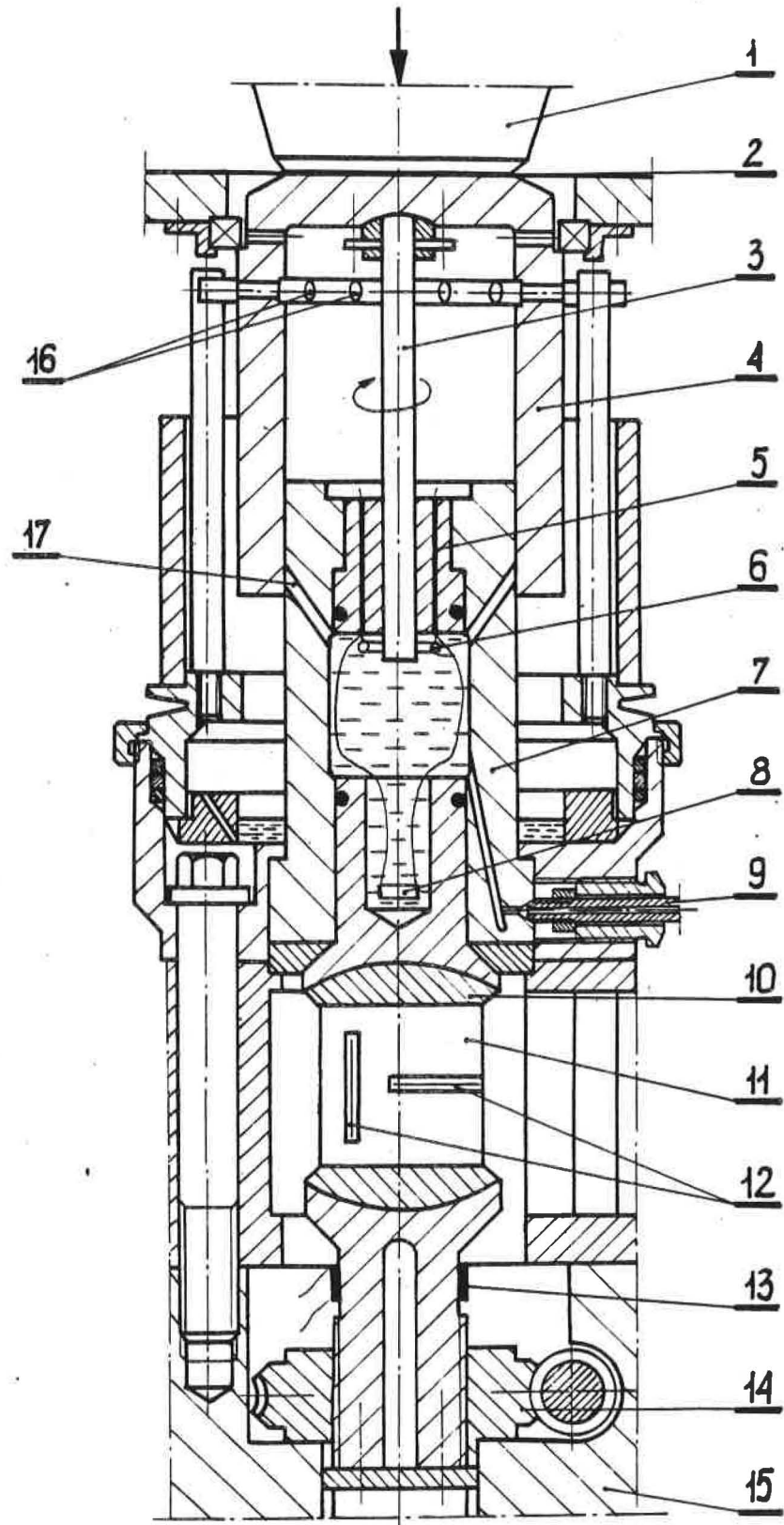


Fig.1. Cross section of triangular pressure pulse generator.

in the same way as it is in dead weight testers. The pressure drops when the side holes (16) and (17) begin to cover each other so that the pressure drop time depends only on dynamical, axially symmetrical outflow of the liquid medium throughout a widening gap.

For the generation of pressure simple pile driver system as a source of energy has been employed. The standard load falling down from the definite height strikes an elastic plate, rigidly connected to the piston (3), causing the movement of the piston and resulting increase of pressure. Since this moment the potential energy of falling down load is converted into potential energy of liquid closed in pressure chamber.

The pulse rise time can be calculated from the formula:

$$t = \frac{s}{\sqrt{2gh}} \quad (1)$$

where : h - height of the fall of the load  
s - medium compressing length

whereas the maximum pressure in pulse can be calculated from the formula :

$$P_{max} = \frac{2mg}{A_{eff}} \quad (2)$$

where : m - mass of the load  
A<sub>eff</sub> - effective area

Thus adjusting the height and selecting appropriate value of the falling mass it was possible adjust the shape of pressure pulses in terms of both time and pressure.

In practice the highest pressure obtained by authors was approaching 500 MPa, whereas the pulse rise time was about 5 msec. for the height of 5m.

Unfortunately there was not possible to calculate theoretically the time of pressure fall. Rough calculation taking into account flow of the liquid through the side holes has given pressure drop time of 20 - 50 μsec., whereas experimental results taken from the analysis of the CRO picture have indicated about 100 μsec.

#### THE EXPERIMENTAL RESULTS OF CALIBRATION OF RESISTANCE-PRESSURE TRANSDUCERS

Using the generator described above the authors have made several experiments of various materials commonly used for pressure measurements. The first measurements have been performed on manganin coils of resistance 100Ω and 500Ω, using the normal Wheatstone bridge with C.R.O. connected to the output of the bridge. The dependence R(t) = f(p(t)) for manganin has been shown in fig.2a. Since the first measurements have indicated excellent linearity of manganin it was very essential to find out what was the source of relatively long "droop time", by the independent measurement. For this reason the authors have made a modification of the lower part of pressure generator, fixing the metal block (no.11 in fig.1) with the strain gauges fixed to its surface. Both independent (fig.2b) and simultaneous (fig.2c) measurements of R(t) of strain gauges and manganin have given the same time dependence of pressure and the same value of pressure in the chamber. Thus they have finally proved that the "droop time" was relatively long due to the finite time of outflow. In most of the experiments the castor oil medium has been applied. Although the large viscosity of it has highly contributed to the observed droop time, the selection of

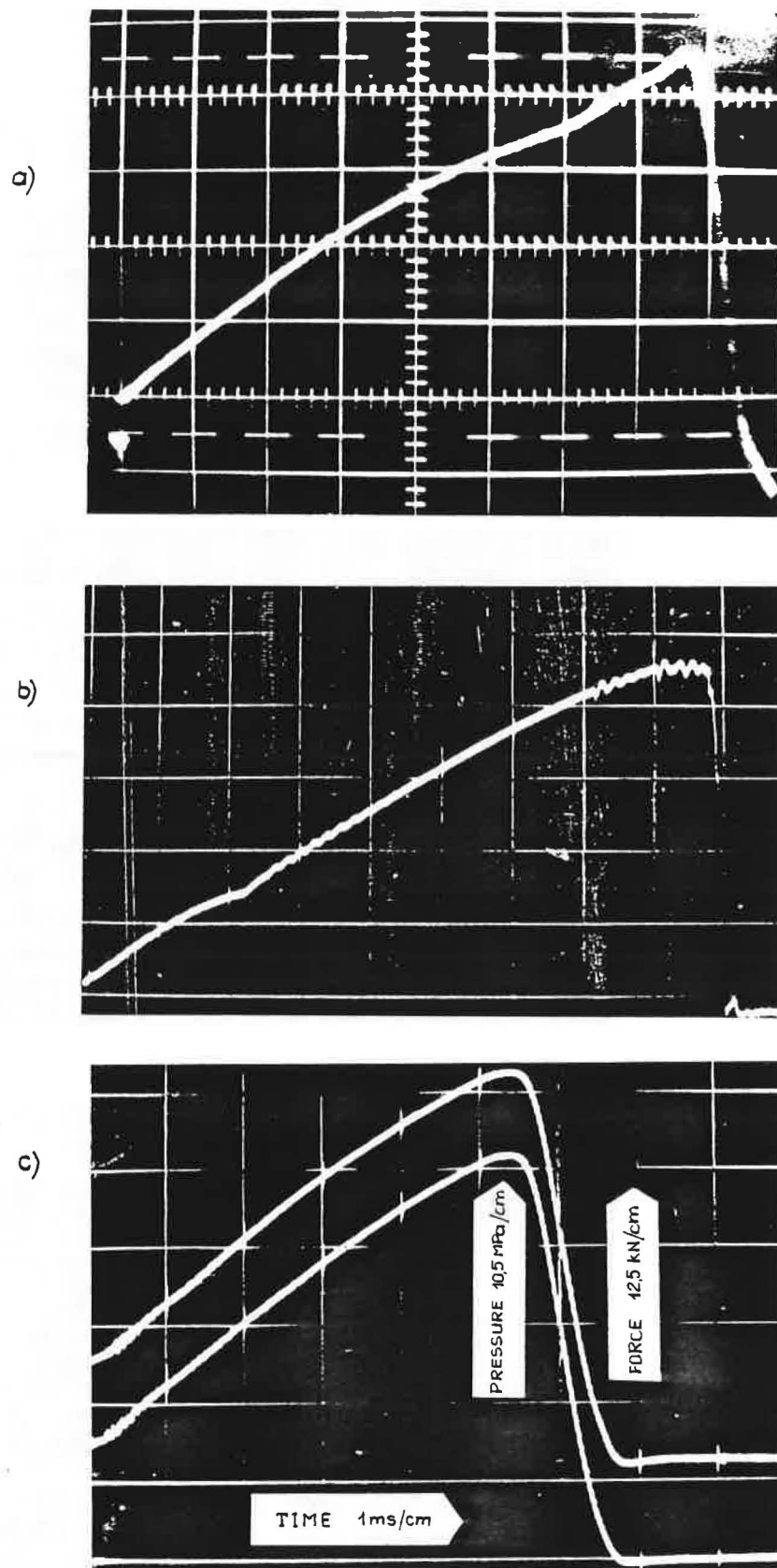


Fig. 2. CRO pictures of the pressure and stress dependence on time a) for manganin transducer, b) for strain gauge fixed to the base, c) for manganin and strain gauge simultaneously.

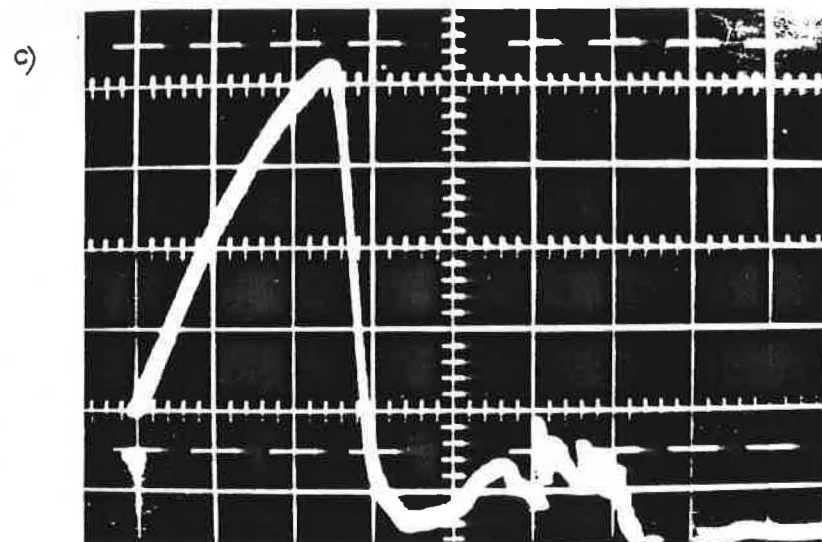
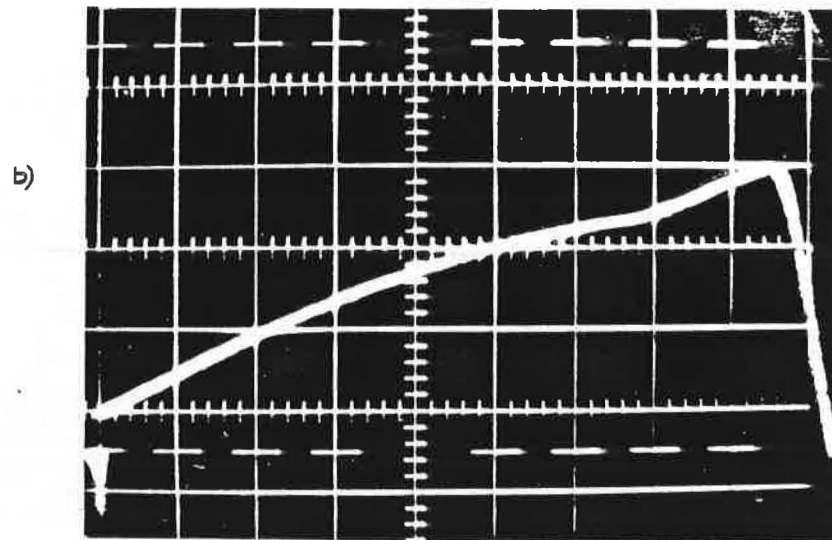
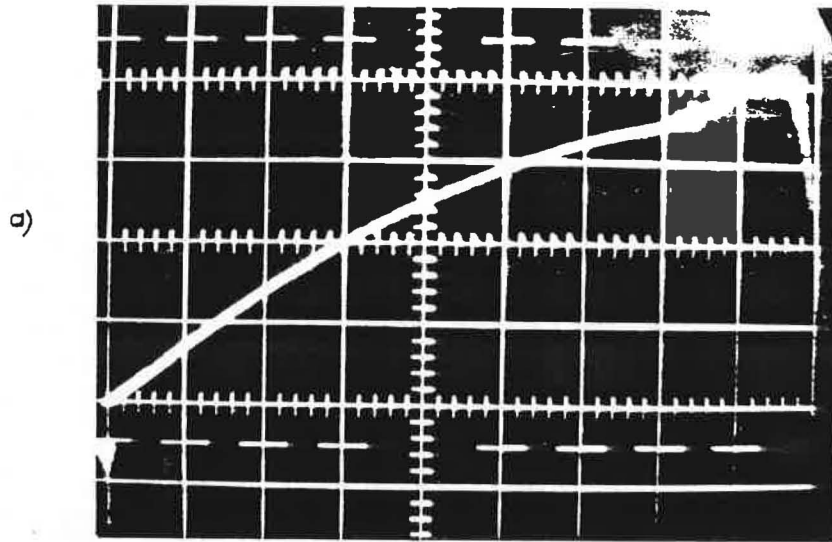


Fig. 3. CRO pictures of the pressure dependence on time for :  
 a) Zerantin transducer, b) Au-Cr transducer c) tellurium.

operational amplifier with the capacitance , holding the peak value of the output voltage from the bridge and supplying it to the digital voltmeter. The recorded peak amplitude was not different from the theoretically calculated more then 5% .

The results of calibration of other materials are shown in figures : 3a - zeranin ,3b - Au-Cr alloy , 3c - tellurium. It is only in case of tellurium the authors have observed nonlinear effects and kind of reaction in form of oscillations after the decompression. The magnitude of those effects rather disqualifies tellurium as a material for making transducers of dynamic pressures.

#### CONCLUSIONS

Presented results have shown usefulness of triangle pressure generator for dynamic calibration of resistive transducers of pressure. It seems to be for dynamic pressures a device analogue to the dead weight piston gauge for static pressures.

Although it is too early to speak about dynamic pressure standard , it is possible to test with help of it the resistive transducers even with accuracy about 5 % .

#### REFERENCES

- [1] J.Schwepe et al. NBS Monograph 67,250,1963
- [2] R.O.Smith Trans.ASME ,723, Dec 1964
- [3] R.Wisniewski, A.J.Rostocki. Polish Patent P184322, 1979
- [4] R.Wisniewski, A.J.Rostocki, W.Bock . Proc. VII-th AIRAPT Int.Conf. p.176, Le Creusot, France 1979 .
- [5] R.Wisniewski, M.Trombik. Przegląd Gorniczy no.7/8,256,1984

The 700 MPa Intercomparisons of the National High Pressure Standards of the USSR, GDR, and Hungary

Borovkov V.M., Tarassov V.E., Atanov Yu.A. (VNIIFTRI)  
Lippman H., Sterner L., Arendt H. (ASMW)  
Gyarmati B., Sarkani G. (OMH)

The intercomparisons of the National High Pressure Standards for liquid media were carried out up to 700 MPa by the metrology laboratories of the USSR (VNIIFTRI), German Democratic Republic (ASMW) and Hungary (OMH) to provide an East-European regional contribution to the International High Pressure comparisons initiated by the CCM Working Group "High Pressures".

In 1986 VNIIFTRI sent to ASMW and OMH its proposals about the various aspects of the forthcoming measurements. A few months later the metrologists from both laboratories came to Moscow to acquaint themselves with the standard instruments and methods adopted in the USSR in the high-pressure piston-gauge comparisons. All technical aspects of the forthcoming comparisons were discussed in detail.

The intercomparisons were accomplished by means of small-size transfer standards: a pressure multiplier (MULTIBAR) and standard manganin cell. Both are described in detail in the foregoing paper.

Prior to the actual intercomparisons the metrological characteristics of the transfer standards were thoroughly studied. The partial errors contributing to the total error were determined and calibrations against the USSR National High-Pressure Standard performed. The relevant statistical parameters together with the pressure drift values were found. All the measurements were repeated after the transfer standards had been brought back after the intercomparisons in GDR and Hungary. The numerical data obtained are shown in Tables 1 and 2. The total error of the MULTIBAR is seen to be so small as to be neglected in the evaluations of high-pressure scale agreement.

Table 1

## Metrological Characteristics of the MULTIBAR

No	Parameter	Value, ppm
1	Sensitivity threshold	4
2	Uncertainty due to piston rotation drive	8
3	Standard deviation of pressure reproduction	40
4	Multiplication factor change after 100 hour operation	70
5	Multiplication factor change during intercomparisons in GDR and Hungary	40

Table 2

## Metrological Characteristics of the Manganin Gauge

No	Parameter	Value
1	Nominal resistance, Ohm	96
2	Sensitivity threshold, MPa	0.002
3	Standard deviation, MPa	0.08
4	Drift during the comparisons, MPa	0.12

The standards intercompared. (i) The USSR National High-Pressure Standard (GOST 8.094-73) is an instrumental complex based on a 1500 MPa piston gauge with hydraulic multiplier. The residual bias is 2 parts in 10,000 and standard deviation is 40 ppm. The low-pressure and high-pressure piston-cylinder assemblies are made of steel. The nominal diameter of the high-pressure piston is 3 mm. The geometry of the assembly has been carefully measured. The piston shape does not deviate from the perfect cylinder more than 0.05  $\mu\text{m}$ . The re-entrant cylinder supports the piston over the entire engagement length, permitting one to neglect the end effects. The special profile of the cylinder ensures very low leakage rates and enables computer-aided calculations of effective area.

The pressure unit reproduced by the National High-Pressure Standard is compatible with that reproduced by the USSR Primary Pressure Standard (up to 6 MPa). The uncertainty of effective area at any pressure is reduced down to 50 ppm with corrections

made for (a) the real geometry of piston-cylinder assembly; (b) physical properties of pressure-transmitting liquids at high pressures (measured at VNIIFTRI); (c) elastic distortion found from the solution of the Lamé problem (with elastic constants of the specific steel samples determined by ultrasonic methods); (d) assumptions used in solving the Lamé problem under operation conditions in terms of linear elasticity theory; and (e) non-linear effects observed in distortion of piston-cylinder assembly.

Earlier the USSR High-Pressure Standard was directly compared with that of Poland and by means of a manganin cell with France. The indirect evidence of agreement with reference piston gauges maintained at the USA, UK and Japan was obtained through accurate determinations of the mercury fixed point at 0° C (the present VNIIFTRI value being equal to 756.97 MPa). The results of all previous comparisons diverged less than the combined error of instruments involved. In most cases the results coincided within 0.02 %.

(ii) The National High-Pressure Standard maintained at ASMW (GDR) is based on a Budenberg piston gauge manufactured in 1953. It uses a 10-to-1 lever-arm multiplier and steel piston-cylinder assembly. The nominal piston diameter is 2.5 mm. The uncertainty due to distortion is estimated to be 0.02 %. The uncertainty due to the mechanical rotation drive has not been determined. The maximum pressure equals 600 MPa, the normalized uncertainty being 0.05 %.

Another ASMW high-pressure standard is a Harwood Engineering piston gauge manufactured in 1968. It employs a steel cylinder and tungsten carbide piston of nominal diameter 2.5 mm. A mixture of oil and petroleum ether ("white gasoline") is used as a pressure transmitting liquid. Due to high volatility of petroleum ether the mixture is unstable. This may cause perceptible variations in the pressure dependence of the effective area. The overall error is estimated to be 1 part in 1000. During the intercomparisons reported here, the manganin cell has been calibrated against this piston gauge.

(iii) The OMH primary gauge was manufactured in Riga (USSR) and certified by VNIIM (Leningrad) in 1967. The piston is loaded through a rod with ball joints at the ends. The instrument has a simple piston-cylinder unit made of steel, with piston having the nominal diameter of 1.75 mm. The overall error is 0.05 %.

The intercomparisons procedure and results. Of all known comparison methods, the most accurate and efficient seems to be a pressure-sensing method using a high-pressure valve and two manganin cells [1]. This method is routinely used in VNIIFTRI in calibrations and metrological certifications involving standard piston gauges. With resolution better than 0.1 kPa readily attained at any pressure, two piston gauges can be balanced in about one minute. Unfortunately, there was no high-pressure valve available at ASMW and OMH, so that a flow-sensing (cross-float) method had to be applied. Its relative resolution is about 0.01 %, and a single balancing takes up to a half-hour. The effective areas of the local low-pressure standard piston gauges used to select the MULTIBAR input pressure values were preliminarily measured against the National Standards of GDR and Hungary. The MULTIBAR output pressures were measured by the National High-Pressure Standards at the levels multiple of 100 MPa in the range from 100 to 600 MPa. The comparison data were expressed in terms of pressure dependence of the MULTIBAR multiplication factor. Some of the intercomparisons characteristics are summarized in Table 3.

Table 3  
Maximum Divergence of High Pressure Scales

Transfer device	Nat'l scales compared	Maximum divergence, %	Standard deviation of result, %
MULTIBAR	USSR - GDR (I)	0.036	0.007
	USSR - Hungary	0.052	0.004
	GDR (I)- Hungary	0.088	
Manganin gauge	USSR - GDR (I)	0.07	0.02
	USSR - GDR (II)	0.09	0.04

The high pressure scales of the USSR, GDR and Hungary are found to coincide within the normalized uncertainty limits. The higher apparent effective area values of piston gauges of GDR and Hungary may result from the errors in measurements of elastic constants of materials used in manufacturing the piston-cylinder assembly and/or because of the clearance increase at the

ends of the engagement length due to technological defects or wear.

During the intercomparisons we found what additional measures would be helpful in ensuring the higher accuracy of pressure reproduction and comparison. In fact, the experimental methods of investigating liquid flow in the clearance have been recently refined. Another version of multiplier, the MULTIBAR-C, has been developed. With a mass of only 3.8 kg, it permits pressure measurements to be performed in the range from 25 kPa to 1.2 GPa.

As it was mentioned before, the pressure-sensing technique should be preferred in the next international comparisons. The local laboratories have to be equipped with a high-pressure valve and a sensitive d.c. resistance bridge with resolution 1 part in  $10^8$ . A set of transfer standards should include a pressure multiplier and two manganin cells. A mercury freezing cell may be also included as an optional device.

In terms of economy and logistics, it is advisable to compare pressure scales both in the medium and high ranges at the same time since the same complex of measuring instruments is employed.

#### R e f e r e n c e

1. High Pressure Research. Ed. by E.V. Zolotykh, Izdatel'stvo standartov, Moscow, 1987

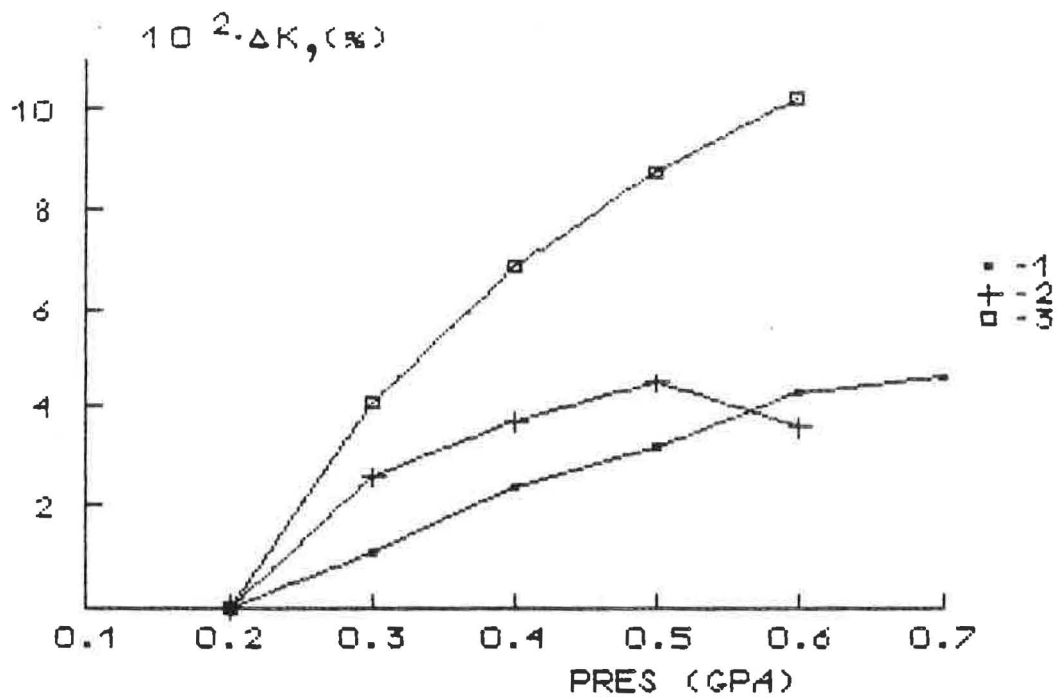


Fig. 1. Fractional increment  $\Delta K$  of MULTIBAR multiplication factor vs pressure. 1 - USSR; 2 - Hungary; 3 - GDR

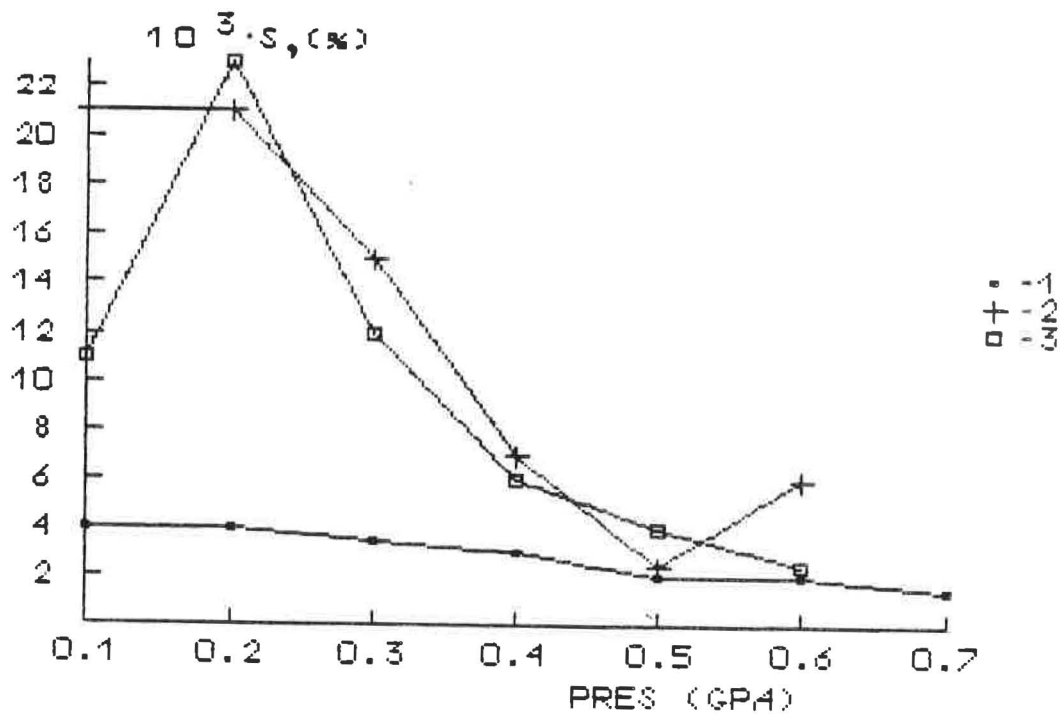


Fig. 2. Standard deviation of cross-float measurements. 1 - USSR; 2 - Hungary; 3 - GDR

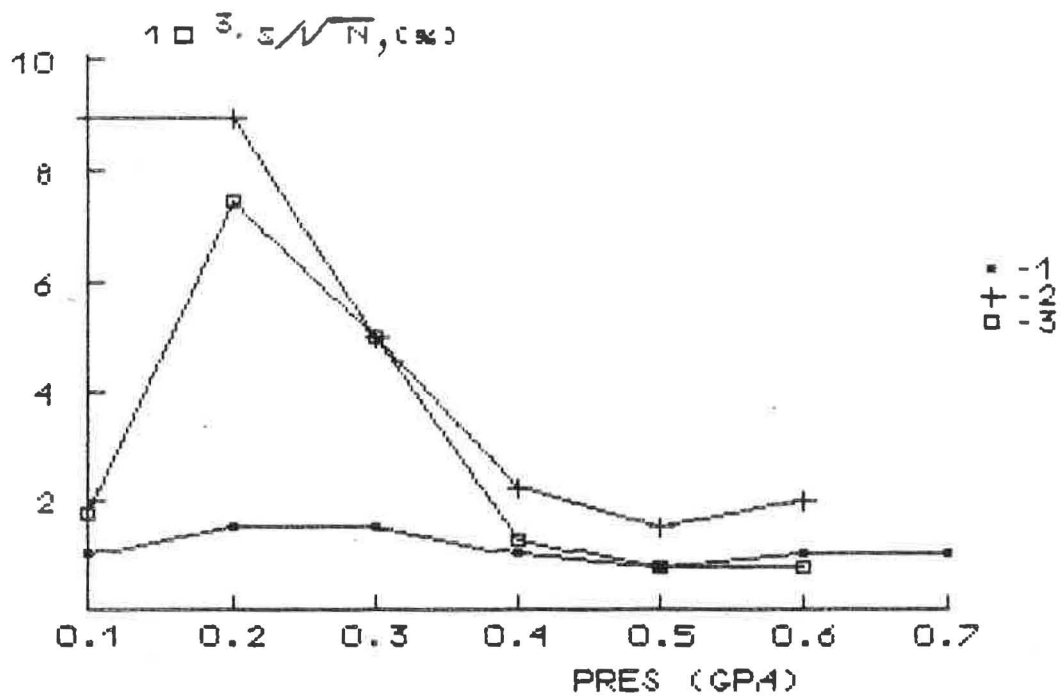


Fig. 3. Standard deviation of mean values of cross-float measurements. 1 - USSR; 2 - Hungary; 3 - GDR

Pressure Fixed Points Based on the  
Carbon Dioxide Vapor Pressure at 273.16 K and the  
 $H_2O(I) - H_2O(III) - H_2O(L)$  Triple-Point

Noel Bignell  
CSIRO  
Division of Applied Physics  
Lindfield, NSW, Australia

and

Vern E. Bean  
National Institute of Standards and Technology  
Center for Basic Standards  
Gaithersburg, Maryland, USA

ABSTRACT

*The vapor pressure of carbon dioxide in equilibrium with the liquid at 273.16 K has been measured and found to be  $3.48608 \pm .00017$  MPa. Results were found to depend upon the purity of the carbon dioxide. Samples prepared by heating analytical reagent quality sodium bicarbonate were of sufficient purity to be suitable for use as a pressure fixed point.*

*The pressure of the  $H_2O(I)-H_2O(III)-H_2O(L)$  triple-point has also been measured and found to be  $208.829 \pm 0.025$  MPa.*

INTRODUCTION

Fixed points are valuable since they provide:

1. A method of comparison among laboratories.
2. A method for calibration of secondary standards.
3. An invariant for periodic comparisons of primary standards.

Herein we report our recent measurements on two pressure fixed points that are in the range of piston gages, the vapor pressure of carbon dioxide in equilibrium with the liquid at a temperature fixed at the triple-point of water (defined to be 273.16 K or 0.01 °C), which is in the neighborhood of 3.5 MPa, and the pressure of the triple-point of  $H_2O(I)$  (the ordinary ice),  $H_2O(III)$  (a high pressure polymorph of ice), and liquid  $H_2O$ , which is in the neighborhood of -22 °C and 209 MPa.

CARBON DIOXIDE VAPOR PRESSURE

(a) Apparatus

The general arrangement of the apparatus is shown in Fig. 1. The surfaces exposed to the carbon dioxide are stainless steel and the volume the vapor must fill has been kept low to reduce the equilibrium time. This was done by using small diameter capillary tubing and by making special small-volume fittings for connections.

The capillary tube leading from the bomb to the differential pressure transducer (DPT) passed through an aluminum block in good thermal contact with the stem of the triple point cell where it passes through the surrounding ice bath. This tempering technique greatly reduced the heat conducted down the tubing into the bomb.

The pressure was measured with a piston gage, operated in the absolute mode using nitrogen gas. The DPT serves as a separator between the nitrogen and the carbon dioxide. All the tubing in the measurement circuit from the piston gage to the sample bomb was covered with insulation to reduce the effect of room temperature changes.

#### (b) Carbon Dioxide Samples

Four carbon dioxide samples were used.

Sample (i) was prepared by distillation of industrial grade carbon dioxide.

Sample (ii) was prepared by heating sodium bicarbonate of analytical reagent quality. The following reaction occurs:



The apparatus used to conduct this chemical reaction is shown in Fig. 2 and was mostly devoted to the removal of the one molecule of water that is generated for each molecule of carbon dioxide. The gas was first passed through a cold trap maintained at  $-55^\circ\text{C}$  by an alcohol and dry ice mixture and then through two drying tubes, one filled with anhydrous calcium sulfate and the final one filled with glass fibers coated with phosphorus pentoxide, an extremely efficient desiccant [1]. The carbon dioxide was collected by condensing it in a cylinder cooled in liquid nitrogen.

Sample (iii) was commercially-prepared "research grade" carbon dioxide specified as having a total content of carbon monoxide, nitrogen, oxygen and argon of less than 20 ppm; water, 4.5 ppm; and hydrocarbons, 0.2 ppm.

Sample (iv) was commercially prepared as 99.999% pure by a different supplier.

#### (c) Results

The results for the four samples are shown in Fig. 3 where the pressure is plotted vertically and equal intervals along the horizontal axis represent the progression from one measurement to another, that is the evacuation and refilling of the DPT. The measurements on samples (i) and (ii) settle to constant values which are estimated from the mean of the measurements made after settling as:

- (i) 3.486072 MPa standard deviation  $15 \times 10^{-6}$  MPa
- (ii) 3.486084 MPa standard deviation  $12 \times 10^{-6}$  MPa

Combining the data from both samples, the average value is  $3.48608 \pm 0.00017$  MPa.

As discussed in the next section, the other samples gave pressure values which did not stop reducing with successive measurements and so were not used in the final result.

There are three main sources of error: the piston gage pressure, the head correction, and the triple point cell temperature. The piston gage has been calibrated using primary standards and the total uncertainty (one standard deviation) in the pressure at the reference level is 48 Pa. The head correction is -298 Pa with an uncertainty of 12 Pa. The uncertainty in pressure produced by the temperature uncertainties is due to the difference in temperature an individual triple point cell may have from 0.01 °C. According to IPTS 68 [2] this should be less than 0.2 mK which corresponds to a pressure of 18 Pa. The manufacturer of the cell claims the error lies between zero and 0.1 mK but the larger error will be used here. Combining these uncertainties by taking the square root of the sum of the squares [3], and multiplying that result by three, the overall uncertainty at the 99.7 percent confidence level is 165 Pa.

#### (d) Discussion

When the differential pressure transducer was pumped out and refilled from the sample bomb, the vapor pressure would be expected to re-establish itself to its previous value. For samples (i) and (ii) this is true after the first few measurements. The large initial drop in vapor pressure shown by samples (i) and (iii) is considered to be due to the presence of permanent gases dissolved in the liquid which are boiled off and removed with the vapor thus purifying the remaining liquid. This is the basis of a method of purification of cylinders of industrial grade carbon dioxide given by Keulemans [4].

After the large decreases in vapor pressure sample (iii) continues to exhibit small decreases with each removal of vapor and its replacement by evaporation of the liquid. This behavior is thought to be due to the concentration of water in solution in the carbon dioxide liquid. Morrison [5], in experiments on the effect of water on the critical temperature of carbon dioxide, has shown that the liquid phase is richer in water than the vapor phase in equilibrium with it. There is a chemical interaction between the two types of molecules causing the vapor pressure to be lower than for pure carbon dioxide and lower than the simple application of Raoult's Law would suggest. As the DPT is evacuated and refilled with each new sample, the relative concentration of water in the sample increases. Thus the vapor pressure continues to fall below the value found for the samples of carbon dioxide which were free of water, samples (i) and (ii), for which special care was taken to remove the water. Sample (i), which was prepared from industrial gas was dry but presumably contained permanent gases, so that it showed the initial large drops in vapor pressure whereas sample (ii), prepared from sodium bicarbonate and comparatively free of both permanent gases and water, did not. These two samples after several initial measurements re-established their vapor pressures at virtually the same value after each measurement. Sample (iv) was used twice to fill the bomb; the first filling is shown as (iv)a and the second as (iv)b in Fig. 3. In both cases it shows no initial large drop but does exhibit the small drops in pressure with each measurement. This behavior is interpreted as being due to very few permanent gas impurities but some water content. The more rapid decrease in vapor pressure shown for the last couple of measurements by samples (iii) and (iv)b seems due to

the more rapid concentration of water which would occur when the sample is nearly depleted.

#### H<sub>2</sub>O(I) - H<sub>2</sub>O(III) - H<sub>2</sub>O(L) TRIPLE-POINT

The phase diagram of Fig. 4 shows the H<sub>2</sub>O(I) - H<sub>2</sub>O(III) - H<sub>2</sub>O(L) triple-point and the region of stability of the various phases of water around it.

##### (a) Apparatus

The triple-point cell designed for this measurement is shown in Fig. 5. The cell is made of maraging steel, chosen to keep the mass, and hence the thermal bulk of the vessel, as small as possible. The water sample was designed to fill as much of the pressure volume as possible so that its volume changes had the maximum possible effect on the pressure of the system. The connections were made with capillary tubing to minimize the volume of the pressurizing fluid and the heat input to the vessel. The cell is contained in a vacuum flask for thermal stability.

A sample of distilled water of about 50 ml was placed in a deformable sack made from a laminate of polyethylene and polyester. The water was boiled to remove dissolved gases. For the final measurements the metal parts in contact with the sample were gold plated to avoid rust contamination.

A platinum resistance thermometer whose well extended into the interior of the sack containing the sample was used to measure sample temperature. The cell was cooled by blowing cold nitrogen gas into the vacuum flask around the cell and warmed with an electrical heater wound on the cell.

The schematic diagram of the apparatus used to measure the triple-point pressure is shown in Fig. 6. The oil-operated piston gage was calibrated using the pressure standards maintained by the National Institute of Standards and Technology. It was separated from the cell by a differential pressure transducer with constant volume valves in series and parallel for checking the zero. This is necessary both to isolate the different liquids used in the cell and in the piston gage, heptane and oil, and to prevent a slight pressure difference between the cell and the piston gage from driving the cell beyond the limits of its stability.

##### (b) Attainment of the triple-point condition

It is necessary to establish the three phases, H<sub>2</sub>O(I), H<sub>2</sub>O(III) and the liquid, simultaneously in the cell. This cannot be done simply by establishing the pressure and temperature of the triple-point, as the liquid is quasi-stable in the stability regions of the solids and the system would simply persist in the liquid state. Before a new solid phase will form it is generally necessary to penetrate some distance into its region of stability.

The triple-point was approached along the path shown in the phase diagram of Fig. 4. The pressure in the cell was increased, at room temperature, to 280 MPa then the cell was cooled down gradually until, at about -31 °C, a transition was observed by the sudden increase in temperature and a slow drop in pressure. This was the transition to

H<sub>2</sub>O(III) which is more dense than the liquid. Though this transition occurred in the region of stability of H<sub>2</sub>O(II), any of this phase which formed would change to H<sub>2</sub>O(III) when the system rapidly increased its temperature and moved into the H<sub>2</sub>O(III) region of stability. After this sudden rise in temperature there was a slow fall which is due to the loss of heat to the cell and pressurizing fluid.

The pressure was then reduced, as shown in Fig. 4, until at some point in the region of stability of H<sub>2</sub>O(I), a transition was again observed by an abrupt increase in pressure, though this time the temperature change was quite small. H<sub>2</sub>O(I) and H<sub>2</sub>O(III) were now present and the system had established an equilibrium between these two phases. At this stage the pressure of the system became more stable and was controlled by this equilibrium. Because the boundary between the two phases is almost parallel to the temperature axis, temperature changes have a small effect on the equilibrium pressure.

The cell was then warmed until the two phases began to melt and the third phase was formed at the triple-point. A plot of temperature against time showed when this melting occurred by a decrease in the rate of warming. As the apparatus warmed up the pressure was measured by balancing the pressure in the cell against the piston gage. When the system had not yet reached the triple-point condition, the balance pressure drifted downward but became quite stable when the triple-point condition had been reached. The temperature range corresponding to the stable pressure condition extends over about 80 mK. In this range the pressure is independent of temperature but at higher temperatures the pressure increases with temperature. Attempts to alter the pressure of the system by adjustment of the screw press result in the re-establishment of the same stable pressure after only about a minute. By cooling periodically and using the screw press to keep both phases I and III present, the system can be kept in the triple-point condition indefinitely.

### (c) Results

The piston gage pressures, with the usual corrections, were used to calculate the absolute pressures in the triple-point cell by the addition of measured atmospheric pressure and a small correction for the head of pressurizing fluid between the piston gage reference level and the cell level. Five runs were made and the results of the last three are shown in Fig. 7. The pressures of each of the runs were averaged and the values of these averages and the standard deviations are given in Table I. After the first three runs, the cell was disassembled and inspected. Some traces of rust were found on the metal parts in contact with the water. These parts were then gold-plated before the last two runs were done. Even though the contamination by rust seems to have little effect on the results, only the two runs after the gold-plating have been averaged for the final result of  $208.829 \pm 0.025$  MPa.

The standard deviation of the 24 readings of the last two runs is 0.0036 MPa which constitutes a measure of the reproducibility of the triple-point pressure. The other uncertainty of the measurement is the calibration uncertainty of the piston gage. The piston gage was calibrated against standards and the estimated uncertainty at 210 MPa is 0.025 MPa. The combined uncertainty from both sources expressed as the root-mean-square at the 99.7 percent confidence level is 0.025 MPa.

The uncertainty in the estimation of the triple-point temperature is dominated by the range over which the condition of pressure stability was observed to extend, from -22.18 °C to -22.25 °C, and so the triple-point is taken as  $-22.22 \pm 0.04$  °C.

#### REFERENCES

1. J. E. Still, H. J. Cluley, *The Analyst* 97, 1-16, (1972)
2. H. Preston-Thomas, *Metrologia* 12, 7-17, (1976)
3. *Metrologia*, 17, 73, (1981)
4. A. I. M. Keulemans, *Gas Chromatography* (Reinhold N.Y. 1957) pp. 213-4
5. G. Morrison, *J. Phys. Chem.* 85, 759-761, (1981)

Table I. The means and standard deviations of five runs together with the combined mean and standard deviation of the last two runs.

Run	Readings	Mean (MPa)	Standard Deviation (MPa)
1	9	208.823	0.0041
2	3	208.823	0.011
3	6	208.829	0.0057
4	10	208.827	0.0034
5	14	208.832	0.0051
4 & 5	24	208.829	0.0036

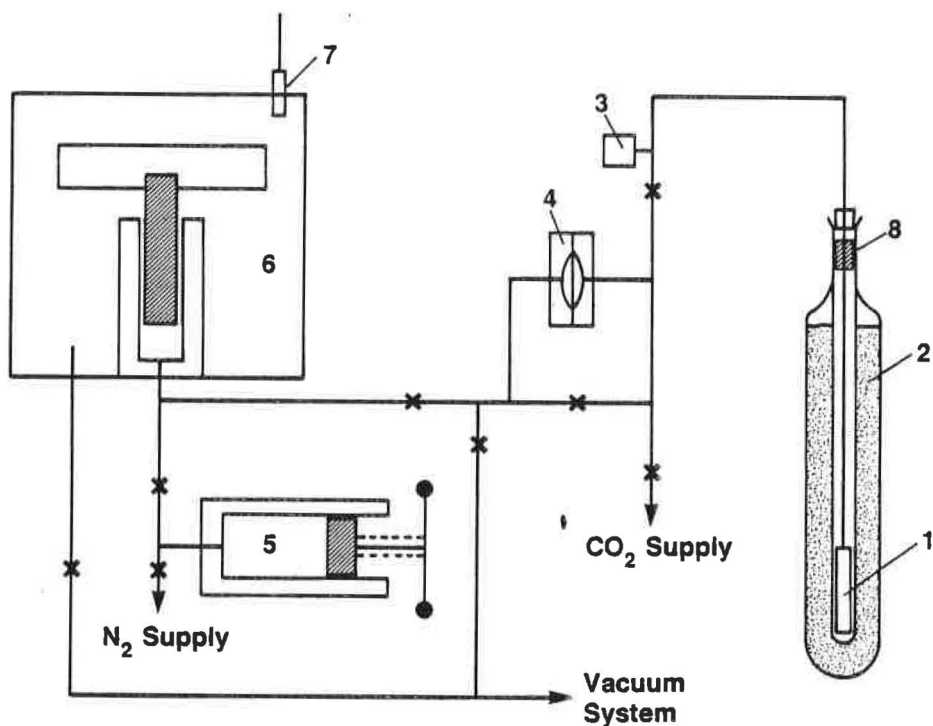


Fig. 1. The apparatus used to measure the vapor pressures. 1, sample bomb; 2, triple point cell; 3, pressure transducer; 4, differential pressure transducer; 5, volume adjuster; 6, piston gage with evacuated cover for absolute mode; 7, vacuum gage; 8, aluminum block.

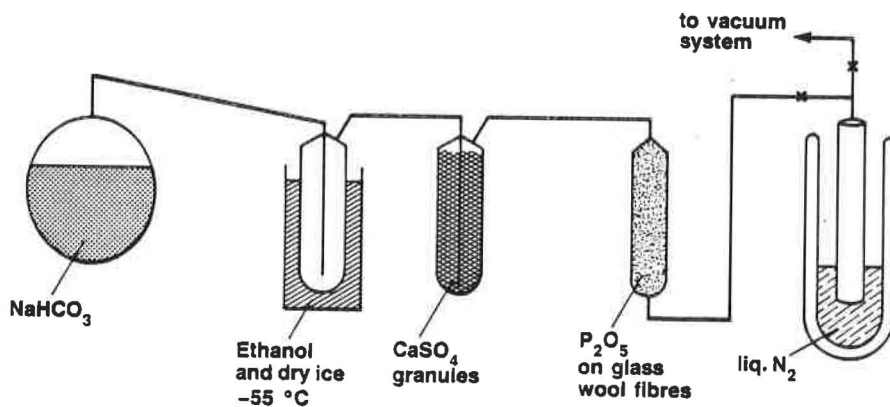


Fig. 2. Diagram of the apparatus used to make the carbon dioxide for sample (ii).

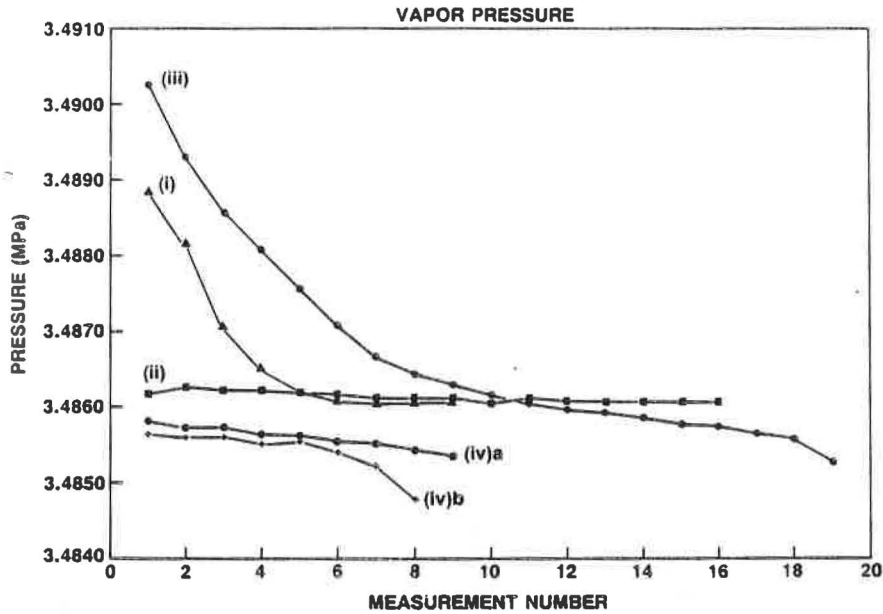


Fig. 3. The measured vapor pressures for samples (i) to (iv) plotted against the measurement number, a number representing the sequence in which the measurements were performed.

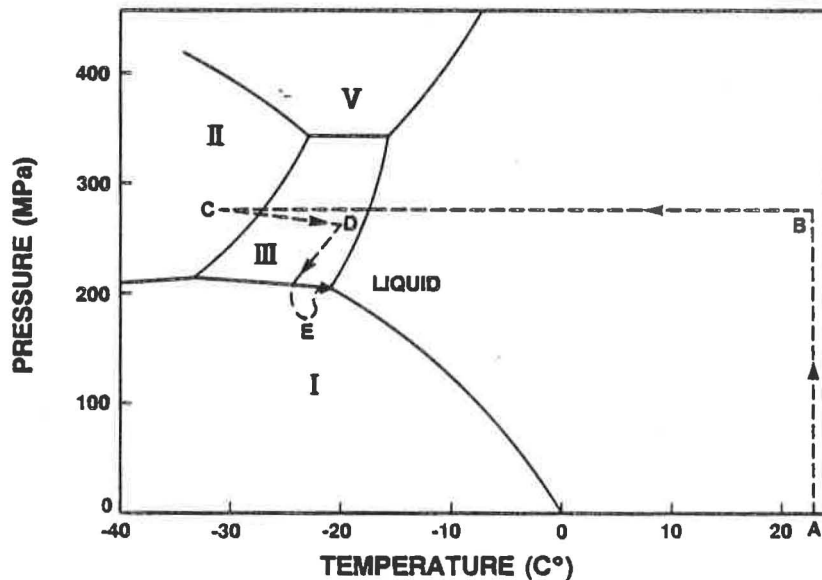


Fig. 4. Part of the phase diagram of water showing the triple-point between the liquid and two solid forms, I and III. The path taken by the cell to establish the three phases in equilibrium is also shown. At A the cell is at room temperature and pressure. The pressure is increased at room temperature to B and then the cell is cooled until at C a transition to a solid occurs when both pressure and temperature move spontaneously to D. At this stage the water is in form III. The pressure is then reduced until at E another transition occurs to form I. By warming the cell the system can be moved to the triple-point condition when melting produces the liquid form and the three phases are present.

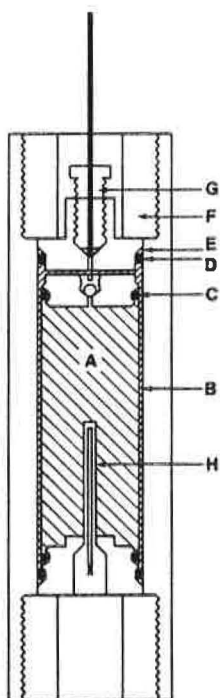


Fig. 5. The pressure vessel and sample container. A, sample of water; B, pressure fluid, heptane; C, "O" ring for sealing sample in plastic sack; D, "O" ring for sealing pressure vessel; E, anti-extrusion ring; F, jam nut; G, gland nut and conical seal for high pressure capillary tubing; H, thermometer well.

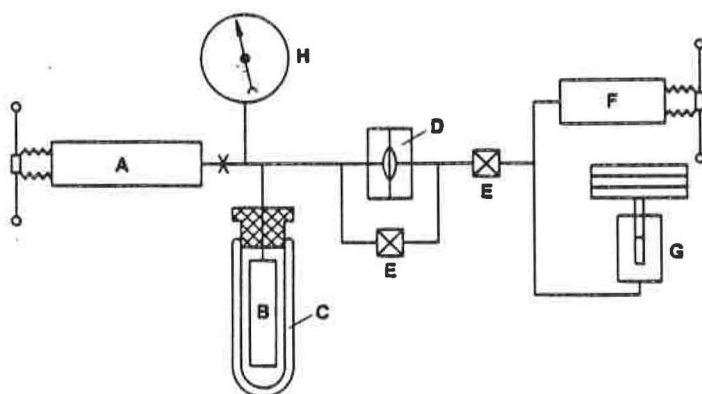


Fig. 6. The schematic of the apparatus used to measure the pressure produced by the triple-point cell. A, screw press for heptane; B, pressure vessel; C, vacuum flask; D, differential pressure gage; E, constant volume valves; F, screw press for piston gage pressure fluid; G, piston gage; H, Bourdon gage.

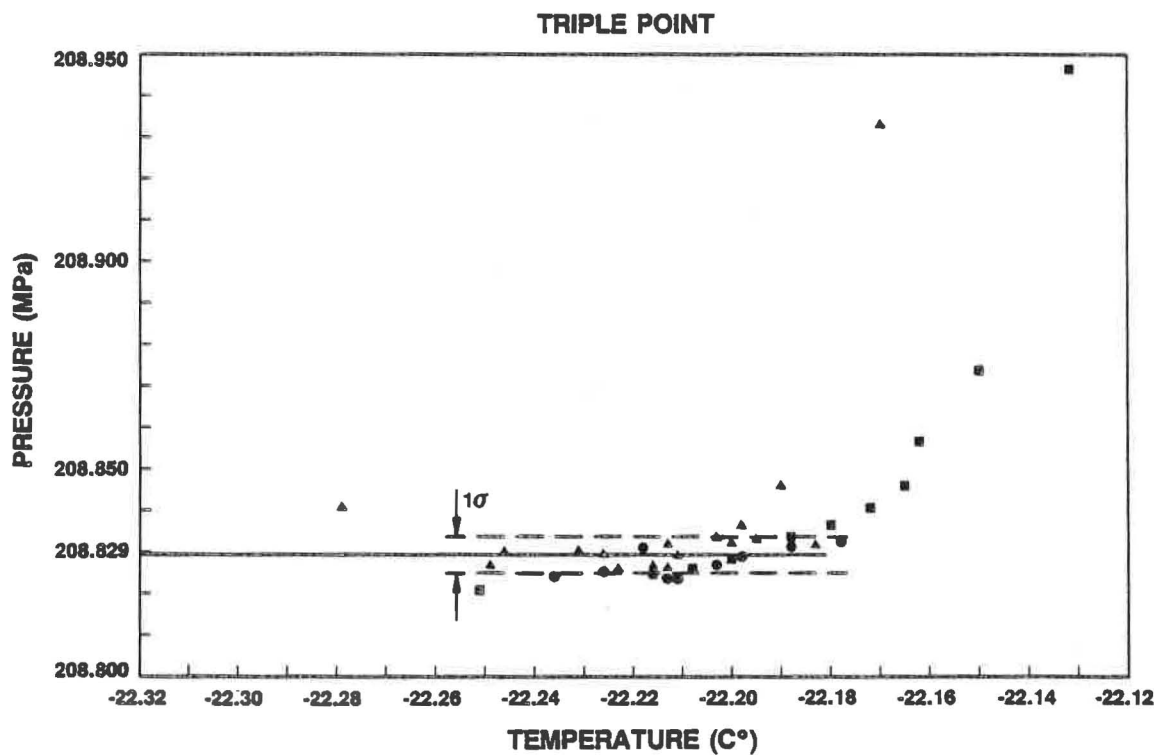


Fig. 7. A plot of the temperature recorded by the platinum resistance thermometer against the pressure as measured by the piston gage in the immediate vicinity of the triple-point for runs 3, 4, and 5.

LIST OF CONTRIBUTORS - II

(alphabetic order and page of the paper in the present monograph)

H. Arendt 168  
Yu.A. Atanov 132, 168  
V.E. Bean 22, 81, 125, 175  
L. Bianchi 147  
N. Bignell 175  
V.M. Borovkov 132, 168  
P.C. Cresto 12  
J.P. Damion 161  
P. Delajoud 114  
R.E. Edsinger 81  
C.D. Ehrlich 81  
D.B. Francis 53  
B. Gyarmati 168  
P. Hilsch 62  
R.W. Hyland 105  
J. Jäger 62, 141  
G. Klingenberg 1  
J.C. Legras 41  
H. Lippmann 168  
R. Maghenzani 12  
GF. Molinar 12, 147  
A. Ooiwa 67  
J. Rogowski 73  
A.J. Rostocki 27, 73, 162  
G. Sarkani 168  
R. Sendys 27  
Sheng-Yi Tang 105  
K. Solis 53  
L. Sterner 168  
P.R. Stuart 31, 95  
V.E. Tarassov 132, 168  
C.R. Tilford 105  
B.E. Welch 81  
D. Wisniewski 27  
R. Wisniewski 27, 73, 162  
S. Yamamoto 157  
Yaw-Poo Lin 22

